The role of RER1 in the assembly and transport of TREM2-DAP12 complex and cellular lipid metabolism

Doctoral thesis

to obtain a doctorate (MD/PhD)

from the Faculty of Medicine

of the University of Bonn

Yanxia Liu

from Hohhot, Inner Mongolia, China

2025

Written with authorization of

the Faculty of Medicine of the University of Bonn

First reviewer: Prof. Dr. Jochen Walter (University of Bonn, Germany)

Second reviewer: Prof. Dr. Thorsten Lang (University of Bonn, Germany)

Day of oral examination: 23.07.2025

From Clinic for Parkinson, Sleep and Movement Disorders, Center for Neurology

Table of Contents

List of abbreviations

aa	Amino acids
ABCA1	Transporter proteins ATP-binding cassette transporter 1
ABCG1	ATP Binding Cassette Subfamily G Member 1
ABCG8	ATP Binding Cassette Subfamily G Member 8
AChR	Acetylcholine Receptor
AD	Alzheimer's disease
ALDQ	Automatic Lipid Droplet Quantification
ANOVA	Analysis of variance
APOC1	Apolipoprotein C1
ApoE	Apolipoprotein E
APP	Amyloid beta precursor protein
Aβ	Amyloid-beta
BSA	Bovine serum albumin
cDNA	Complementary DNA
CEs	Cholesterol esters
Chlo	Chloroquine
CHX	Cycloheximide
CLEC5A	C-type lectin domain containing 5A
CMA	Chaperone-mediated autophagy
CMT disease	Charcot-Marie-Tooth disease
CNS	Central nervous system
Co-IP	Co-Immunoprecipitation
COP	Coat protein complex
COPI	Coat protein complex I
COPII	Coat protein complex II
crRNA	CRISPR RNA
CSF	Colony-stimulating factors
CTFs	C-terminal fragments
CYP51A1	Cytochrome P450 Family 51 Subfamily A Member 1
cyto D	Cytochalasin D
DAM	Disease-associated microglia

DAP12	DNAX-activating protein of 12 kDa
DAPI	4′,6-diamidino-2-phenylindole
DCs	Dendritic cells
DEGs	Differentially expressed genes
DHCR7	7-Dehydrocholesterol Reductase
DMEM	Dulbecco's Modified Eagle Medium
DMSO	Dimethyl sulfoxide
DNA	Deoxyribonucleic acid
DTT	Dithiothreitol
E1	Ub activating enzyme
E2	Ub conjugating enzyme
E3	Ub ligase
EBP	Emopamil Binding Protein
ELOVL6	Elongation of Very Long Chain Fatty Acids Protein 6
EMPs	erythro-myeloid progenitors
EOAD	Early-onset Alzheimer’s disease
ER	Endoplasmic reticulum
ERAD	ER-associated degradation
ERES	ER exit sites
ERGIC	ER-Golgi intermediate compartment
FABP5	Fatty Acid Binding Protein 5
FADS2	Fatty Acid Desaturase 2
FAs	Fatty acids
FASN	Fatty Acid Synthase
FBS	Fetal Bovine Serum
FcR	Fc receptor
FDFT1	Farnesyl Diphosphate Farnesyltransferase 1
FL	Full-length
FTD	Frontotemporal dementia
$GABA_A$	γ-Aminobutyric acid type A receptor
GAPDH	Glycerinaldehyd-3-phosphat-Dehydrogenase
GC-FID	chromatography-flame ionization detection

GC-MS-SIM	GC-mass spectrometry selected ion monitoring
Gly	Glycine
GO	Gene Ontology
HDEL	Histidine-Aspartic acid-Glutamic acid-Leucine
HDL	High density lipoprotein
HEK	Human embryonic kidney
HMGCR	HMG-CoA reductase
HMGCS1	3-Hydroxy-3-Methylglutaryl-Coenzyme A Synthase 1
HPRT1	Hypoxanthine phosphoribosyltransferase 1
Hsp60	Heat shock protein 60
ICC	Immunocytochemistry
ICD	Intracellular domain
IDOL	Inducible Degrader of the Low-Density Lipoprotein
IFN-γ	Interferon-gamma
INSIG1	Insulin-induced gene 1 protein
iPSC	Induced pluripotent stem cell
ITAM	Immunoreceptor tyrosine-based activation motifs
ITIM	Immunoreceptor tyrosine-based inhibitory motif
KARAPs	Killer cell activating receptor-associated polypeptides
KARs	Killer cell activating receptors
KDEL	Lys-Asp-Glu-Leu
KEGG	Kyoto Encyclopedia of Genes and Genomes
KIR	Killer cell inhibitory receptor
ko	Knock out
Lac	Lactacystin
LB	Lysogeny broth
LC3	Microtubule-associated protein 1A/1B-light chain 3
LDAM	Lipid-droplet-accumulating microglia
LDL	Low density lipoprotein
LDLR	Low density lipoprotein receptor
LDs	Lipid droplets
LIPG	Lipase G

LOAD	Late-onset Alzheimer’s disease
LPL	Lipoprotein Lipase
LPS	Lipopolysaccharide
LRP1	Low density lipoprotein receptor-related protein 1
LSS	Lanosterol Synthase
LXR	Activate liver X receptor
MAM	Mitochondrial-associated membrane
MAP	Mitogen-activated protein
MDL-1	Myeloid DAP12 associating lectin 1
MG132	Carbobenzoxy-L-leucyl-L-leucyl-L-leucine
mRNA	Messenger ribonucleic acid
MSMO1	Methylsterol Monooxygenase 1
MYLIP	Myosin Light Chain Interacting Protein
nAChR	Skeletal muscle nicotinic acetylcholine receptor
NEDD4-2	neural precursor cell expressed developmentally downregulated gene 4-like
NHD	Nasu-Hakola disease
NHEJ	Non-homologous end joining
NK cell	Nature killer cell
NKp44	44-kD surface molecule in NK cells
NMR	Nuclear Magnetic Resonance
NPC1	Nieman-Pick C proteins 1
NSDHL	NAD(P) Dependent Steroid Dehydrogenase-Like
P/S	Penicillin/Streptomycin
PBS	Phosphate buffer saline
PBST	Phosphate-Buffered Saline, 0.1 % Tween® 20 Detergent
PDI	Protein disulfide isomerase
PEN2	Presenilin Enhancer 2
PFA	Paraformaldehyde
PI3K	Phosphatidylinositol 3-kinase
PKC	Protein kinase C
PLCγ	Phospholipase Cγ

PLL	Poly-L-Lysine Hydrobromide
PLOSL	Polycystic lipomembranous osteodysplasia with sclerosing leucoencephalopathy
PMA	Phorbol 12-Myristate 13-Acetate
PMP22	Peripheral myelin protein 22
PS1	Presenilin 1
PSEN1	Presenilin 1
PSYK	Phospho-SYK
qRT-PCR	Quantitative Reverse Transcription polymerase chain reaction
RA	Retinoic acid
RER1	Retention in Endoplasmic Reticulum Sorting Receptor 1
RNA seq	RNA sequencing
RNP	Ribonucleoprotein
RT	Room temperature
SC5D	Sterol-C5-Desaturase
SCAP	Sterol regulatory element-binding protein Cleavage-Activating Protein
SCD5	Stearoyl-CoA Desaturase 5
SDS	Sodium dodecyl sulfate
SDS-PAGE	sodium dodecyl sulphate-polyacrylamide gel electrophoresis
SEM	Standard Error of Mean
sgRNAs	Single guide RNAs
shRNA	Small hairpin RNA
Siglec	Sialic acid-binding immunoglobulin (Ig)-like lectin
SIRPβ1	Signal-regulatory protein β1
SOC	Super Optimal broth with Catabolite repression
SQLE	Squalene Epoxidase
SREBP2	Sterol response element-binding protein 2
SYK	Spleen tyrosine kinase
TAGs	Triacylglycerols
TBS	Tris-Buffered Saline
TBST	Tris-Buffered Saline, 0.1 % Tween® 20 Detergent

TCR	T-cell receptor
TDPC	Homodimer within tetradecyl phosphocholine
TM	Transmembrane
TM7SF2	Transmembrane 7 Superfamily Member 2
TMD	Transmembrane domain
TNF-α	Tumor necrosis factor-alpha
TPM	Transcript per million
TracrRNA	Transactivating crRNA
TREM1	Triggering receptor expressed on myeloid cell 1
TREM2	Triggering receptor expressed on myeloid cell 2
TREM3	Triggering receptor expressed on myeloid cell 3
Ttyh1	Protein tweety homolog 1
TYROBP	Tyrosine kinase binding protein
Ub	Ubiquitin
UBC	Ubiquitin C
UPS	Ubiquitin-proteasome system
Vitamin D3	1,25-Dihydroxyvitamin D3
VLDL	Very low density lipoprotein
wt	Wild type
ZAP70	ζ-chain-associated protein kinase

1 Introduction

1.1 Monocytes/macrophages and microglia

1.1.1 Monocytes/macrophages

Human mononuclear phagocytes mainly include three types of cells: circulating monocytes, macrophages and dendritic cells (DCs) (Hume et al., 2019).

Monocytes are circulating blood cells and represent a type of leukocytes (white blood cell). They represent about 10% of peripheral leukocytes in humans (Yona & Jung, 2010). They originate in the bone marrow and circulate in the bloodstream. Monocytes serve as a precursor to macrophages and dendritic cells (Randolph et al., 1999, van Furth et al., 1979, Yona & Jung, 2010). Monocytes have high mobility and can reach any part of the organism (Yona & Jung, 2010). Additionally, the half-life time of monocytes is only around three days in humans, enabling the continuous repopulation of tissue macrophages and in particular the ephemeral dendritic cells (Geissmann et al., 2003, Randolph et al., 1998, Serbina & Pamer, 2006, van Furth & Cohn, 1968).

Macrophages are present across various organs throughout the body and mainly include tissue-resident macrophages, which are derived from yolk sac erythro-myeloid progenitors (EMPs), and monocyte-derived macrophages, which are developed from hematopoietic stem cells (HSCs) (Jenkins & Allen, 2021, Mass et al., 2023, Park et al., 2022). During embryonic stages, EMPs develop to either pre-macrophages, which colonize embryonic tissues and differentiate into tissue-specific macrophages during organogenesis (Gomez Perdiguero et al., 2015, Mass et al., 2016), or to monocytes, which additionally contribute to the pool of tissue-specific macrophages (Dick et al., 2022, Gomez Perdiguero et al., 2015, Hoeffel et al., 2015). During tissue damage, monocytes are recruited to inflamed tissues and differentiate into monocyte-derived macrophages (Park et al., 2022). Macrophages express many membrane receptors, including phagocytic receptors, toll-like receptors, and scavenger receptors, which mediate phagocytosis and inflammatory responses (Gilroy et al., 2004, Gordon, 2007, Gordon & Plüddemann, 2017, Gordon et al., 2020, Lawrence et al., 2002, Mass et al., 2023).

1.1.2 Microglia

Microglia are the principal resident immune cells (5-20% of total cells in brain) in the central nervous system (CNS), and originate from primitive myeloid precursors in the yolk-sac during early hematopoiesis that migrate to CNS (Ginhoux et al., 2010). Microglia express various membrane receptors, including toll-like receptors, CD36 and triggering receptor expressed on myeloid cell 2 (TREM2, Fig.1.1), which bind to many ligands, such as lipopolysaccharide (LPS) and β-amyloid (Aβ), leading to their activation to trigger release of inflammatory mediators and/or phagocytosis (El Khoury et al., 2003, Ibach et al., 2021, Stewart et al., 2010). Microglia have several important functions in the central nervous system (CNS). They help maintain CNS homeostasis and monitor infections or injuries. During brain development, they assist in synaptic pruning and support brain plasticity. When activated, they also respond to inflammation (Kettenmann et al., 2013, Schafer & Stevens, 2015, Tremblay, 2011, Tremblay et al., 2011). Traditionally, activated microglia are distinguished as classically activated microglia (M1 type) and alternatively activated microglia (M2 type). M1 type of microglia secrete pro-inflammatory cytokines, including tumor necrosis factor-α (TNF-α), interleukin6 (IL-6), IL-1, IL-1β, and chemokines, and express nicotinamide adenine dinucleotide phosphate (NADPH) oxidase and matrix metalloproteinases (MMP)-12. M2 type of microglia release anti-inflammatory cytokines and plays a neuroprotective role (Qin et al., 2023). However, this classical definition is oversimplified as RNA sequencing revealed a broader transcriptional profile than M1 and M2 types (Xue et al., 2014). *In vivo* single-cell RNA sequencing also demonstrated more complex phenotypes of activated microglia in both mouse and human brain, even differences were found in the subpopulations of microglia between mouse and human brain (Hammond et al., 2019, Masuda et al., 2019, Olah et al., 2020, Salamanca et al., 2019). In addition, differential microglia subtypes were also observed in different CNS disorders, such as amyotrophic lateral sclerosis and Alzheimer's disease (AD) (Chiu et al., 2013, Keren-Shaul et al., 2017).

Microglia have been involved in the development and pathogenesis of neurodegenerative diseases, including AD (Althafar, 2022, Heneka et al., 2024). In the early stage of AD pathology, microglia are activated and help with the clearance of Aβ plaques in the brain of AD mouse models and this phagocytotic process involves different receptors of

microglia, including TREM2, Fc receptor and others (Bard et al., 2000, Grubman et al., 2021, Keren-Shaul et al., 2017). The deletion of microglia led to the increased Aβ deposition in an organotypic hippocampal slice culture (OHSC) system with an in vivo-like microglial-neuronal environment and the replenishment of primary microglia reverse the deposition of Aβ, indicating the importance of microglia for the clearance of Aβ plaques (Hellwig et al., 2015). However, in later stage of AD pathology, microglial phagocytosis may contribute to synapse loss and neuronal loss (Dejanovic et al., 2022, Huang & Lemke, 2022). Thus, microglial phagocytosis of Aβ, synapses and neurons may affect AD onset and progression (Heneka et al., 2024).

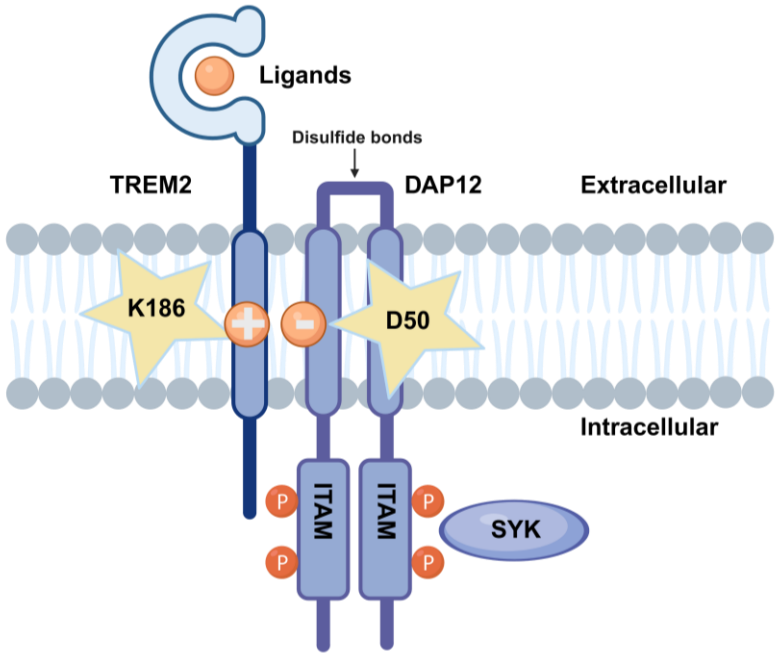

Fig. 1.1 TREM2-DAP12 complex and signaling. The interaction of TREM2 and DAP12 is mediated by the positively charged lysine residue (K186) and the aspartic acid residue (D50) in the transmembrane domain (TMD) of TREM2 and DAP12, respectively. As a result of the ligation of TREM2, the ITAM motif's tyrosine residues become phosphorylated, activating downstream targets via SYK kinase. Created with BioRender.com.

1.2 The DNAX-activating protein of 12 kDa (DAP12)

KARAP (killer cell activating receptor-associated protein), also called DNAX-activating protein 12 kDa (DAP12) or TYROBP (tyrosine kinase binding protein), is a type I transmembrane protein. It was firstly identified and defined by Olcese and colleagues (Olcese et al., 1997). They discovered a group of disulfide-linked dimers specifically

connected with killer cell activating receptors (KARs), isoforms of killer cell inhibitory receptor (KIR). Lanier and colleagues firstly found that human DAP12 gene is located in chromosome 19q13.1, close to KIR genes, indicating the genetic connection between KIR and DAP12 genes (Lanier et al., 1998b). DAP12 is expressed in lymphoid cells and myeloid lineage cells, including nature killer (NK) cells, subsets of B and T cells, monocyte/macrophages, granulocytes, DCs, mast cell (Lanier & Bakker, 2000, Tomasello et al., 1998), osteoclasts, oligodendrocytes and microglia (Kaifu et al., 2003).

1.2.1 Structure

Lanier et al. were the first to identify the amino acid sequence of human DAP12 (Lanier et al., 1998b), which contains 113 amino acids (aa) with a predicted signal sequence of 27 aa followed by a 14 aa short extracellular domain, a transmembrane (TM) domain with 24 aa and a cytoplasmic domain with 48 aa.

In the extracellular domain, there are two cysteine residues (C33 and C35) connecting two monomers to a homodimer by disulfide bonds. In the transmembrane domain (TMD), there is a negatively charged aspartic acid residue at position 50 (D50) that mediates interaction with positively charged residues (lysine, K; arginine, R) in the TMD of co-immunoreceptors (Fig. 1.1) (Lanier et al., 1998a). Nuclear Magnetic Resonance (NMR) analysis revealed that the TMDs of a DAP12 dimer form parallel left-handed alpha helices. Notably, two conserved polar residues, including the aspartic acid residue at position 50 (D50) and the threonine residue at position 54 (T54), are essential contributors to the homodimerization process (Call et al., 2010). Molecular dynamics simulation studies also revealed the importance of polar residues in the TM-TM association in the membrane bilayer (Wei et al., 2013). Two immunoreceptor tyrosine-based activation motifs (ITAM) are present in the cytoplasmic domain including Y91xxL94 and Y102xxL105, which are responsible for DAP12 mediated cell signaling (Tomasello et al., 1998).

1.2.2 Associations with immunoreceptors

DAP12 interacts with two types of immunoreceptors, including members of the C-type lectin receptor and immunoglobulin-like receptor superfamilies.

1.2.2.1 DAP12 interacting receptors of the C-type lectin receptors superfamily

CD94/NKG2 comprise a subfamily of C-type lectin receptors which is predominantly expressed on the plasma membrane of nature killer cells and subsets of T cells. CD94 and one NKG2 isoform form heterodimers. There are five types of NKG2 glycoproteins, including NKG2A, -2B, 2C -2E, -2H, which binds to CD94 by disulfide bonds (Brooks et al., 1997, Carretero et al., 1997, Lazetic et al., 1996, Sullivan et al., 2007). The cytoplasmic domain of NKG2A and its alternatively spliced variant NKG2B contain an immunoreceptor tyrosine-based inhibitory motif (ITIM), which can be phosphorylated to inhibit the function of NK cells (Houchins et al., 1997, Le Dréan et al., 1998). The remaining NKG2 isoforms, including NKG2C/E/H, however, do not contain an ITIM, resulting in NK cell activation when ligated (Cantoni et al., 1998, Houchins et al., 1997). A basic lysine residue is present in the TMD of NKG2C/E/H but not in NKG2A, which mediates the interaction of NKG2C/E/H and DAP12. Indeed, the activation of NK cell by NKG2C ligation is dependent on DAP12 (Lanier et al., 1998a). It was also shown that DAP12 is necessary for the expression of the CD94/NKG2C heterodimeric receptor on the plasma membrane (Lanier et al., 1998a).

Similar to the activating and inhibitory receptors expressed in human NK cells, murine NK cells also have Ly49 receptors which contains both activating and inhibitory types, such as Ly49D and Ly49H, which belong to activating receptors and the arginine (R) residue in the TMD of Ly49 receptors is responsible for the interaction with DAP12 for NK cell activation (Makrigiannis et al., 1999, Mason et al., 1998, McVicar et al., 1998, Rahim & Makrigiannis, 2015).

The 44-kD surface molecule of NK cells (NKp44), which is expressed by activated NK cells, is also a C-type lectin receptor that interacts with DAP12 (Campbell et al., 2004, Parodi et al., 2019, Vitale et al., 1998). The interaction of NKp44 and DAP12 is mediated by the lysine residue (K) in NKp44 and the aspartic acid residue (D) in DAP12 (Campbell et al., 2004).

Additionally, DAP12 is associated with myeloid DAP12 associating lectin 1 (MDL-1), also known as C-type lectin domain containing 5A (CLEC5A), an exclusively monocyte and macrophage lectin, belonging to the superfamily of C type lectins and is a type II

transmembrane protein (Bakker et al., 1999, Gingras et al., 2002). It pairs with DAP12 due to a charged lysine (K) residue in the TMD of MDL-1 (Bakker et al., 1999).

1.2.2.2 DAP12 interacting receptors of the immunoglobulin-like superfamily

Another type of function related receptor expressed in NK cells are KIRs, which were firstly found as DAP12 co-receptors. KIRs belong to Immunoglobulin-like receptors superfamily and similar to CD94/NKG2, KIRs also have an ITIM in the cytoplasmic domain mediating the inhibition function of NK cells (KIR2DL and KIR3DL). A KIR lacking an ITIM (KIR2DS) contains a basic lysine residue in the TMD for interaction with DAP12 and thereby mediates the activation function of NK cells (Biassoni et al., 1996, Campbell et al., 1998, Lanier et al., 1998b, Olcese et al., 1997).

The Triggering Receptor Expressed on Myeloid Cells (TREMs) are activating receptors of the Ig superfamily that are expressed on human myeloid cells and interact with DAP12 by lysine residues (K) in TMD of the receptor, including TREM1, TREM2 (Fig. 1.1) and TREM3 (Bouchon et al., 2000, Chung et al., 2002).

It is also found that signal-regulatory protein 1 (SIRP1) is an activating receptor expressed on myeloid cells, including monocytes and dendritic cells, that associates with DAP12 (Dietrich et al., 2000, Tomasello et al., 2000). Moreover, SIRPβ1 has similar characteristics like the activating receptors in NK cells, which have a basic lysine residue in the TMDs and have short cytoplasmic domains without the signaling transduction function (Dietrich et al., 2000, Wilson et al., 2000).

The sialic acid-binding immunoglobulin (Ig)-like lectin (Siglec) is found on the surface of many immune cells that specifically recognize glycan chains containing sialic acids (Angata et al., 2006, Cao & Crocker, 2011, Crocker et al., 2007). Similar to other Ig-like receptors, there are both inhibitory and activating receptors in the Siglec superfamily. Inhibitory signaling is mediated by ITIM in the cytoplasmic domain of inhibitory receptors, such as Siglec-11 and Siglec-5. Accordingly, Siglec-16 and Siglec-14 are activating receptors which are paired to Siglec-11 and Siglec-5 respectively (Angata et al., 2006, Angata et al., 2002). The activating receptors has no ITIM in the cytoplasmic domain and instead there is a charged lysine residue or arginine residue in the TMD of Siglec-16 and Siglec-14, respectively, which mediates the interaction with DAP12 (Cao & Crocker, 2011).

It was shown that Siglec-H, which is only expressed in mouse, interacts with DAP12 by lysine residue (Blasius et al., 2006, Zhang et al., 2006).

1.2.3 Signaling and regulation of cell function

Olcese et al. found that DAP12 can be phosphorylated on tyrosine and serine residues upon binding of ligands to KIRs (Olcese et al., 1997). Another early study from Lanier and colleagues confirmed that DAP12 has an ITAM in the cytoplasmic domain, which is homologous with ITAM in the cytoplasmic tail of human T-cell receptor (TCR)-associated CD3 chains and the Fc receptor (FcR) γ-chain. DAP12 ITAM is phosphorylated by SRC-family kinases after receptor ligation, and spleen tyrosine kinase (SYK) or ζ-chain-associated protein kinase of 70 kDa (ZAP70) are recruited (Lanier et al., 1998b). As recruited SYK is phosphorylated (PSYK), it triggers additional molecules to be activated, including phosphatidylinositol 3-kinase (PI3K), phospholipase Cγ (PLCγ), AKT (also known as protein kinase B) (Chiesa et al., 2006, Jiang et al., 2002, McVicar & Burshtyn, 2001, Turnbull & Colonna, 2007, Vivier et al., 2004).

In NK cells, activation of the DAP12-associated immunoreceptors elevates the intracellular calcium levels and initiates the mitogen-activated protein (MAP) kinase pathway, subsequently triggering the production of cytokines and chemokines as well as cell-mediated cytotoxicity (Lanier & Bakker, 2000). Bakker et al and Tomasello et al showed that the DAP12-deficiency in mice impaired the function of activating immunoreceptors in NK cells, accumulated DCs in the peripheral tissues and inhibited Th1 responses (Bakker et al., 2000, Tomasello et al., 2000b). However, the identification of DAP12-associated receptors TREMs showed both activatory and inhibitory functions of DAP12 (Turnbull & Colonna, 2007). Which function of DAP12-coreceptors signaling shows is dependent on the avidity of ligand binding to its coupled receptors: when the associated receptors bind to the ligands with high avidity, it shows strong and prolonged activation, leading to pro-inflammatory responses and enhanced immune cell function. However, if DAP12-associated receptors bind to low-avidity ligands, the activation of DAP12 ITAM is partial. The interaction with low-avidity ligands may not provide sufficient stimulation to fully activate DAP12-mediated signaling pathways. Partial activation of DAP12 can lead to inhibitory signaling, suggesting a dual regulatory role of DAP12 in

immune responses (Blasius et al., 2004, Fuchs et al., 2005, Hamerman et al., 2006, Hamerman et al., 2005, Turnbull et al., 2006).

Hickman and colleagues unearthed a cluster of 100 transcripts exhibiting significant enrichment in microglia during a sensing activity. 44 of 100 transcripts are directly or indirectly associated with DAP12, indicating DAP12 as a central hub within this intricate network termed the "sensome" (Hickman et al., 2013). Keren-Shaul et al recently defined a microglial phenotype termed “disease-associated microglia” (DAM) and TROBP exhibited significant upregulation in the hypothesized initial phase of microglial transition from the baseline "homeostatic state" to the DAM phenotype (Keren-Shaul et al., 2017).

1.2.4 Implications in disease

Polycystic lipomembranous osteodysplasia with sclerosing leucoencephalopathy (PLOSL), also known as Nasu-Hakola disease (NHD), is a hereditary recessive disease. The symptoms of patients include progressive presenile frontal-lobe dementia, bone cysts, and fractures. Moreover, patients with NHD usually experience mortality in their fourth or fifth decade of life (Paloneva et al., 2000, Verloes et al., 1997).

The chromosomal locus for this disease was identified at 19q13.1, which was subsequently determined to encode DAP12 (Pekkarinen et al., 1998a, Pekkarinen et al., 1998b). The early studies showed that loss-function mutants of DAP12, including the deletion of exons 1-4 in Finnish patients and a homozygous single-base deletion in exon 3 in a Japanese patient, resulted in NHD disease (Paloneva et al., 2000). Surprisingly, there are no abnormalities in NK cell function of those patients, though DAP12 is originally identified as a crucial transmembrane adapter protein for several immunoreceptors in NK cells (Paloneva et al., 2000). Based on the symptoms (bone cysts and presenile dementia) of the NHD patients, Kaifu and colleagues hypothesized DAP12 could be involved in bone modeling and brain myelination. Therefore, they generated DAP12-deficient mouse model and demonstrated they exhibited osteopetrosis and de-myelinization of the central nervous system (Kaifu et al., 2003).

One study found that several variants of DAP12 might also contribute to the risk of early-onset Alzheimer’s disease (EOAD) (Pottier et al., 2016).The researchers observed those rare DAP12 variants in 9 out of 1110 EOAD patients, but none of them was detected in

1826 controls. Those rare mutations are including G2E, R23C, V47A, D50_L51ins14, R80W, I84V and S89L (Pottier et al., 2016). D50_L51ins14 mutation led to a significant reduction of TREM2, which might indicate a loss of TREM2/DAP12 function and further contribute to the pathophysiology of AD. However, there is so far no evidence whether and how other six mutations affect DAP12 and TREM2 biology.

It is also found that DAP12 is involved in late-onset Alzheimer's disease (LOAD). Zhang et al performed a gene regulatory networks analysis in more than 1000 brain tissues obtained from post-mortem persons who diagnosed of LOAD and the controls by whole-genome genotyping and DAP12 gene was identified as a crucial regulator and up-regulated in LOAD (Zhang et al., 2013).

By crossing *DAP12*$^{-/-}$ mice with APP transgenic (APPswe/PSEN1dE9) mice, researchers found that in both wt and APP transgenic mice, deleting DAP12 had no effect on the overall number of microglia in the cortex and hippocampus, but reduced clustering of microglia around Aβ plaques (Haure-Mirande et al., 2017, Haure-Mirande et al., 2019). Notably, APP transgenic (APPswe/PSEN1dE9) mice lacking DAP12 performed normally in learning behavior assays and electrophysiology recordings at both 4 and 8 months of age (Haure-Mirande et al., 2019). Similarly, crossing the tau transgenic (*MAPT*^{P301S}) with *DAP12*$^{-/-}$ mice resulted in improved learning behavior and enhanced synaptic function, despite an increase in tau phosphorylation stoichiometry and trans-neuronal tau diffusion in the absence of DAP12 (Audrain et al., 2019). A consistent observation in both APPswe/PSEN1dE9 and MAPT^{P301S} mice, when crossed with homozygously deleted DAP12, was a reduction in the levels of the complement protein C1q, suggesting that the removal of DAP12 contributes to positive effects on learning behavior and synaptic functions, partially mediated by a reduction in C1q levels (Audrain et al., 2019, Haure-Mirande et al., 2019). They also overexpressed DAP12 in mice and crossed those mice with APPswe/PSEN1dE9 and MAPT^{P301S} mice to further investigate the effects of elevated DAP12 on modification of microglial phenotype and AD pathogenesis (Audrain et al., 2021). They found that DAP12 mRNA was increased in recruited microglia in either wt or APPswe/PSEN1dE9 and MAPT^{P301S} transgenic mice. Moreover, the overexpression of DAP12 decreased the brain amyloid burden in APPswe/PSEN1dE9 mice and increased

the phosphorylation of TAU in MAPT^{P301S} mice while not altering the total number of microglia in the brain.

1.3 The triggering receptor expressed on myeloid cells 2 (TREM2)

1.3.1 Cell type-specific expression

TREM2 was firstly identified in 2000 and is encoded on human chromosome 6 (Bouchon et al., 2000). TREM2 was found to be expressed on macrophages, immature DCs, osteoclasts, granulocytes in the periphery (Bouchon et al., 2000, Bouchon et al., 2001, Hu et al., 2014, Kaifu et al., 2003, Turnbull et al., 2006). In the central nervous system (CNS), TREM2 shows a much higher expression on microglia compared to that on neurons and other glia (Bouchon et al., 2000, Bouchon et al., 2001, Colonna, 2003, Hickman & El Khoury, 2014, Hickman et al., 2013, Sessa et al., 2004). However, the expression of TREM2 on circulating monocytes is not consistent. Previously, TREM2 was shown to be only expressed in macrophages, differentiated from monocytes (Cella et al., 2003), not in monocytes or only expressed on a small subset of monocytes in both humans and mice (Forabosco et al., 2013, Kiialainen et al., 2007, Song et al., 2017, Tserel et al., 2010, Wang et al., 2016). Several recent studies found that TREM2 is expressed in several blood cell types, including monocytes, granulocytes, in both human and mice (Chan et al., 2015, Hu et al., 2014, Mori et al., 2015, Ozaki et al., 2017, Satoh et al., 2012, Tan et al., 2017, Wu et al., 2015).

1.3.2 Structure

TREM2 is a type I transmembrane protein. It contains a single extracellular immunoglobulin-like domain of the V-type with N-linked glycosylation sites, which binds to its ligands (Bouchon et al., 2001, Gawish et al., 2015, Kober et al., 2016, Park et al., 2015a, Park et al., 2016). The TMD of TREM2 contains a positively charged lysine (K186) residue, which facilitates the association with DAP12. TREM2 has a short intracellular domain, which lacks known cytoplasmic signaling elements (Bouchon et al., 2000, Colonna, 2003).

1.3.3 Soluble TREM2 (sTREM2)

Full-length (FL) TREM2 is cleaved by a Disintegrin and Metalloproteinase Domain-Containing Protein 10 (ADAM10), a protein containing a disintegrin and metalloproteinase domain, leading to the shedding of its ectodomain and the generation of C-terminal fragments (CTFs) (Bouchon et al., 2001, Kleinberger et al., 2014, Wunderlich et al., 2013). The shed ectodomain is known as soluble TREM2 (sTREM2) and secreted extracellularly (Kleinberger et al., 2014, Ma et al., 2016, Wunderlich et al., 2013). TREM2 CTFs undergo intramembrane proteolysis through γ-secretase, resulting in the release of its intracellular domain (ICD) (Wunderlich et al., 2013). Inhibition of γ-secretase cleavage of TREM2 promotes accumulation of CTFs while TREM2 FL is unaffected (Glebov et al., 2016, Park et al., 2015a, Wunderlich et al., 2013). It is shown that the deletion of DAP12 decreased sTREM2 production (Wu et al., 2015).

1.3.4 Ligands

Binding to the ligands could activate TREM2 and further lead to phosphorylation of ITAM in the C-terminus of DAP12, further regulating several cellular functions, including survival, proliferation, differentiation, chemotaxis, phagocytosis and inflammatory responses (Jay et al., 2017, Walter, 2016).

Studies have revealed that TREM2 binds to both exogenous ligands from pathogens and endogenous ligands. For the exogenous ligands, TREM2 has been found to recognize components from bacteria, including anionic bacterial products, pertussis and cholera toxins (Daws et al., 2003, Kawabori et al., 2015, N'Diaye et al., 2009, Phongsisay, 2015, Phongsisay et al., 2015a, Phongsisay et al., 2015b, Phongsisay et al., 2017, Poliani et al., 2015, Quan et al., 2008, Takahashi et al., 2005, Wang et al., 2015b). For the endogenous ligands, TREM2 was shown to bind to heat shock protein 60 (Hsp60), anionic, zwitterionic, myelin-associated lipids, anionic lipid, lipoproteins, nucleic acid released from apoptotic cells (Cannon et al., 2012, Hsieh et al., 2009, Kawabori et al., 2015, Kober et al., 2016, Phongsisay, 2015, Poliani et al., 2015, Stefano et al., 2009, Wang et al., 2015b). Apolipoprotein E (APOE), one of the ligands of TREM2, is recognized as the most significant risk factor for LOAD and has been revealed to regulate the clearance and aggregation of amyloid-beta (Aβ) in both cellular and mouse models (Daws et al., 2003,

Kanekiyo et al., 2011, Liu et al., 2013, Strittmatter et al., 1993, Tai et al., 2014, Verghese et al., 2013). Studies have demonstrated that the interaction between APOE and TREM2 in microglia enhances the phagocytosis of apoptotic neurons bound to APOE, thus linking these two high-risk factors for LOAD (Atagi et al., 2015, Bailey et al., 2015).

1.3.5 Implications in disease

Loss-of-function variants in TREM2 have been found so far that cause or rise the risks of several neurodegenerative diseases. It was firstly shown that several variants of TREM2 caused NHD (Dardiotis et al., 2017, Fenoglio et al., 2007, Klünemann et al., 2005, Numasawa et al., 2011, Paloneva et al., 2002, Satoh et al., 2016, Soragna et al., 2003). For example, TREM2 K186N mutation, originally found in a Norwegian family with NHD, interrupts the association of TREM2 with DAP12 and results in the impairment of TREM2-DAP12 signaling (Jay et al., 2017, Paloneva et al., 2002). However, another study later showed that TREM2 K186N variant did not display maturation or surface expression defect (Sirkis et al., 2017). A recent study demonstrated that splicing defects were likely contributing to pathogenicity in TREM2 K186N variant (Kiianitsa et al., 2024).

Other mutations of TREM2, localized mainly in exon 2 (IgV domain) have been found in other forms of neurodegenerative disease. For example, whole-exome sequencing revealed homozygous TREM2 mutations Q33X, T66M, and Y38C in patients with a frontotemporal dementia (FTD)-like clinical diagnosis (Guerreiro et al., 2013b). The TREM2 mutations T66M and Y38C have been shown to affect the trafficking and processing of TREM2, leading to reduced cell surface expression and increased localization of TREM2 in the ER, further impairing the ability to facilitate phagocytic activity (Ibach et al., 2021, Kleinberger et al., 2014, Kober et al., 2016, Park et al., 2015a, Varnum et al., 2017). Moreover, TREM2 variants T66M and Y38C also led to the reduction of sTREM2 release, impairment of glycosylation as well as protein folding of TREM2 and further enhanced proteasomal degradation (Jay et al., 2017, Kleinberger et al., 2014, Park et al., 2015b, Piccio et al., 2016).

The TREM2 R47H variant was originally found in two genome-wide sequencing studies that significantly increased the risk of LOAD (Guerreiro et al., 2013a, Jonsson et al., 2013), and the risk level was comparable to APOE ε4 (Guerreiro et al., 2013a, Hooli et al., 2014,

Jonsson et al., 2013). This mutation is located in the extracellular domain of TREM2 and leads to diminished affinity of TREM2 for its ligands (Jonsson et al., 2013, Kober et al., 2016, Wang et al., 2015b). Microglia expressing the R47H heterozygous variant of TREM2 showed reduced presence around amyloid plaques in AD mouse models (Cheng-Hathaway et al., 2018). Further, the R47H variant impairs microglial survival and inflammation (Zhong et al., 2017). Other variants, such as D87N, R62H, L211P, T96K, and H157Y, have also been linked to an increased risk of Alzheimer's disease. (Jay et al., 2017).

1.4 Protein sorting and quality control in the endoplasmic reticulum (ER)

Proteostasis, also known as protein homeostasis, is a cellular process ensuring the proper concentration, structure, binding interactions and localization of proteins (Balch et al., 2008). This mechanism involves a comprehensive network of pathways governing protein synthesis, folding, transport, and degradation (Hanley & Cooper, 2020).

The ER is a dynamic membranous organelle in eukaryotic cells and has many functions, including protein synthesis, lipid metabolism and trafficking, calcium homeostasis, and redox regulation (Harada et al., 2022, Schwarz & Blower, 2016). The ER protein quality control process protects against the accumulation of abnormal proteins in eukaryotic cells (Sun & Brodsky, 2019). The quality control in the ER ensures that only properly folded and assembled soluble and membrane proteins could be further transported to Golgi. It was shown that combination of five strategies is involved in the regulation of this process, including selective capture by coat protein complex II (COPII) carrier vesicles, inclusion via fluid and membrane bulk flow, retention within the ER, retrieval from post-ER compartments and ER-associated degradation (ERAD) (Barlowe & Helenius, 2016).

1.4.1 Selective cargo capture by coat protein complex II (COPII) carrier vesicles

The transport of fully folded and oligomerized proteins, also called cargo, is a selective process which is dependent on the recognition of export signals and motifs of cargo by specific adaptors, receptors and coat proteins. Then the cargos could be further sorted into COPII vesicles at endoplasmic reticulum exit sites (ERES) (see Fig. 1.2). COPII coat assembly at the ERES requires Sec12, an ER integral membrane protein, and Sec16, an

ER peripheral membrane protein (Connerly et al., 2005, Saito et al., 2014, Shaywitz et al., 1997, Zanetti et al., 2011). Selective cargo capture by COPII carrier vesicles ensures the packaging of the correct cargo for transit to the Golgi complex.

1.4.2 Inclusion via fluid and membrane bulk flow

Some proteins may be included in transport vesicles as part of the bulk flow of fluid and membrane components and this process is independent on receptors, adaptors and specific export motif. While not as selective as other mechanisms, this inclusion process contributes to the overall efficiency of protein transport.

1.4.3 Selective retention within the ER

Certain proteins are retained within the ER to prevent their incorporation into transport vesicles. This retention mechanism ensures that proteins could not proceed to the Golgi complex before they are fully folded and oligomerized. Moreover, resident ER proteins like molecular chaperones are retained within the ER to exert their physiological function (Ellgaard et al., 1999, Teasdale & Jackson, 1996).

1.4.4 Selective retrieval from post-ER compartments

Proteins that have reached post-ER compartments, mainly including ER-Golgi intermediate compartment (ERGIC) and *cis*-Golgi, but are not fully folded or assembled, need to be returned to the ER for further processing or quality control (e.g. ER resident proteins), are selectively retrieved via retrograde vesicle transport. This process involves retrieval signals localized in the different domains of proteins.

In the C-terminal ends of some soluble ER-resident proteins, including binding immunoglobulin protein (BiP) and protein disulfide isomerase (PDI), there are H/KDEL (His-Asp-Glu-Leu or Lys-Asp-Glu-Leu) motifs as retrieval signals, which could be recognized by the KDEL receptor (Munro & Pelham, 1987, Semenza et al., 1990).

For the transmembrane proteins that cycle between the ER and the ERGIC/Golgi complex, the di-lysine sorting signals (KKXX or KXKXX) in their C-terminals are found to be recognized by the coat protein complex I (COPI) coat and retrieved to ER (Papanikou & Glick, 2014). Another retrieval signal found in the C-terminal sequences of the subunits of

some membrane protein complexes, such as G-protein coupled receptor 1 for gamma-aminobutyric acid ($GABA_BR1$), the delta opioid receptor, the N-methyl-D-aspartate (NMDA) receptor (NR), the ATP-sensitive potassium channel subunit (Kir6.1), and the longer isoform of transmembrane protein 63B (TMEM63B), mediating the ER retention of those proteins, is the arginine-based RXR motif, which is also recognized by COPI (Aziz et al., 2014, Margeta-Mitrovic et al., 2000, Michelsen et al., 2005, Shiwarski et al., 2019, Wu et al., 2023). However, the RXR motifs could be masked when subunits of the respective transmembrane protein complexes are fully assembled, leading to the further transport to cell surface.

The polar or charged residues in the TMD of some transmembrane proteins are another important retrieval signals. Research has shown that a single charged residue in a TMD is enough to retain/retrieve a protein, unless the residue is masked by complex assembly or folding. It remains largely unknown how sorting motifs in TMDs are recognized and localized in the ER. Currently, the best-characterized mechanism suggests that a protein called Retention in Endoplasmic Reticulum Sorting Receptor 1 (RER1) recognizes TMDs and ensures their localization in the ER (Sato et al., 2001). RER1 is a tetraspanin transmembrane protein with a COPI sorting signal in the C-terminal tail and it binds to escaped ER membrane proteins or subunits of plasma membrane protein complexes in post-ER compartments and retrieves the proteins to ER via COPI vesicles (Boehm et al., 1997b, Bonifacino et al., 1991, Cosson et al., 2013, Füllekrug et al., 1997, Sato et al., 2003). RER1 will be described in more details below. This retrieval mechanism ensures the maintenance of proper protein localization and function within the cell.

1.4.5 ER-associated degradation (ERAD)

Protein quality control in ER also regulates the degradation of proteins that are improperly folded by ER-associated degradation (ERAD) process (Klausner & Sitia, 1990, Krshnan et al., 2022). Briefly, proteins, which are not correctly folded, could be retro-translocated from the ER into the cytosol and further be ubiquitinylated and degraded by proteasomes (Brodsky & McCracken, 1999, Jarosch et al., 2002, Tsai et al., 2002, Wu & Rapoport, 2018). The ERAD pathway is crucial to maintain ER homeostasis.

Overall, the concerted action of these mechanisms orchestrates the selective and efficient transport and turnover of newly synthesized proteins from the ER to the Golgi complex, essential for cellular function and homeostasis (Barlowe & Helenius, 2016).

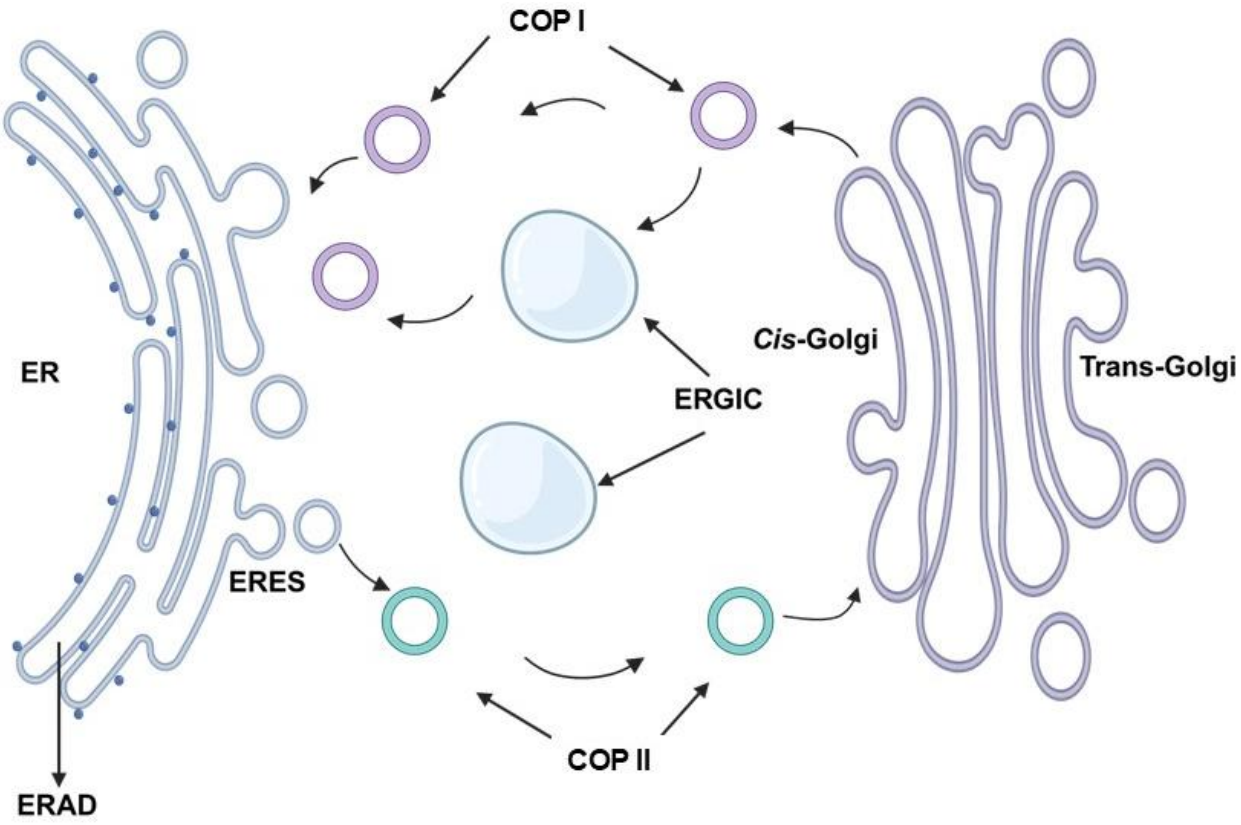

Fig. 1.2 Proteins transport between ER and *cis*-Golgi. Cargo at ER exit sites (ERES) can be transported to Golgi complex by COPII vesicles. Not fully folded proteins, unassembled subunits of complexes or escaped ER-resident proteins are retained/retrieved from ERGIC (ER-Golgi intermediate compartment) and the *cis*-Golgi by COPI vesicles. Figure adapted from Barlowe & Helenius, 2016. Created with BioRender.com.

1.5 Protein degradation pathways

Proteins undergo continuous turnover by degradation and new synthesis. Within eukaryotic cells, damaged proteins are eliminated mainly through proteasomal and lysosomal pathways. While these pathways operate independently, they are closely interconnected (Khaminets et al., 2016). Typically, proteasomes manage short-lived and soluble misfolded proteins through the ubiquitin-proteasome system (UPS), while lysosomes handle degradation of long-lived proteins, insoluble protein aggregates,

organelles, macromolecules, and intracellular pathogens, involving pathways such as endocytosis, phagocytosis, or autophagy (Zhao et al., 2022).

1.5.1 The ubiquitin-proteasome system (UPS)

Cellular proteasomes are large catalytic protease complexes that are found in eukaryotic cells' cytoplasm and nucleus (Voges et al., 1999, Wójcik & DeMartino, 2003). The 26S proteasome is composed of two subunits, including a central barrel-shaped 20S proteasome which consists of α and β subunits and is responsible for protein digestion, and a 19S regulatory particle which catalyzes the entry of substrate proteins and ensures the specificity for protein substrates (Glickman & Ciechanover, 2002, Groll et al., 2000, Heinemeyer et al., 2004, Kisselev & Goldberg, 2001, Majumder & Baumeister, 2019, Murata et al., 2009, Voges et al., 1999).

Ubiquitin (Ub) plays a vital role as a cofactor, crucial for the effective functioning of the proteasome. Substrate proteins for ubiquitin-proteasome pathway are covalently linked to the 76-residue ubiquitin protein and this process involves three enzymes, including an Ub activating enzyme(E1), an Ub conjugating enzyme (E2), and an Ub ligase (E3) (Baumeister et al., 1998, Glickman & Ciechanover, 2002). E1 activates the C-terminal glycine (Gly) of Ub and then transfers it to the E2, which cooperates with E3 to attach it to the substrate protein (Dikic, 2017, Hershko & Ciechanover, 1992, Lecker et al., 2006). For degradation of proteins, after the repeated reactions with three enzymes, substrate proteins are polyubiquitinated and recognized by the proteasome. Subsequently, ubiquitination tag is removed, allowing the unfolding of proteins and further digestion into small peptide fragments in the core of the proteasome complex. These fragments are processed by intracellular peptidases to produce amino acids, which are then recycled into new proteins (see Fig. 1.3) (Baumeister et al., 1998, Bochtler et al., 1999, Glickman & Ciechanover, 2002).

Inhibition of the proteasome results in the accumulation of numerous polyubiquitinated proteins within cells, which leads to growth arrest and programmed cell death (apoptosis). This accumulation of large molecular weight Ubiquitin-protein complexes ultimately induces apoptosis (Driscoll & Dechowdhury, 2010, Molineaux, 2012, Murata et al., 2009, Nalepa et al., 2006, Sterz et al., 2008).

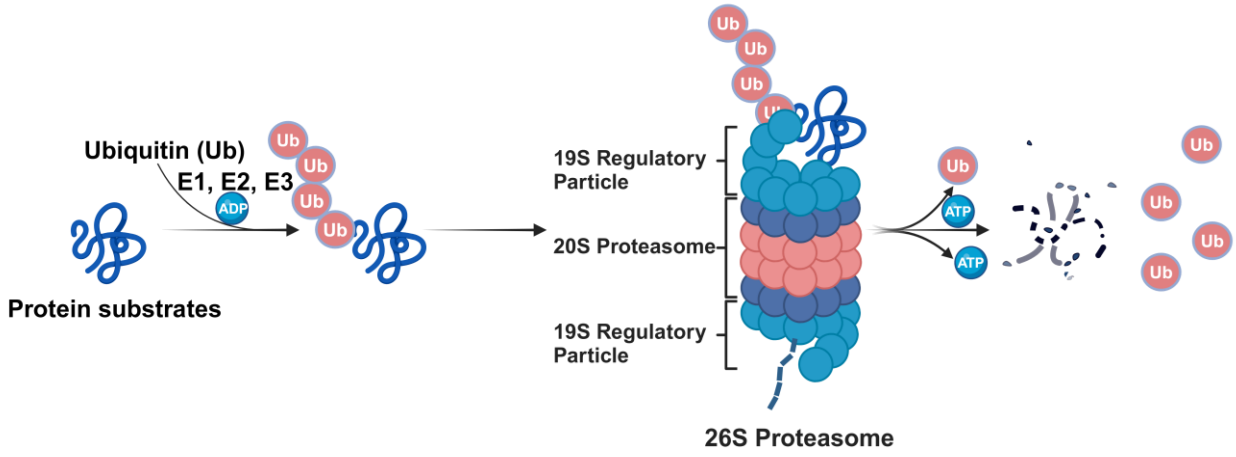

Fig. 1.3 Degradation of protein by proteasome. The protein to be degraded is polyubiquitinated by ubiquitin ligases, including E1, E2 and E3, followed by the transport to proteasome. Ubiquitinated proteins are recognized by 19S regulatory particles and then the ubiquitin chain of the protein is removed and the protein enters into the proteasome. The protein is further digested into small peptide fragments in the core of the proteasome complex (20S proteasome). Figure adapted from Molineaux, 2012. Created with BioRender.com.

1.5.2 Endo-lysosomal degradation pathway and autophagy

The lysosome is a membrane-bound dynamic organelle involved in the degradation of proteins. Lysosomes, uncovered by Christian de Duve in the 1950s, were found to harbor proton-pumping vacuolar ATPases, which regulate the pH of the luminal environment within the range of 4.6–5.0 (Luzio et al., 2007, Mellman et al., 1986). Lysosomes receive molecules for degradation from distinct pathways, including endocytosis, phagocytosis and autophagy (Luzio et al., 2007). Endocytosis serves for the uptake of extracellular and surface-localized molecules (Doherty & McMahon, 2009), while phagocytosis rather refers to the degradation of larger extracellular components, such as apoptotic cells and microorganisms in lysosomes (Lancaster et al., 2019).

Autophagy can be classified into microautophagy, chaperone-mediated autophagy (CMA) and macroautophagy, involving lysosomal activity (Mauthe et al., 2018, Mizushima & Komatsu, 2011). It was identified that microautophagy directly degrades engulfed autophagic cargo (Schuck, 2020), while CMA could selectively degrade proteins by the involvement of chaperones and directly transports proteins across the lysosome membrane (Kaushik & Cuervo, 2018).

Macroautophagy (hereafter autophagy) is the most well-known type of autophagy, which is induced by cellular stressors, including starvation, and pathogen infection (Schuck, 2020). Autophagy can be categorized into two types: nonselective autophagy, which is initiated in response to starvation, and selective autophagy, which is triggered by the presence of pathogens during infection, damaged organelles (mitophagy, lysophagy, ER-phagy, ribophagy) and aggregated proteins (aggrephagy) (Vargas et al., 2023, Zaffagnini & Martens, 2016). During autophagy, an essential step involves the creation of a dual-membrane organelle termed the autophagosome. This organelle emerges from a curved membrane, referred to as the isolation membrane or phagophore (Kraft & Martens, 2012, Suzuki et al., 2001). As this membrane expands, it encloses segments of the cytoplasm. Upon closure, these membranes transform into autophagosomes, entrapping cytoplasmic content within. Following fusion with the lysosome (or vacuole in yeast), the enclosed material is degraded (Feng et al., 2014, Kraft & Martens, 2012, Wang et al., 2015a, Zaffagnini & Martens, 2016).

In neurodegenerative diseases, it was shown that impaired autophagy could lead to the accumulation of misfolded proteins and affect the normal cellular function (Menzies et al., 2011). For example, there is a higher accumulation of autophagosome in the brains of AD patients comparted with controls (Nixon et al., 2005). In addition, dysfunction in autophagy has been demonstrated to increase the accumulation of insoluble tau species (Li et al., 2017). The induction of autophagy by rapamycin increases the clearance of Aβ and improves the cognitive function of AD mouse model (Di Meco et al., 2020).

While the UPS and autophagy-lysosomal systems are distinct mechanisms for degradation, Ub plays a significant role as an interaction mediator between these two degradation pathways. During ubiquitin-dependent autophagy, ubiquitinated aggregates and organelles are recognized by autophagy receptors and this process relies on the Ub chain length (Khaminets et al., 2016). Treatment with the proteasome inhibitor MG132 (carbobenzoxy-L-leucyl-L-leucyl-L-leucine) in human SHG-44 glioma cells resulted in reduced cell proliferation alongside the stimulation of autophagy, evidenced by increased levels of Beclin-1 and LC3 (microtubule-associated protein 1A/1B-light chain 3), two critical proteins involved in autophagosome formation (Ge et al., 2009). Additionally, autophagy was also induced by proteasome inhibition in cultured cardiomyocytes and

retinal pigment epithelial cells (Kyrychenko et al., 2014, Tang et al., 2014). These findings suggest a compensatory mechanism wherein autophagy is upregulated in response to inhibition or defects of UPS. In general, it was shown that UPS and autophagy-lysosomal pathways collaborate in the degradation of substrates (Zhao & Goldberg, 2016, Zhao et al., 2015).

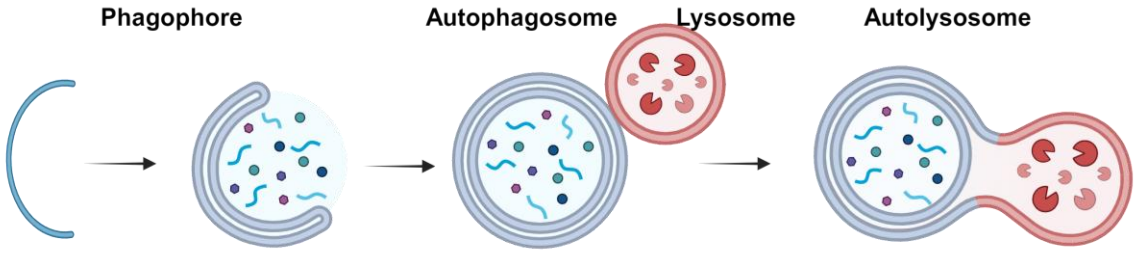

Fig. 1.4 Mechanism of macroautophagy. The initiation of autophagy is the formation of a phagophore, which enfolds different intracellular components, including misfolded proteins, aggregated proteins, damaged organelles and pathogens to form the mature autophagosome. Upon fusion with lysosomes, the autophagosome transforms into the autolysosome, where the content is finally degraded and recycled. Figure adapted from Khaminets et al., 2016. Created with BioRender.com.

1.6 The Retention in Endoplasmic Reticulum Sorting Receptor 1 (RER1)

RER1 has been identified as a sorting receptor for the retrieval of ER-resident proteins, immature/misfolded proteins, and unassembled components of transmembrane protein complexes mediated by the COPI-dependent pathway (Boehm et al., 1997a, Sato et al., 1995, Sato et al., 2001). Additionally, RER1 is so far the only identified sorting receptor for TMD-based retrieval and retention signals (Annaert & Kaether, 2020).

1.6.1 Structure and localization

RER1 gene was firstly identified in yeast in 1993 and it encoded for a 188 amino acids protein (Nishikawa & Nakano, 1993). Human RER1 gene was firstly described in 1997 and it contains 196 amino acids (Füllekrug et al., 1997). There are 4 putative transmembrane domains in RER1 protein, forming a W-topology and both N- and C-terminals face the cytosol (Füllekrug et al., 1997). RER1 mainly localizes at ERGIC and *cis*-Golgi in yeast and mammalian cells (Sato et al., 1995, Valkova et al., 2011). RER1 binds to COPI by the di-lysine like motif and tyrosine residues in the C-terminal region.

With the assistance of the COPI complex, RER1 undergoes cycling between ER and Golgi (Boehm et al., 1997a, Cosson et al., 2013, Sato et al., 2001).

1.6.2 Substrates

Initially, RER1 was identified as a sorting receptor required for proper transport of Sec12 between the ER and Golgi in yeast (Nishikawa & Nakano, 1993). Later, more substrates, including misfolded, immature and unassembled proteins, were identified in yeast and mammalian cells. In yeast, many ER membrane proteins, including Sed4, Sec71, Sec63, and Mns1, need RER1 to retrieve from Golgi back to ER (Sato et al., 1997, Sato et al., 2001, Sato et al., 1996). RER1 mutants leads to the mis-localization of the substrate proteins to the trans-Golgi or the vacuole in yeast (Boehm et al., 1997a, Sato et al., 1997, Sato et al., 2003). There is a tyrosine residue in the fourth transmembrane domain of RER1, which is essential for its binding to Sec12 but not Sec71, indicating the presence of distinct binding modes for various substrates (Sato et al., 2003). Moreover, by retrieving unassembled components, RER1 could regulate the assembly process of transmembrane complexes, as exemplified by the reduction of fully assembled yeast iron transporter when RER1 was deleted, since RER1 is responsible for the retrieval of unassembled Fet3, a subunit of the yeast iron transporter (Sato et al., 2004). It was also demonstrated that the binding of RER1 to those yeast substrates is dependent on the existence of spaced polar residues in the TMDs of those substrates (Sato et al., 2003).

In mammalian cells, subunits of γ-secretase were found as the first substrates, including unassembled presenilin enhancer 2 (PEN2) and immature nicastrin (Nct) (Hara et al., 2018, Kaether et al., 2007, Park et al., 2012, Spasic et al., 2007). γ-Secretase is an intramembrane protease complex, composed of presenilin (PS) 1 or PS2, Nct, anterior pharynx-defective phenotype 1 (Aph1) and PEN2 (Haass, 2004). Many substrates of γ-secretase have been discovered, including Notch receptors, APP and TREM2 (Haapasalo & Kovacs, 2011, Jurisch-Yaksi et al., 2013b, Wunderlich et al., 2013). It was shown that RER1 interacts with immature Nct by three polar aa residues in the TMD of Nct (Spasic et al., 2007) and also binds to unassembled PEN2 by the asparagine (N) residue in the first TMD of PEN2 (Kaether et al., 2007). It could be that RER1 is part of a quality control mechanism that allows complexes to exit the ER once they are fully assembled, as evidenced by the findings wherein RER1 knockdown increases the cell-surface

localization of assembled γ-secretase complex and PEN2 (Kaether et al., 2007, Spasic et al., 2007). Thus, RER1 negatively regulates the assembly of the γ-secretase complex and contributes to total cellular γ-secretase activity.

Valkova and colleagues identified the unassembled α1-subunits of skeletal muscle nicotinic acetylcholine receptor (nAChR) as the next substrate of RER1 in mammalian cells (Valkova et al., 2011). In the first TMD of nAChR, there is an asparagine-based motif that aids in its retention in the ER until assembly, similar to the motif in PEN2 that binds to RER1 (Kaether et al., 2007, Wang et al., 2002). The study found that RER1 only binds to unassembled nAChRα1 subunit, not the fully assembled nAChR complex or other subunits. When RER1 is knocked down *in vitro*, unassembled nAChRα1 escapes the ER and is likely degraded in lysosomes. A knockdown of RER1 in mouse skeletal muscle using small hairpin RNA (shRNA) resulted in a reduction in the size of neuromuscular junctions as well as the amount of fully assembled nAChR (Valkova et al., 2011).

In the peripheral nervous system, RER1 interacts with the peripheral myelin protein 22 (PMP22), a plasma membrane-resident protein that is necessary for myelin synthesis. PMP22 mutants can accumulate excessively in the ER and cause Charcot-Marie-Tooth disease (CMT) (Hara et al., 2014, Marinko et al., 2021). It was found that RER1 interacts with PMP22 wt and mutants, including PMP22 L16P and G150D. One of the disease causal mutants, PMP22(L16P), is partially released from the ER by loss of RER1 (Hara et al., 2014).

Rhodopsin, the pigment in photoreceptor cells, has also been found as a substrate of RER1 (Yamasaki et al., 2014). The immature wild-type rhodopsin could be transported to the post-Golgi compartments when RER1 was knocked down while it was accumulated in the ER when RER1 is overexpressed. A disease-related mutant of rhodopsin G51R was also retained in the ER and the silence of RER1 leads to the exit of rhodopsin G51R mutant from ER to the cell surface or localization in lysosome.

In addition, targeted deletion of RER1 in Purkinje cells exhibited age-related motor impairments and the depletion of Purkinje cells. Subsequent investigations revealed that the deletion of RER1 in Purkinje cells impairs the formation of action potentials associated with a significant reduction in the Nav1.6 voltage-gated Na^+ channel subunit within the

axon initial segment. The substantial decrease in both Nav1.6 and Nav1.1 channels, consequent to RER1 deletion in the brain, suggested a potential role for RER1 in retrieving Nav subunits, similar to its involvement with nAChR. However, as of now, there has been no identification of direct binding between RER1 and Nav channel subunits or any specific retrieval motif within them (Valkova et al., 2017).

It was shown that overexpression of RER1 strongly decreased the levels of α-synuclein (αSyn), which might be due to the degradation of αSyn by the proteasome. However, overexpressing a loss-of-function variant of RER1, with a 25-amino-acid deletion in the C-terminal part, only slightly reduced α-synuclein levels, suggesting a critical role, of this sequence proper function of RER1 (Park et al., 2017). *In vivo*, RER1 was co-localized with Lewy bodies which contained αSyn in the brain tissues from patients diagnosed with dementia with Lewy bodies (Park et al., 2017). It was also demonstrated that RER1 binds to an E3 ubiquitin-protein ligase NEDD4 (neural precursor cell expressed developmentally down-regulated protein 4), which is also a regulator of αSyn degradation (Park et al., 2017).

The interactome profile of RER1 in epileptic mice hippocampus identified several potential cargos that are related to synaptic functions. For example, γ-Aminobutyric acid type A receptor ($GABA_A$) subunit 1 is demonstrated to interact with RER1 (Liu et al., 2022).

As known so far, the studies on the effects of RER1 on the stoichiometry of complex subunits have controversial results. Unassembled heteromeric complex subunits are retrieved from the cis-Golgi by RER1. Depending on where the complex is assembled, this can increase or decrease its likelihood of being assembled. Based on this, Annaert and Kaether proposed two models for RER1 function (Annaert & Kaether, 2020): Retrieval of individual subunits of protein complexes from the cis-Golgi will increase the assembly probability if the complex is usually assembled in the ER. Therefore, the subunits will be decreased if RER1 is absent and a further reduction in the level of complexes assembled in plasma membranes will be achieved. For example, knockout or knockdown of RER1 results in reduced levels of γ-secretase, AChR and voltage-gated Na^+ channels at the plasma membrane (Hara et al., 2018, Valkova et al., 2011, Valkova et al., 2017). Oppositely, if complex assembly occurs preferentially in the ERGIC or cis-Golgi, retrieving unassembled subunits from the Golgi decreases the likelihood of complex assembly. As a consequence, RER1 deficiency leads to increased levels of the respective protein

complexes at the plasma membrane. Research on nicastrin and tweety homolog 1 (Ttyh1) has shown that loss of RER1 leads to more complexes at the plasma membrane (Kim et al., 2018, Spasic et al., 2007). Both studies showed that reduction of RER1 levels led to an increase in the level of γ-secretase complex at the plasma membrane as well as its activities.

1.6.3 Implications in cellular homeostasis and diseases

It was shown that RER1 is involved in several diseases, including Charcot-Marie-Tooth (CMT) disease, Parkinson's disease and pancreatic cancer (Chen et al., 2019, Hara et al., 2014, Marinko et al., 2021, Park et al., 2017). In CMT disease, RER1 mediates the excessive accumulation of pathogenic protein mutants (PMP22 L16P and G150D) in ER and further contributes to the pathogenesis of the disease (Hara et al., 2014, Marinko et al., 2021). However, there are no clear mechanisms identified in the roles of RER1 in Parkinson's disease and pancreatic cancer.

Studies showed that loss of RER1 induced ER stress in yeast, nematode and mouse models (Ghavidel et al., 2015, Hara et al., 2018). It is also suggested that RER1 could enhance competitive cell survival in *Drosophila* by alleviating the proteotoxic stress (Paul et al., 2024). These findings support the important role of RER1 in regulating ER proteostasis, indicating that its function is conserved in different species (Annaert & Kaether, 2020).

Deleting RER1 systemically in mice led to prenatal lethality, and forebrain-specific knockout resulted in early postnatal lethality (Hara et al., 2018, Valkova et al., 2011, Valkova et al., 2017), while mice with knockout of RER1 specifically in the Purkinje cells of the cerebellum showed normal polarization and differentiation of Purkinje cells and normal development of the cerebellum (Valkova et al., 2017).

RER1 could regulate Notch signaling in murine neuronal stem cells. However, results from two studies are controversial. Hara et al concluded that the deficiency of RER1 reduced γ-secretase activity and therefore downregulated Notch signaling and inhibited the development of murine neuronal stem cells (Hara et al., 2018). In contrast, Kim et al. found that Ttyh1 membrane protein bound to RER1 and led to the degradation of RER1, further resulting in an increase of γ-secretase activity and Notch signaling, suggesting that

RER1 negatively regulates Notch signaling mediated development of murine neuronal stem cells (Kim et al., 2018).

Moreover, several lines of evidence have been unveiled about the role of RER1 in the regulation of Aβ accumulation indirectly by modifying γ-secretase. Tanabe et al. showed that RER1 could be ubiquitinated and degraded by another ubiquitin ligase, synoviolin, further modulating Aβ generation by regulating γ-secretase (Tanabe et al., 2012). Similarly, decreased RER1 enhances Aβ production by increasing γ-secretase assembly or activity (Choi et al., 2023, Dries & Yu, 2008, Jiang et al., 2014, Mullard, 2007). Moreover, the downregulation of RER1 by cortisol prompted the translocation of mature PSEN1 into the ER's mitochondrial-associated membrane (MAM) via the endocytic recycling pathway, representing a rate-limiting step. This process led to the accumulation of Aβ in mitochondria, culminating in mitochondrial dysfunction and cell death. Conversely, the reintroduction of RER1 reduced the presence of PSEN1 in MAM, thereby preventing the accumulation of Aβ in mitochondria (Choi et al., 2023). In addition, a recent study demonstrated that RER1 undergoes ubiquitination by the E3 ligase NEDD4-2 and further degradation by the proteasomal pathway (Liu et al., 2022). Accumulation of RER1 in brain when the ubiquitination process was inhibited by partial deletion of *NEDD4-2* increases the susceptibility to ER stress and seizures (Liu et al., 2022).

Another study revealed that the absence of RER1 in zebrafish and mammalian cells shortened cilia and impaired their function, which might be due to the increased γ-secretase complex assembly and activity followed by enhanced Notch signaling as well as reduced Foxj1a expression (Jurisch-Yaksi et al., 2013a).

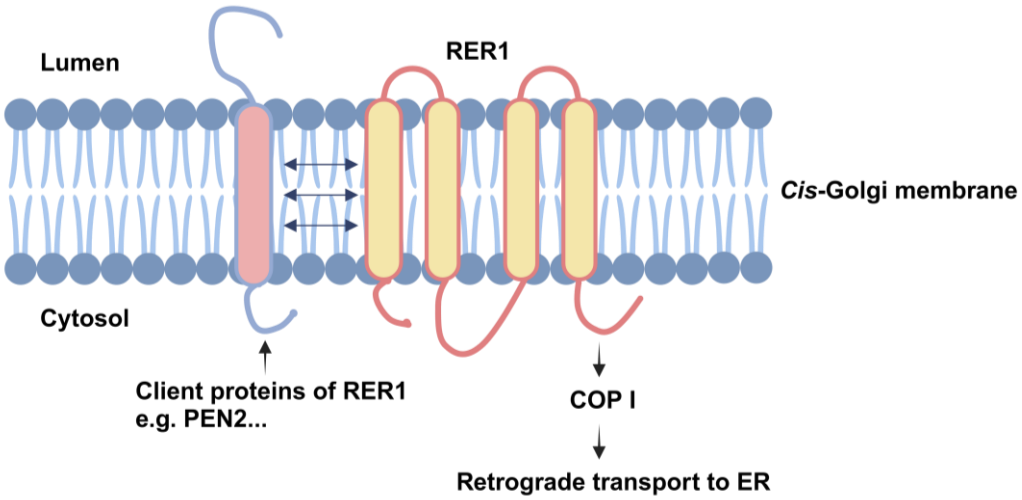

Fig. 1.5 RER1-mediated retrieval of transmembrane proteins. Within the cis-Golgi compartments, RER1 engages with the transmembrane domain (TMD) of client proteins, including presenilin enhancer 2 (PEN2), nicastrin and others. Subsequently, the cytosolic domain of RER1 interacts with the COPI complex, facilitating the return of client proteins to the endoplasmic reticulum (ER). Figure adapted from Cosson et al., 2013. Created with BioRender.com.

1.7 Lipid droplets

Lipid droplets (LDs) are dynamic cytoplasmic organelles found in most cells, which store fatty acids (FAs) in the form of neutral lipid, including triacylglycerols (TAGs) and cholesterol esters (CE), and are critically important for energy metabolism. They are surrounded by a phospholipid monolayer composed of phospholipids and associated proteins, including perilipin proteins (Barbosa & Siniossoglou, 2017b, Greenberg et al., 1991, Griseti et al., 2024, Gross & Silver, 2014, Henne et al., 2018, Kory et al., 2016). Besides the lipid storage for energy metabolism, LDs can also store other lipids, such as hydrophobic vitamin and signaling precursors. In addition, LDs plays a vital role in reduction of ER and oxidative stress, and also assist the maturation, storage, and turnover of proteins (Welte & Gould, 2017).

In immune system, evidences indicate LDs serve as structural markers of activation of immune cells and inflammation, such as macrophages and macroglia, as well as regulates the inflammatory responses of those cells (Bozza & Viola, 2010, den Brok et al., 2018, Stephenson et al., 2024, van Dierendonck et al., 2022). Accumulation of TAGs was found in LDs of LPS activated pro-inflammatory macrophages by increasing uptake of FAs and

synthesis of TAG, and reducing TAG hydrolysis (Feingold et al., 2012, van Dierendonck et al., 2022). The activation of human iPSC-derived microglia and microglia cell line N9 by LPS treatment also led to accumulation of TAG-rich LDs (Khatchadourian et al., 2012, Stephenson et al., 2024). Additionally, LDs accumulation was observed in human iPSC microglia with the Alzheimer's disease-associated APOE4 genotype (Stephenson et al., 2024). Importantly, biosynthesis and catabolism of TAGs are necessary for the transcription and secretion of proinflammatory cytokines and chemokines in response to extrinsic stimuli as well as the activation-associated phagocytosis of multiple substrates including the disease-associated amyloid-beta peptide (Stephenson et al., 2024). However, another study showed that LDs were strongly accumulated in microglia with aging in both mouse and human brains and further impaired phagocytosis of the cells, leading to the increased production of reactive oxygen species and secretion of proinflammatory cytokines (Marschallinger et al., 2020). Taken together, these results indicate not only the importance of lipid metabolism in function of microglia, but also the adverse effects of overloaded lipid droplets in microglia.

Excessive LDs storage in immune cells is related to different diseases, including obesity, diabetes, atherosclerosis, and neurodegenerative disorders (Accad et al., 2000, Farmer et al., 2020, Koliwad et al., 2010, Nagle et al., 2009, Walther & Farese, 2012). Strong accumulation of LDs mainly containing excessive esterified cholesterol in macrophages results in formation of foam cell accumulated in the arterial wall during atherosclerosis, which is the hallmark of this disease (Florance & Ramasubbu, 2022, Fowler et al., 1985, Libby, 2002, Ross, 1993). In obese mice, increased accumulation of lipids in adipose tissue macrophages led to the polarization of macrophages to pro-inflammatory phenotype, further contributed to chronic inflammation and insulin resistance in adipose tissue (Prieur et al., 2011). In addition, lipid-droplet-accumulating microglia (LDAM) represent a dysfunctional and proinflammatory state in the aging brain and they were also observed in both chimeric human-mouse AD models and AD patients who carried homozygous APOE ε4 allele (APOE4/4) (Claes et al., 2021, Haney et al., 2024, Marschallinger et al., 2020).

Therefore, it is crucial to investigate the potential regulators of lipid metabolism in immune cells. Previous studies showed lipid droplets (LDs) were accumulated in mouse embryonic

fibroblast under genetic and pharmacological inhibition of γ-secretase (Fabiano et al., 2024, Gutierrez et al., 2020), which might be due to the impairment of γ-secretase function. RER1 deletion in the HAP1 cell line leads to the reduction of PEN2, Nicastrin and presenilin 1 (PS1), which affects γ-secretase assembly (Hara et al., 2018). So, it is also important to explore if RER1 regulates lipid metabolism in immune cells.

1.8 Aim of the thesis

The interaction between TREM2 and DAP12 in brain immune cells, including microglia, holds significant implications for neurodegenerative diseases. Research has unveiled that mutations in both TREM2 and DAP12 underlie NHD and that coding sequence variants increase the risk of various other neurodegenerative disorders, indicating the important role of TREM2-DAP12 signaling in CNS function.

DAP12, functioning as an adaptor molecule, forms complexes with multiple co-receptors, regulating various cellular responses. The interaction between DAP12 and its co-receptors is mediated through charged residues within TMD of immunoreceptors. Previous investigations have demonstrated a role of DAP12 in TREM2 expression and cellular trafficking pathways, however, little attention has been given to understanding how DAP12 and its interacting receptor are regulated in terms of metabolism and cellular transport.

In this thesis, the primary objective was to explore the impact of TREM2 on the turnover, degradation, and intracellular trafficking of DAP12. By delving into the dynamics of this relationship, a deeper understanding of how TREM2 modulates the fate of DAP12 within cells shall be attained. In addition, the potential involvement role of RER1 in the subcellular transport and metabolism of TREM2 and DAP12 was also investigated. Furthermore, we also explored the function of RER1 in lipid metabolism in both undifferentiated and differentiated THP-1 cells.

This thesis aims to uncover the complex regulatory mechanisms behind DAP12 and its co-receptors' metabolism and intracellular trafficking, offering new insights for treating neurodegenerative diseases. Through careful experimentation and analysis, this research seeks to expand our understanding of the interactions between TREM2, DAP12, and

related molecule, RER1, ultimately guiding the development of targeted therapies to reduce the impact of neurodegenerative diseases.

2 Material and methods

2.1 Materials

2.1.1 Chemicals, reagents and enzymes

Name	Supplier and catalog number
Phorbol 12-myristate-13-acetate (PMA)	Cat# P8139, Sigma-Aldrich, Steinheim, Germany
Lipofectamine™ 2000 Transfection Reagent	Cat# 11668-019, Invitrogen, Carlsbad, USA
Cas9 enzyme	Cat# 1081061, IDT, Coralville, USA
RNAiMAX	Cat# 13778-150, Invitrogen, Carlsbad, USA
Cycloheximide	Cat# C4859-1ML, Sigma-Aldrich, Steinheim, Germany
Lactacystin	Cat# L6785-.2MG, Sigma-Aldrich, Steinheim, Germany
MG132	Cat# C2211-5MG, Sigma-Aldrich, Steinheim, Germany
Chloroquine	Cat# C6628-25G, Sigma-Aldrich, Steinheim, Germany
N-dodecyl-β-d-Maltoside	Cat# D4641, Sigma-Aldrich, Steinheim, Germany
Bio-Rad protein assay dye	Cat# 5000006, Bio-Rad, Hercules, USA
Bovine serum albumin (BSA)	Cat# 8076.3, Thermo Fisher Scientific, Waltham, USA
Novex™ NuPAGE™ MES SDS Running Bufferr	Cat# NP0002, Invitrogen, Carlsbad, USA
Protease inhibitor cocktail	Cat# 04693116001, Sigma-Aldrich, Steinheim, Germany

Phosphatase inhibitor cocktail	Cat# 4906837001, Sigma-Aldrich, Steinheim, Germany
RNase-Free DNase	Cat# 79254, QIAGEN, Hilden, Germany
Poly-L-Lysine Hydrobromide (PLL)	Cat# P6282, Sigma-Aldrich, Steinheim, Germany
Boric acid	Cat# B6768, Sigma-Aldrich, Steinheim, Germany
Sodium tetraborate	Cat# B9876, Sigma-Aldrich, Steinheim, Germany
Paraformaldehyde (PFA)	Cat# 16005-1KG-R, Sigma-Aldrich, Steinheim, Germany
Triton X-100	Cat# 3051.2, Carl Roth, Karlsruhe, Germany
4′,6-diamidino-2-phenylindole (DAPI)	Invitrogen, Carlsbad, USA
Immu-Mount™	Cat# 9990402, Fisher Scientific, USA
Ibidi mounting medium	Cat# 50011, Ibidi, Gräfelfing, Germany
Sepharose Protein G beads	Cat# 101242, Invitrogen, Carlsbad, USA
Cytochalasin D (cyto D)	Cat# C8273, Sigma-Aldrich, Steinheim, Germany
pHrodo™ Red *E.coli* BioParticles™	Cat# P35361, Invitrogen, Carlsbad, USA
LD540 dye	A gift from Christoph Thiele

2.1.2 Buffers and solutions

Name	**Composition**
10X Phosphate buffer saline (PBS)	1.3 M NaCl, 26.8 mM KCl, 100 mM $Na_2HPO_4.7H_2O$, 17.6 mM KH_2PO_4, pH 7.4
Hypotonic buffer	10 mM Tris-HCl, 1 mM EDTA, 1 mM EGTA in dH_2O, pH 7.6

Lysis buffer for isolation of cellular proteins	1% n-dodecyl-β-d-Maltoside, 50 mM Tris–HCl (pH 8.0), 150 mM NaCl, 1 mM EDTA, 1.5 mM $MgCl_2$, 10 % glycerol
Washing buffer for Co-Immunoprecipitation (Co-IP)	50 mM Tris-HCl (pH 8.0), 150 mM NaCl, 1 mM EDTA, 1.5 mM $MgCl_2$, 10 % glycerol
5x SDS loading buffer without Dithiothreitol (DTT)	125 mM Tris, 10 % SDS, 50 % Glycerol, Bromophenol blue
Tris-Buffered Saline (TBS)	50 mM Tris, 150 mM NaCl, pH 7.5
Tris-Buffered Saline, 0.1 % Tween® 20 Detergent (TBST)	50 mM Tris, 150 mM NaCl, pH 7.5, 0.1 % Tween20
Novex™ NuPAGE™ MES SDS Running Buffer (20x)	1M MES, 1M Tris, 20mM EDTA and 2 % SDS (Invitrogen, Carlsbad, USA)
1x Blotting buffer	10 % Isopropanol, 5 mM Tris, 200 mM Glycine
10x Ponceau	2 % Ponceau S, 30 % trichloroacetic acid
Blocking buffer for western immunoblotting	5 % skim milk powder in TBST
0.1 M borate buffer	40.1 mM boric acid, 10 mM sodium tetraborate, pH 8.4
4 % Paraformaldehyde (PFA)	20 g PFA in 500 mL PBS
0.1 % Triton X-100	100 µL Triton X-100 in 100 mL PBS
Phosphate-Buffered Saline, 0.1 % Tween® 20 Detergent (PBST)	1X PBS, 0.1 % Tween
Blocking buffer for immunocytochemistry (ICC)	3 % BSA in PBST
Solution for preparing the antibody for ICC	1 % BSA in PBST

2.1.3 Kits

Kits	**Supplier**

Nucleobond™Xtra Maxi-Kit	Cat# 740414.100, Macherey-Nagel, Düren, Germany
Pierce™ BCA Protein Assay Kit	Cat# 23225, Thermo Fisher Scientific, Waltham, USA
RNeasy® Midi Kit	Cat# 75144, QIAGEN, Hilden, Germany
RevertAid First Strand cDNA Synthesis Kit	Cat# K1622, Thermo Fisher Scientific, Waltham, USA
QuantiTect® SYBR® Green PCR Kit	Cat# 204145, QIAGEN, Hilden, Germany
AlphaLISA® SureFire® Ultra™ Kit	Cat# U5387, Perkin Elmer, Waltham, USA

2.1.4 Cell lines

Cell line	Description	Reference/Source
Human embryonic kidney (HEK) 293 cells	Human embryonic kidney cells	ATCC, CRL-1573
HEK293 Flp-In cells	HEK293 cells with a Flp-In locus	R75007, Invitrogen, Carlsbad, USA
HEK293 Flp-In DAP12 wt	HEK293 Flp-In cells stably expressing DAP12 wt	Generated previously in the lab by Melanie Ibach
HEK 293 Flp-In myc-TREM2-FLAG_T2A_DAP12	HEK 293 Flp-In cells stably expressing myc-TREM2-FLAG_T2A_DAP12	Generated previously in the lab by Melanie Ibach
HEK 293 Flp-In myc-TREM2 K186N-FLAG_T2A_DAP12	HEK 293 Flp-In cells stably expressing myc-TREM2 K186N-FLAG_T2A_DAP12	Generated previously in the lab by Melanie Ibach
HEK 293 Flp-In DAP12 D50A	HEK 293 Flp-In cells stably expressing DAP12 D50A	Generated previously in the lab by Melanie Ibach
HEK 293 Flp-In myc-	HEK 293 Flp-In cells	Generated previously in the

TREM2-FLAG_T2A_DAP12 D50A	stably expressing myc-TREM2-FLAG_T2A_DAP12 D50A	lab by Melanie Ibach
THP-1 cells	A monocyte cell line isolated from the peripheral blood of an acute monocytic leukemia patient	ATCC, TIB-202

2.1.5 Culture media and supplements

Name	**Composition**	**Supplier and catalog number**
Dulbecco's Modified Eagle Medium (DMEM), GlutaMAX™ Supplement	-	Cat# 31966-921, Gibco, Waltham, USA
Fetal Bovine Serum (FBS)	-	Cat# P30-3306, PAN-Biotech, Aidenbach, Germany
Penicillin/streptomycin (P/S)	-	Cat# 15140-122, Gibco, Waltham, USA
Trypsin 0.05 %/EDTA 0.02 %	-	Cat# P10-0235SP, PAN-Biotech, Aidenbach, Germany
Hygromycin B	-	Cat# ant-hg-5, InvivoGen, San Diego, USA
RPMI 1640	-	Cat# 21875-034, Gibco, Waltham, USA
β-Mercaptoethanol	-	Cat# M7522-100mL, Sigma-Aldrich, Steinheim, Germany
Dimethyl sulfoxide (DMSO)	-	Cat# 4720.3, Carl Roth, Karlsruhe, Germany

Opti-MEM Reduced Serum medium	-	Cat# 11058-021, Gibco, Waltham, USA
Super Optimal broth with Catabolite repression (SOC)	0.5 % yeast extract, 2 % Tryptone, 10 mM NaCl, 2.5 mM KCl, 20 mM $MgSO_4$, 20 mM Glucose	-
Lysogeny broth (LB) Medium	-	Cat# X968.3, Carl Roth, Karlsruhe, Germany
LB agar plates	Respective Medium + 15 g/L Agar + Selection antibiotics Ampicilin – µg/mL	-
Freezing medium	10 % Dimethyl Sulfoxide (DMSO) in FBS	-

2.1.6 Oligonucleotides

Name	**Sequence 5’ - 3’**	**Application**	**Reference/Source**
TREM2 CRISPR RNA (crRNA)	GCCATCACAGACGATACCCT	Knock out of TREM2	IDT, Coralville, USA
RER1 CRISPR RNA (crRNA)	TGTGCGATGGGTCGTGACCAC	Knock out of RER1	IDT, Coralville, USA
Transactivating crRNA (tracrRNA)	-	Knock out of TREM2 and RER1	IDT, Coralville, USA
DAP12 primer for Real-Time qRT-PCR	QT00077518	Real-Time qRT-PCR	QIAGEN, Hilden, Germany

TREM2 primer for Real-Time qRT-PCR	QT00063868	Real-Time qRT-PCR	QIAGEN, Hilden, Germany
Hypoxanthine phosphoribosyltransferase 1 (HPRT1)	QT00059066	Real-Time qRT-PCR	QIAGEN, Hilden, Germany
Ubiquitin C (UBC) forward	ATTTGGGTCGCGGTTCTTG	Real-Time qRT-PCR	Accession number M26880
Ubiquitin C (UBC) reverse	TGCCTTGACATTCTCGATGGT	Real-Time qRT-PCR	Accession number M26880
Primer for sanger sequence of RER1 ko	ACATCACGCCCAGGTAACG	Sanger sequence	7549494, Eurogentec
Primer for sanger sequence of TREM2 ko	GTGTCTTGCCCCTATGACTCC	Sanger sequence	7549487, Eurogentec

2.1.7 Primary antibodies

Antibody	**Origin**	**Dilution**	**Reference**
Anti-DAP12 (DAP12.1* (0.620 mg/mL) and DAP12.2* (0.582 mg/mL))	Rabbit polyclonal	WB (DAP12.1): 8.4 µL in 5 mL Co-IP (DAP12.2): 5 µg (8.6 µL)	In house*
Anti-DAP12 (12492, D7G1X)	Rabbit polyclonal	ICC: 1:200	Cell Signaling Technologies, Danvers, USA

Anti-TREM2 (AF1828 or AF18281)	Goat polyclonal	WB: 1:1000 Stimulation for signaling: 10 µg/mL	R&D Systems, Minneapolis, USA
Anti-TREM2 (4B2A3)	Mouse monoclonal	Stimulation for signaling: 10 µg/mL	In house (Ibach et al., 2021)
Anti-TREM2 (9D11)	Rat monoclonal	WB: 1:1000	Haass lab (Schlepckow et al., 2017)
Anti-Calnexin (AB2301)	Rabbit polyclonal	WB: 1:1000	Millipore, Burlington, USA
Anti-Calnexin (ab112995, 6F12BE10)	Mouse monoclonal	ICC: 1:1000	Abcam, Cambridge, UK
Anti-Ubiquitinylated proteins (04-263, FK2)	Mouse monoclonal	WB: 1:1000	Millipore, Burlington, USA
Anti-Actin (A1978, AC-15)	Mouse monoclonal	WB: 1:1000	Sigma-Aldrich, Steinheim, Germany
Anti-Glycerinaldehyd-3-phosphat-Dehydrogenase (GAPDH) (sc-47724, 0411)	Mouse monoclonal	WB: 1:1000	Santa Cruz Biotechnology, Dallas, USA
Anti-Amyloid-Precursor-Protein (APP) (BLD-802801, C1/6.1)	Mouse monoclonal	WB: 1:1000	BioLegend, San Diego, USA

Anti-Alpha 1 Sodium Potassium ATPase (ab7671, 464.6)	Mouse monoclonal	ICC: 1:500	Abcam, Cambridge, UK
Anti-Giantin (ab37266, 9B6)	Mouse monoclonal	ICC: 1:100	Abcam, Cambridge, UK
Anti-ERGIC53 (LMAN1) (MA5-25345, OTI1A8)	Mouse monoclonal	ICC: 1:100	Thermo Fisher Scientific, Waltham, USA
Anti-RER1 (R4407)	Rabbit polyclonal	WB: 1:300	Sigma-Aldrich, Steinheim, Germany
Anti-RER1 (MBS418574)	Goat polyclonal	WB: 1:300 ICC: 1:100	Mybiosource
Anti-spleen tyrosine kinase (SYK) (80460, 4D10)	Mouse monoclonal	WB: 1:1000	Cell Signaling Technologies, Danvers, USA
Anti-Phospho-SYK (Tyr525/526) (2710, C87C1)	Rabbit Monoclonal	WB: 1:1000	Cell Signaling Technologies, Danvers, USA
Anti-Perilipin 2 (610102, AP125)	Mouse monoclonal	WB: 1:100 ICC: 1:100	PROGEN Biotechnik GmbH, Heidelberg, Germany
Anti-CYP51A1 (13431-1-AP)	Rabbit polyclonal	WB: 1:1000	Proteintech, Planegg-Martinsried Germany

Anti-LDLR (EP1553Y, ab52818)	Rabbit Monoclonal	WB: 1:1000	Abcam, Cambridge, UK
Anti-LRP1 (ab92544)	Rabbit polyclonal	WB: 1:1000	Abcam, Cambridge, UK
Anti-NPC1 (ab36983)	Rabbit Monoclonal	WB: 1:1000	Abcam, Cambridge, UK
Anti-ABCA1 (NB400-105)	Rabbit polyclonal	WB: 1:500	Novus Biologicals, Centennial, USA
Anti-APOE (E6D7, ab1906)	Mouse monoclonal	WB: 1:1000	Abcam, Cambridge, UK

*The anti-DAP12 antibodies DAP12.1 and DAP12.2 were generated by inoculation of rabbits with the peptide CITETESPYQELQGQ and CDVYSDLNTQRPYYK, respectively.

2.1.8 Secondary antibodies

Antibody	**Origin**	**Dilution**	**Reference**
IRDye 680 RD donkey anti rabbit	Donkey	1:5000	Cat# 926-68073, Li-COR Biosciences, Bad Homburg, Germany
IRDye 800 CW donkey anti goat	Donkey	1:5000	Cat# 926-32214, Li-COR Biosciences, Bad Homburg, Germany
IRDye 800CW donkey anti mouse	Donkey	1:5000	Cat# 926-32212, Li-COR Biosciences, Bad Homburg, Germany
IRDye 680 RD donkey anti mouse	Donkey	1:5000	Cat# 926-68072, Li-COR Biosciences,

			Bad Homburg, Germany
IRDye 800CW goat anti rat	Goat	1:5000	Cat# 926-32219, Li-COR Biosciences, Bad Homburg, Germany
Alexa Fluor 546-conjugated Anti-rabbit	Donkey	1:500	Cat# A10040, Invitrogen, Carlsbad, USA
Alexa Fluor 488-conjugated Anti-mouse	Donkey	1:500	Cat# A21202, Invitrogen, Carlsbad, USA
Horseradish peroxidase conjugated goat anti-rat	Goat	1:25000	Cat# 612-103-120, Rockland, Gilbertsville, USA
Horseradish peroxidase conjugated rabbit anti-goat	Rabbit	1:25000	Cat# A-5420, Sigma-Aldrich, Steinheim, Germany

2.1.9 Software

Software	**Application**	**Origin**
Microsoft Office 2021	Writing, and data analysis	Microsoft Corporation, Redmond, USA
Adobe Illustrator	Figures preparation	Adobe, San Jose, USA
GraphPad Prism 9	Data plotting	GraphPad Software Inc., San Diego, USA
I-control 1.11	Data acquisition via infinite M200PRO	Tecan, Männedorf, Switzerland

Image Studio Lite Ver 4.0	Data acquisition via Li-cor Odyssey CLx	Li-cor Biosciences GmbH, Bad Homburg, Germany
Quantity One®	Data acuisition via Chemidoc XRS Imager	Bio-Rad, Hercules, USA
Fiji, ImageJ	Image analysis	Wayne Rasband, National Institute of Health, USA

2.1.10 Instruments

Instrument	**Manufacturer**
Cell culture hoods	Amersham, GE Healthcare, Chicago, USA
Cell culture incubator 37°C/5% CO_2	Binder, Tuttlingen, Germany
Centrifuge 5415 R	Eppendorf, Wesseling, Germany
ChemiDoc XRS	Bio-Rad, Hercules, USA
Electrophoresis power supply	Amersham, GE Healthcare, Chicago, USA
Cell counter (CytoSMART™)	Corning, New York, USA
NanoPhotometer P-class P330	Implen, Munich, Germany
Tecan infinite M200Pro reader	Tecan, Männedorf, Switzerland
XCell4 SureLock Mini- Cell/ Midi-Cell	Thermo Fisher Scientific, Waltham, USA
PeqLap electrophoresis system	Peqlab Life Sciences, Erlangen, Germany
Blotting chamber	Amersham, GE Healthcare, Chicago, USA
Thermomixer	Eppendorf, Wesseling, Germany
VS-Homogenizer	Visitron Systems GmbH, Puchheim, Germany
Chemidoc XRS Imager	Bio-Rad, Hercules, USA
Odyssey® CLx (Li-cor)	Li-COR Biosciences, Bad Homburg, Germany
Microscope AxioVert 200 M with AxioCam MR R3 camera	Carl Zeiss, Oberkochen, Germany

Zeiss ApoTome	Carl Zeiss, Oberkochen, Germany
Tecan Spark reader	Tecan, Männedorf, Switzerland
Keyence BZ-X800	Keyence, Neu-Isenburg, Germany
Zeiss Axio Observer	Carl Zeiss, Oberkochen, Germany

2.2 Cell culture

Human embryonic kidney (HEK) 293 cells and HEK293 Flp-In cells were cultured in Dulbecco's Modified Eagle Medium (DMEM, Gibco, Waltham, USA), supplemented with 10 % heat-inactivated Fetal Bovine Serum (FBS, PAN-Biotech, Aidenbach, Germany), 1 % penicillin/streptomycin (P/S, Gibco, Waltham, USA) in an atmosphere containing 5 % CO_2 at 37 °C. Cells were split when the confluence reached 80-90 %. For detaching, cells were washed with prewarmed phosphate buffer saline (PBS), followed by incubation with PBS containing 0.05 % trypsin and 0.02 % EDTA (PAN-Biotech, Aidenbach, Germany). The process was stopped by resuspending the cells in fresh DMEM supplemented with 10 % FBS and 1 % P/S. Aliquots of the cell suspension were transferred to new dishes containing the appropriate cell culture medium. Plasmid transfected HEK293 Flp-In cells were cultured in DMEM, supplemented with 10 % (v/v) heat-inactivated FBS, 1 % (v/v) P/S, with 200 µg/mL Hygromycin B (InvivoGen, San Diego, USA) in an atmosphere containing 5 % CO_2 at 37 °C. The splitting method was the same with HEK 293 cells (Liu et al., 2024).

For long-term storage of HEK293 and HEK293 Flp-In cells, the cells were centrifuged at 200 xg for 3 mins after trypsinization and then suspended in FBS containing 10 % (v/v) dimethyl sulfoxide (DMSO, Carl Roth, Karlsruhe, Germany). The cell suspension was transferred to cryo-vials and stored at -80 °C, or in liquid nitrogen.

THP-1 cells were cultured in T75 flasks with RPMI 1640 medium (Gibco, Waltham, USA), supplemented with 10 % FBS, 1 % P/S, 0.05 µM β-Mercaptoethanol (Sigma-Aldrich, M7522, Germany) in a cell incubator with 5 % CO_2 at 37 ℃. Cells were split before the cell concentration reached 1,000,000 cells/mL (Liu et al., 2024).

After collecting THP-1 cells from the T75 flasks, they were centrifuged at 163 x g for 8 min and supernatants were discarded. A cryoprotectant containing 90 % FBS and 10 % DMSO

was then added to resuspended cell pallets. For long-term storage, the cell suspension was transferred to cryo-vials and stored at -80 °C or in liquid nitrogen.

To thaw both HEK 293 cells and THP-1 cells, we put the cryo-vials in a 37 °C water bath and when a small ice crystal remained in the solution, further cultivation was conducted with the partially thawed solution mixed with fresh culture medium in sterile flasks or dishes.

2.3 Counting and seeding of cells

In order to determine the cell number before seeding cells for further experiments, 10 µl of the trypsinized pure cell suspension was placed into a Neubauer chamber and counted with an automatic cell counter (CytoSMART^{TM}, Corning, New York, USA). Accordingly, cells were seeded for certain numbers in dishes or plates for experiments.

2.4 Differentiation of THP-1 cells by phorbol 12-myristate-13-acetate (PMA)

THP-1 cells were differentiated with 5 ng/mL phorbol 12-myristate-13-acetate (PMA, Sigma-Aldrich, Steinheim, Germany) into macrophage-like cells for 48 h. PMA was prepared in RPMI 1640 supplemented with 10 % FBS, 1 % P/S, 0.05 µM β-Mercaptoethanol. Afterwards, PMA was removed and differentiated cells were kept in complete RPMI 1640 medium for 1 day (Park et al., 2007). Then, differentiated cells were used for further experiments.

2.5 Plasmid DNA transformation of competent *E.coli*

One µg of respective plasmid DNA was mixed with DH5alpha bacteria and incubated on ice for 30 minutes to allow the plasmid DNA to attach. Afterwards, bacterial membranes were permeabilized using a heat shock at 42 °C for 45 seconds. After cooling on ice for 2 minutes, the bacteria were cultured in 1 mL of Super Optimal Broth with Catabolite Repression (SOC) medium supplemented with 0.1 % ampicillin in a shaking incubator for 1 h at 37 °C with 75 rpm shaking speed. Afterwards, for the expansion of the plasmid that already existed in the lab, 1 mL mixture was transferred to 250 mL Lysogeny broth (LB,

Carl Roth, Karlsruhe, Germany) medium supplemented with 0.1 % ampicillin in Erlenmeyer flasks for further culture overnight in a shaking incubator at 37 °C. The shaking speed was set to 200 rpm.

2.6 Cultivation of bacteria and plasmid DNA Maxiprep

The bacteria were incubated in a shaking incubator at 37°C overnight at a shaking speed of 200 rpm. The next day, plasmid preparation was carried out using the NucleoBond™ Xtra Maxi-Kit (Macherey-Nagel, Düren, Germany), following the manufacturer's instructions. To summarize, pelleted cells were resuspended in buffers containing lysis and neutralization enzymes. Centrifugation followed by loading of the clear supernatant onto a DNA binding column. DNA was washed, eluted, precipitated with isopropanol, and washed with ethanol. The DNA was centrifuged and resuspended in DNase-free H_2O, followed by determination of plasmid DNA concentrations by the NanoPhotometer P-Class P330 (Implen, Munich, Germany) and stored at -20 °C for future cell transfection.

2.7 Cell transfection

Five µg of the respective DNA plasmid was mixed with 200 µL Opti-MEM Reduced Serum medium (Gibco, USA). Lipofectamine 2000 (7.5 µL; Thermo Fisher Scientific, Waltham, USA) was mixed with 200 µL Opti-MEM Reduced Serum medium (Gibco, Waltham, USA) by flicking and incubated for 5 min at room temperature (RT). Lipofectamine 2000 and the respective plasmid constructs were mixed and incubated for 20 min at RT. Meanwhile the cells were washed twice with PBS and kept in culture medium (DMEM) without any supplements. The DNA-Lipofectamine mixtures were dropwise added to cells cultured in 6 cm diameter dishes and incubated for 16 h at 37 °C, 5% CO_2 (Liu et al., 2024).

For stable transfections of HEK293 Flp-In cells, a co-transfection of 7.2 µg pOG44 (Invitrogen, Carlsbad, USA) encoding Flp recombinase and 0.8 µg of the respective cDNA construct in a pcDNA5/FRT vector (Invitrogen, Carlsbad, USA) was performed. Medium was changed 24 h after transfection, and supplemented with 200 µg/mL Hygromycin B for selection of cells expressing the target gene of interest (Ibach et al., 2021, Liu et al., 2024).

2.8 Generation of TREM2 ko and RER1 ko THP-1 cell lines

CRISPR RNA (crRNA) and transactivating crRNA (tracrRNA, IDT, Coralville, USA) duplex, representing single guide RNAs (sgRNAs) for targeting TREM2 (IDT, Coralville, USA) or RER1 (IDT, Coralville, USA) were designed and obtained from Integrated DNA technologies (IDT, USA). For preparation of RNA duplexes, crRNA and tracrRNA were diluted to the same concentration (1 μM) and mixed. The mixed RNAs were heated at 95 °C for 5 min and cooled down at RT. Cas9 enzyme (IDT, 1081061, USA) was diluted to a concentration of 1 μM in Opti-MEM Reduced Serum medium. For each well of a 96-well tissue culture plate, 1.5 μL sgRNA (crRNA and tracrRNA duplex, 1 μM) and 1.5 μL Cas9 enzyme (1 μM) were mixed in 22 μL Opti-MEM Reduced Serum medium and incubated at RT for 5 min to assemble the ribonucleoprotein (RNP) complexes. Next, RNP complexes (25 μL) were mixed with lipofectamine RNAiMAX (Invitrogen, Carlsbad, USA, 1.2 μL) and Opti-MEM Reduced Serum medium (23.8 μL) and incubated at RT for 20 min to form transfection complexes. Meanwhile, THP-1 cells were washed with PBS and diluted to 400,000 cells/mL in complete media without antibiotics. Afterwards, 50 μL of the transfection solution containing the RNP complexes were transferred into one well of a 96-well plate. Hundred μL of the cell suspension (40,000 cells) were added to yield a final concentration of RNP complexes of 10 nM, and the plate was incubated for 4 h. Single-cell clones were obtained by diluting the cells to 1 cell/100 μL and cultured in 96-well plates. Single-cell clones were further expanded and analyzed for protein expression and DNA sequencing (Liu et al., 2024).

2.9 Limiting dilution cloning

Single cell clones were obtained by limiting dilution cloning. The stably transfected cells were counted and seeded in 96-well plates at a density of 1 cell/100 μL per well. Cells were cultured until the single cell clones were detectable by microscopy, followed by further expansion and verification for protein expression and DNA sequencing (Liu et al., 2024).

2.10 Cycloheximide chase assay

To determine the turnover of proteins, cycloheximide chase assay was performed. HEK 293 Flp-In cells and differentiated THP-1 cells were treated with 100 µg/mL cycloheximide (Sigma-Aldrich, Steinheim, Germany) for different time periods, including 2 h, 4 h, 8 h for HEK293 Flp-In cells and 4 h, 8 h for differentiated THP-1 cells. Untreated cells were used as control. Cells were collected at indicated time points for further analysis.

2.11 Assessment of protein degradation pathway by inhibitors of proteasome and lysosome

HEK 293 Flp-In and differentiated THP-1 cells were treated with inhibitors of either proteasomal or lysosomal activity. Lactacystin (Sigma-Aldrich, Steinheim, Germany, 10 µM) and MG132 (Sigma-Aldrich, Steinheim, Germany, 10 µM) were used as inhibitors for the proteasome and chloroquine (50 µM, Sigma-Aldrich, Steinheim, Germany) was used as an inhibitor for lysosomes. Cells were treated with the inhibitors for 4 h and collected for further cellular membrane isolation.

2.12 Preparation of cellular membrane fractions

For preparation of cellular membranes, cells were washed once with ice cold PBS, scraped in an appropriate volume of hypotonic buffer (10 mM Tris-HCl, 1 mM EDTA, 1 mM EGTA in dH2O, pH 7.6) supplemented with protease inhibitor cocktail (Sigma-Aldrich, Steinheim, Germany) and collected in tubes. Cells were incubated on ice for 10 min and subsequently homogenized using a syringe with a 0.6 mm cannula, drawing 20 times. After centrifugation for 10 min at 200 x g and 4 °C, the resultant supernatant was transferred into a new tube and centrifuged for 1 h at 16,000 x g and 4 °C. The supernatant was removed and the remaining pellet was considered as a crude membrane fraction. For extraction of proteins, the membrane fraction was resuspended in lysis buffer (1% n-dodecyl-β-d-maltoside (Sigma-Aldrich, Steinheim, Germany), 50 mM Tris–HCl (pH 8.0), 150 mM NaCl, 1 mM EDTA, 1.5 mM MgCl2, 10 % glycerol) supplemented with protease inhibitor and phosphatase inhibitor cocktail (Sigma-Aldrich, Steinheim, Germany), and

incubated for 20 min on ice. The lysate was centrifuged for 10 min at 16,000 x g and 4 °C and the supernatant used either for co-immunoprecipitation or direct analysis by sodium dodecyl-sulfate polyacrylamide gel electrophoresis (SDS-PAGE) and western immunoblotting (Liu et al., 2024).

2.13 Determination of protein concentrations

Protein concentrations were measured by either the Pierce™ BCA Protein Assay Kit (Thermo Fisher Scientific, Waltham, USA) or the Bradford method according to the instruction of the providers.

2.14 Sodium dodecyl sulphate-polyacrylamide gel electrophoresis (SDS-PAGE)

Samples were mixed with SDS sample buffer with or without dithiothreitol (DTT, 100 mM) as indicated and heated for 5 min at 95 °C. Proteins were separated using pre-cast NuPAGE Novex Bis-Tris Gels 4-12 % (Invitrogen, Carlsbad, USA), NuPAGE running chambers, and NuPAGE MES SDS Running Buffer (Invitrogen, Carlsbad, USA) at 150 V (Liu et al., 2024).

2.15 Western immunoblotting

Proteins were transferred onto nitrocellulose membranes by wet transfer technique at a constant current of 400 mA for 1 h and 45 min. After blocking for 1 h with constant agitation in Tris-Buffered Saline, 0.1 % Tween® 20 Detergent (TBST) containing 5 % milk powder, membranes were incubated over night at 4 °C in primary antibodies diluted in TBST. Membranes were washed 3 times for 5 min, and incubated in TBST containing the respective secondary antibody conjugated either with horseradish peroxidase or a fluorophore (IRDye800CW, 680RD, Li-COR Biosciences, Germany) for 1 h at RT. After washing the membrane 3 times for 5 min, signals were detected using a Chemidoc XRS Imager (Bio-Rad, USA) or Odyssey® CLx (Li-COR Biosciences, Germany). ImageJ (NIH, USA) was used for quantitative analysis of the blots (Liu et al., 2024).

2.16 Real-Time Quantitative Reverse Transcription PCR (Real-Time qRT-PCR)

Total RNA was extracted from THP-1 cells by RNeasy® Mini Kit (QIAGEN, Hilden, Germany) and genomic DNA was removed by using RNase-Free DNase (QIAGEN, Hilden, Germany).

Single-stranded cDNA was generated from total RNA by reverse transcription using a RevertAid First Strand cDNA Synthesis Kit (Thermo Fisher Scientific, Waltham, USA) according to the manufacturer's instructions.

Quantitative PCR was performed using QuantiTect® SYBR® Green PCR Kit (QIAGEN, Hilden, Germany). The primers for DAP12 (QIAGEN, Hilden, Germany) and TREM2 (QIAGEN, Hilden, Germany) were purchased from QIAGEN. The mRNA levels of DAP12 and TREM2 were normalized to Hypoxanthine phosphoribosyltransferase 1 (HPRT1, QIAGEN, Hilden, Germany) and Ubiquitin C (UBC, accession number M26880, forward ATTTGGGTCGCGGTTCTTG and reverse TGCCTTGACATTCTCGATGGT) expression in each sample (Liu et al., 2024).

2.17 Immunocytochemistry

Coverslips and ibidi dishes (Ibidi, Gräfelfing, Germany) were incubated with a solution of 1X Poly-L-Lysine Hydrobromide (PLL, Sigma-Aldrich, Steinheim, Germany) diluted in distilled water (10XPLL: 5 mg PLL in 50 mL 0.1 M borate buffer (pH 8.4, 2.48 g/L boric acid (Sigma-Aldrich, Steinheim, Germany), 3.8 g/L sodium tetraborate (Sigma-Aldrich, Steinheim, Germany) for 2 h. Afterwards, the solution was removed and the coverslips and ibidi dishes were washed with PBS for 3 times and used for further experiments. Cells were seeded on PLL coated coverslips or ibidi dishes (ibidi, Gräfelfing, Germany) and fixed with 4 % paraformaldehyde (PFA, Sigma-Aldrich, Steinheim, Germany) in PBS for 20 min. After washing 3 times with PBS, cells were permeabilized in PBS containing 0.1 % Triton X-100 (Carl Roth, Karlsruhe, Germany) for 15 min at RT, followed by blocking in PBS containing 0.1 % Tween® 20 (PBST) supplemented with 3 % bovine serum albumin (BSA) for 1 h. Cells were incubated with primary antibodies diluted in PBST containing 1 % BSA at RT for 1 h and washed 3 times with PBST. Afterwards, cells were incubated with

secondary antibodies diluted in PBST containing 1 % BSA with addition of 4′,6-diamidino-2-phenylindole (DAPI, Invitrogen, Carlsbad, USA) for 1 h at RT and washed 3 times with PBST followed by two washes with PBS. Subsequently, the coverslips were mounted on microscopic slides using Immu-Mount™ (Thermo Fisher Scientific, Waltham, USA). Samples processed on Ibidi dishes were mounted using Ibidi mounting medium (ibidi, Gräfelfing, Germany). Images were taken with a Zeiss microscope (AxioVert 200) supplied with a Zeiss ApoTome using a 63/1.4 objective and EGFP, DsRed and DAPI fluorescence filter sets. Images were processed with ImageJ (NIH, USA) (Liu et al., 2024).

For quantitative image analysis, images were randomly captured with identical camera settings within individual experiments. Analysis of colocalization was done with the colocalization processing module (Coloc 2) of Fiji ImageJ. A total number of at least 65 cells for each experimental condition was scored by a person blind to the samples (Liu et al., 2024).

For the LD540 staining in differentiated THP-1 cells, cells were incubated with 0.05 µg/mL LD540 dye for 30 minutes after fixation with 4 % PFA. Subsequently, cells were washed with PBS for three times before ibidi mounting medium were added to the dishes.

Images were taken with a Zeiss microscope (AxioVert 200) supplied with a Zeiss ApoTome using a 63/1.4 objective and DsRed and DAPI fluorescence filter sets. Images were processed with ImageJ (NIH, USA). For quantitative image analysis, images were randomly captured with identical camera settings within individual experiments. Analysis of LDs number and volume was done with Automatic Lipid Droplet Quantification (ALDQ) plugin of Fiji ImageJ according to a previous publication (Exner et al., 2019). A total number of at least 424 cells was included for each experimental condition in ALDQ quantification. Analysis of perilipin 2 intensity was performed in ImageJ and at least 408 cells for each experimental condition.

2.18 Co-immunoprecipitation

Cellular membrane lysates were incubated with 5 µg of the indicated antibodies for 4 h at RT. Afterwards, 20 µL Sepharose Protein G beads (Invitrogen, Carlsbad, USA) were added to the samples and incubated for 1 h at RT. Beads were collected by centrifugation,

washed for 2 times with the buffer (50 mM Tris–HCl (pH 8.0), 150 mM NaCl, 1 mM EDTA, 1.5 mM $MgCl_2$, 10% glycerol) and 1 time with PBS. Bound proteins were denatured at 95 °C for 5 min in 2xSDS sample buffer and subjected to western immunoblotting analysis (Liu et al., 2024).

2.19 Stimulation of TREM2-DAP12 signaling pathway by anti-TREM2 antibodies

Anti-TREM2 antibodies, including AF1828 (R&D Systems, Minneapolis, USA) and 4B2A3 (in house made) (Ibach et al., 2021), were used for the stimulation of TREM2-DAP12 signaling. Differentiated THP-1 cells in 96 well plates were washed with RPMI 1640 medium (without the supplement FBS and P/S) three times and then treated with 50 µL AF1828 (10 µg/mL in RPMI 1640) or 4B2A3 (10 µg/mL in RPMI 1640) antibody solutions for 10 min at 37 °C. Cells without or with IgG treatment were used as negative controls. Afterwards, cells were lysed with Lysis Buffer-Ultra (AlphaLISA® SureFire® Ultra™ p-SYK (Tyr525/526) Assay Kit, Perkin Elmer, Waltham, USA) for 10 min and cell lysates were used for AlphaLISA assay.

2.20 AlphaLISA technology

Detection of phospho-SYK (PSYK) in cell lysates was performed according to manufacturer's instructions (AlphaLISA® SureFire® Ultra™, Perkin Elmer, USA). Briefly, cells were lysed with Lysis Buffer-Ultra (included in the kit, AlphaLISA® SureFire® Ultra™ p-SYK (Tyr525/526) Assay Kit, Perkin Elmer, ALSU-PSYK-A500, USA) for 10 min. Ten µL of cell lysates were transferred into a 384well Optiplate (Perkin Elmer, 6007680, USA) and incubated with 5 µL acceptor beads prior to 5 µl donor beads for 1 h in the dark, respectively. The luminescence signals were measured using a Tecan Spark reader (Tecan, Switzerland) with standard AlphaLISA settings (Liu et al., 2024).

2.21 Phagocytosis assay

Cells were seeded at a density of 100,000 cells/well into 96-well flat-bottom plates with black wall (Greiner Bio-one, Frickenhausen, Germany) or black ibiTreat 96-well µ-plates

(ibidi, Gräfelfing, Germany) and were cultured for 48 h in complete RPMI 1640 medium (10 % FBS, 1 % P/S) in presence of 5 ng/mL of PMA and recovered in normal medium for 1 day without PMA. On the day of the experiment, cells were pre-incubated with or without 10 µM cytochalasin D (cyto D, Sigma-Aldrich, Steinheim, Germany) for 30 min before the addition of 0.5 mg/mL pHrodo™ Red E.coli BioParticles™ (1 mg/mL, Invitrogen, Carlsbad, USA) diluted in live cell imaging solution (Thermo Fisher Scientific, Waltham, USA). Fluorescence was analyzed using an Infinite M200Pro reader (Tecan, Männedorf, Switzerland) at the indicated time points. For direct view of the uptake of pHrodo™ Red *E.coli* BioParticles by differentiated THP-1 cells, fluorescence signals at 568 nm as well as bright field images were taken using a Keyence BZ-X800 microscope with a 40/0.60 objective, and processed using ImageJ (NIH, USA). For the quantification of phagocytosis, pHrodo fluorescence intensity of samples incubated with cyto D was subtracted (Liu et al., 2024).

2.22 Detection of LD540 fluorescence by flow cytometry

Undifferentiated THP-1 cells were washed with PBS for three times after collecting and counting and incubated with 0.5 µg/mL lipophilic dye LD540 in 1x DPBS for 20 mins in a cell incubator with 5 % CO_2 at 37 °C. Afterwards, the cells were washed twice with DPBS and resuspend in the same solution. All samples were analyzed by FACSAria II flow cytometer (BD Biosciences, San Jose, USA) by exciting with a 488 nm laser and collecting the fluorescence emission at 530 nm. FlowJo (BD Biosciences, San Jose, USA) was used for data processing.

2.23 Quantification of cholesterol, non-cholesterol sterols and oxysterols in THP-1 cells

THP-1 undifferentiated and differentiated cells were harvested and washed three times with PBS. Samples were stored at −80 °C until analysis. Sterols and oxysterols were quantified in undifferentiated and differentiated THP-1 cells. The cells were dried in a speedvac concentrator (12 mbar; SpeedVac DNA 130-230 Vacuum Concentrator, Thermo Scientific, Darmstadt, Germany) and weighed. Cholesterol, non-cholesterol sterols, and oxysterols were extracted using chloroform/methanol (2:1; vol/vol)). After

alkaline hydrolysis, the concentrations of the sterols and oxysterols were measured with gas chromatography-flame ionization detection (GC-FID) or GC-mass spectrometry selected ion monitoring (GC-MS-SIM) by Anja Kerksiek and Prof. Dr. Dieter Lütjohann as previously described (Šošić-Jurjević et al., 2019).

2.24 Lipidomic analysis by Tandem mass spectrometry

500.000 cells of THP-1 undifferentiated and differentiated cells were collected washed three times with PBS. Samples were stored at −80 °C until analysis. Lipid extraction was performed as previously described (Yaghmour et al., 2021). Briefly, 500 µl of extraction mix, including containing methanol:chloroform 5/1 and internal standard mix (containing 240 pmol pPC 31:1, 210 pmol phosphatidylethanolamine (PE) 31:1, 396 pmol PC 31:1, 98 pmol phosphatidylserine (PS) 31:1, 56 pmol phosphatidic acid 31:1, 51 pmol phosphatidylglycerol 28:0, 39 pmol lysophosphatidate 17:0, 35 pmol lysophosphatidylcholine; 17:1, 38 pmol lysophosphatidylethanolamine (LPE) 17:1, 32 pmol ceramide 17:0, 99 pmol SM 17:0, 55 pmol glucosylceramide 12:0, 339.7 pmol triacylglycerol (TAG) 50:1, 111 pmol cholesteryl ester (CE) 17:1, 64 pmol diacylglycerol (DAG) 31:1, and 103 pmol monoglyceride 17:1), was quickly added to one sample and followed by sonication for 30 s in the bath sonicator. Subsequently, the samples were centrifuged at 20.000 x g for 2 min and the supernatants were transferred into new tubes for further process. 200 µl chloroform and 800 µl 1% acetic acid in water were added into the samples to induce phase separation. The samples were shaken manually for 5 second and centrifuged at 20.000 x g for 2 min. The upper phase was carefully removed and discarded. The entire lower phase was transferred into a new tube and evaporated in the centrifuge at 45 °C for 20 min. 1 mL spray buffer (2-propanol:methanol:water 8/5/1+10 mM ammonium acetate) was added into the samples and sonicated for 5 min.

Mass spectra were acquired using a Thermo Q-Exactive Plus spectrometer equipped with a standard heated ESI source. Direct injection was performed with a Hamilton syringe driven by a syringe pump and managed via the Tune instrument control software. MS1 spectra, with a resolution of 280,000, were collected across 100 m/z windows from 250 to 1,200 m/z in positive mode and 950 to 1,300 m/z in negative mode. MS/MS spectra, also with a resolution of 280,000, were recorded using data-independent acquisition in 1 m/z

windows, covering 200 to 1,200 m/z in positive mode and 950 to 1,300 m/z in negative mode. The raw data were converted to .mzML files using MSConvert and analyzed with LipidXplorer software. For further analysis, absolute amounts were calculated using internal standard intensities, followed by the calculation of the mol% for the identified lipids. Lipidomic analysis by Tandem mass spectrometry was performed by Mohamed H. Yaghmour and Prof. Dr. Christoph Thiele.

2.25 RNA sequencing

Total RNA was extracted from THP-1 cells by RNeasy® Mini Kit (QIAGEN, Hilden, Germany) according to the manufacturer's instructions and genomic DNA was removed by using RNase-Free DNase (QIAGEN, Hilden, Germany). Transcriptome library construction was performed by QuantSeq 3'-mRNA Library Prep for Illumina (Lexogen, Vienna, Austria). Single-end 100-base reads were generated by NovaSeq 6000 sequencing system.

Raw reads were filtered by using SOAPnuke (https://github.com/BGI-flexlab/SOAPnuke) (Cock et al., 2010) and mapped to human reference genome (Homo_sapiens_NCBI_GCF_000001405.40_GRCh38.p14) by Hierarchical Indexing for Spliced Alignment of Transcripts (HISAT, http://www.ccb.jhu.edu/software/hisat) (Kim et al., 2015) and aligned to the reference genes by using Bowtie2. The matched reads were calculated as transcript per million (TPM). Differentially expressed genes (DEGs) were identified using DESeq2, with thresholds set at an adjusted p-value (Qvalue) < 0.05 and |log2FoldChange| ≥ 1, and the results were visualized using heatmaps and volcano plots. Kyoto Encyclopedia of Genes and Genomes (KEGG) function enrichment analysis was performed to identify the associated biochemical and signal transduction pathways. The functional enrichment analysis of Gene Ontology (GO) was performed to explore the potential roles of the differentially expressed mRNAs. Both enrichment analyses were performed by using the online Dr. Tom software (https://biosys.bgi.com), with a Q value < 0.05 as significance threshold.

2.26 Statistics analysis

Data were analyzed using GraphPad Prism 9 (GraphPad Software Inc., San Diego, USA). After testing for normality, all data were analyzed by one-way ANOVA, followed by post hoc Tukey's multiple comparisons test or Student's t-test (unpaired, two-tailed). A p-value less than 0.05 was considered as statistically significant (*p <0.05; **p <0.01; ***p <0.001; ****p <0.0001). Information on the number of experiments and replicates is provided in the figure legends.

3 Results

3.1 Differentiation of THP-1 cells into macrophage-like cells

TREM2-DAP12 complex is expressed in lymphoid and myeloid lineage cells, including monocytes and macrophages. The human monocytic leukemia cell line THP-1, although only expressing Fc receptors and C3b receptors and lacking surface and cytoplasmic immunoglobulins, can express more surface immunoglobulins when it is differentiated into macrophage-like cell by PMA (Daigneault et al., 2010, Schwende et al., 1996, Tsuchiya et al., 1982). Therefore, we included THP-1 as a cell line endogenously expressing TREM2 and DAP12 complex and PMA was used for differentiating the cells into macrophage-like cells. PMA, an analog of diacyl glycerol, can activate PKC, in particular the classical and the novel PKC isoforms (Liu & Heckman, 1998), which can initiate differentiation of THP-1 cells into macrophages (Ansa-Addo et al., 2010, Tsuchiya et al., 1982). Since high concentration of PMA might upregulate the expression of some genes in differentiated macrophages, which could overwhelm gene expression increases induced by other stimuli (Abe et al., 1991, Kohro et al., 2004), different PMA concentrations and treatment time were tested in the study to optimize the PMA concentration and treatment time.

In the present study, different PMA concentrations, including 5 ng/mL, 10 ng/mL, 20 ng/mL and 50 ng/mL and different treatment time points, including 48 h and 72 h, were tested for the differentiation of THP-1 cells. The results showed that both TREM2 and DAP12 protein were endogenously expressed by undifferentiated THP-1 monocytes but at a low level (Fig. 3.1 A, PMA 0 ng/mL, 48 h and 72 h). Differentiation with PMA strongly increased expression of both, DAP12 and TREM2 at the mRNA and protein level. While there was no significant difference of DAP12 and TREM2 protein expression among different PMA concentrations and treatment time (Fig.3.1 A), therefore the protocol for differentiating THP-1 cells into macrophage-like cells with 5 ng/mL PMA for 48 h followed by 1 day recovery (culturing the cells in the absence of PMA) was used in the following experiments. Moreover, SDS-PAGE analysis under reducing (with DTT) and non-reducing conditions (without DTT) revealed that DAP12 predominantly exists in dimeric forms (Fig. 3.1 A). The low levels of monomeric DAP12 might represent a pool of DAP12 before dimerization. As

expected, DAP12 dimers dissociated to monomers under reducing conditions (Fig. 3.1 A). However, the monomers derived from dissociated DAP12 dimers under reducing conditions showed slower migration in SDS gels as compared to the monomeric DAP12 pool detected under non-reducing conditions (Fig. 3.1 A). It remains to be determined whether the different migration of monomers is due to altered glycosylation or phosphorylation states of DAP12 before and after dimerization. Detection of mRNA levels of DAP12 and TREM2 was further performed by real-time qRT-PCR in THP-1 cells differentiated with 5 ng/mL PMA for 48 h. The results showed that DAP12 mRNA increased for approximately ten times while TREM2 mRNA elevated for more than twenty times after differentiation (Fig. 3.1 B and C) (Liu et al., 2024).

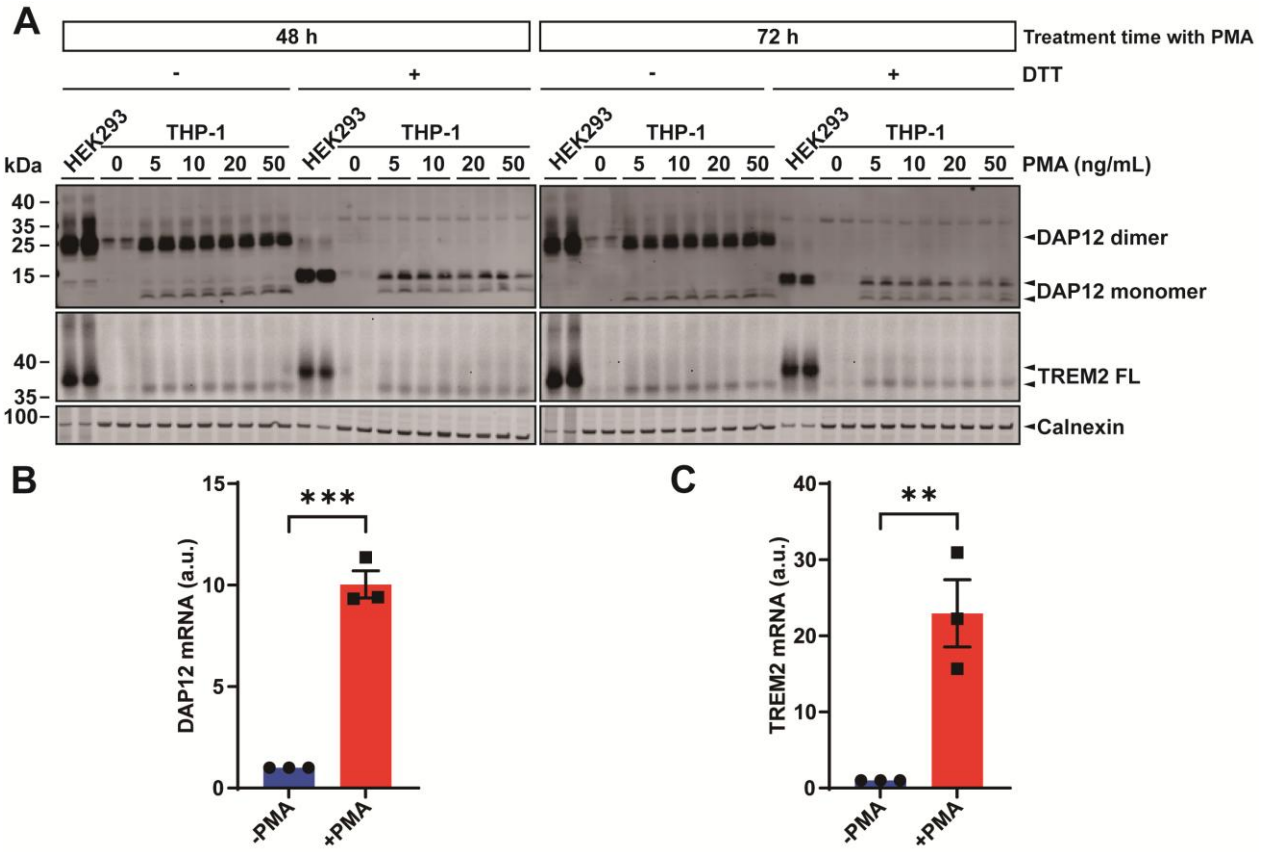

Fig. 3.1 Differentiation of THP-1 cells into macrophage-like cells increases endogenous expression of TREM2 and DAP12. (A) Comparison of DAP12 and TREM2 expression levels in THP-1 wt cells differentiated with PMA at the indicated concentrations and incubation times followed by one day recovery in normal RPMI 1640 after PMA removal. HEK293 cells transiently transfected with a bicistronic TREM2 wt+DAP12 wt construct served as positive control. Membrane proteins were isolated, and samples

prepared under reducing (with dithiothreitol (DTT)) or non-reducing (without DTT) conditions, and analyzed by western immunoblotting. TREM2 FL: TREM2 full-length protein. (B)-(C) Comparison of the DAP12 and TREM2 mRNA levels in differentiated (5 ng/mL PMA, 48 h + 1 day recovery) and undifferentiated THP-1 wt cells by real-time qRT-PCR. Values represent Mean ± SEM of three independent experiments. Each data point represents the mean value of an individual experiment. Student's t-test (unpaired, two-tailed). **p <0.01, ***p <0.001. Figure adapted from Liu et al. 2024.

3.2 Generation of TREM2 knockout THP-1 cell lines

To further investigate the effects of TREM2 on DAP12 metabolism, transport and signaling transduction function, TREM2 knockout (TREM2 ko) THP-1 cells were generated by Clustered Regularly Interspaced Short Palindromic Repeat/ CRISPR associated protein 9 (CRISPR/Cas9) technology. The CRISPR/Cas9 technology for genome editing has been a popular method because of its convenience, efficiency and robustness (Cho et al., 2013). The system requires two short RNA molecules, a sequence-specific CRISPR RNA (crRNA) and a conserved, transactivating crRNA (tracrRNA) that interact through partial homology to form a crRNA:tracrRNA duplex that is often called the guide RNA (gRNA). Furthermore, the guide RNA is mixed with Cas9 nuclease to form a ribonucleoprotein (RNP) in vitro (Kim et al., 2014). By lipofectamine transfection of RNP into cells (Zuris et al., 2015), the gRNA guides and triggers Cas9 to cleave double-stranded DNA targets, activating the non-homologous end joining (NHEJ) system, including insertion, deletion and frameshift mutation. Single cell clones of and TREM2-ko were selected by limiting dilution cloning assay and many cell clones for TREM2 ko were obtained.

To check the knock out of the target genes, membrane fractions of cells were isolated and analyzed by western immunoblotting. It was shown that several cell clones had no TREM2 protein expression compared with wt THP-1 cells (Fig. 3.2 A). One of the clones (T2D4 for TREM2 ko cells) was further confirmed by DNA sanger sequencing. It was shown that T2D4 has a four base pair deletion in the respective target gene (Fig. 3.2), and was further used in the study.

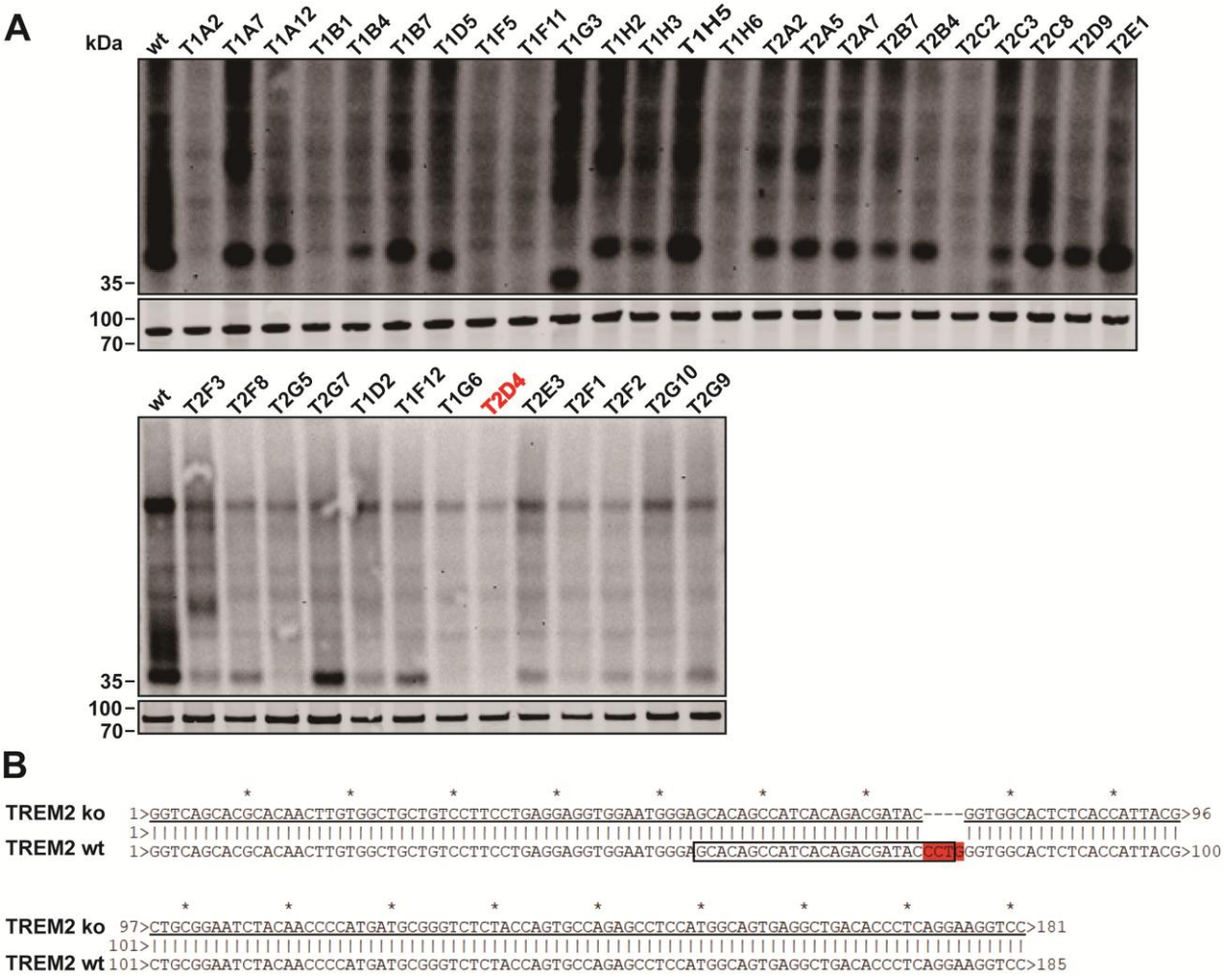

Fig. 3.2 Generation of TREM2 knockout THP-1 cell line by CRISPR/CAS9 technology. (A) TREM2 protein was detected by western immunoblotting in TREM2 ko and wt THP-1 differentiated cells with TREM2 antibody (AF1828). (B) DNA sanger sequencing of TREM2 in CRISPR/Cas9-mediated THP-1 TREM2 ko cells. DNA was extracted and the primer 5'-GTGTCTTGCCCCTATGACTCC-3' used for DNA sequencing. The sequence of the gRNA used for TREM2 targeting is indicated by the box. The arrow indicated deleted bases pairs in the TREM2 sequence. Figure adapted from Liu et al. 2024.

3.3 The interaction of DAP12 and TREM2 is mediated by the aspartic acid residue (D50) in the transmembrane domain of DAP12 and the lysine residue (K186) in the transmembrane domain of TREM2

The interaction between DAP12 and its co-receptors has been found to be mediated by charged amino acid residues, including the negatively charged aspartic acid residue (D50) in the TMD of DAP12 and the positively charged basic residues in the transmembrane

domain of co-receptors, including lysine or arginine residues (Lanier et al., 1998a). TREM2 interacts with DAP12 via the lysine residue in position 186 (K186) in the TMD (Bouchon et al., 2001). Here, we confirmed that the lysine residue (K186) in the TREM2 TMD and the aspartic acid residue (D50) in DAP12 TMD are involved in the interaction between TREM2 and DAP12 by co-immunoprecipitation assay. In particular, the anti-TREM2 antibody 4B2A3 co-precipitated DAP12, and anti-DAP12 antibody DAP12.2 co-precipitated TREM2 in the lysates of HEK 293 cell transiently overexpressing TREM2 wt and DAP12 wt proteins. In contrast, co-IP was abrogated in cells expressing the TREM2 K187N variant (Fig. 3.3 A) as well as DAP12 D50A variant (Fig. 3.3 B) which confirm that the lysine residue in transmembrane domain of TREM2 and aspartic acid residue in DAP12 TMD mediate TREM2 binding to DAP12 (Liu et al., 2024).

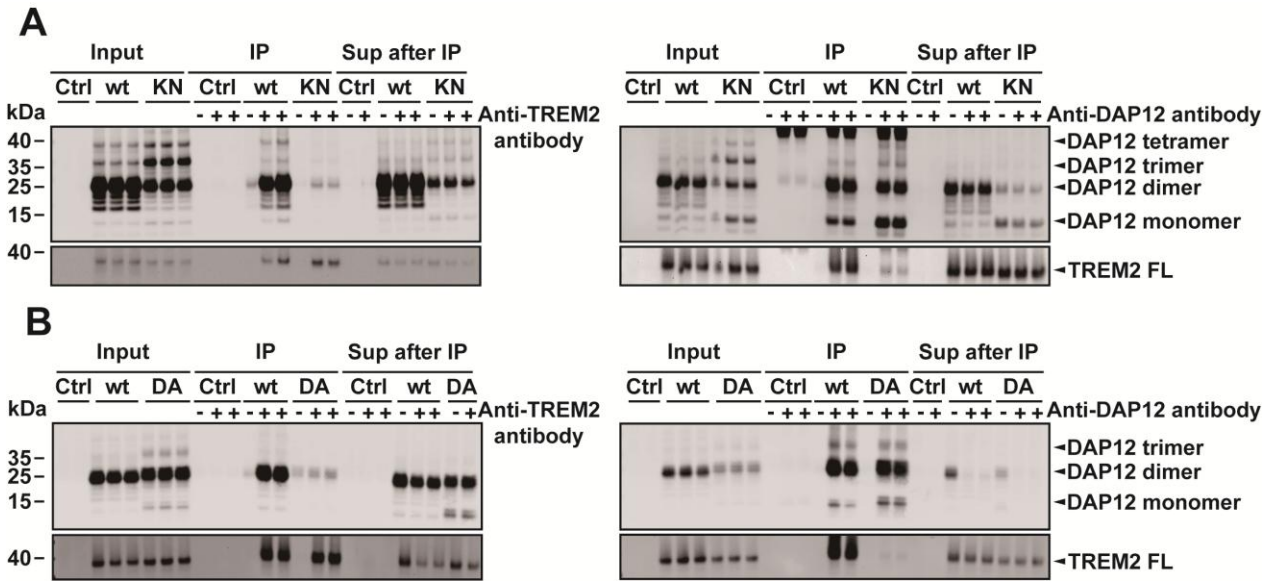

Fig 3.3 Analysis of the interaction between different TREM2 and DAP12 variants. (A) HEK293 cells were transiently co-transfected with TREM2 wt+DAP12 wt (wt) or TREM2 K186N+DAP12 wt (KN). Non-transfected HEK 293 cells served as control (Ctrl). Membrane proteins were extracted and subjected to co-immunoprecipitation with anti-TREM2 antibody (4B2A3) or anti-DAP12 antibody (DAP12.2). TREM2 FL: the full length of TREM2. (B) HEK293 cells were transiently co-transfected with TREM2 wt+DAP12 wt (wt) and TREM2 wt+DAP12 D50A (DA). Non-transfected HEK 293 cells served as control (Ctrl). Non-transfected HEK 293 cells served as control (Ctrl). Membrane proteins were extracted and subjected to co-immunoprecipitation with anti-TREM2 antibody (4B2A3) or anti-DAP12 antibody (DAP12.2). TREM2 FL: TREM2 full length protein. Figure adapted from Liu et al. 2024.

3.4 Deficiency of TREM2 results in decreased expression of DAP12

To investigate whether TREM2 affects DAP12 metabolism, we analyzed expression levels and stability of DAP12 in TREM2 wt and TREM2 ko THP-1 cells that were differentiated with PMA into a macrophage-like phenotype (Daigneault et al., 2010, Schwende et al., 1996, Tsuchiya et al., 1982).

Interestingly, compared with wt cells, protein levels of both monomeric and dimeric DAP12 were significantly decreased in TREM2 ko cells, with the reduction of dimeric DAP12 being stronger than that of monomeric DAP12 (Fig. 3.4 A-C). However, the level of DAP12 mRNA was even slightly increased in the TREM2 ko cells compared with wt cells (Fig. 3.4 D).

3.5 Increased degradation of DAP12 in the absence of TREM2 interaction

It has been reported that DAP12 stabilizes TREM2 CTFs (Zhong et al., 2015). However, it is not known if TREM2 also stabilizes DAP12. To figure out how TREM2 ko led to decreased DAP12 levels, the stability of DAP12 in TREM2 ko cells was assessed. Cycloheximide (CHX) chase assay is commonly used in molecular biology to investigate the stability or half-life of a protein within the cells. The assay involves treating cells with cycloheximide, a translation inhibitor that halts protein synthesis by binding to the ribosome (Buchanan et al., 2016, Obrig et al., 1971). By measuring the decrease in protein levels over time after CHX treatment, we can assess the stability of the targeted protein.

Here, cycloheximide (CHX) chase assays revealed increased degradation of DAP12 dimers in TREM2 ko cells as compared to TREM2 expressing cells. The half-life time of DAP12 dimers in wt cells was about 6.12 h, while it was about 3.06 h in TREM2 ko cells (Fig. 3.4 E, G, H). However, the turnover of the monomeric DAP12 pool was not significantly affected by TREM2 deficiency (Fig. 3.4 F) (Liu et al., 2024).

To further investigate the effects of TREM2 on DAP12 metabolism and subcellular transport without potential interference by other immune receptors that might interact with DAP12, we chose HEK293 Flp-In cells that allow expression of cDNAs from a defined genetic locus (O'Gorman et al., 1991). This model was applied previously to study

TREM2-DAP12 expression and signaling (Ibach et al., 2021, Kleinberger et al., 2014). Cell clones were generated that stably express a bicistronic cDNA construct encoding TREM2 and DAP12 separated by a T2A linker sequence to ensure stoichiometric expression of both proteins. In addition, stable clones were generated expressing DAP12 alone or together with the TREM2 K186N mutation associated with NHD. This mutation is known to prevent the interaction with DAP12 (Paloneva et al., 2002, Sirkis et al., 2017). Defective interaction of the TREM2 K186N variant with DAP12 was verified by co-IP (Fig. 3.3 A). Protein chase experiments revealed strongly increased degradation of both monomeric and dimeric DAP12 in cells expressing no TREM2 or the TREM2 K186N mutant (Fig. 3.5 A-C) as compared to cells that co-express TREM2 wt, thereby partially verifying the results obtained with the THP-1 cell model (Liu et al., 2024).

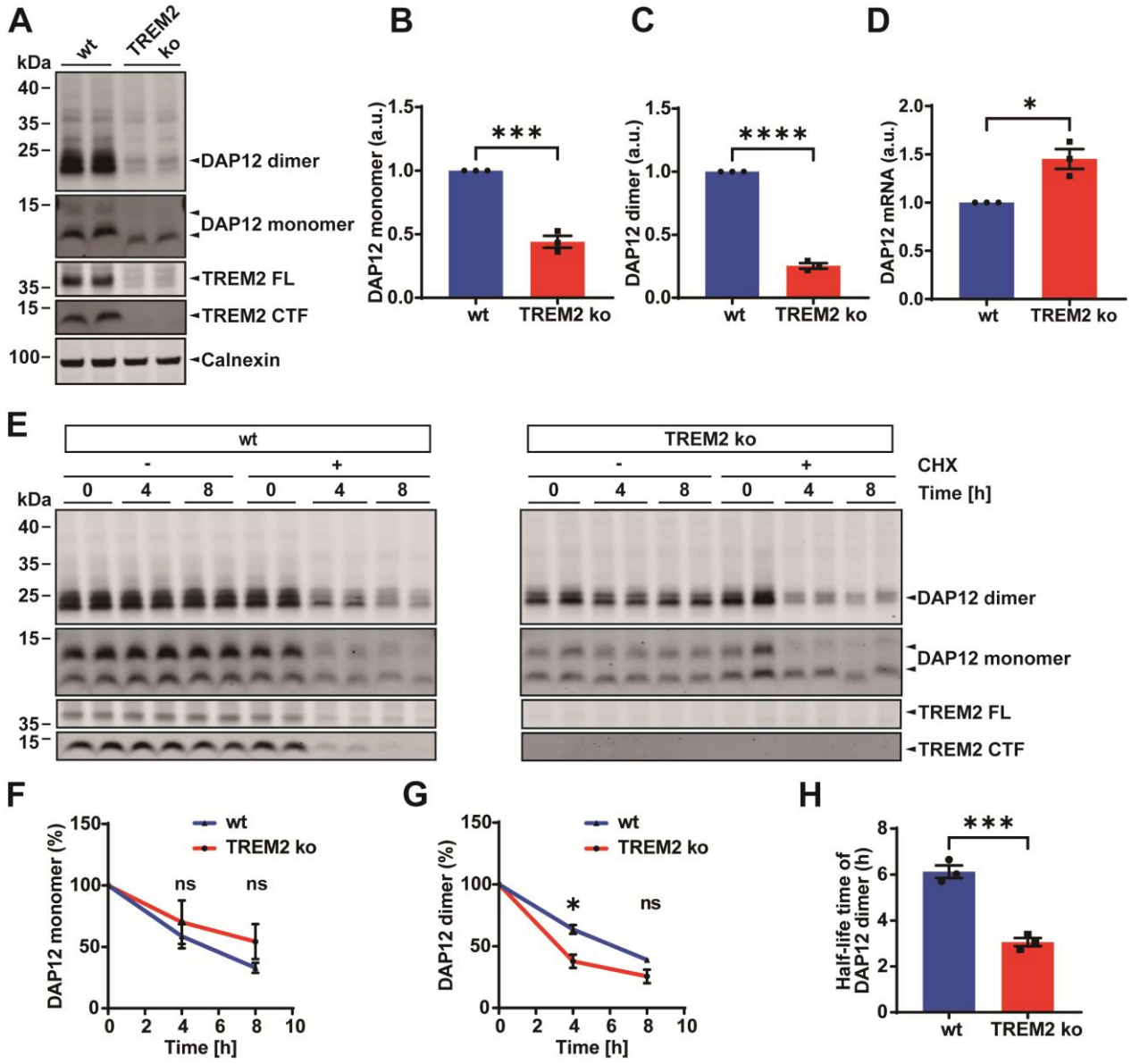

Fig. 3.4 Increased turnover of DAP12 in the absence of TREM2 in THP-1 cells. Detection of DAP12 in macrophage-like differentiated THP-1 wt and TREM2 knockout (ko) cells. Cellular membranes were isolated and the indicated proteins analyzed by western immunoblotting. TREM2 FL: TREM2 full length protein; TREM2 CTF: TREM2 C-terminal fragment. (B) and (C) Quantification of monomeric and dimeric DAP12 by western immunoblotting (as shown in A). Monomeric and dimeric DAP12 was normalized to calnexin present in the membrane fraction. Mean ± SEM of three independent experiments each performed with duplicate or triplicate samples. Each data point represents the mean value of an individual experiment. Student's t-test (unpaired, two-tailed). ***p <0.001, ****p <0.0001. (D) Comparison of the DAP12 mRNA levels in differentiated THP-1 wt andTREM2 ko cells by real-time RT-PCR. Values represent Mean ± SEM of three independent experiments. Each data point represents the mean value of an individual experiment. Student's t-test (unpaired, two-tailed). *p <0.05. (E) Analysis of DAP12 stability in THP-1 wt and TREM2 ko cells. THP-1 differentiated

macrophage-like wt and TREM2 ko cells were incubated with cycloheximide (CHX, 100 µg/mL) or without (Ctrl) for the indicated time points. Cellular membranes were isolated and the indicated proteins were analyzed by western immunoblotting. (F)-(H) Quantification of DAP12 turnover upon cell treatment with CHX. The level of DAP12 was normalized against the level of DAP12 in non-treated control cells at corresponding time points. The half-life time of DAP12 dimer was about 6.12 h in wt cells, and 3.06 h in TREM2 ko cells (D). Mean ± SEM of three independent experiments each performed with duplicate samples. Each data point represents the mean value of an individual experiment. Student's t-test (unpaired, two-tailed). *p <0.05, ***p <0.001. The statistical differences marked with the asterisk (*) and no significance (ns) are between wt and TREM2 ko cells at 4 h and 8 h, respectively. Figure adapted from Liu et al. 2024.

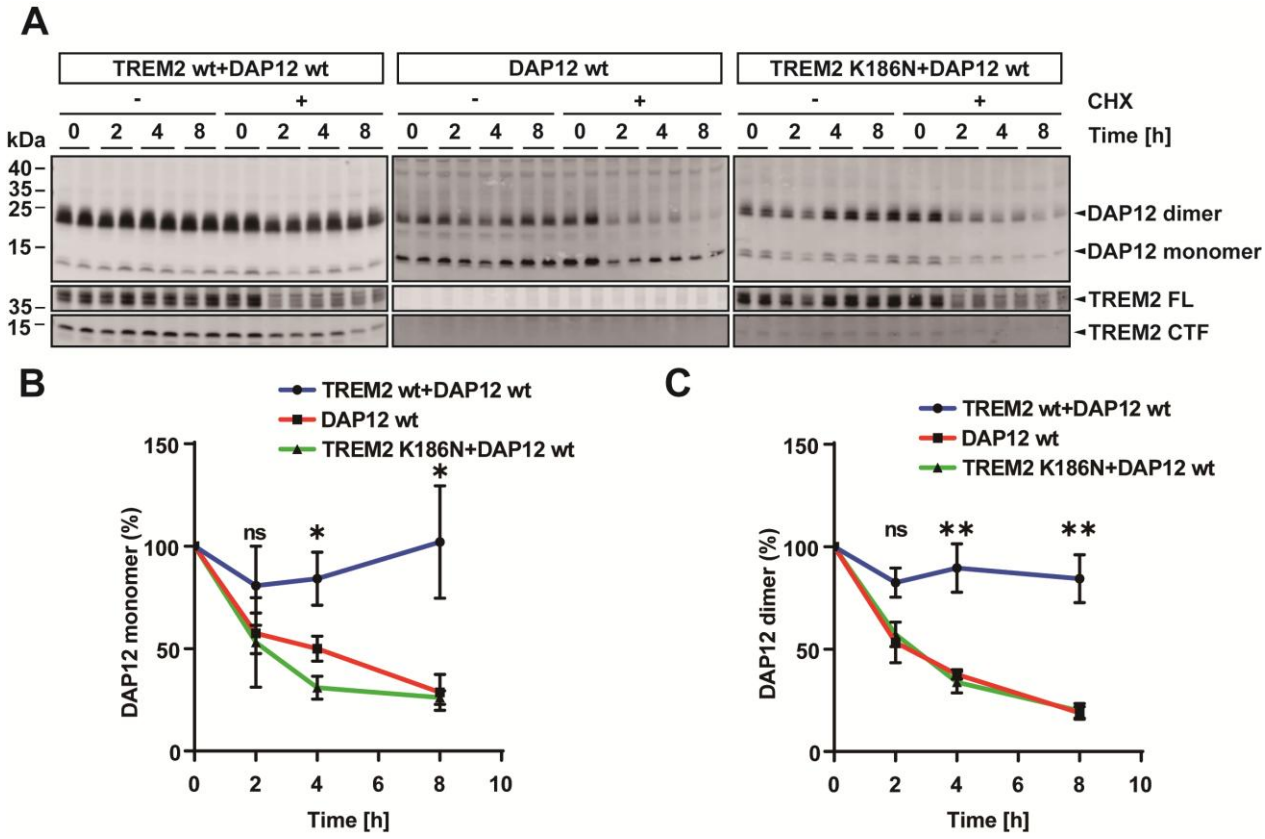

Fig. 3.5 Absence of TREM2 or the disease-associated TREM2 K186N destabilizes DAP12. (A) HEK293 Flp-In cells stably overexpressing the indicated proteins were incubated without (Ctrl) or with cycloheximide (100 µg/mL) for the indicated time points. Cellular membranes were isolated. DAP12 and TREM2 were detected by western immunoblotting. TREM2 FL: TREM2 full length protein; TREM2 CTF: TREM2 C-terminal fragment. (B)-(C) Quantification of DAP12 levels at the indicated time periods upon cell treatment with CHX (t=0 h was set a 100%). The level of DAP12 was normalized against the level of DAP12 in non-treated control cells at the corresponding time points. Data represent the Mean ± SEM of three independent experiments each performed with duplicate samples. One-way ANOVA (post hoc Tukey's multiple comparisons test). Statistical significance of differences at the individual time points is indicated by asterisks

(*p <0.05; **p <0.01; ns, not significant). No significant difference was observed between cells overexpressing DAP12 only or together with the TREM2 K186N mutant. Figure adapted from Liu et al. 2024.

3.6 The absence of TREM2 interaction increases degradation of DAP12 by the proteasome

Next, we wanted to characterize the degradation systems involved in DAP12 turn-over. There are two major pathways for protein degradation, the ubiquitin-proteasome pathway, which mainly degrades short-lived proteins and soluble misfolded proteins (Cao et al., 2019, Lee et al., 2013), and the autophagy-lysosomal pathway, which is responsible for degradation of entire organelles, protein aggregates, and cargo in cytoplasmic vesicular compartments (Nixon et al., 2005). In these experiments, lactacystin and MG132 were used as proteasome inhibitors, while lysosomal activity was inhibited by chloroquine. After 4 h treatment, lactacystin and MG132 had little if any effect on dimeric DAP12 levels in THP-1 wt cells (Fig. 3.6 A and C). In contrast, both proteasomal inhibitors strongly elevated levels of dimeric DAP12 in TREM2 ko cells, indicating that TREM2 deficiency caused increased proteasomal degradation of dimeric DAP12 (Fig. 3.6 A and C). Inhibition of proteasomal activity also slightly increased levels of monomeric DAP12 in both wt and TREM2 ko cells (Fig. 3.6 B and F). Notably, proteasomal inhibition also led to the accumulation of DAP12 trimers, particularly pronounced in TREM2 ko cells, albeit at a much lower level as compared to dimeric DAP12 (Fig. 3.6 A). Chloroquine had no effect on DAP12 levels in either genotype (Fig. 3.6 B, C, F and G). The treatment of THP-1 wt cells with lactacystin and MG132 decreased levels of full-length TREM2 (TREM2 FL, Fig. 3.6 D). In contrast, MG132 rather increased levels of the C-terminal fragments (CTFs) of TREM2 (Fig. 3.6 E). Cell treatment with lactacystin also tended to increase levels of TREM2 CTFs, but this effect was not statistically significant. TREM2 CTFs derive from the full-length protein by ectodomain shedding and remain inserted into cellular membranes (Kleinberger et al., 2014, Wunderlich et al., 2013). The inhibition of lysosomal activity by chloroquine had no significant effect on TREM2 CTFs (Fig. 3.6 E), suggesting that the degradation of TREM2 CTFs rather involves proteasomal activity than lysosomal activity (Liu et al., 2024).

Then, we also validated these results obtained from differentiated THP-1 cells by using HEK293 cells stably transfected with TREM2 wt+DAP12 wt, DAP12 wt alone, TREM2 K186N+DAP12 wt cDNA. The inhibition of proteasomal activity significantly increased levels of dimeric DAP12 in HEK293 cells expressing DAP12 alone or together with the TREM2 K186N mutant, but not in cells co-expressing TREM2 wt, while the lysosomal inhibitor, chloroquine didn't affect levels of dimeric DAP12 in all three conditions (Fig. 3.7 C, G and I). In line with the results obtained from THP-1 cells, levels of monomeric DAP12 were much lower as compared to that of dimeric DAP12 in HEK293 cell model with the overexpression of TREM2 and DAP12 variants (Fig. 3.7). Levels of monomeric DAP12 were significantly affected by proteasome inhibition only in cells co-expressing the TREM2 K186N mutant. Levels of monomeric DAP12 also tended to be increased in cells expressing only DAP12 or co-expressing DAP12 together with TREM2 wt, but the differences were not statistically significant (Fig. 3.7 B, F and H). DAP12 trimers were detectable in cells overexpressing TREM2 K186N and DAP12 wt upon treatment with proteasome inhibitors (Fig. 3.7 A) (Liu et al., 2024).

In cells co-expressing DAP12 wt with the TREM2 K186N variant, lactacystin tended to increase levels of TREM2 CTF while the treatment of MG132 significantly increased levels of TREM2 CTF (Fig. 3.7 K). The inhibition of lysosomal activity by chloroquine had no significant effect on TREM2 CTFs in both TREM2 wt or TREM2 K186N expressing cells (Fig. 3.7 K), suggesting that the degradation of TREM2 CTFs rather involves proteasomal activity than lysosomal activity. Together, these data demonstrate destabilization of DAP12 in the absence of TREM2 involving increased degradation by the proteasome. Proteasomal activity could also contribute to the degradation of TREM2 CTFs (Liu et al., 2024).

To prove that chloroquine indeed inhibited lysosomal activity under our experimental conditions, we detected APP CTFs that are known to be partially degraded by lysosomes (Haass et al., 1992, Karaca et al., 2014, Tamboli et al., 2011). Consistent with previous findings (Jaeger et al., 2010, Tien et al., 2016), APP CTFs accumulated upon cell treatment with chloroquine (Liu et al., 2024).

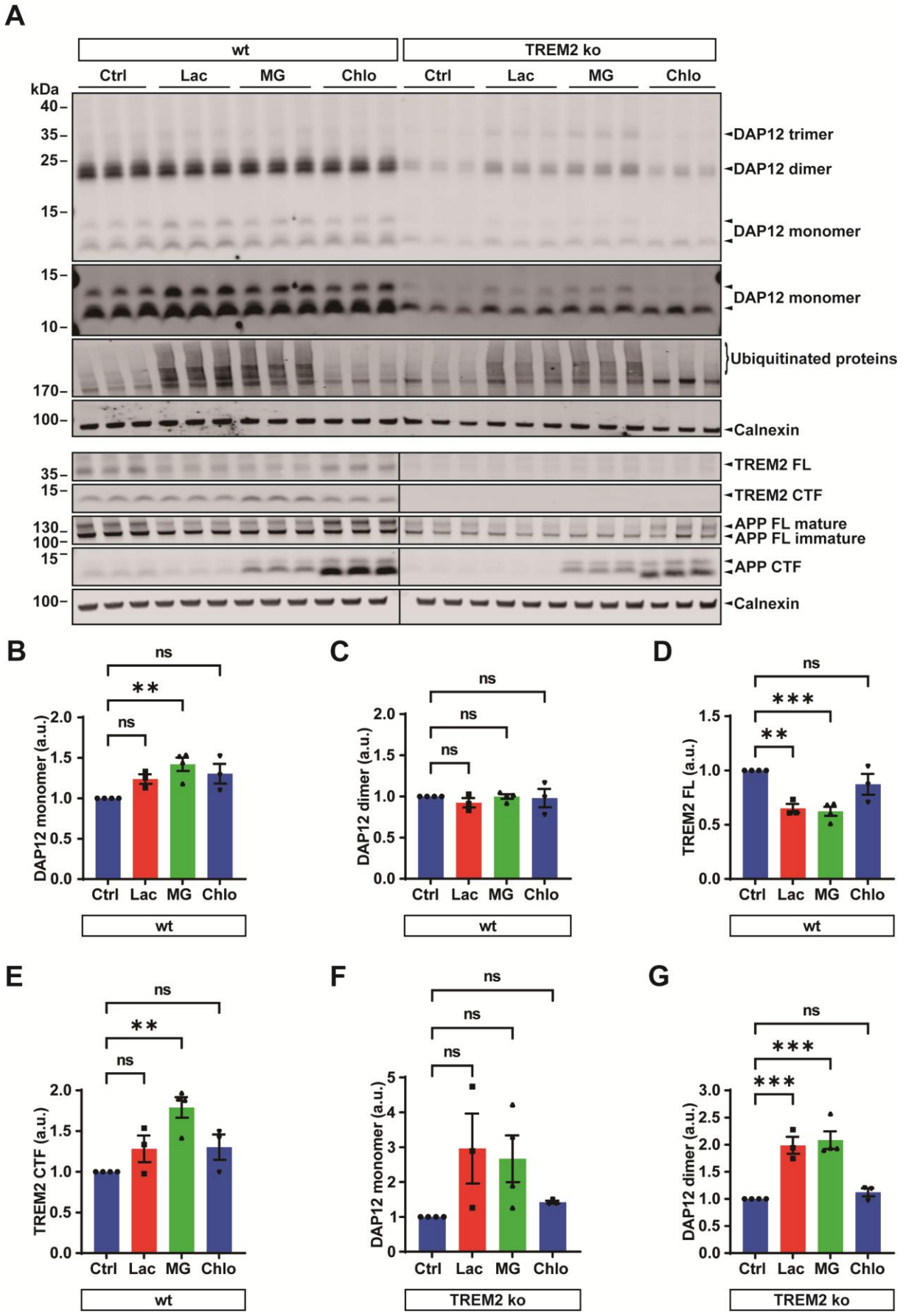
A
wt
TREM2 ko
Ctrl
Lac
MG
Chlo
kDa
40
35
25
15
10
170
100
DAP12 trimer
DAP12 dimer
DAP12 monomer
Ubiquitinated proteins
Calnexin
TREM2 FL
TREM2 CTF
APP FL mature
APP FL immature
APP CTF
B
DAP12 monomer (a.u.)
C
DAP12 dimer (a.u.)
D
TREM2 FL (a.u.)
E
TREM2 CTF (a.u.)
F
DAP12 monomer (a.u.)
G
DAP12 dimer (a.u.)
ns
**
***

Fig. 3.6 Characterization of degradation pathways for DAP12 and TREM2 in THP-1 cell model. (A) THP-1 wt and TREM2 ko cells were treated with MG132 (MG, 10 μM), lactacystin (Lac, 10 μM), chloroquine (Chlo, 50 μM) or without (Ctrl) for 4 h. Cellular membranes were isolated and the indicated proteins were detected by western immunoblotting. Ubiquitinated proteins and amyloid precursor protein (APP) were detected as positive controls for efficient inhibition of proteasomal and lysosomal activity, respectively. TREM2 FL: TREM2 full length protein; TREM2 CTF: the C-terminal fragment of TREM2. (B), (C), (D), (E), (F) and (G) Quantification of DAP12 monomer, dimer, and TREM2 FL and CTFs levels as shown in A. (B) DAP12 monomer in wt; (C) DAP12 dimer in wt; (D) TREM2 FL in wt; (E) TREM2 CTF in wt, (F) DAP12 monomer in TREM2 ko, (G) DAP12 dimer in TREM2 ko. Indicated proteins were normalized against the loading control protein calnexin. Mean ± SEM of three or four independent experiments each performed with duplicate or triplicate samples. One way ANOVA (post hoc Tukey's multiple comparisons test). *p <0.05, **p <0.01, ***p <0.001. Figure adapted from Liu et al. 2024.

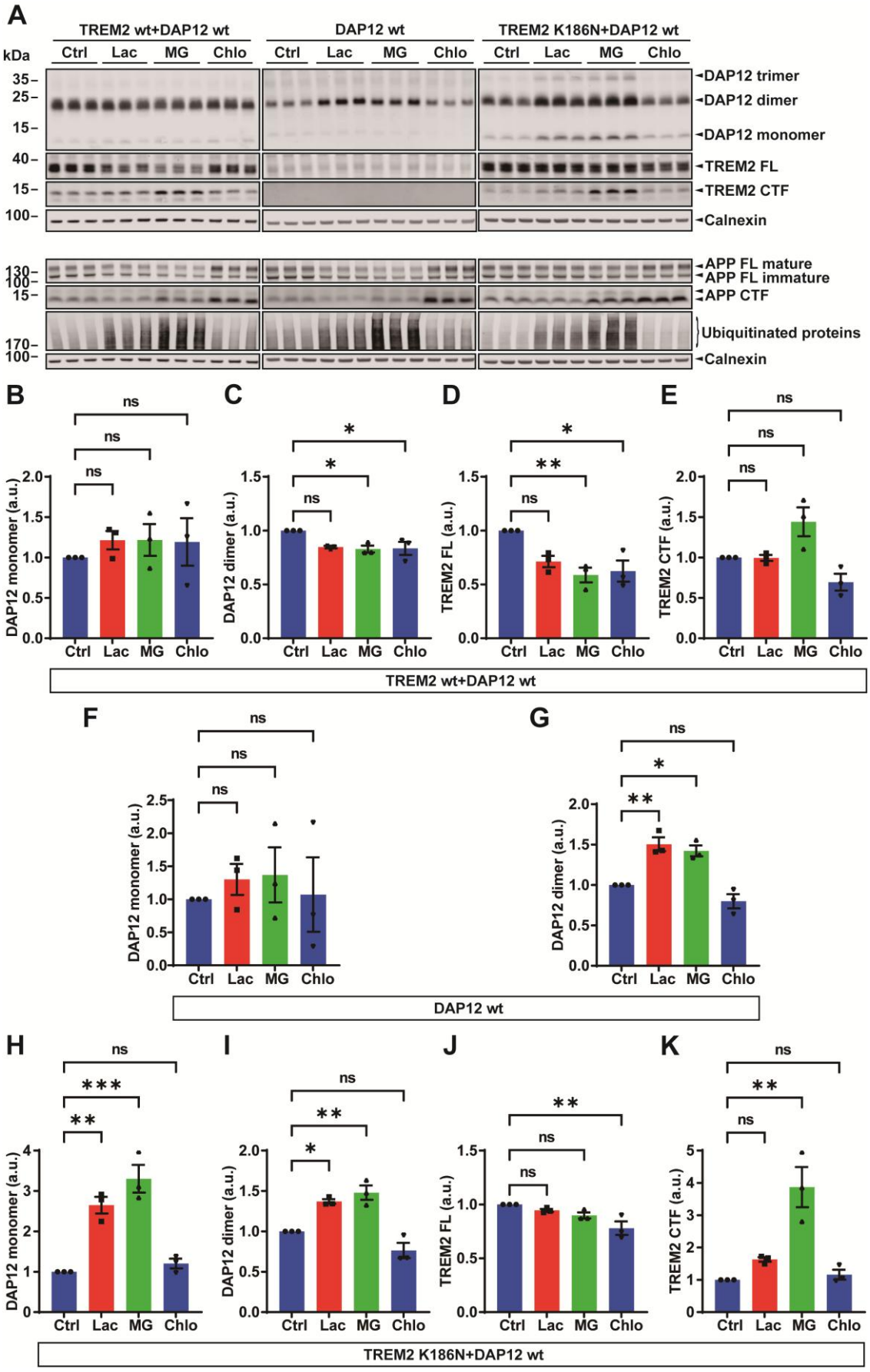
A
TREM2 wt+DAP12 wt
DAP12 wt
TREM2 K186N+DAP12 wt
Ctrl Lac MG Chlo
kDa
35
25
15
40
15
100
DAP12 trimer
DAP12 dimer
DAP12 monomer
TREM2 FL
TREM2 CTF
Calnexin
130
100
15
170
100
APP FL mature
APP FL immature
APP CTF
Ubiquitinated proteins
Calnexin
B
DAP12 monomer (a.u.)
C
DAP12 dimer (a.u.)
D
TREM2 FL (a.u.)
E
TREM2 CTF (a.u.)
ns
*
**
TREM2 wt+DAP12 wt
F
DAP12 monomer (a.u.)
G
DAP12 dimer (a.u.)
DAP12 wt
H
DAP12 monomer (a.u.)
I
DAP12 dimer (a.u.)
J
TREM2 FL (a.u.)
K
TREM2 CTF (a.u.)
***
TREM2 K186N+DAP12 wt

Fig. 3.7 Characterization of degradation pathways for DAP12 and TREM2 in HEK293 cells overexpressing TREM2 and DAP12 variants. (A) Cells overexpressing DAP12 wt alone or in combination with TREM2 wt or TREM2 K186N variants were treated with MG132 (MG, 10 µM), lactacystin (Lac, 10 µM), chloroquine (Chlo, 50 µM) or without (Ctrl) for 4 h. Cellular membranes were isolated and the indicated proteins were detected by western immunoblotting. Ubiquitinated proteins and amyloid precursor protein (APP) were detected as positive controls for efficient inhibition of proteasomal and lysosomal activity, respectively, TREM2 FL: TREM2 full length protein; TREM2 CTF: TREM2 C-terminal fragment. (B)-(K) Quantification of DAP12 monomer, dimer, TREM2 FL and CTFs levels. (B) DAP12 monomer in TREM2 wt-DAP12 wt; (C) DAP12 dimer in TREM2 wt-DAP12 wt; (D) TREM2 FL in TREM2 wt-DAP12 wt; (E) TREM2 CTF in TREM2 wt-DAP12 wt, (F) DAP12 monomer in DAP12 wt, (G) DAP12 dimer in DAP12 wt, (H) DAP12 monomer in TREM2 K186N-DAP12 wt; (I) DAP12 dimer in TREM2 K186N-DAP12 wt; (J) TREM2 FL in TREM2 K186N-DAP12 wt; (K) TREM2 CTF in TREM2 K186N-DAP12 wt. Indicated proteins were normalized to calnexin. Mean ± SEM of three independent experiments each performed with triplicate samples. One way ANOVA (post hoc Tukey's multiple comparisons test). *p <0.05, **p <0.01, ***p <0.001. Figure adapted from Liu et al. 2024.

3.7 Retention of unassembled DAP12 in early secretory compartments

Next, TREM2 and DAP12 were detected by immunocytochemistry. In TREM2 wt+DAP12 wt expressing cells, DAP12 mainly localized on the cell surface together with TREM2 (Fig. 3.8). DAP12 showed mainly intracellular vesicular localization and little if any expression at the plasma membrane in cells expressing no TREM2 or the TREM2 K186N mutation (Fig. 3.8). These data indicate that the interaction with TREM2 not only stabilizes DAP12, but is also required for efficient transport of DAP12 to the cell surface. It should be noted that the TREM2 K186N variant is still prominently detected at the plasma membrane, implying that DAP12 is not required for surface transport of TREM2 (Liu et al., 2024).

The subcellular localization of DAP12 was analyzed in more detail by co-staining for several marker proteins of distinct subcellular compartments. First, co-staining of DAP12 and alpha 1 sodium potassium ATPase (α1 Na+/K+ ATPase) confirmed localization of DAP12 at the cell surface in TREM2 wt-DAP12 wt expressing cells. The colocalization of DAP12 and α1 Na+/K+ ATPase was significantly reduced in cells that express DAP12 wt alone or together with the TREM2 K186N mutant (Fig. 3.9 A and E). DAP12 also colocalized with Giantin in TREM2 wt-DAP12 wt expressing cells, a marker for the Golgi compartment (Fig. 3.9 B and F). The colocalization of DAP12 and Giantin was significantly lower in cells expressing no TREM2. The colocalization of DAP12 and Giantin also tended to be decreased in TREM2 K186N-DAP12 wt expressing cells as compared to TREM2

wt-DAP12 wt expressing cells, although the difference was not statistically significant. More importantly, in cells expressing no TREM2 or the TREM2 K186N mutant, DAP12 showed strongly elevated colocalization with calnexin (Fig. 3.9 D and H) and ERGIC53 (Fig. 3.9 C and G), two marker proteins for the ER and the ER Golgi intermediate compartment, respectively. Together, these data indicate efficient retention and/or retrieval of DAP12 in compartments of the early secretory pathway when the protein is not incorporated into a complex with TREM2 (Liu et al., 2024).

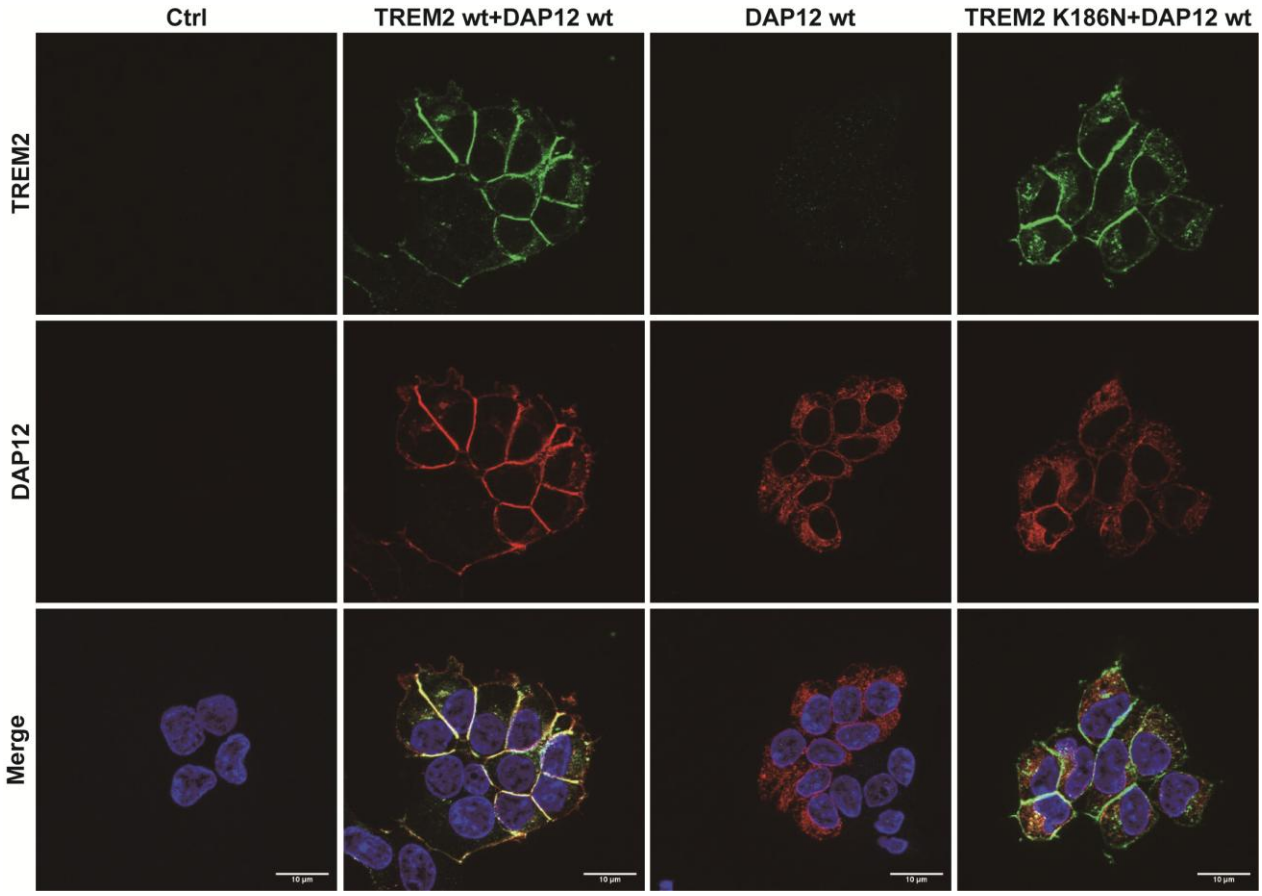

Fig. 3.8 Absence of TREM2 or the disease-associated TREM2 K186N reduces its expression at the cell surface. Immunocytochemical detection of DAP12 and TREM2 in HEK293 Flp-In cells stably expressing the indicated proteins. Representative images are shown. TREM2 (green) and DAP12 (red) were detected with antibodies 4B2A3 and D7G1X, respectively, and appropriate secondary antibodies as described in the Method section. Nuclei were stained with DAPI. Scale bar = 10 µm. Figure adapted from Liu et al. 2024.

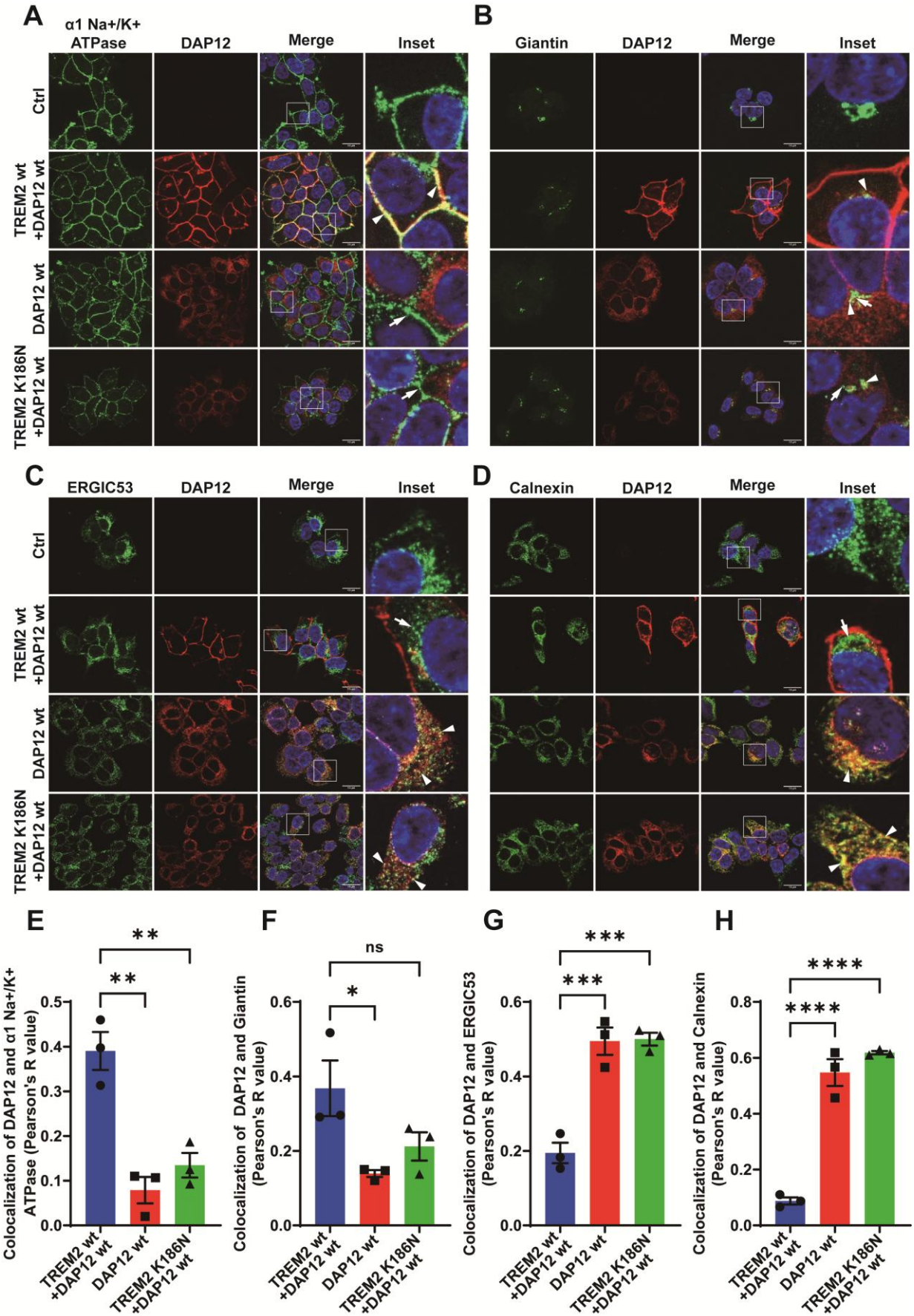
A
α1 Na+/K+ ATPase
DAP12
Merge
Inset
Ctrl
TREM2 wt +DAP12 wt
DAP12 wt
TREM2 K186N +DAP12 wt
B
Giantin
DAP12
Merge
Inset
C
ERGIC53
DAP12
Merge
Inset
D
Calnexin
DAP12
Merge
Inset
E
Colocalization of DAP12 and α1 Na+/K+ ATPase (Pearson's R value)
F
Colocalization of DAP12 and Giantin (Pearson's R value)
G
Colocalization of DAP12 and ERGIC53 (Pearson's R value)
H
Colocalization of DAP12 and Calnexin (Pearson's R value)
TREM2 wt +DAP12 wt
DAP12 wt
TREM2 K186N +DAP12 wt
ns

Fig. 3.9 DAP12 accumulates in early secretory compartments in the absence of TREM2 interaction. (A)-(D) Immunocytochemical detection of DAP12 in HEK293 Flp-In cells stably overexpressing DAP12 alone (DAP12) or together with TREM2 (TREM2+DAP12) or the TREM2 K186N mutant (TREM2 K186N+DAP12). Representative images are shown. Cells were co-stained for DAP12 (red) and the indicated marker proteins alpha 1 sodium potassium ATPase (α1 Na+/K+ ATPase, plasma membrane), giantin (cis- and medial-Golgi network), ERGIC53 (ER Golgi intermediate compartment) or calnexin (endoplasmic reticulum) (green). Nuclei were counterstained with DAPI. The colocalization of two proteins is indicated by arrow heads and the indicated marker proteins are indicated by arrows. Scale bar =10 µm. (E)-(H) Pearson's R value was measured for quantification of colocalization of DAP12 with the respective maker proteins. Values represent Mean ± SEM of three independent experiments. Each data point represents the mean value of an individual experiment. One way ANOVA (post hoc Tukey's multiple comparisons test). *p <0.05, **p <0.01, ***p <0.001, ****p <0.0001. Figure adapted from Liu et al. 2024.

3.8 The aspartic acid residue in the transmembrane domain is critical for retention of unassembled DAP12 in early secretory compartment

Previous studies found that charged or polar amino acid residues in TMDs could mediate the retention of select proteins in or retrieval to the ER (Bonifacino et al., 1991). To explore whether the single aspartic acid residue (D) at position 50 in the TMD of DAP12 is potentially responsible for the retention of unassembled DAP12, we mutated this residue to an alanine residue (A). It has been shown previously that this mutation prevents electrostatic interaction, and thus, the complex formation with TREM2 (Feng et al., 2006, Zhong et al., 2015). This effect was verified by coimmunoprecipitation assays (Fig. 3.3 B). It has also been shown that overexpressed DAP12 D50A with an N-terminal FLAG-tag in Ba/F3 cells could be detected by flow cytometry with an anti-FLAG antibody indicating expression of this mutant at the cell surface, in contrast to the DAP12 wt protein (Lanier et al., 1998a). Our immunocytochemical analysis showed similar results as the DAP12 D50A variant with or without additional TREM2 expression partially localized at the cell surface (Fig. 3.10). Then, we analyzed the subcellular localization of DAP12 wt and the DAP12 D50A mutant in the presence or absence of TREM2 in more detail. Interestingly, in cells expressing DAP12 D50A alone or together with TREM2 wt, DAP12 D50A was detected at the plasma membrane and in the Golgi compartment as indicated by the colocalization with α1 Na+/K+ ATPase (Fig. 3.11 A and E) and with Giantin (Fig. 3.11 B and F), respectively. The colocalization of DAP12 D50A with α1 Na+/K+ ATPase (Fig.

3.11 A and E) or with Giantin (Fig. 3.11 B and F) was very similar as that for DAP12 wt when co-expressed with TREM2 wt, and significantly higher than that of DAP12 wt in the absence of TREM2. Moreover, the colocalization of DAP12 D50A with calnexin (Fig. 3.11 D and H) and ERGIC53 (Fig. 3.11 C and G) was reduced as compared to that of the DAP12 wt protein in the absence of TREM2, even it was not a significant decrease for ERGIC53. As DAP12 D50A does not interact with TREM2, it can also be ruled out that TREM2 wt (when co-expressed) assisted in the transport of this DAP12 mutant in the secretory pathway. Together, these data indicate that the negatively charged D50 residue in the transmembrane domain plays a crucial role in the retention of DAP12 in early secretory compartments in the absence of proper interaction with TREM2 (Liu et al., 2024).

Retention of transmembrane proteins, in particular of some components of multiprotein complexes, can be mediated by RER1 that recognizes polar amino acids within their TMDs (Kaether et al., 2007, Sato et al., 2003). Thus, the potential interaction of RER1 with DAP12 was first tested by co-immunoprecipitation (Fig. 3.12 A). DAP12 wt efficiently co-precipitated with RER1 in the absence of TREM2. In contrast, co-expression of DAP12 wt with TREM2 strongly reduced the co-precipitation of RER1 with DAP12. The co-precipitation of RER1 with DAP12 D50A, either expressed alone or together with TREM2, was also strongly reduced, indicating that RER1 recognizes the polar D50 residue of DAP12 when it is not interacting with TREM2 (Liu et al., 2024).

We also noticed that DAP12 wt, but not DAP12 D50A, formed increased levels of SDS resistant trimers and tetramers when expressed in the absence of TREM2 (Fig. 3.3 A and B, Fig. 3.12 A). A similar observation was made previously, and it had been proposed that DAP12 interacting immunoreceptors compete with additional DAP12 molecules for interaction with covalently linked DAP12 dimers during complex assembly (Knoblich et al., 2015). However, further work is required to dissect whether oligomerization of DAP12 in the absence of TREM2 modulates the interaction with RER1. The interaction of DAP12 and RER1 was also confirmed in macrophage-like differentiated THP-1 cells endogenously expressing both proteins (Fig. 3.12 B and C) (Liu et al., 2024).

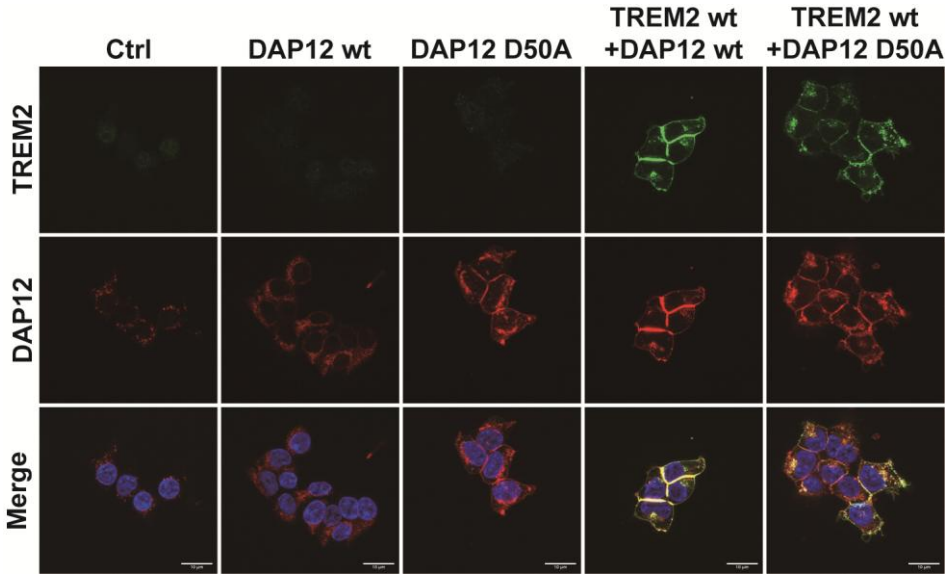

Fig. 3.10 Immunocytochemical detection of DAP12 in HEK293 Flp-In cells stably overexpressing DAP12 wt or DAP12 D50A with or without TREM2 wt. Non-transfected HEK293 Flp-In cells as control. Representative images are shown. TREM2 (4B2A3 antibody) is shown in green and DAP12 (D7G1X antibody) in red. Nuclei were counterstained with DAPI. Scale bar = 10 µm. Figure adapted from Liu et al. 2024.

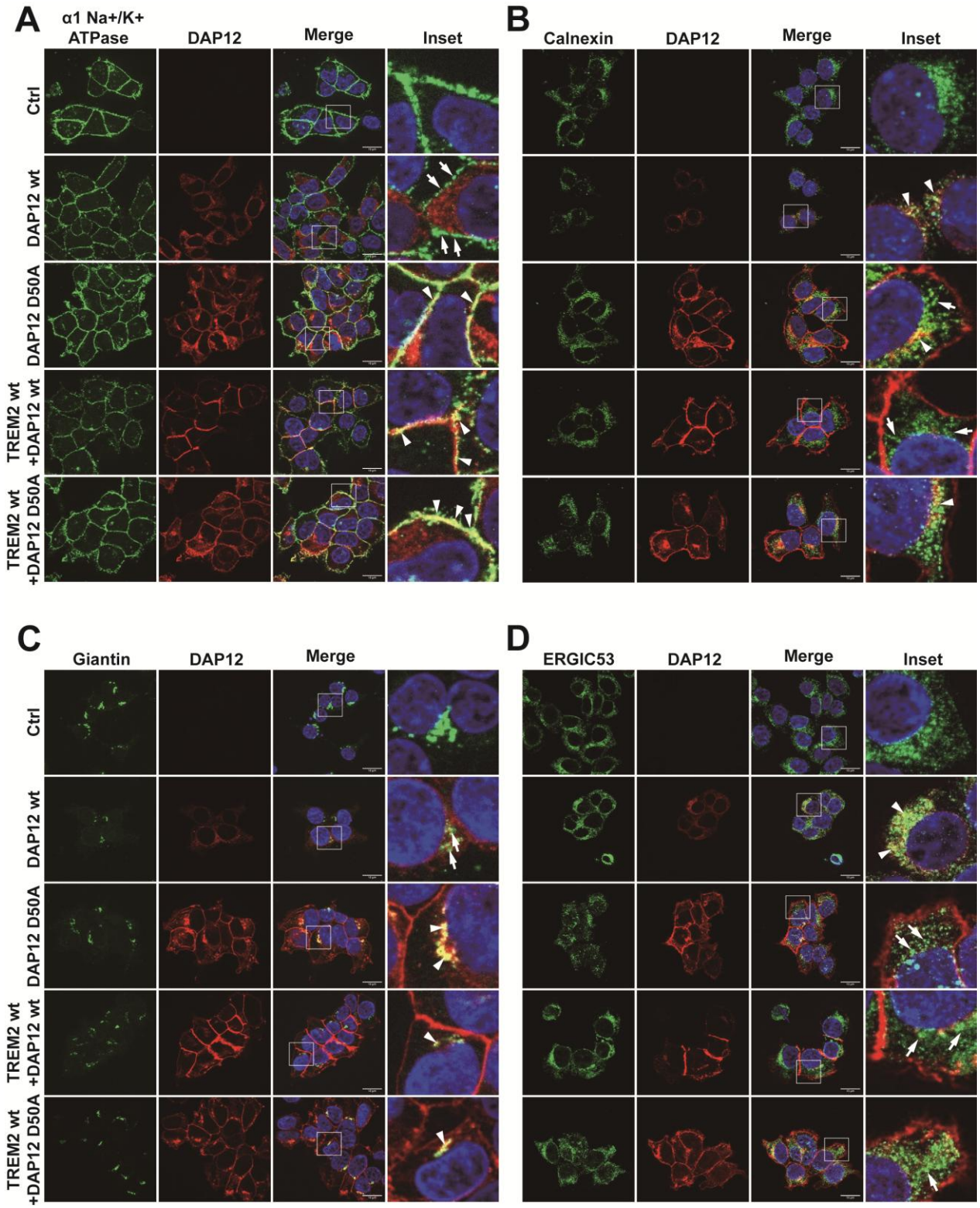
A
α1 Na+/K+ ATPase
DAP12
Merge
Inset
B
Calnexin
DAP12
Merge
Inset
C
Giantin
DAP12
Merge
D
ERGIC53
DAP12
Merge
Inset
Ctrl
DAP12 wt
DAP12 D50A
TREM2 wt +DAP12 wt
TREM2 wt +DAP12 D50A

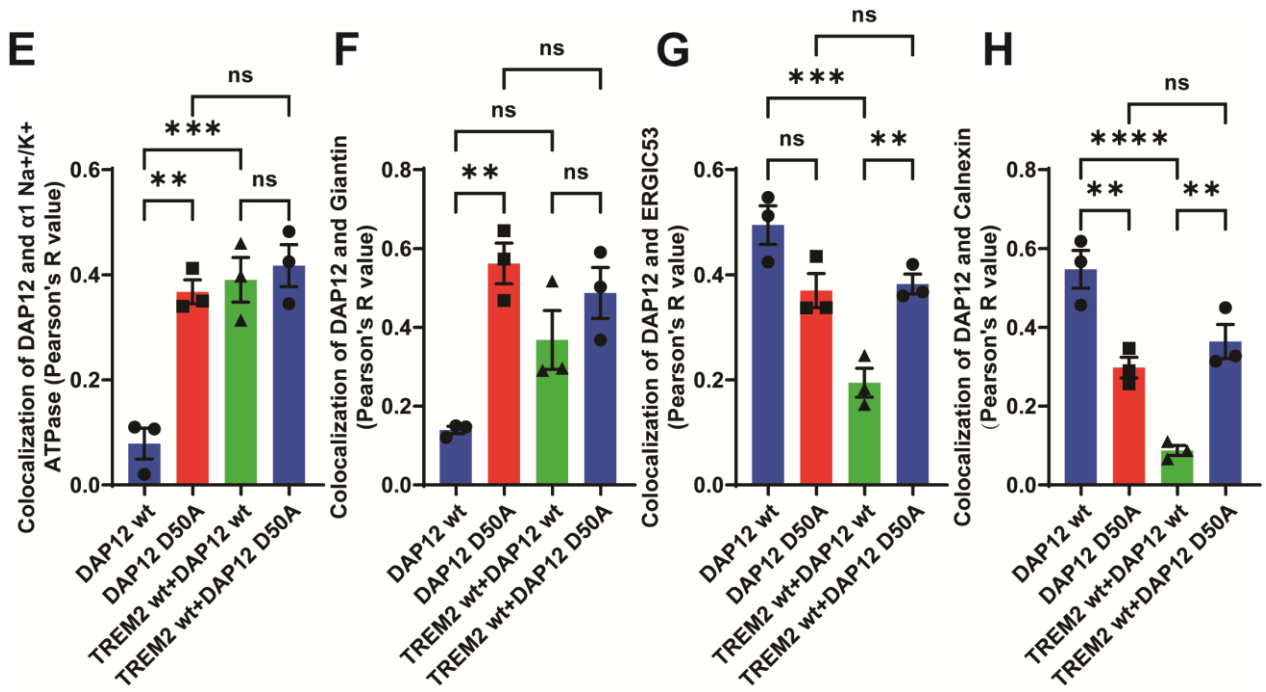

Fig. 3.11 Critical role of D50 within the transmembrane domain of DAP12 for the retention in early secretory compartments. (A)-(D) subcellular localization of DAP12 in HEK293 cells stably transfected with DAP12 D50A variants. HEK293 Flp-In cells were stably transfected with DAP12 wt, DAP12 D50A, TREM2 wt+DAP12 wt and TREM2 wt+DAP12 D50A constructs. Non-transfected HEK293 Flp-In cells (Ctrl) were used as control. Shown are representative images. Cells were co-stained for DAP12 (red) and the indicated marker proteins alpha 1 sodium potassium ATPase (α1 Na+/K+ ATPase, plasma membrane), giantin (cis- and medial-Golgi network), ERGIC53 (ER Golgi intermediate compartment) or calnexin (endoplasmic reticulum) (green). Nuclei were counterstained with DAPI. The colocalization of two proteins is indicated by arrow heads and the indicated marker proteins are indicated by arrows. Scale bar =10 µm. (E)-(H) Pearson's R value was measured for quantification of colocalization of DAP12 with the respective maker proteins. Values represent Mean ± SEM of three independent experiments. Each data point represents the mean value of an individual experiment. One way ANOVA (post hoc Tukey's multiple comparisons test). **p <0.01, ***p <0.001, ****p <0.0001. Figure adapted from Liu et al. 2024.

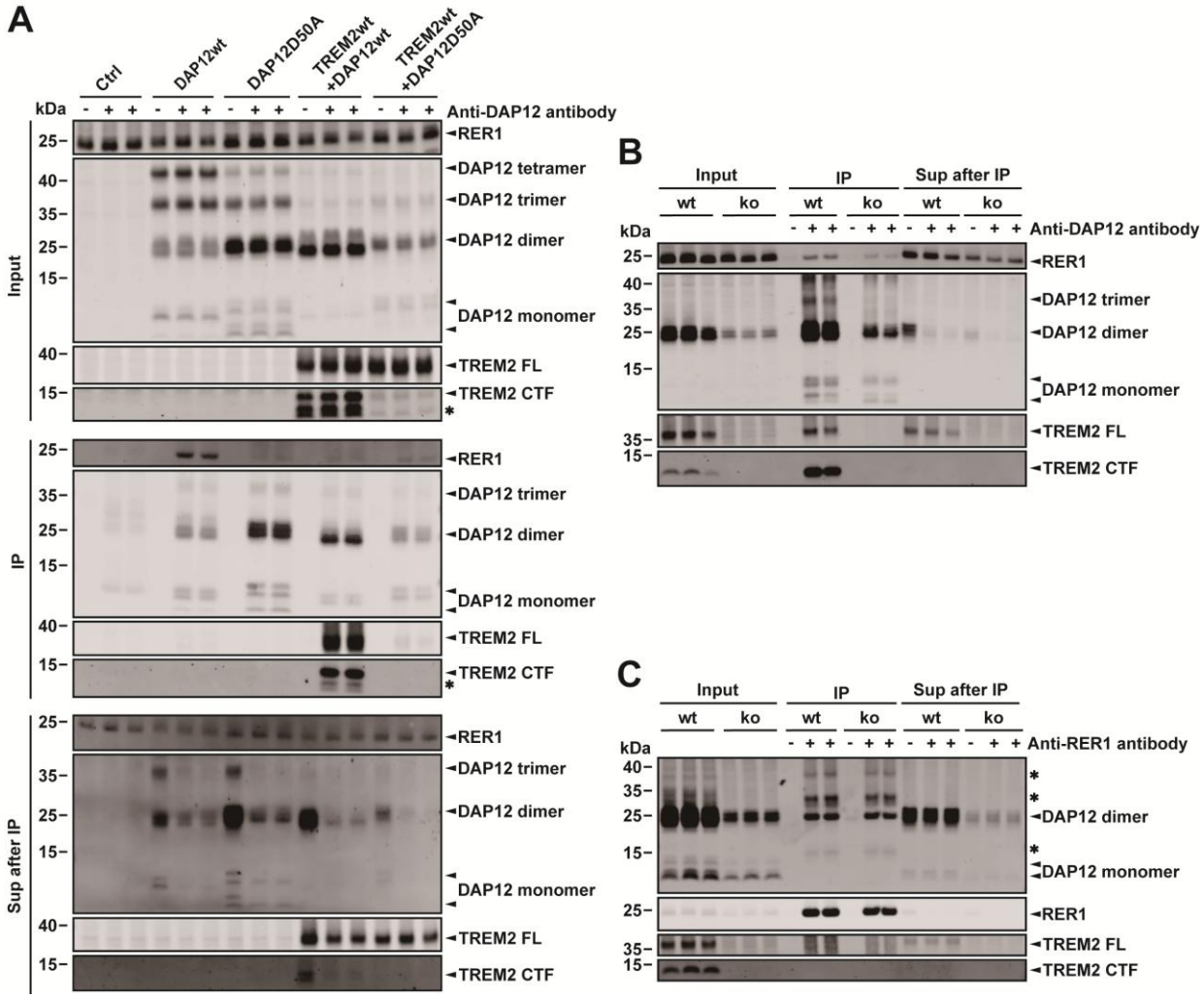

Fig. 3.12 Interaction of DAP12 with RER1. (A)–(C) HEK293 cells overexpressing the indicated proteins (A) or macrophage-like differentiated THP-1 wt and TREM2 ko cells (B and C) were subjected to co-immunoprecipitation as described in the Methods section. Cellular membranes were isolated and the indicated proteins in immunoprecipitate (IP) and the remaining supernatant (Sup after IP) were detected by western immunoblotting. The 'Input' represents an aliquot of the cell lysate before IP containing 20 µg of total protein Three independent experiments were performed. TREM2 FL: TREM2 full length protein; TREM2 CTF: TREM2 C-terminal fragment. The bands marked with asterisks (*) are unspecific signals from the anti-RER1 antibody which was used in the IP. Figure adapted from Liu et al. 2024.

3.9 RGR motif in the cytoplasmic domain does not affect the retention of unassembled DAP12 in early secretory compartments

An arginine-based RXR retrieval signal in the cytoplasmic domains of the subunits of some heteromeric membrane proteins, such as potassium channels, could also mediate

retention/retrieval of the unassembled proteins by the interaction with COPI (Michelsen et al., 2005). An RXR (70RGR72) motif is also present in the cytoplasmic domain of DAP12. To explore whether this RXR motif plays a role in the retention or retrieval of unassembled DAP12, the R residues at position 70 and 72 were mutated to alanine residues (A). Immunocytochemical analysis showed that DAP12 70AGA72 without the co-expression of TREM2 was localized intracellularly, while DAP12 70AGA72 with the co-expression of TREM2 was expressed on the cell surface, which was similar to the localization of the DAP12 wt. Intracellular localization was also observed with a DAP12 variant with combined mutations of the D50A, and the R70A and R72A residues (Fig. 3.13).

Then, we further investigated the subcellular localization of DAP12 70AGA72 mutant with or without the co-expression of TREM2 as well as DAP12 D50A 70AGA72 mutant in the absence of TREM2 by analyzing the colocalization of DAP12 with maker proteins for different organelles and plasma membrane. We observed that DAP12 70AGA72 mutant without the co-expression of TREM2 was mainly detected in the ER and ERGIC as indicated by the colocalization with calnexin (Fig. 3.14 F and H) and with ERGIC53 (Fig. 3.14 E and G), respectively, which was very similar as that for DAP12 wt without the co-expression of TREM2 (Fig. 3.14 E, F, G, and H). DAP12 70AGA72 mutant with the co-expression of TREM2 was detected at the cell surface as indicated by the colocalization with α1 Na+/K+ ATPase (Fig. 3.14 A and C) and the colocalization of DAP12 70AGA72 with α1 Na+/K+ ATPase in the presence of TREM2 was significantly higher than that for DAP12 70AGA72 in the absence of TREM2 (Fig. 3.14 A and C) while the colocalization of DAP12 70AGA with calnexin (Fig. 3.14 F and H) and ERGIC53 (Fig. 3.14 E and G) in the presence of TREM2 was significantly reduced as compared to that of the DAP12 70AGA72 protein in the absence of TREM2. Moreover, the double mutations of DAP12, DAP12 D50A 70AGA72 was detected in early Golgi structures, as indicated by the colocalization with Giantin (Fig. 3.14 B and D), which was similar with that for DAP12 D50A mutant (Fig. 3.14 B and D). However, DAP12 D50A 70AGA was also partially colocalized with ERGIC53 (Fig. 3.14 E and G) and calnexin (Fig. 3.14 F and H), and the colocalization of DAP12 D50A 70AGA with ERGIC53 and calnexin was higher than that for DAP12 D50A mutant, even it was not a significant increase for calnexin.

Together, these data indicate that the RGR motif in the intracellular domain had little effect on the subcellular localization of DAP12 in early secretory compartments.

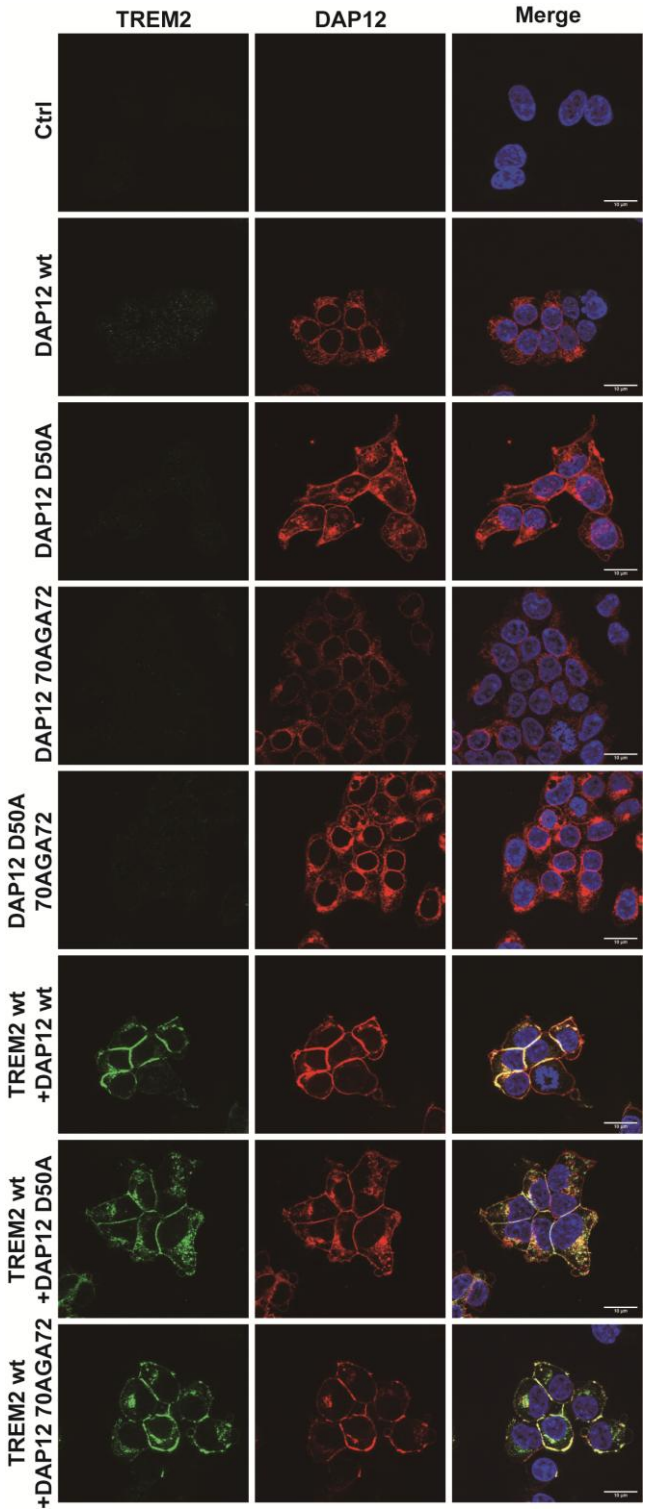

Fig. 3.13 Immunocytochemical detection of DAP12 in HEK293 Flp-In cells stably overexpressing DAP12 wt, DAP12 D50A or DAP12 70AGA with or without TREM2 wt. HEK293 Flp-In cells were stably transfected with DAP12 wt, DAP12 D50A, DAP12 70AGA72, DAP12 D50A 70AGA72, TREM2 wt+DAP12 wt, TREM2 wt+DAP12 D50A and TREM2 wt+DAP12 70AGA72 constructs. Non-transfected HEK293 Flp-In cells as control. Representative images are shown. TREM2 (4B2A3 antibody) is shown in green and DAP12 (D7G1X antibody) in red. Nuclei were counterstained with DAPI. Scale bar = 10 µm.

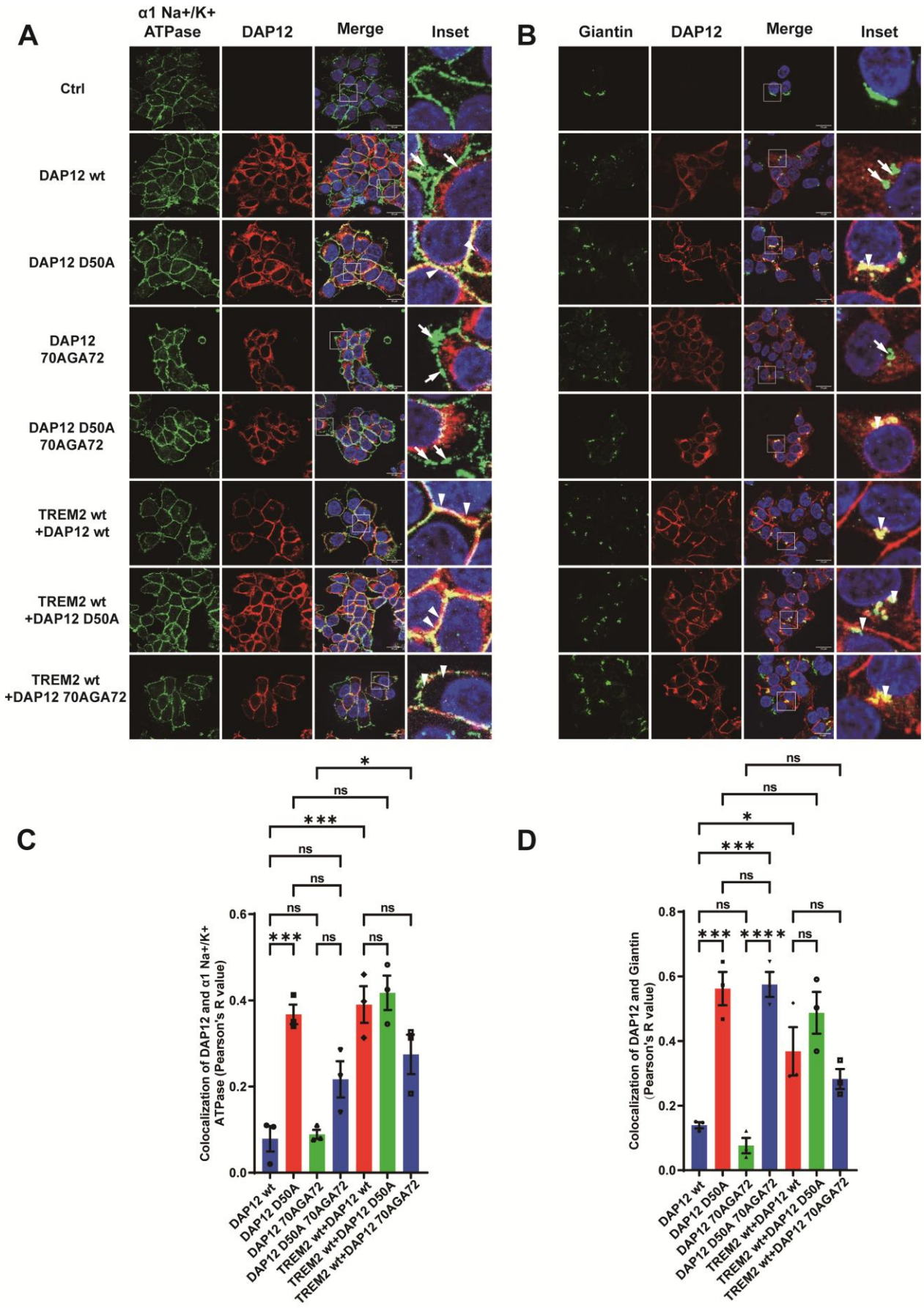
A
α1 Na+/K+ ATPase
DAP12
Merge
Inset
Ctrl
DAP12 wt
DAP12 D50A
DAP12 70AGA72
DAP12 D50A 70AGA72
TREM2 wt +DAP12 wt
TREM2 wt +DAP12 D50A
TREM2 wt +DAP12 70AGA72
B
Giantin
DAP12
Merge
Inset
C
Colocalization of DAP12 and α1 Na+/K+ ATPase (Pearson's R value)
D
Colocalization of DAP12 and Giantin (Pearson's R value)
DAP12 wt
DAP12 D50A
DAP12 70AGA72
DAP12 D50A 70AGA72
TREM2 wt+DAP12 wt
TREM2 wt+DAP12 D50A
TREM2 wt+DAP12 70AGA72

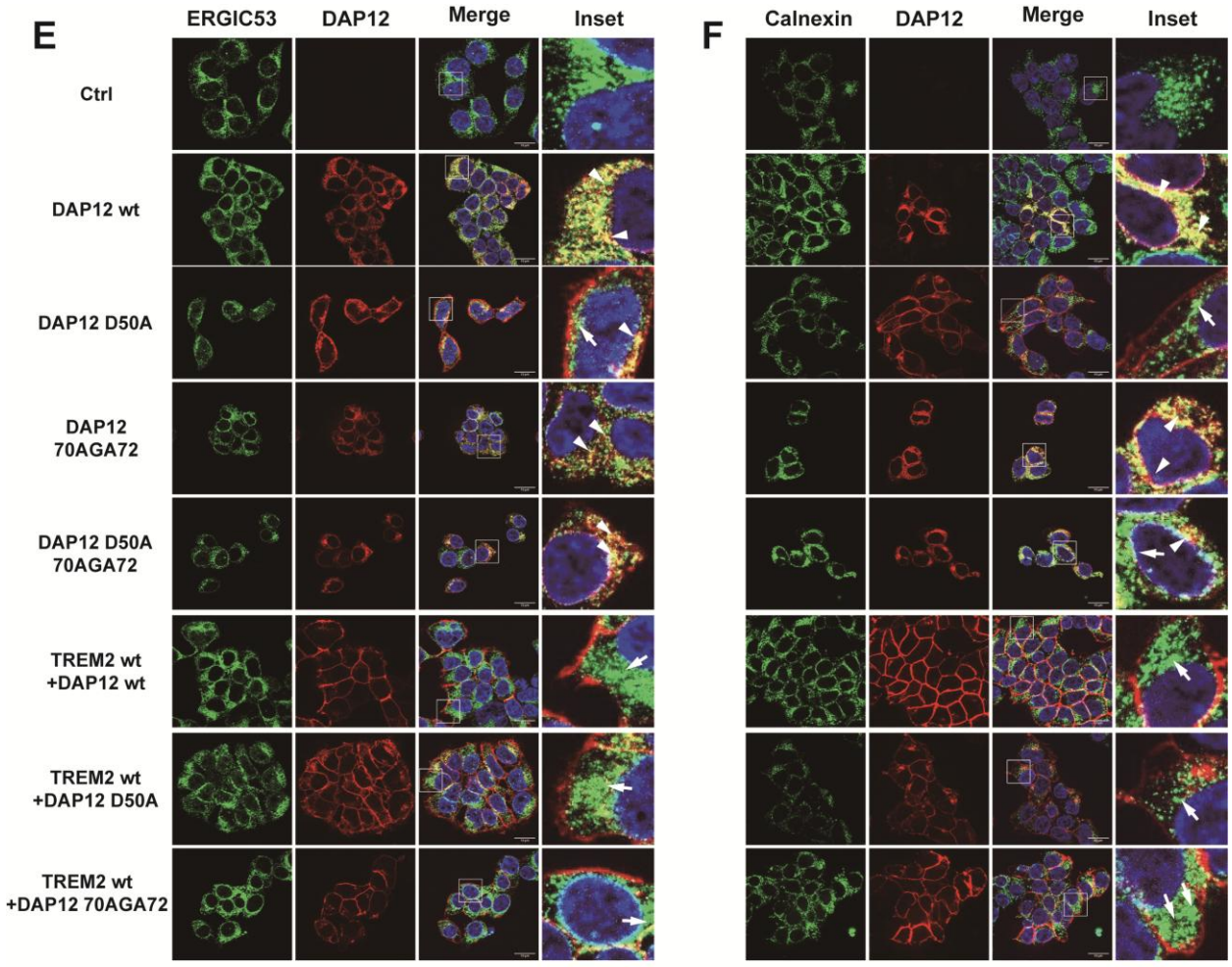
E
ERGIC53
DAP12
Merge
Inset
Ctrl
DAP12 wt
DAP12 D50A
DAP12 70AGA72
DAP12 D50A 70AGA72
TREM2 wt +DAP12 wt
TREM2 wt +DAP12 D50A
TREM2 wt +DAP12 70AGA72
F
Calnexin
DAP12
Merge
Inset

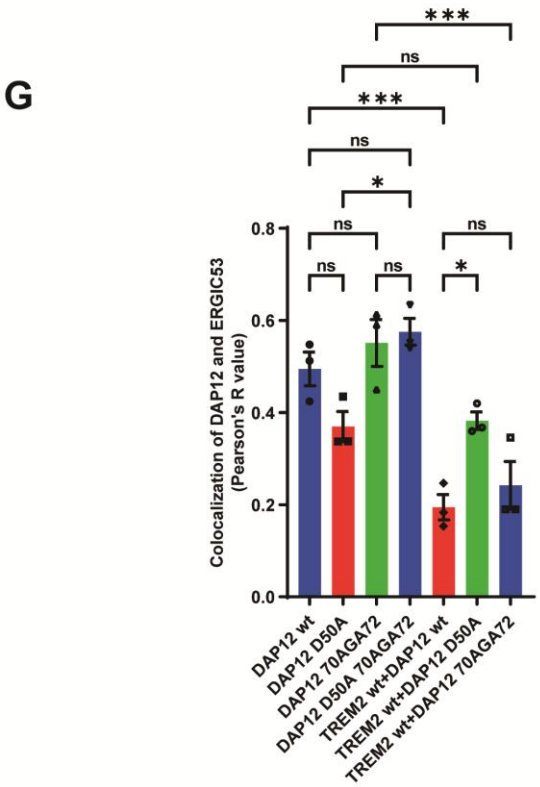
G
Colocalization of DAP12 and ERGIC53 (Pearson's R value)
0.0
0.2
0.4
0.6
0.8
***
ns
***
ns
*
ns
ns
ns
*
DAP12 wt
DAP12 D50A
DAP12 70AGA72
DAP12 D50A 70AGA72
TREM2 wt+DAP12 wt
TREM2 wt+DAP12 D50A
TREM2 wt+DAP12 70AGA72

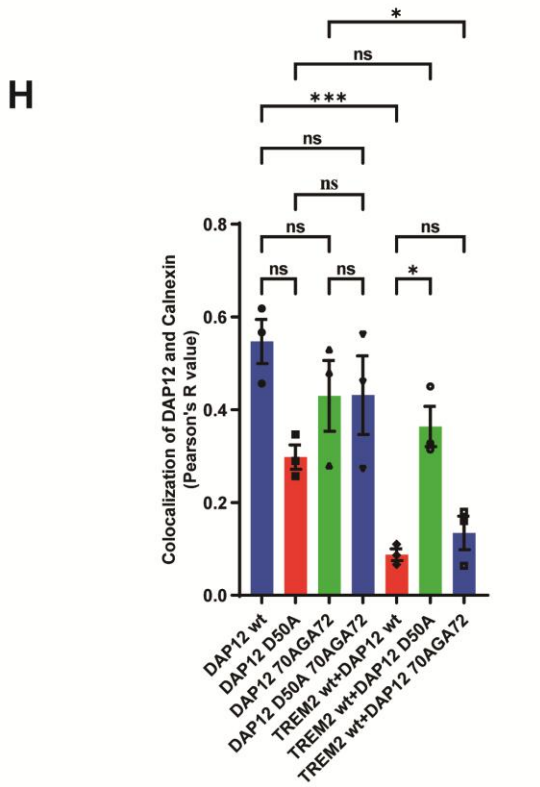
H
Colocalization of DAP12 and Calnexin (Pearson's R value)
0.0
0.2
0.4
0.6
0.8
*
ns
***
ns
ns
ns
ns
ns
*
DAP12 wt
DAP12 D50A
DAP12 70AGA72
DAP12 D50A 70AGA72
TREM2 wt+DAP12 wt
TREM2 wt+DAP12 D50A
TREM2 wt+DAP12 70AGA72

Fig. 3.14 RGR motif in the cytoplasmic domain doesn't affect the retention of unassembled DAP12 in early secretory compartments. (A), (B), (E) and (F) subcellular localization of DAP12 in HEK293 cells stably transfected with DAP12 D50A, DAP12 70AGA72 and DAP12 D50A 70AGA72 variants. HEK293 Flp-In cells were stably transfected with DAP12 wt, DAP12 D50A, DAP12 70AGA72, DAP12 D50A 70AGA72, TREM2 wt+DAP12 wt, TREM2 wt+DAP12 D50A and TREM2 wt+DAP12 70AGA72 constructs. Non-transfected HEK293 Flp-In cells (Ctrl) were used as control. Shown are representative images. Cells were co-stained for DAP12 (red) and the indicated marker proteins alpha 1 sodium potassium ATPase (α1 Na+/K+ ATPase, plasma membrane), giantin (cis- and medial-Golgi network), ERGIC53 (ER Golgi intermediate compartment) or calnexin (endoplasmic reticulum) (green). Nuclei were counterstained with DAPI. The colocalization of two proteins is indicated by arrow heads and the indicated marker proteins are indicated by arrows. Scale bar =10 µm. (C), (D), (G) and (H) Pearson's R value was measured for quantification of colocalization of DAP12 with the respective maker proteins. Values represent Mean ± SEM of three independent experiments. Each data point represents the mean value of an individual experiment. One way ANOVA (post hoc Tukey's multiple comparisons test). *p <0.05, ***p <0.001, ****p <0.0001.

3.10 RER1 deletion strongly decreases protein levels of DAP12 and TREM2

To further explore the role of RER1 in TREM2-DAP12 assembly, we knocked out the RER1 gene in THP-1 cells by CRISPR/CAS9 technology, and selected single cell clones by limiting dilution assay. To check the knock out RER1, membrane fractions of cells were isolated and analyzed by western immunoblotting. Several different cell clones had no detectable RER1 protein expression compared with wt THP-1 cells, respectively (Fig. 3.15 A). DNA sanger sequencing showed that one of the ko clones, R1C7, has a 14 base pair deletion and was used for the following experiments (Fig. 3.15 B).

Surprisingly, the deletion of RER1 led to decreased levels of both, DAP12 and TREM2, in differentiated THP-1 cells (Fig. 3.15 C-F). The strong decrease of both proteins was not associated with significant changes of DAP12 and TREM2 mRNA levels, although there was a trend to decreased TREM2 mRNA expression (Fig. 3.15 G and H) (Liu et al., 2024).

CHX chase assay were performed to investigate if the strong decrease of DAP12 and TREM2 in RER1 ko cells is due to low protein stability. The results showed that there was no significant difference of DAP12 turnover between wt and RER1 ko cells, indicating that RER1 deletion might not affect DAP12 turnover (Fig. 3.16 A-C). In addition, the remaining TREM2 FL in RER1 ko cells after CHX treatment for 4 h was significantly more than that

in wt cells, indicating that RER1 deletion decreased the turnover of TREM2 FL (Fig. 3.16 D) (Liu et al., 2024).

Notably, proteasomal inhibition (by MG132 treatment) partially stabilized DAP12 dimer in RER1 ko cells (Fig. 3.17 A-C, E-F). Both proteasomal and lysosomal inhibition did not increase the level of TREM2 FL in RER1 ko cells, indicating that proteasomal and lysosomal degradation is not involved in the degradation of TREM2 in RER1 ko cells (Fig. 3.17 A, D and G). However, additional posttranscriptional and/or posttranslational mechanisms could contribute to the strong decrease of DAP12 and TREM2 proteins in RER1 ko cells (Liu et al., 2024).

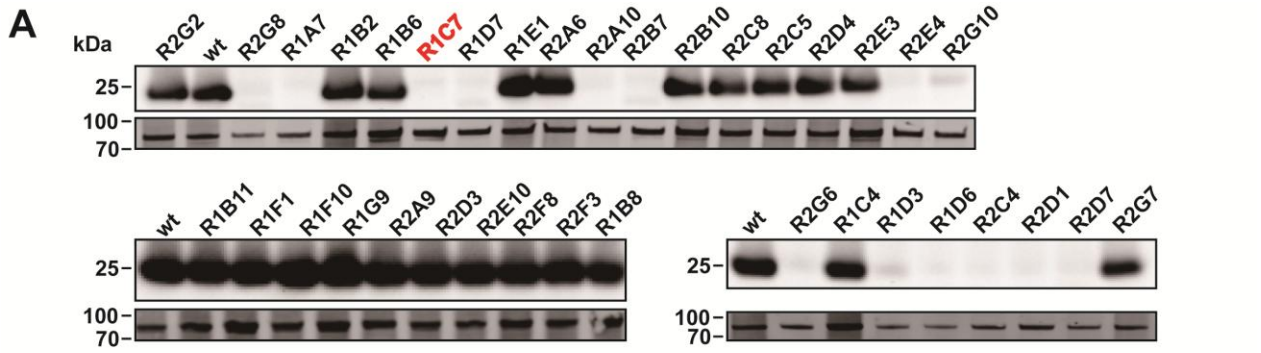
A
kDa
R2G2
wt
R2G8
R1A7
R1B2
R1B6
R1C7
R1D7
R1E1
R2A6
R2A10
R2B7
R2B10
R2C8
R2C5
R2D4
R2E3
R2E4
R2G10
25
100
70
wt
R1B11
R1F1
R1F10
R1G9
R2A9
R2D3
R2E10
R2F8
R2F3
R1B8
wt
R2G6
R1C4
R1D3
R1D6
R2C4
R2D1
R2D7
R2G7

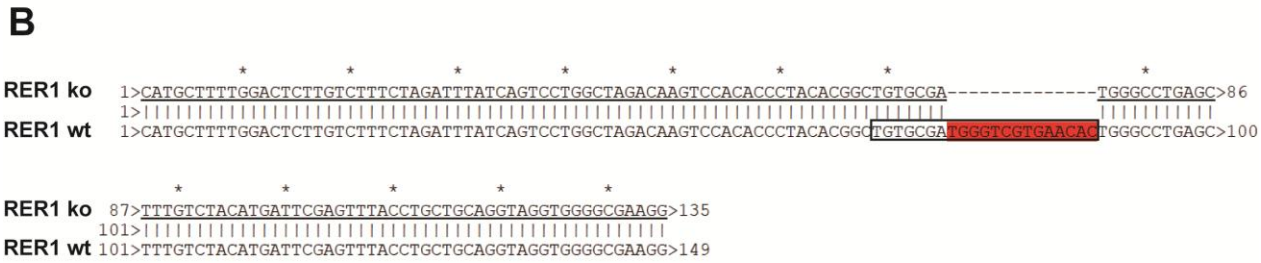
B
RER1 ko 1>CATGCTTTTGGACTCTTGTCTTTCTAGATTTATCAGTCCTGGCTAGACAAGTCCACACCCTACACGGCTGTGCGA----------TGGGCCTGAGC>86
RER1 wt 1>CATGCTTTTGGACTCTTGTCTTTCTAGATTTATCAGTCCTGGCTAGACAAGTCCACACCCTACACGGCTGTGCGAAGGGTCGTGAACACTGGGCCTGAGC>100
RER1 ko 87>TTTGTCTACATGATTCGAGTTTACCTGCTGCAGGTAGGTGGGGCGAAGG>135
RER1 wt 101>TTTGTCTACATGATTCGAGTTTACCTGCTGCAGGTAGGTGGGGCGAAGG>149

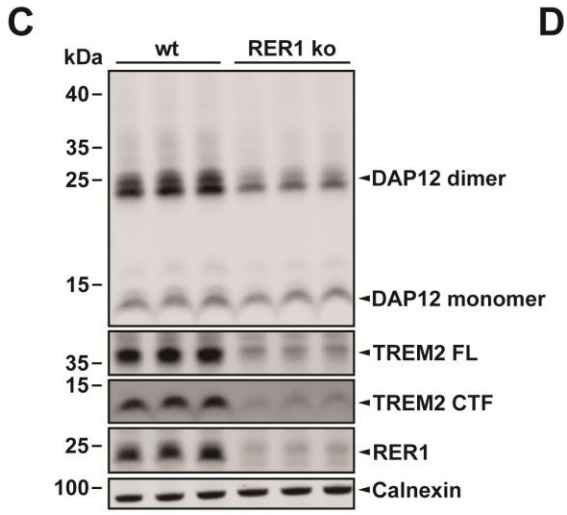
C
kDa
wt
RER1 ko
40
35
25
15
35
15
25
100
DAP12 dimer
DAP12 monomer
TREM2 FL
TREM2 CTF
RER1
Calnexin

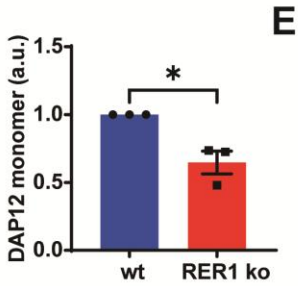
D
DAP12 monomer (a.u.)
1.5
1.0
0.5
0.0
*
wt
RER1 ko

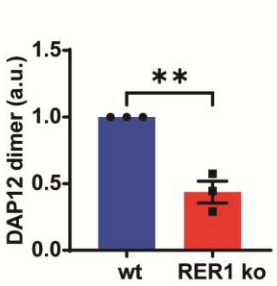
E
DAP12 dimer (a.u.)
1.5
1.0
0.5
0.0
**
wt
RER1 ko

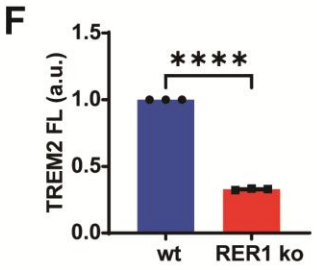
F
TREM2 FL (a.u.)
1.5
1.0
0.5
0.0
****
wt
RER1 ko

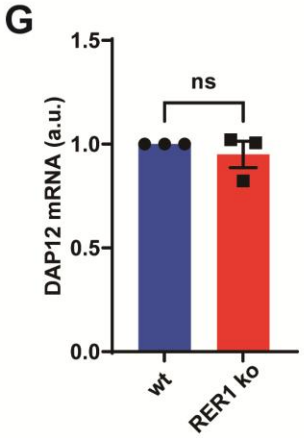
G
DAP12 mRNA (a.u.)
1.5
1.0
0.5
0.0
ns
wt
RER1 ko

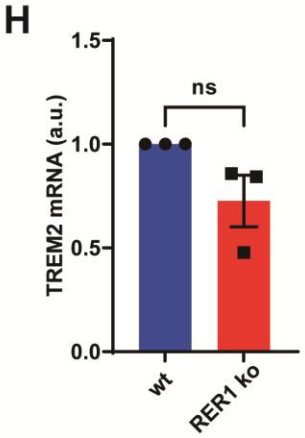
H
TREM2 mRNA (a.u.)
1.5
1.0
0.5
0.0
ns
wt
RER1 ko

Fig. 3.15 Detection of DAP12 and TREM2 in THP-1 wt and RER1 ko differentiated macrophage-like cells (A) RER1 protein was detected by western immunoblotting in different RER1 ko clones and wt THP-1 differentiated cells with RER1 rb antibody. wt worked as control. (B) DNA sanger sequence of RER1 in CRISPR/Cas9-mediated THP-1 RER1 ko cells. DNA was extracted and the primer 5'- ACATCACGCCCAGGTAACG-3' used for DNA sequencing. The sequence of the gRNA used for targeting of RER1is indicated by the box. The arrow indicated deleted bases pairs in the RER1 sequence. (C) Western immunoblotting analysis of the indicated proteins in purified membranes from macrophage-like differentiated THP-1 wt and RER1 ko cells. TREM2 FL: TREM2 full length protein. TREM2 CTF: TREM2 C-terminal fragment. (D)-(F) Quantification of DAP12 and TREM2 FL expression by western immunoblotting. (D) DAP12 monomer; (E) DAP12 dimer; (F) TREM2 FL. Levels of the indicated proteins were normalized to levels of calnexin present in the membrane fraction. Data represent the Mean ± SEM of three independent experiments each performed with triplicate samples. Each data point represents the mean value of an individual experiment. Student's t-test (unpaired, two-tailed). *p <0.05, **p <0.01, ****p <0.0001. (G)-(H) Comparison of the DAP12 and TREM2 mRNA levels in differentiated THP-1 wt and RER1 ko cells by real-time qRT-PCR. Values represent Mean ± SEM of three independent experiments. Each data point represents the mean value of an individual experiment. Student's t-test (unpaired, two-tailed). Figure adapted from Liu et al. 2024.

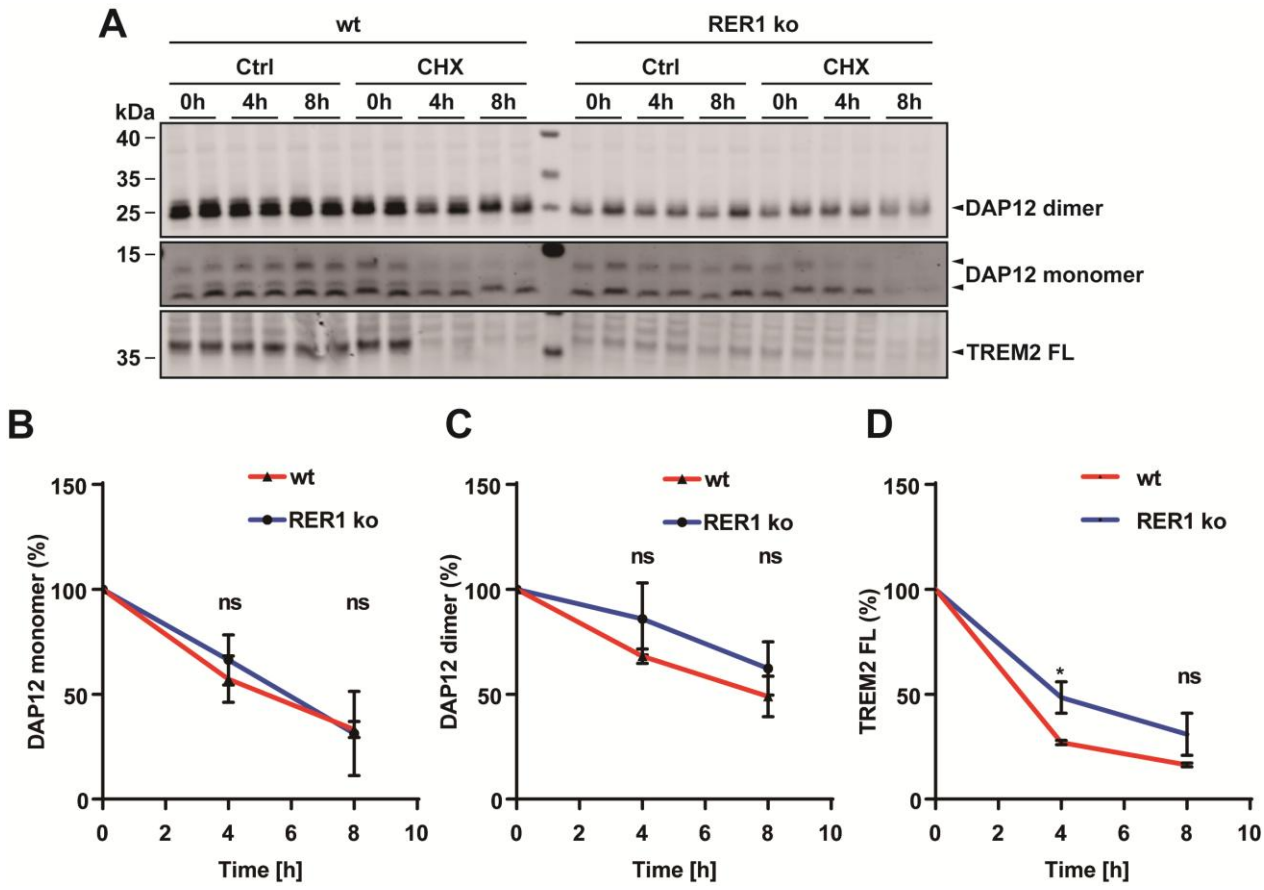

Fig. 3.16 RER1 deletion doesn’t alter DAP12 turnover. (A) Differentiated THP-1 wt and RER1 ko cells were incubated with cycloheximide (CHX, 100 µg/mL) or without (Ctrl) for the indicated time points. Cellular membranes were isolated, and DAP12 and TREM2 detected by western immunoblotting. TREM2 FL: TREM2 full length protein; TREM2 CTF: TREM2 C-terminal fragment. (B)-(D) Quantification of DAP12 and TREM2 levels at the indicated time periods upon CHX treatment (t=0 h was set a 100%). The levels of DAP12 and TREM2 were normalized against the level of DAP12 in non-treated control cells at corresponding time points. Mean ± SEM of three independent experiments each performed with duplicate samples. One-way ANOVA (post hoc Tukey's multiple comparisons test). *p <0.05. There were no statistically significant differences (ns) in the levels of DAP12 between wt and RER1 ko cells at 4 h and 8 h, respectively. Levels of TREM2 FL were significantly increased in RER1 ko cells at 4 h. Figure adapted from Liu et al. 2024.

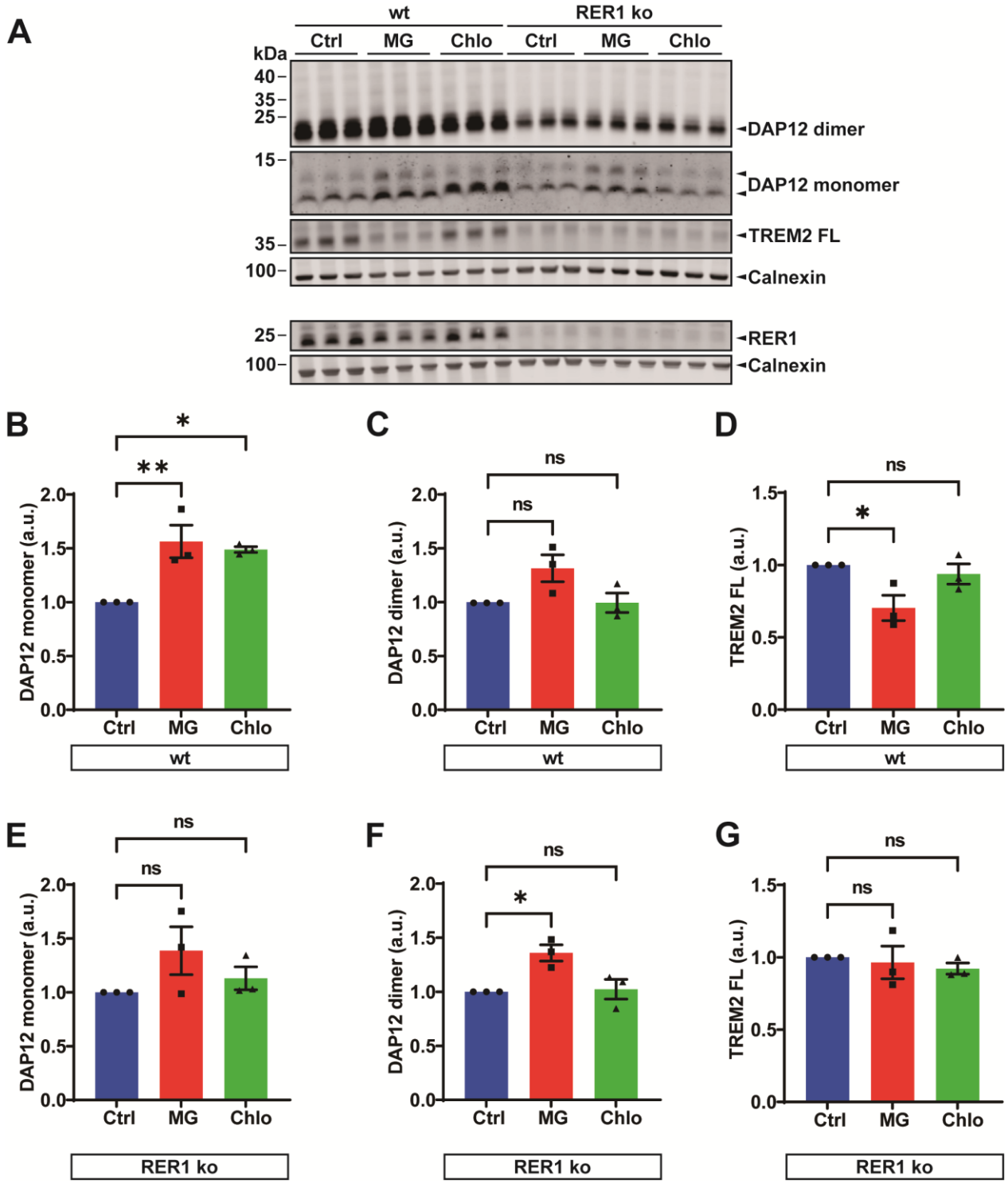

Fig. 3.17 Characterization of degradation pathways for DAP12 and TREM2 in RER1 ko macrophage-like cells. (A) THP-1 wt and RER1 ko macrophage-like cells were treated with MG132 (MG, 10 μM) or chloroquine (Chlo, 50 μM) or without (Ctrl) for 4 h. Membrane proteins were extracted from isolated membranes and analyzed by western immunoblotting. TREM2 FL: TREM2 full length protein; TREM2 CTF: TREM2 C-terminal fragment. (B)-(G) Quantification of DAP12 and TREM2 levels by western immunoblotting

in (A). Dimeric and monomeric DAP12, TREM2 FL were normalized against calnexin. Values represent Mean ± SEM of three independent experiments. Each data point represents the mean value of an individual experiment. One way ANOVA (post hoc Tukey's multiple comparisons test). *p <0.05, **p <0.01. Figure adapted from Liu et al. 2024.

3.11 RER1 deletion leads to the inhibition of TREM2-DAP12 signaling upon stimulation with TREM2 antibodies

TREM2-DAP12 signaling can be specifically stimulated by cross-linking anti-TREM2 antibodies (Ibach et al., 2021, Schlepckow et al., 2020, Wang et al., 2020). Therefore, the monoclonal 4B2A3 and the polyclonal AF1828 anti-TREM2 antibodies were used to specifically stimulate TREM2-DAP12 signaling, and phosphorylation of SYK (pSYK) in macrophage-like differentiated human THP-1 cells was detected (Fig. 3.18 A and B). TREM2 ko cells, used as a negative control, did not respond to the incubation with either anti-TREM2 antibody. In contrast, THP-1 wt cells showed a 2-fold increase in pSYK levels upon stimulation with monoclonal antibody 4B2A3 and more than 4-fold increase with polyclonal antibody AF1828. Interestingly, consistent with the significant decrease of TREM2 and DAP12 expression levels, neither antibody stimulated the phosphorylation of SYK in RER1 ko cells (Fig. 3.18 A and B). Similarly, phosphorylated SYK was only detectable in wt cells not in RER1 ko cells by western immunoblotting upon cell treatment with antibodies 4B2A3 or AF8128 while total SYK was similarly expressed in both wt and RER1 ko cells. Together, these combined data further support a loss-of-function in the TREM2-DAP12 signaling capacity in RER1 ko cells (Liu et al., 2024).

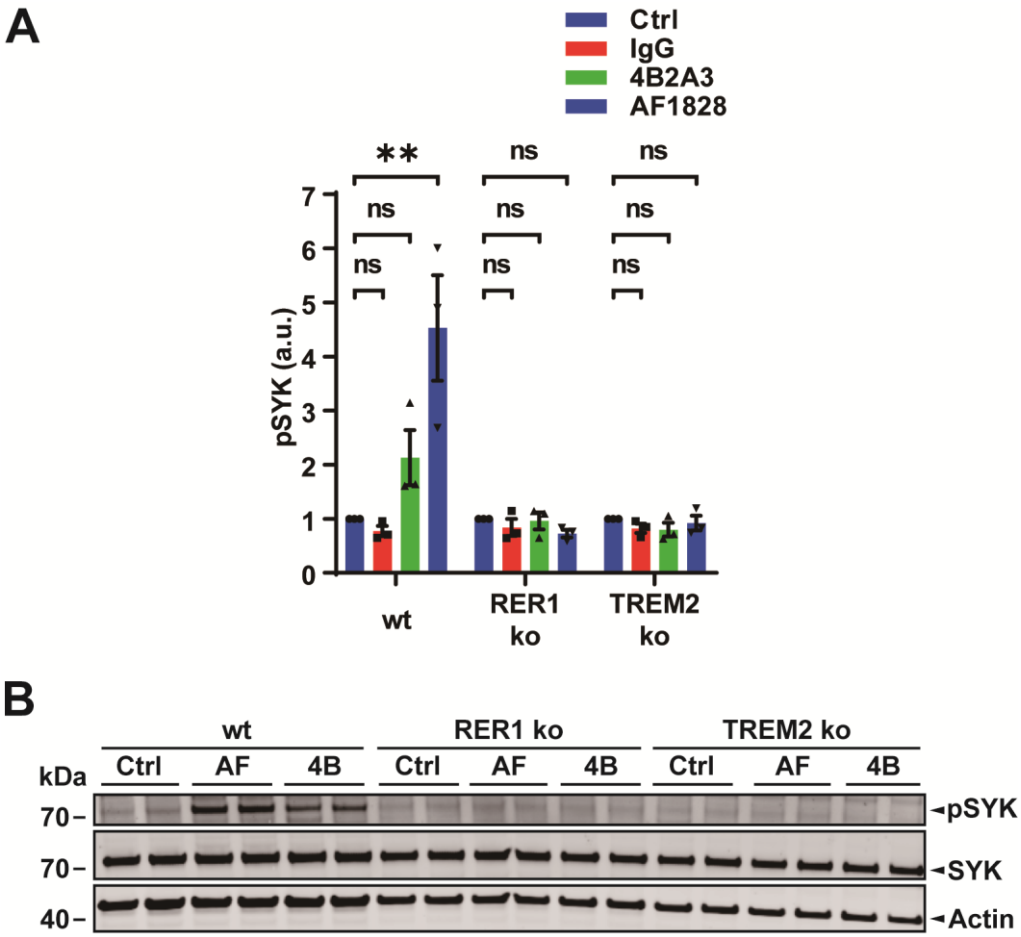

Fig. 3.18 Deletion of RER1 impairs TREM2-DAP12 signaling. (A) Differential activation of TREM2-DAP12 signaling in THP-1 wt and RER1 ko cells. Macrophage-like differentiated THP-1 cells were incubated with or without 10 µg/mL of the respective anti-TREM2 antibody (4B2A3 or AF1828) for 10 min. Treatment with an isotype control antibody (IgG) served as a negative control, and THP-1 TREM2 ko cells served as additional controls. After treatment, cells were lysed (whole cell lysates) and phosphorylated SYK (pSYK) detected by AlphaLISA technology. Data represent the Mean ± SEM of three independent experiments each performed with quadruplicate samples. Each data point represents the mean value of an individual experiment. One-way ANOVA (post hoc Tukey's multiple comparisons test). ** p <0.01. (B) Detection of SYK and pSYK in lysates of the indicated cells by western immunoblotting. AF: AF1828; 4B: 4B2A3. Figure adapted from Liu et al. 2024.

3.12 RER1 deletion impairs phagocytosis of macrophage-like cells differentiated from THP-1 cells

We observed the deletion of RER1 decreased the expression level of both TREM2 and DAP12. Therefore, we wanted to assess if RER1 deletion also affected macrophage-like

function of THP-1 cells and analyzed phagocytosis of pHrodo-labeled *E.coli* bioparticles (Fig. 3.19 A). Fluorescence readings over a period of 5 h indicated efficient phagocytosis of these particles by macrophage-like differentiated THP-1 wt cells. As expected, phagocytosis was strongly reduced in TREM2 ko cells. More importantly, the deletion of RER1 also resulted in almost complete inhibition of phagocytic activity (Fig. 3.19 A and B) (Liu et al., 2024).

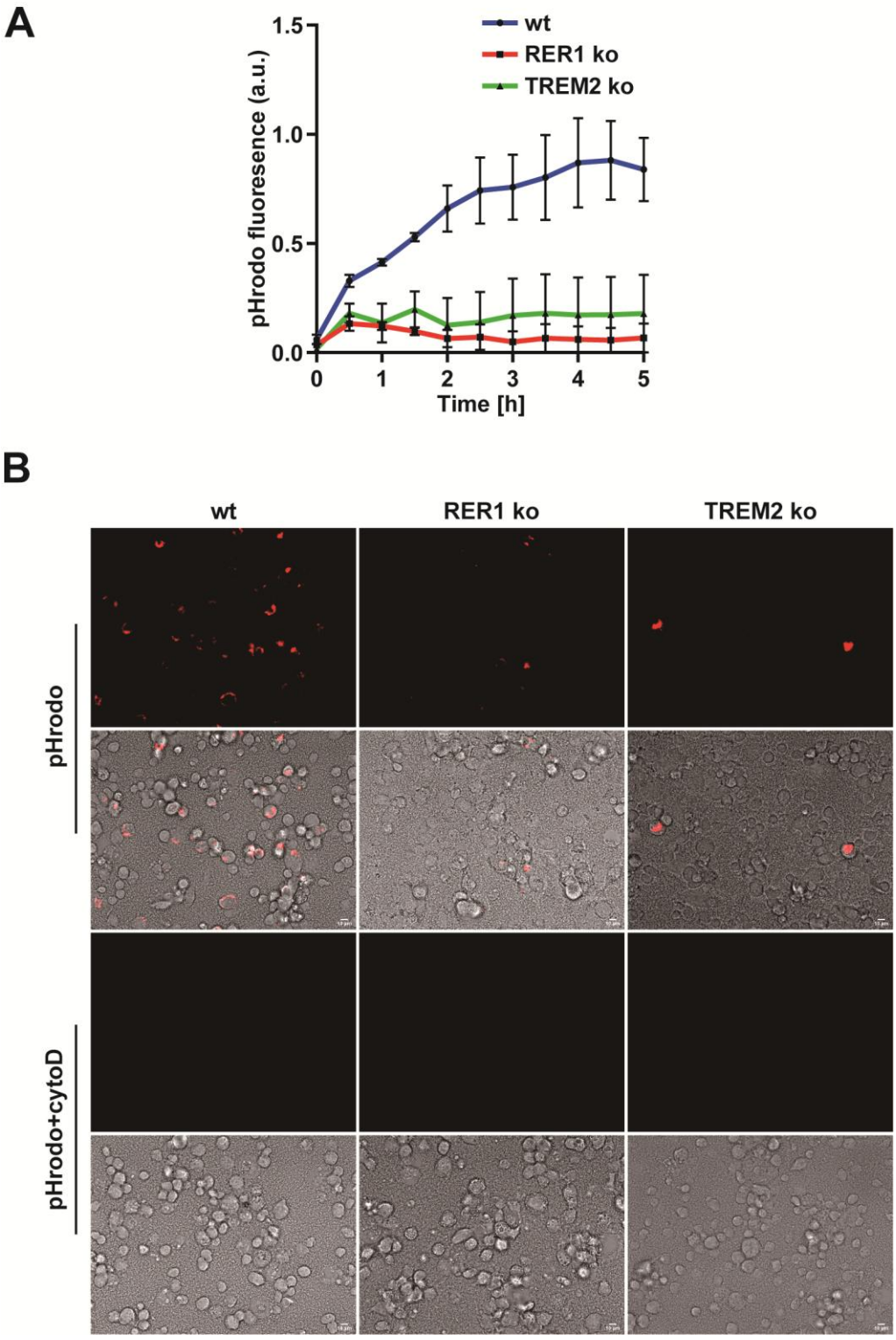

Fig. 3.19 Deletion of RER1 impairs phagocytosis of THP-1 differentiated macrophage-like cells. (A) Phagocytosis of E. coli particles by THP-1 wt and RER1 ko cells. THP-1 wt and RER1 ko cells were seeded in 96-well plates and differentiated to macrophage-like cells by incubation with PMA as described in the Methods section.

pHrodo™ Red *E.coli* BioParticles™ were added to the cells and fluorescence signal was acquired over time using an infinite M200Pro reader for 5 h. Cells pre-treated with cytochalasin D (CytoD, 10 µM) for 30 min served as control. Data represent the Mean ± SEM of two independent experiments each performed with triplicate samples. (B) Representative images of THP-1 wt and RER1 ko cells from the phagocytosis assay (as described in A) were taken at 2 h after addition of pHrodo™ Red *E.coli* BioParticles™. Scale bar = 10 µm. Figure adapted from Liu et al. 2024.

3.13 Accumulation of lipid droplets (LDs) upon RER1 deletion

To assess the role of RER1 in lipid homeostasis of an immune cell model, we first analyzed LDs in monocyte-like undifferentiated and macrophage-like differentiated THP-1 cells upon incubation with the lipophilic dye LD540. Flow cytometry analysis showed significantly increased LD540 fluorescence in RER1 deleted THP-1 cells as compared to wt cells (Fig. 3.20 A and B). Similarly, fluorescence microscopy also revealed a substantially increased number and volume of LDs in RER1 deleted macrophage-like cells compared with wt cells (Fig. 3.20 C-E).

In addition, the lipid droplet coat protein perilipin 2 was also significantly elevated in both RER1 deficient THP-1 monocytes (Fig. 3.21 A and C) and macrophage-like cells (Fig. 3.21 B, D, E and F). These observations strongly suggest that RER1 plays an important role in the metabolism of LDs.

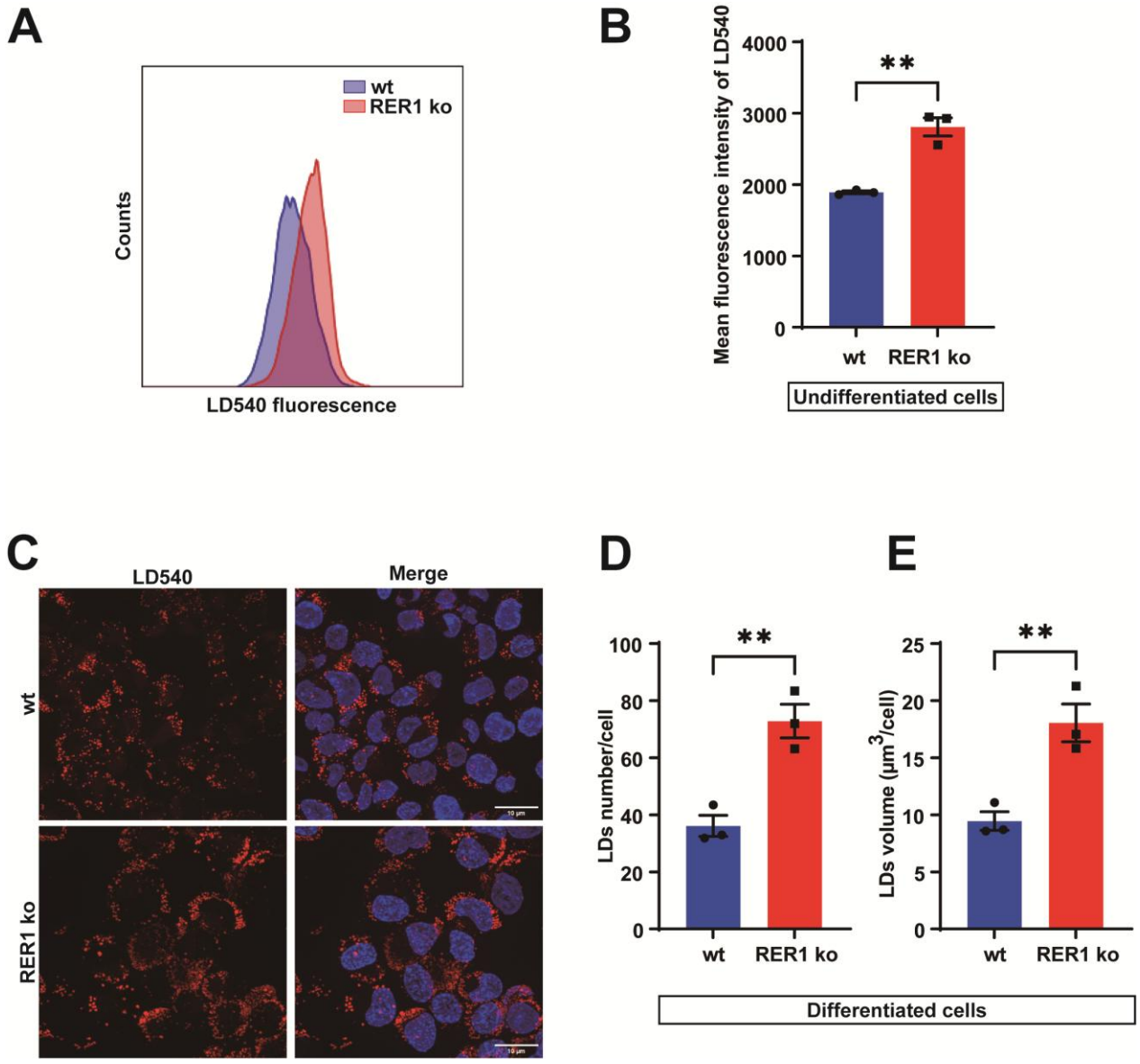

Fig. 3.20: Accumulation of Lipid droplets (LDs) in RER1 ko cells. (A) Comparison of LDs in RER1 ko and wild type (wt) THP-1 undifferentiated cells by flow cytometry. LD540 dye was used for the staining of LDs. (B) Quantification of the median fluorescence intensity (MFI) for LD540 shown in (A). data represent Mean ± SEM of three independent experiments. Each data point represents the mean value of an individual experiment. Student's t-test (unpaired, two-tailed). **p <0.01. (C) Comparison of LDs in RER1 ko and wt THP-1 differentiated cells by LD540 staining. Representative images are shown. Cells were co-stained with the LD540 dye (red) and DAPI (blue) to visualize LDs and nuclei, respectively. Scale bar = 10 µm. LDs numbers (D) and volume (E) per cell were quantified by automated LD quantification (ALDQ) method. Values represent Mean ± SEM of three independent experiments and at least 120 cells in one cell type were included in each experiment. Each data point represents the mean value of an individual experiment. Student's t-test (unpaired, two-tailed). **p <0.01.

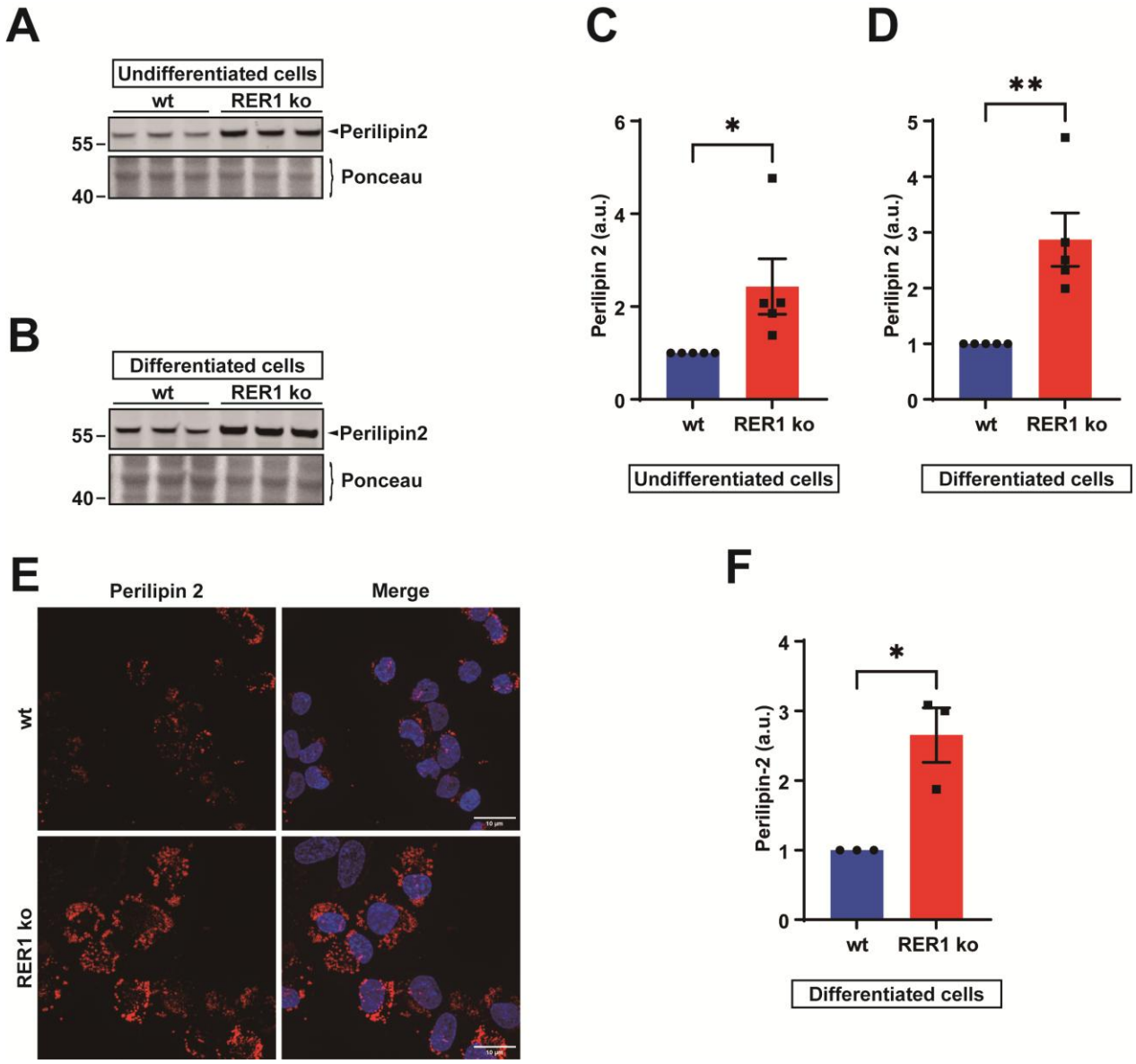

Fig.3.21: Comparison of perilipin 2 in RER1 ko and wt cells by western immunoblotting and immunocytochemistry. (A)-(B) Detection of perilipin 2 in RER1 ko and wt THP-1 undifferentiated (A) and differentiated (B) cells. Cellular membranes were isolated and western immunoblotting was used for the detection of the indicated protein. (C)-(D) Quantification of perilipin2 by western immunoblotting (as shown in A and B). Perilipin 2 was normalized to the full protein stained by ponceau. Data represent Mean ± SEM of five independent experiments with one to three samples per experiment. Each data point represents the mean value of an individual experiment. Student's t-test (unpaired, two-tailed). *p <0.05, **p <0.01. (E) Representative images are shown. Cells were co-stained with the perilipin 2 (red) and DAPI (blue). Scale bar = 10 µm. (F) Quantification of perilipin 2 intensity shown in (E). Three independent experiments were performed and at least 100 cells per experiment for one cell type were included in the quantification. Value represent Mean ± SEM of three independent experiments were used and each data point represents the mean value of an individual experiment. Student's t-test (unpaired, two-tailed). *p <0.05.

3.14 RER1 deletion alters the levels of cholesterol esters (CEs) and triacylglycerols (TAGs)

Since LDs mainly contain CEs and TAGs, comprehensive GC-FID and GC-MS-SIM analyses were performed to detect cholesterol and several metabolites. The total cholesterol level was not much changed in RER1 ko THP-1 monocytes (Fig. 3.22 A) but strongly decreased in RER1 ko macrophage-like cells as compared with wt (Fig. 3.22 G). The levels of free cholesterol were rather increased in both RER1 ko monocytes and macrophage-like cells (Fig. 3.22 B and H). Surprisingly, the level of cholesterol esters was significantly reduced in RER1 ko macrophage-like cells as compared with wt cells (Fig. 3.22 I). In RER1 ko THP-1 monocytes, the level of CEs was also decreased to some extent, but differences were not significant (Fig. 3.22 C).

GC-MS analysis further showed that cells lacking expression of RER1 contained significantly increased levels of the cholesterol precursors lanosterol and desmosterol in monocytic THP-1 cells (Fig. 3.22 D and E), indicating upregulation of *de novo* cholesterol biosynthesis. Since the level of lathosterol was significantly decreased in RER1 deficient cells (Fig. 3.22 F), these data also suggest that this upregulation of cholesterol biosynthesis in RER1 ko monocytic THP-1 cells involves the Bloch pathway rather than the Kandutsch-Russell pathway. Notably, in macrophage-like differentiated THP-1 cells, the knockout of RER1 rather led to strongly reduced levels of cholesterol precursors lanosterol, lathosterol and desmosterol (Fig. 3.22 J-M), indicating a downregulation of *de novo* sterol synthesis.

To further analyze the individual species of CEs, tandem mass spectrometry was performed. In line with our previous measurements (Fig. 3.22), the level of CEs was not much changed in RER1-deficient THP-1 monocytes but was significantly reduced in RER1-deficient macrophage-like cells (Fig. 3.23 A and Fig. 3.24 A). CE (18:1) represented the most produced CEs in THP-1 monocytes and macrophage-like cells (Fig. 3.23 B and Fig. 3.24 B). This species was significantly reduced in RER1 ko macrophage-like cells as compared with wt cells (Fig. 3.24 B). Other species, such as CE (16:0), CE (16:1) and CE (18:2), were also reduced in RER1 ko cells significantly (Fig. 3.24 B). Thus, a decrease in these individual CE species could contribute to the overall decreased CE content in RER1 ko cells.

To obtain more detailed insight into RER1 dependent alterations in the metabolism of LD associated lipids, MS analysis of acylglycerols was performed and the results showed that the direct precursor of TAG, diacylglycerol (DAG) was only increased significantly in RER1 ko macrophage-like differentiated THP-1 cells but not in RER1 ko undifferentiated THP-1 cells (Fig. 3.23 C-D and Fig. 3.24 C-D). The TAGs were significantly increased in both RER1 ko undifferentiated and differentiated cells (Fig. 3.23 E-F and Fig. 3.24 E-F). RER1 ko cells showed elevated levels of most major TAG and DAG species in RER1 ko differentiated cells (Fig. 3.24 D and F). Together, these results indicate complex changes in the cellular lipid composition in RER1-deficient cells and support the contribution of increased acylglycerols to the elevated number of LDs. Additionally, RER1 deficiency had different effects on the cholesterol synthesis in monocytic and macrophage-like THP-1 cells.

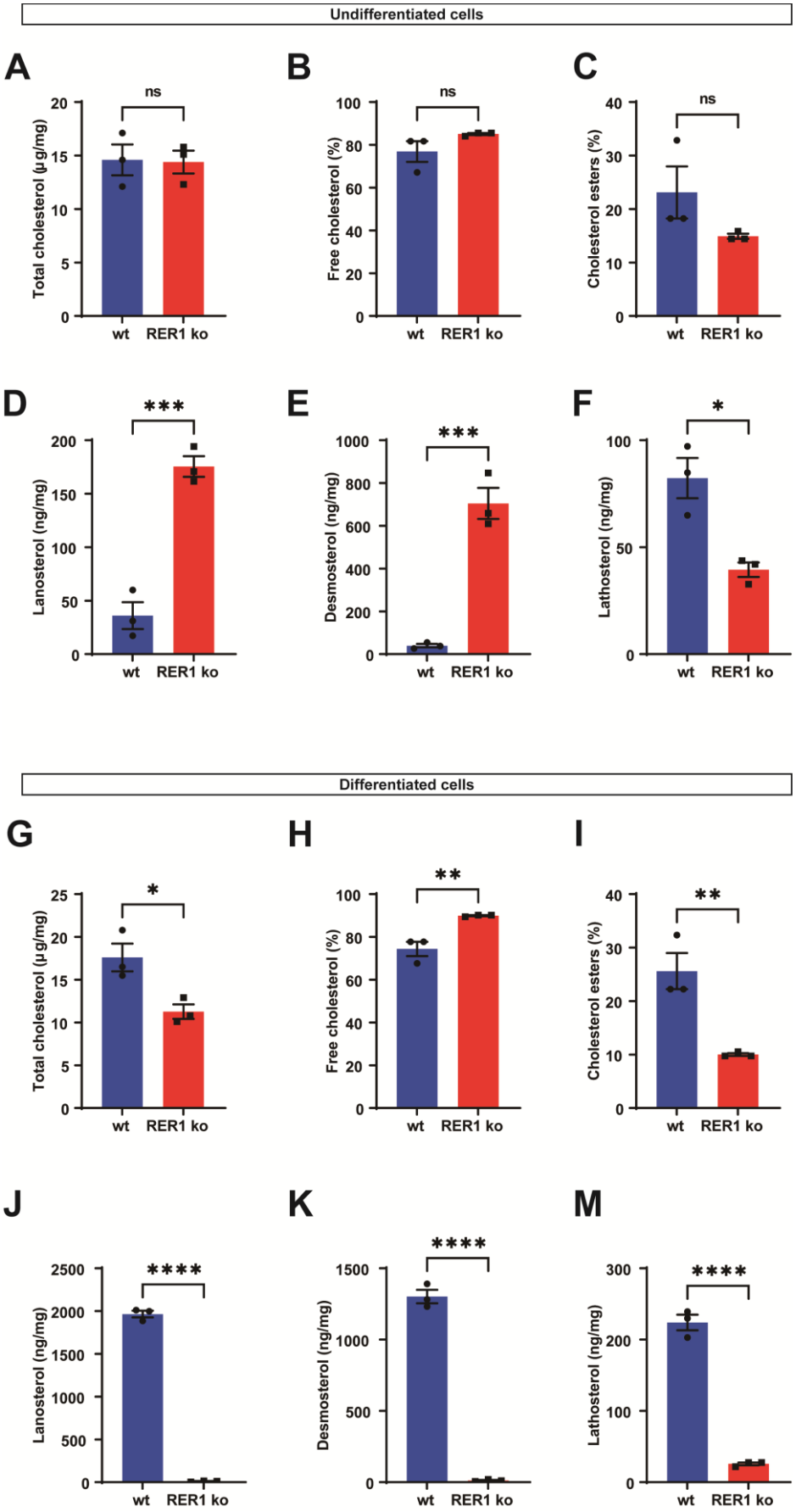
Undifferentiated cells
A
Total cholesterol (µg/mg)
ns
wt
RER1 ko
B
Free cholesterol (%)
ns
C
Cholesterol esters (%)
ns
D
Lanosterol (ng/mg)
***
E
Desmosterol (ng/mg)
***
F
Lathosterol (ng/mg)
*
Differentiated cells
G
Total cholesterol (µg/mg)
*
H
Free cholesterol (%)
**
I
Cholesterol esters (%)
**
J
Lanosterol (ng/mg)
****
K
Desmosterol (ng/mg)
****
M
Lathosterol (ng/mg)
****

Fig. 3.22: Content analysis of a panel of sterols in RER1 ko and wt THP-1 cells, determined by GC-FID and GC-MS. Total cholesterol (A) and (G), free cholesterol (B and H), cholesterol esters (C and I) as well as cholesterol precursors (lanosterol (D and J), desmosterol (E and K), lathosterol (F and M)) were analyzed in undifferentiated (A-F) and differentiated (G-M) THP-1 cells. Data represent Mean ± SEM of three independent experiments each performed with triplicate samples. Each data point represents the mean value of an individual experiment. Student's t-test (unpaired, two-tailed). *p <0.05, **p <0.01, ***p <0.001, ****p <0.0001.

Undifferentiated cells

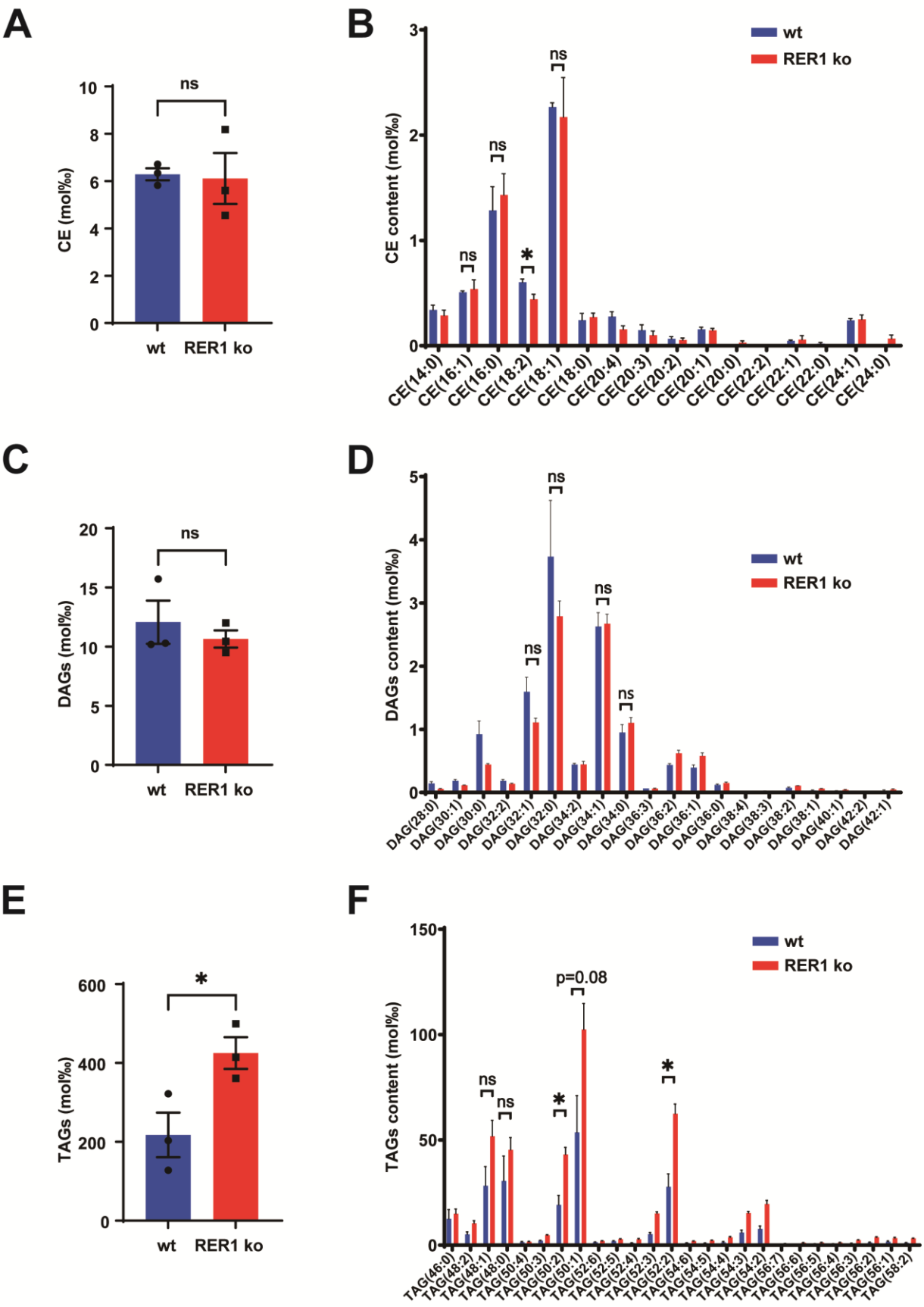

Fig. 3.23: Analysis of cholesterol esters (CEs) species, diacylglycerol (DAGs) species and triacylglycerol (TAGs) species by tandem mass spectrometry in undifferentiated cells. Total CEs (A) and different species (B), total diacylglycerol (C) and different species (D), total triacylglycerol (E) and different species (F) were analyzed in THP-1 undifferentiated cells. Values represent Mean ± SEM of three independent experiments each performed with triplicate samples. Each data point represents the mean value of an individual replicate. Student's t-test (unpaired, two-tailed). *p <0.05.

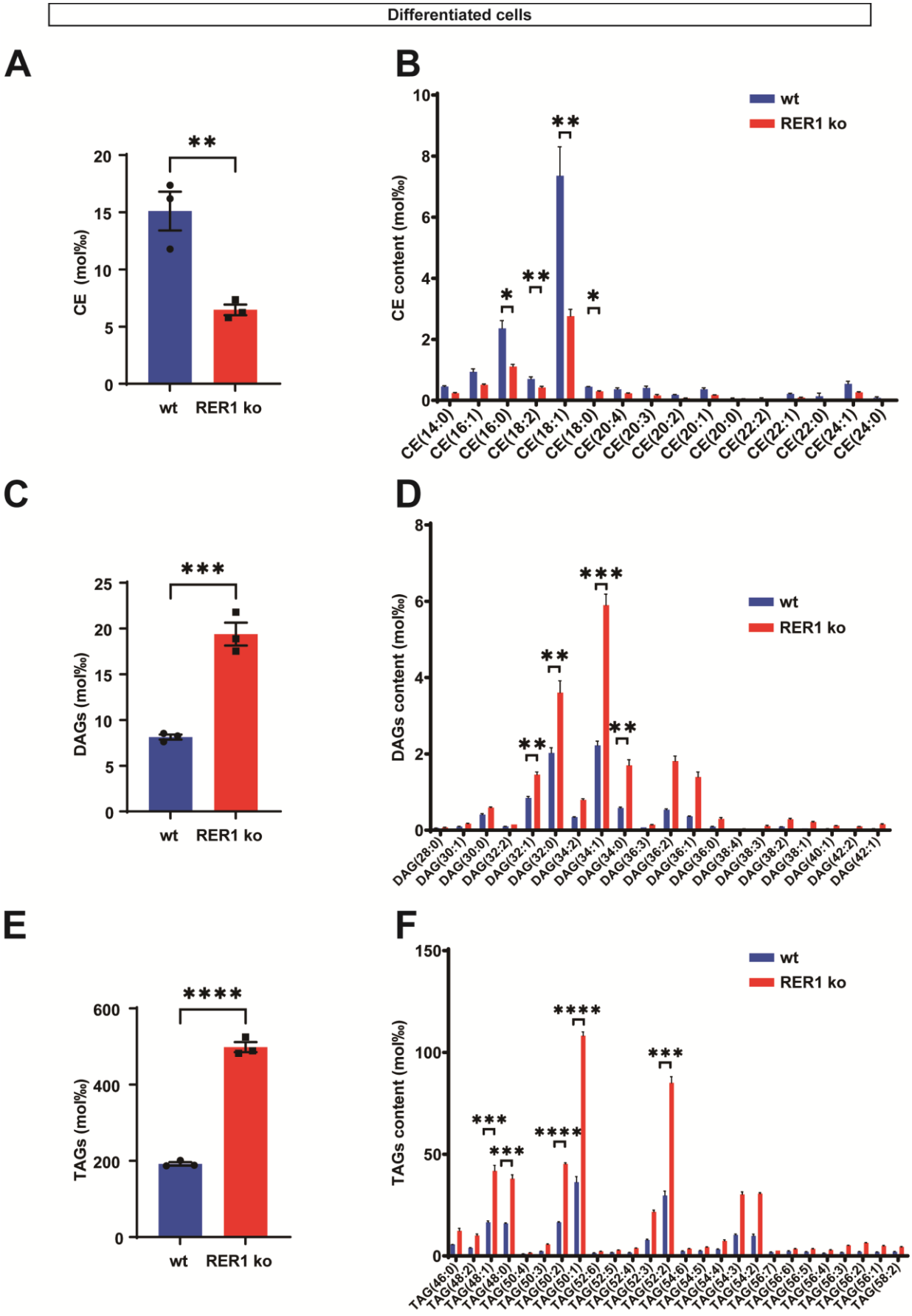
Differentiated cells
A
CE (mol‰)
wt
RER1 ko
B
CE content (mol‰)
wt
RER1 ko
CE(14:0)
CE(16:1)
CE(16:0)
CE(18:2)
CE(18:1)
CE(18:0)
CE(20:4)
CE(20:3)
CE(20:2)
CE(20:1)
CE(20:0)
CE(22:2)
CE(22:1)
CE(22:0)
CE(24:1)
CE(24:0)
C
DAGs (mol‰)
wt
RER1 ko
D
DAGs content (mol‰)
wt
RER1 ko
DAG(28:0)
DAG(30:1)
DAG(30:0)
DAG(32:2)
DAG(32:1)
DAG(32:0)
DAG(34:2)
DAG(34:1)
DAG(34:0)
DAG(36:3)
DAG(36:2)
DAG(36:1)
DAG(36:0)
DAG(38:4)
DAG(38:3)
DAG(38:2)
DAG(38:1)
DAG(40:1)
DAG(42:2)
DAG(42:1)
E
TAGs (mol‰)
wt
RER1 ko
F
TAGs content (mol‰)
wt
RER1 ko
TAG(46:0)
TAG(48:2)
TAG(48:1)
TAG(48:0)
TAG(50:4)
TAG(50:3)
TAG(50:2)
TAG(50:1)
TAG(52:6)
TAG(52:5)
TAG(52:4)
TAG(52:3)
TAG(52:2)
TAG(54:6)
TAG(54:5)
TAG(54:4)
TAG(54:3)
TAG(54:2)
TAG(56:7)
TAG(56:6)
TAG(56:5)
TAG(56:4)
TAG(56:3)
TAG(56:2)
TAG(56:1)
TAG(58:2)

Fig. 3.24: Analysis of cholesterol esters (CEs) species, diacylglycerol (DAGs) species and triacylglycerol (TAGs) species by tandem mass spectrometry in differentiated cells. Total CEs (A) and different species (B), total diacylglycerol (C) and different species (D), total triacylglycerol (E) and different species (F) were analyzed in THP-1 differentiated cells. Values represent Mean ± SEM of three independent experiments each performed with triplicate samples. Each data point represents the mean value of an individual replicate. Student's t-test (unpaired, two-tailed). **p <0.01. ***p <0.001, ****p <0.0001.

3.15 Lipid metabolism related pathways are upregulated in RER1 deleted cells

We also performed RNA sequencing (RNA seq) to assess the potential involvement of RER1 in transcriptional regulation of lipid metabolisms in both monocytes and macrophage-like cells. Hierarchical clustering analysis showed that a large number of genes were robustly changed in RER1 deleted monocytes and macrophage-like cells, as compared with wt monocytes and macrophage-like cells, respectively (Fig. 3.25 A and C). Using the criterion of Qvalue<0.05 and log2 FoldChange≥1, compared with wt undifferentiated cells, 608 upregulated mRNAs and 1062 downregulated mRNAs were found in the RER1 deleted cells (Fig. 3.25 B). Lack of RER1 in macrophage-like cells derived from THP-1 monocytes led to the upregulation of 1423 genes and the downregulation of 1635 genes (Fig. 3.25 D).

Analysis of the upregulated DEGs in RER1 ko cells compared with wt cells based on the KEGG function enrichment revealed that genes related to lipid metabolism were significantly enriched (Fig. 3.26 B and D). The steroid biosynthesis pathway was strongly upregulated in RER1 deficient monocytic THP-1 cells (Fig. 3.26 B) and the genes involved in this pathway were showed in Fig. 3.27 and table 3.1. RER1 ko macrophage-like differentiated THP-1 cells also showed significant upregulation of the pathways 'lipid and atherosclerosis', 'cholesterol metabolism' and 'steroid biosynthesis' (Fig. 3.26 D) as compared wt cells and the genes involved in these three pathways are shown in Fig 3.28 and tables 3.2, 3.3 and 3.4.

For the GO enrichment analysis, the genes were classified into three categories: biological processes, molecular functions, and cellular components. Among the biological processes, the upregulated DEGs in RER1 ko THP-1 monocytes were partially attributed to 'cholesterol biosynthetic process', 'sterol biosynthetic process', 'regulation of lipid

metabolic process', 'steroid biosynthetic process', 'cholesterol biosynthetic process via desmosterol and lathosterol', 'lipid metabolic process' (Fig. 3.29 D) and genes involved in these pathways are shown in Fig. 3.30 and tables 3.5, 3.6, 3.7, 3.8, 3.9 and 3.10. Among the molecular function, upregulated DEGs related to stearoyl-CoA 9-desaturase activity were observed in RER1 deleted THP-1 monocytes (Fig. 3.29 F) and genes involved in this pathway were shown in Fig. 3.31 and table 3.11. However, there were no lipid metabolism related biological processes and molecular function found in the TOP20 of upregulated GO enrichment analysis in RER1 ko macrophage-like cells as compared to wt cells (Fig. 3.32 B, D and F).

Since lipid metabolism related pathways, biological process and molecular functions were enriched in RER1 ko undifferentiated and differentiated THP-1 cells, we further explored the effects of RER1 deletion on the expression of some important proteins involved in lipid metabolism. The levels of lanosterol 14-alpha demethylase (CYP51A1), which is an enzyme known to catalyze the removal of the 14 alpha-methyl group from lanosterol (Lepesheva & Waterman, 2007), were strongly increased in RER1 ko cells as compared to wt cells (Fig. 3.33 A-D). In addition, the increased CYP51A1 protein level corresponded with the increased mRNA of CYP51A1 in RER1 ko cells. In RER1 deleted macrophage-like cells, the proteins related to the uptake, delivery and intracellular transport of cholesterol, including low density lipoprotein receptor (LDLR), low density lipoprotein receptor-related protein 1 (LRP1) and Nieman-Pick C proteins 1 (NPC1), were increased as compared to wt cells (Fig. 3.33 C and E-H). Additionally, the level of ATP binding cassette subfamily A member 1 (ABCA1) and Apolipoprotein E (ApoE) which function during cholesterol efflux in the cellular lipid removal pathway, were also strongly increased in RER1 ko macrophage-like cells as compared to wt cells (Fig. 3.33 C, I and J).

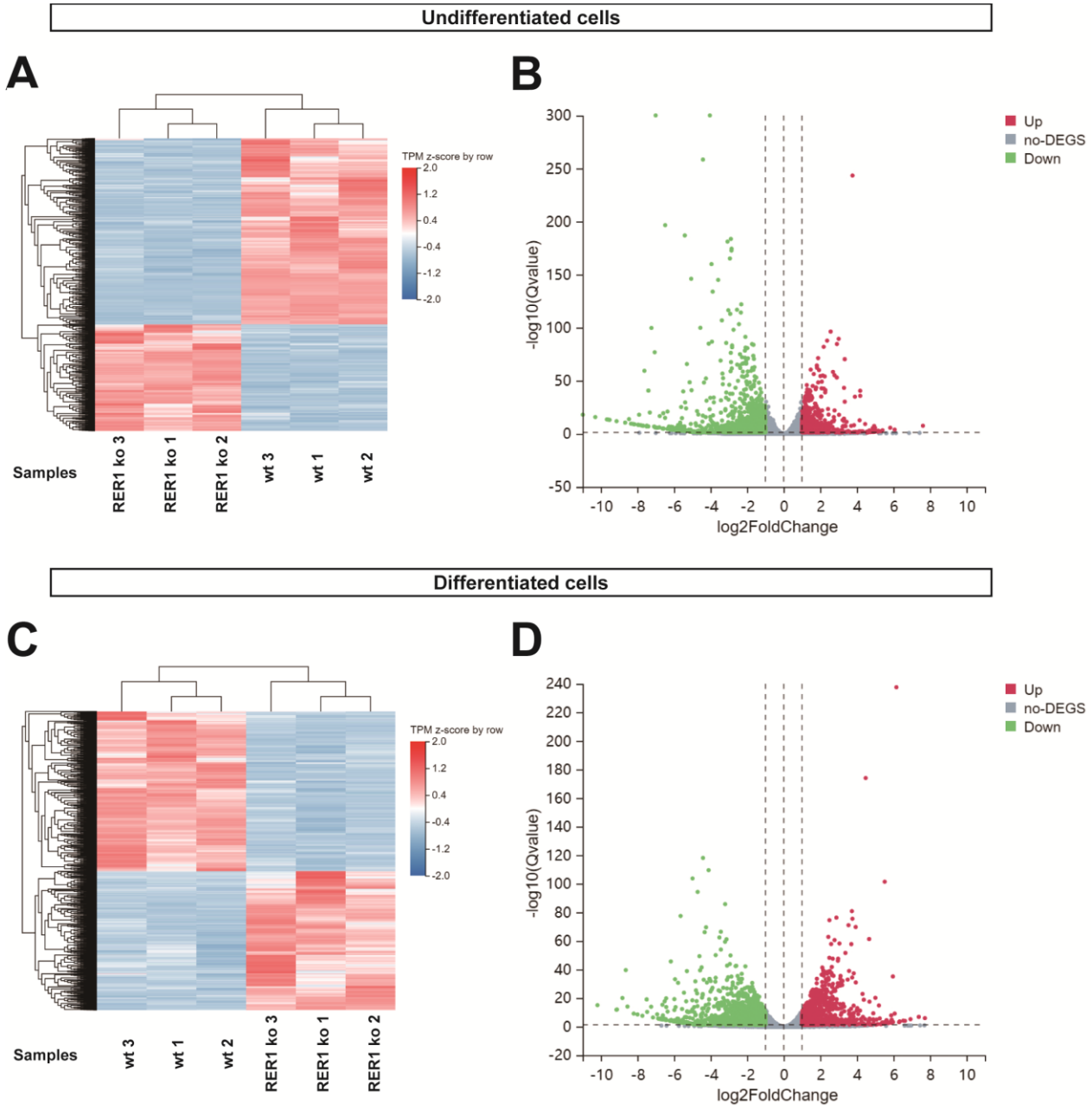

Fig. 3.25: Overview of mRNAs associated with RER1 deletion in THP-1 cells. (A) and (C) The differential cluster analysis between different samples was shown in heatmap. Differentially expressed genes (DEGs) were used to do the hierarchical clustering. (B) and (D) Volcano plot of up-regulation and down-regulation genes, red circles indicate up-regulated mRNAs, and green circles indicate down-regulated mRNAs. DEGs were used to do the hierarchical clustering. y-Axis corresponds to the log10 (Q value, adjust p value), and the x-axis displays the Log2FoldChange value.

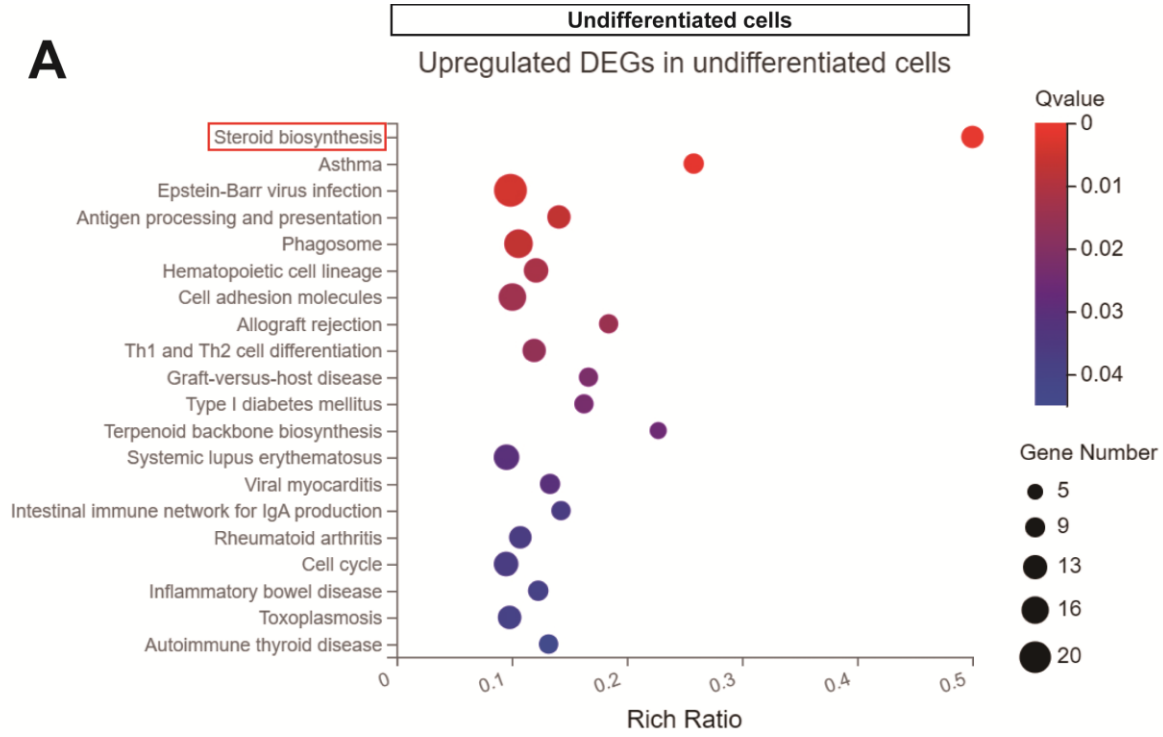
A
Undifferentiated cells
Upregulated DEGs in undifferentiated cells
Steroid biosynthesis
Asthma
Epstein-Barr virus infection
Antigen processing and presentation
Phagosome
Hematopoietic cell lineage
Cell adhesion molecules
Allograft rejection
Th1 and Th2 cell differentiation
Graft-versus-host disease
Type I diabetes mellitus
Terpenoid backbone biosynthesis
Systemic lupus erythematosus
Viral myocarditis
Intestinal immune network for IgA production
Rheumatoid arthritis
Cell cycle
Inflammatory bowel disease
Toxoplasmosis
Autoimmune thyroid disease
0
0.1
0.2
0.3
0.4
0.5
Rich Ratio
Qvalue
0
0.01
0.02
0.03
0.04
Gene Number
5
9
13
16
20

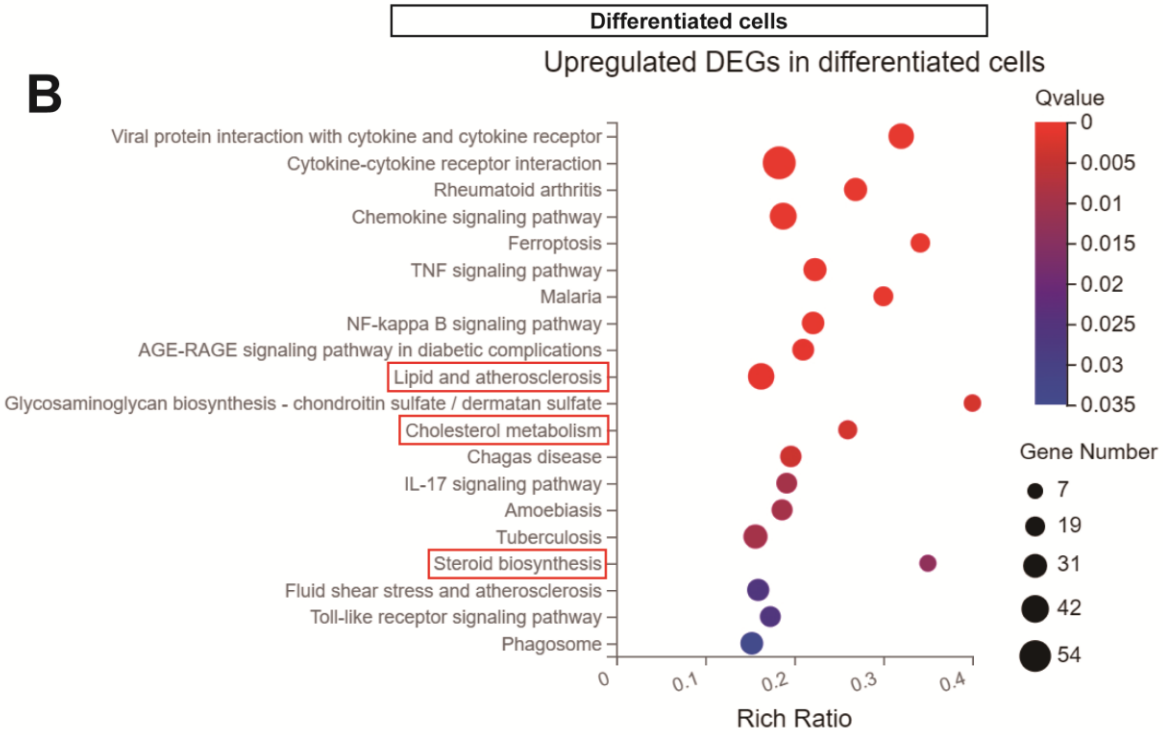
B
Differentiated cells
Upregulated DEGs in differentiated cells
Viral protein interaction with cytokine and cytokine receptor
Cytokine-cytokine receptor interaction
Rheumatoid arthritis
Chemokine signaling pathway
Ferroptosis
TNF signaling pathway
Malaria
NF-kappa B signaling pathway
AGE-RAGE signaling pathway in diabetic complications
Lipid and atherosclerosis
Glycosaminoglycan biosynthesis - chondroitin sulfate / dermatan sulfate
Cholesterol metabolism
Chagas disease
IL-17 signaling pathway
Amoebiasis
Tuberculosis
Steroid biosynthesis
Fluid shear stress and atherosclerosis
Toll-like receptor signaling pathway
Phagosome
0
0.1
0.2
0.3
0.4
Rich Ratio
Qvalue
0
0.005
0.01
0.015
0.02
0.025
0.03
0.035
Gene Number
7
19
31
42
54

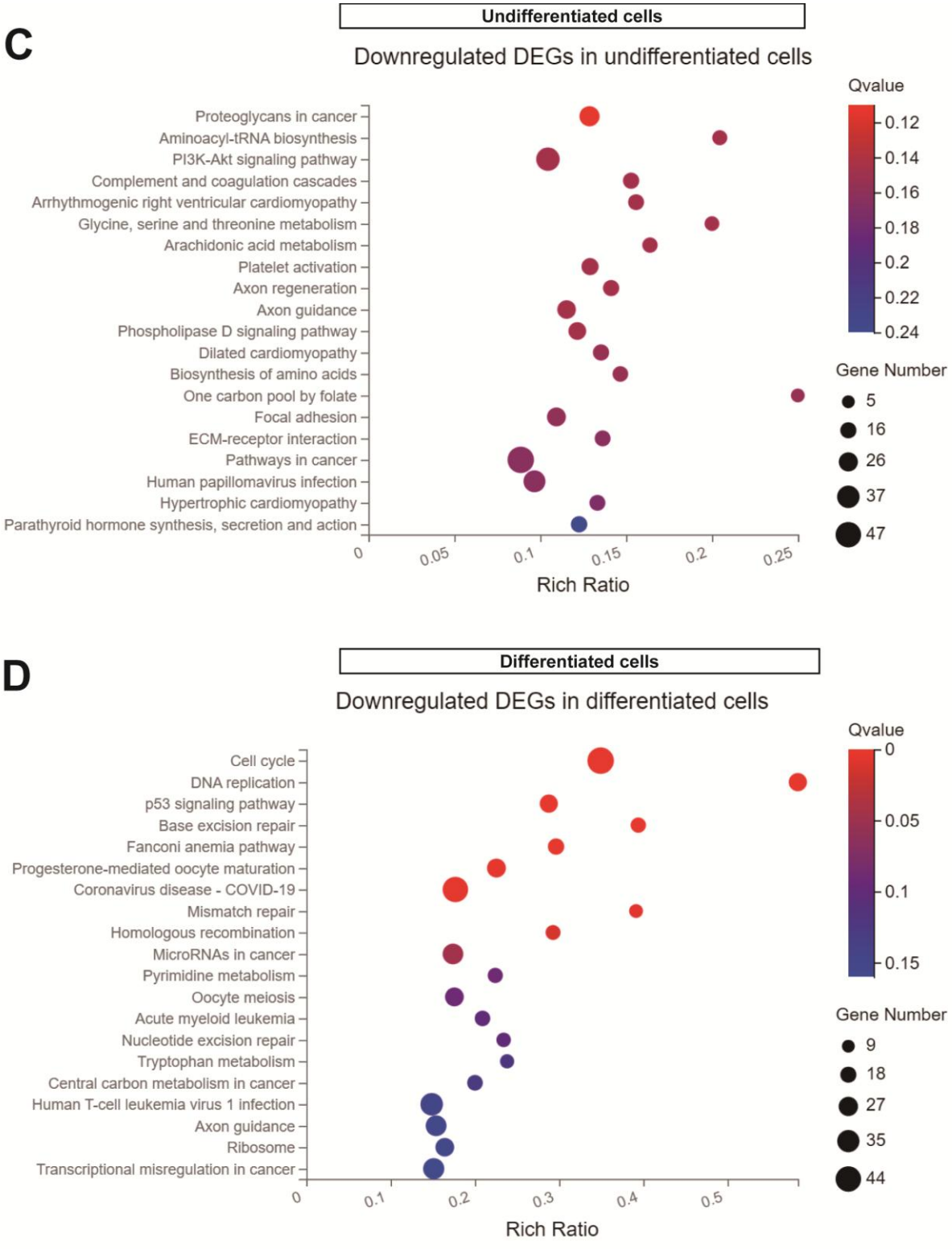

Fig. 3.26: Kyoto Encyclopedia of Genes and Genomes (KEGG) enrichment analysis of differentially expressed gene (DEG) in RER1-deleted and wt THP-1 cells. (A)-(B) KEGG pathway enrichment of genes in the transcriptome of RER1 ko and wt THP-1

undifferentiated cells, down-regulated enrichment (A) and up-regulated enrichment (B). (C)-(D) KEGG pathway enrichment of genes in the transcriptome of RER1 ko and wt THP-1 differentiated cells, down-regulated enrichment (C) and up-regulated enrichment (D). Lipid metabolism related pathways are shown in red rectangular box.

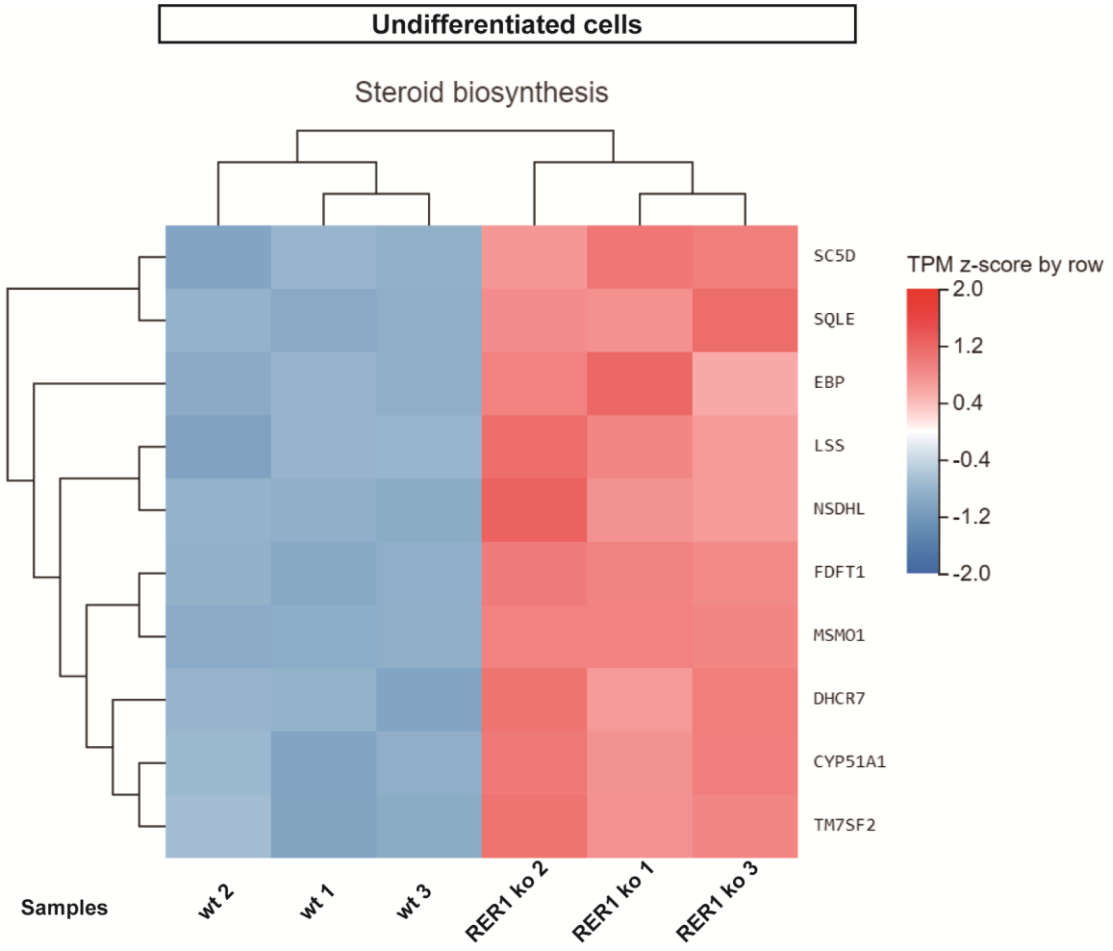

Fig. 3.27 Kyoto Encyclopedia of Genes and Genomes (KEGG) enrichment analysis showed steroid biosynthesis is upregulated in RER1 ko THP-1 undifferentiated cells. Heatmap of 10 genes which are upregulated in steroid biosynthesis pathway. The genes involved in each pathway are shown in table 3.1.

Table 3.1: Upregulation of steroid biosynthesis pathway in RER1 ko undifferentiated THP-1 cells

Gene ID	Gene Symbol	Gene Name	Protein Name	Log2FoldChange (RER1KO_noPMA / WT_noPMA)	Q value (adjust p value) (RER1KO_noPMA / WT_noPMA)
6307	MSMO1	Methylsterol monooxygenase 1	Methylsterol monooxygenase 1	2.0842667	7.25E-50
6713	SQLE	Squalene epoxidase	Squalene monooxygenase	1.882558907	4.64E-72
10682	EBP	EBP cholestenol delta-isomerase	3-beta-hydroxysteroid-Delta(8),Delta(7)-isomerase	1.731975796	3.91E-29
1595	CYP51A1	Cytochrome P450 family 51 subfamily A member 1	Lanosterol 14-alpha demethylase	1.409495453	9.27E-39
50814	NSDHL	NAD(P) dependent steroid dehydrogenase-like	Sterol-4-alpha-carboxylate 3-dehydrogenase, decarboxylating	1.37597262	7.50E-13
1717	DHCR7	7-dehydrocholesterol reductase	7-dehydrocholesterol reductase	1.323759153	2.29E-14
6309	SC5D	Sterol-C5-desaturase	Lathosterol oxidase	1.246517242	8.83E-16
4047	LSS	Lanosterol synthase	Lanosterol synthase	1.185656272	3.53E-07
2222	FDFT1	Farnesyl-diphosphate farnesyltransferase 1	Squalene synthase	1.167520997	1.06E-35
7108	TM7SF2	Transmembrane 7 superfamily member 2	Delta(14)-sterol reductase TM7SF2	1.07297873	5.41E-07

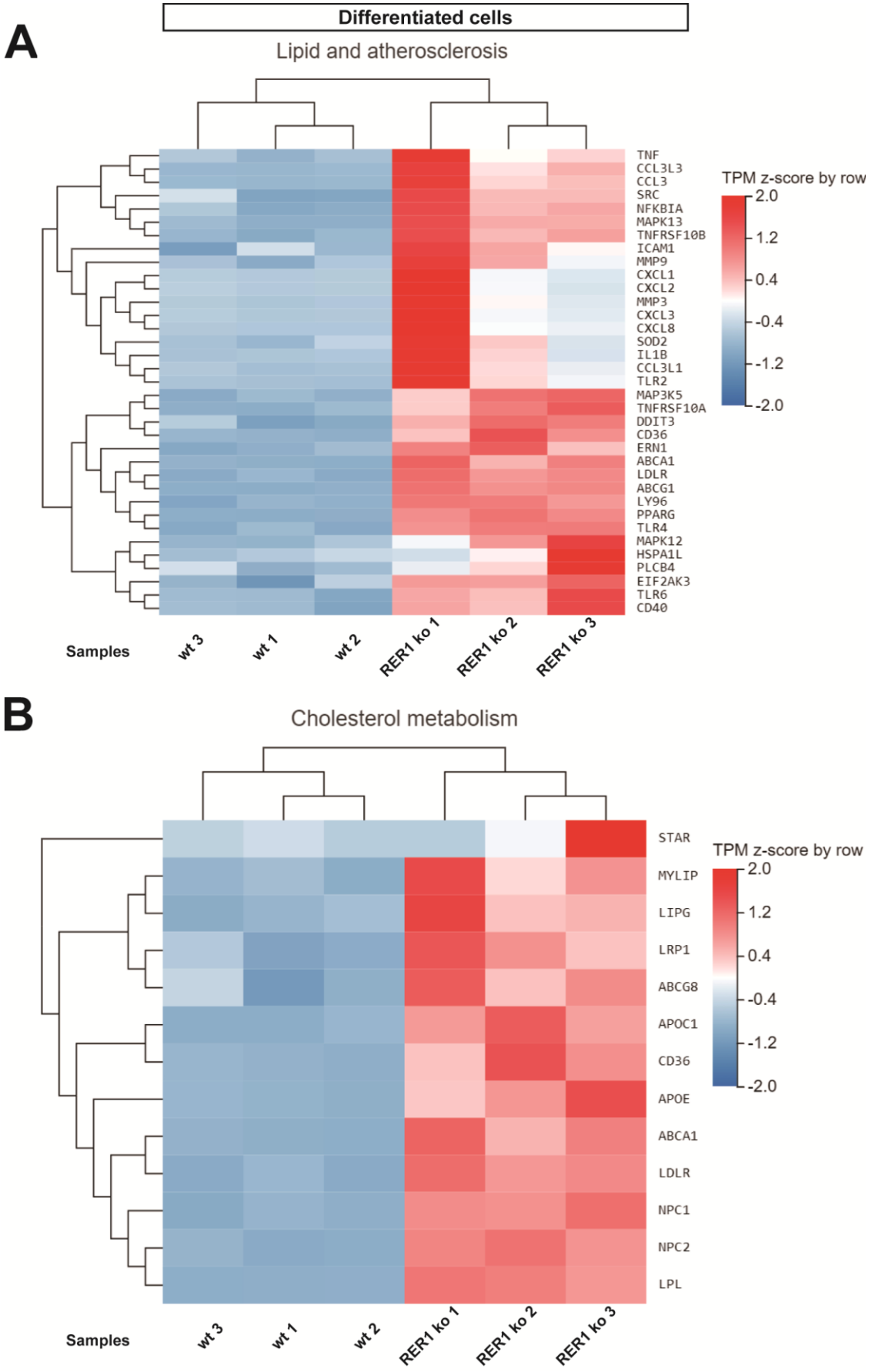
A
Differentiated cells
Lipid and atherosclerosis
TNF
CCL3L3
CCL3
SRC
NFKBIA
MAPK13
TNFRSF10B
ICAM1
MMP9
CXCL1
CXCL2
MMP3
CXCL3
CXCL8
SOD2
IL1B
CCL3L1
TLR2
MAP3K5
TNFRSF10A
DDIT3
CD36
ERN1
ABCA1
LDLR
ABCG1
LY96
PPARG
TLR4
MAPK12
HSPA1L
PLCB4
EIF2AK3
TLR6
CD40
TPM z-score by row
2.0
1.2
0.4
-0.4
-1.2
-2.0
Samples
wt 3
wt 1
wt 2
RER1 ko 1
RER1 ko 2
RER1 ko 3
B
Cholesterol metabolism
STAR
MYLIP
LIPG
LRP1
ABCG8
APOC1
CD36
APOE
ABCA1
LDLR
NPC1
NPC2
LPL
TPM z-score by row
2.0
1.2
0.4
-0.4
-1.2
-2.0
Samples
wt 3
wt 1
wt 2
RER1 ko 1
RER1 ko 2
RER1 ko 3

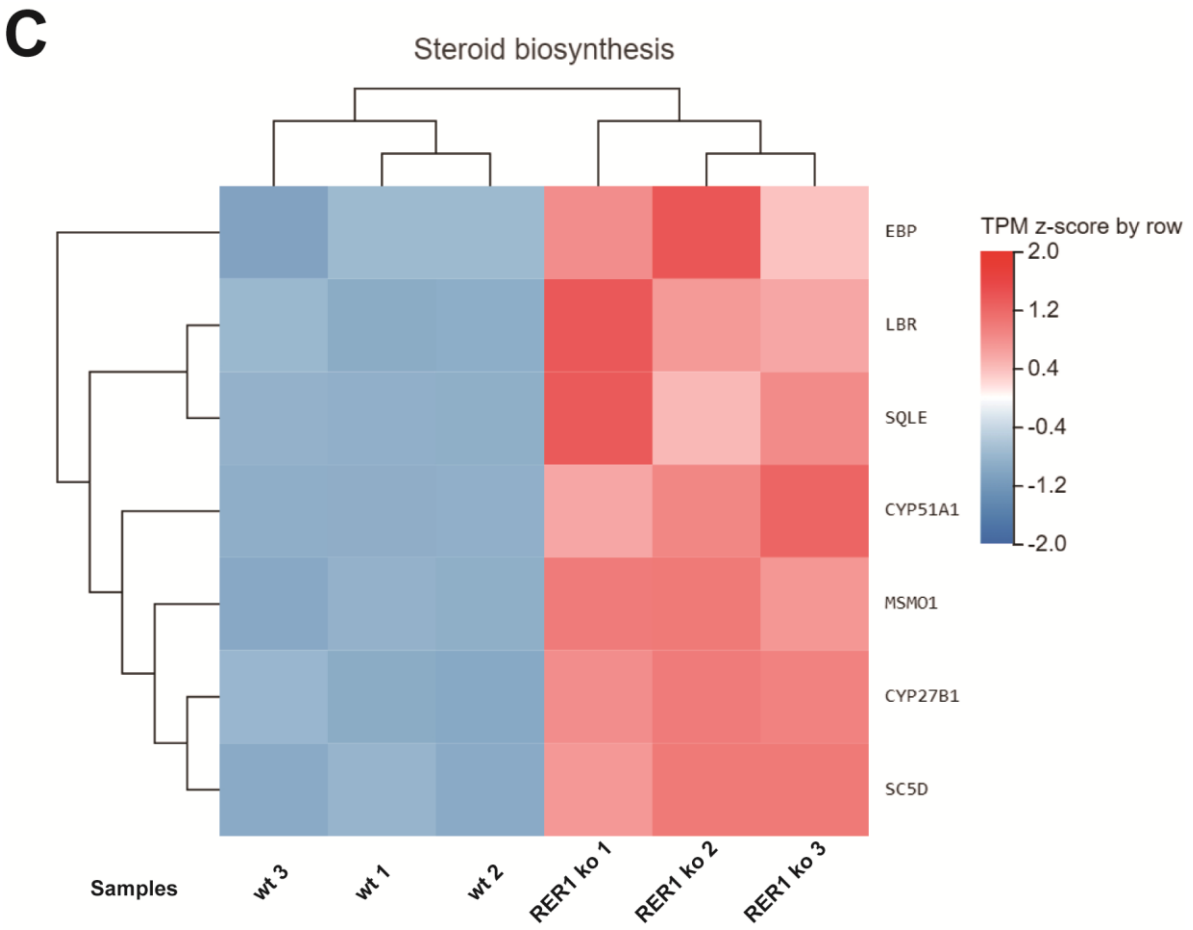

Fig. 3.28: Kyoto Encyclopedia of Genes and Genomes (KEGG) enrichment analysis showed lipid metabolism related pathways are upregulated in RER1 ko THP-1 differentiated cells. Heatmap of lipid metabolism related pathways, including lipid and atherosclerosis (A), cholesterol metabolism (B) and steroid biosynthesis (C). The genes involved in each pathway are shown in table 3.2, 3.3 and 3.4.

Table 3.2: The lipid and atherosclerosis pathway is upregulated in RER1 ko THP-1 differentiated cells

Gene ID	Gene Symbol	Gene Name	Protein Name	Log2FoldChange (RER1KO_noPMA / WT_noPMA)	Qvalue (adjust p value) (RER1KO_noPMA / WT_noPMA)
3576	CXCL8	GCP-1	Interleukin-8	6.066621544	7.57E-10
9619	ABCG1	ATP-binding Cassette Sub-family G Member 1	ATP-binding cassette sub-family G member 1	5.968989539	7.54E-36
2921	CXCL3	CINC-2b	C-X-C motif chemokine 3	5.074361946	1.14E-05
2920	CXCL2	CINC-2a	C-X-C motif chemokine 2	4.905915124	2.59E-05
2919	CXCL1	FSP	Growth-regulated alpha protein	4.893429044	7.38E-06
414062	CCL3L3	D17S1718	C-C motif chemokine 3-like 1	4.689453864	3.39E-18
6348	CCL3	G0S19-1	Acetate--CoA ligase CCL3	4.376888214	1.50E-19
6349	CCL3L1	D17S1718	C-C motif chemokine 3-like 1	4.207976495	5.43E-06
19	ABCA1	ATP binding cassette subfamily A member 1	Phospholipid-transporting ATPase ABCA1	3.934920512	1.87E-70
3553	IL1B	IL-1	Interleukin-1 beta	3.655275635	1.66E-05
4314	MMP3	Matrix metallopeptidase 3	Stromelysin-1	3.647444557	1.00E-07
7124	TNF	Tumor necrosis factor	Tumor necrosis factor	2.751193753	1.79E-04
5468	PPARG	Peroxisome proliferator activated receptor gamma	Peroxisome proliferator-activated receptor gamma	2.627009807	1.00E-20
5603	MAPK13	Mitogen-activated protein kinase 13	Mitogen-activated protein kinase 13	2.322800062	3.24E-15
7099	TLR4	Toll like receptor 4	Toll-like receptor 4	2.306476019	4.30E-18
8797	TNFRSF10A	TNF receptor superfamily member 10a	Tumor necrosis factor receptor superfamily member 10A	2.136574286	4.21E-22
948	CD36	CD36 molecule (CD36 blood group)	Platelet glycoprotein 4	2.128277266	3.03E-26
3949	LDLR	Low density lipoprotein receptor	Low-density lipoprotein receptor	2.105997122	4.50E-29
23643	LY96	Lymphocyte antigen 96	Lymphocyte antigen 96	1.987456241	3.87E-11
6714	SRC	SRC proto-oncogene, non-receptor tyrosine kinase	Proto-oncogene tyrosine-protein kinase Src	1.893996985	0.004275188
7097	TLR2	Toll like receptor 2	Toll-like receptor 2	1.780798796	2.69E-08
6648	SOD2	Superoxide dismutase 2	Superoxide dismutase [Mn], mitochondrial	1.762910654	0.006626211
8795	TNFRSF10B	TNF receptor superfamily member 10b	Tumor necrosis factor receptor superfamily member 10B	1.714914321	4.34E-10
4217	MAP3K5	Mitogen-activated protein kinase 5	Mitogen-activated protein kinase kinase kinase 5	1.648072139	9.28E-11
5332	PLCB4	Phospholipase C beta 4	1-phosphatidylinositol 4,5-bisphosphate phosphodiesterase beta-4	1.435641161	4.88E-04
958	CD40	CD40 molecule	Tumor necrosis factor receptor superfamily member 5	1.420692755	1.87E-10
9451	EIF2AK3	Eukaryotic translation initiation factor 2 alpha kinase 3	Eukaryotic translation initiation factor 2-alpha kinase 3	1.394181327	3.15E-04
3305	HSPA1L	Heat shock protein family A (Hsp70) member 1 like	Heat shock 70 kDa protein 1-like	1.376496254	0.044258948
4318	MMP9	Matrix metallopeptidase 9	Matrix metalloproteinase-9	1.346834459	5.41E-07
1649	DDIT3	DNA damage inducible transcript 3	DNA damage-inducible transcript 3 protein	1.23301527	2.97E-05
2081	ERN1	Endoplasmic reticulum to nucleus	Serine/threonine-protein	1.151335199	2.54E-04
10333	TLR6	Toll like receptor 6	Toll-like receptor 6	1.140748871	7.37E-09
4792	NFKBIA	NFKB inhibitor alpha	NF-kappa-B inhibitor alpha	1.140159714	1.79E-08
3383	ICAM1	Intercellular adhesion molecule 1	Intercellular adhesion molecule 1	1.072405047	7.40E-04
6300	MAPK12	Mitogen-activated protein kinase 12	Mitogen-activated protein kinase 12	1.01158305	0.001110388

Table 3.3: Cholesterol metabolism pathway is upregulated in RER1 ko differentiated THP-1 cells

Gene ID	Gene Symbol	Gene Name/ Alias	Protein Name	Log2FoldChange (RER1KO_noPMA / WT_noPMA)	Qvalue (adjust p value) (RER1KO_noPMA / WT_noPMA)
19	ABCA1	ATP binding cassette subfamily A member 1	Phospholipid-transporting ATPase ABCA1	3.934920512	1.87E-70
348	APOE	Apolipoprotein E	Apolipoprotein E	2.975272472	2.92E-48
4023	LPL	Lipoprotein lipase	Lipoprotein lipase	2.878286259	5.01E-77
4864	NPC1	NPC intracellular cholesterol transporter 1	NPC intracellular cholesterol transporter 1	2.643585611	8.46E-37
341	APOC1	Apolipoprotein C1	Apolipoprotein C-I	2.487522836	1.12E-38
948	CD36	CD36 molecule (CD36 blood group)	Platelet glycoprotein 4	2.128277266	3.03E-26
3949	LDLR	Low density lipoprotein receptor	Low-density lipoprotein receptor	2.105997122	4.50E-29
6770	STAR	Steroidogenic acute regulatory protein	Steroidogenic acute regulatory protein, mitochondrial	2.095579028	0.022716988
4035	LRP1	LDL receptor related protein 1	low-density lipoprotein receptor-related protein 1	2.071860819	2.19E-10
9388	LIPG	Lipase G, endothelial type	Endothelial lipase	1.721075307	2.82E-05
29116	MYLIP	Myosin regulatory light chain interacting protein	E3 ubiquitin-protein ligase MYLIP	1.535327645	2.21E-05
10577	NPC2	NPC intracellular cholesterol transporter 2	NPC intracellular cholesterol transporter 2	1.247088724	5.21E-17
64241	ABCG8	ATP binding cassette subfamily G member 8	ATP-binding cassette sub-family G member 8	1.111005225	0.031282198

Table 3.4: Steroid biosynthesis pathway is upregulated in RER1 ko differentiated THP-1 cells

Gene ID	Gene Symbol	Gene Name	Protein Name	Log2FoldChange (RER1KO_noPMA / WT_noPMA)	Qvalue (adjust p value) (RER1KO_noPMA / WT_noPMA)
6713	SQLE	squalene epoxidase	Squalene monooxygenase	2.520868079	1.01E-39
6307	MSMO1	methylsterol monooxygenase 1	methylsterol monooxygenase 1	2.376808772	8.55E-38
6309	SC5D	sterol-C5-desaturase	Lathosterol oxidase	2.301355407	5.86E-34
1595	CYP51A1	cytochrome P450 family 51 subfamily A member 1	Lanosterol 14-alpha demethylase	2.108690047	4.35E-42
1594	CYP27B1	cytochrome P450 family 27 subfamily B member 1	25-hydroxyvitamin D-1 alpha hydroxylase, mitochondrial	1.543361144	2.93E-04
10682	EBP	EBP cholestenol delta-isomerase	3-beta-hydroxysteroid-Delta(8),Delta(7)-isomerase	1.359461691	3.81E-10
3930	LBR	lamin B receptor	Delta(14)-sterol reductase LBR	1.253023519	1.87E-11

Undifferentiated cells

Downregulated DEGs

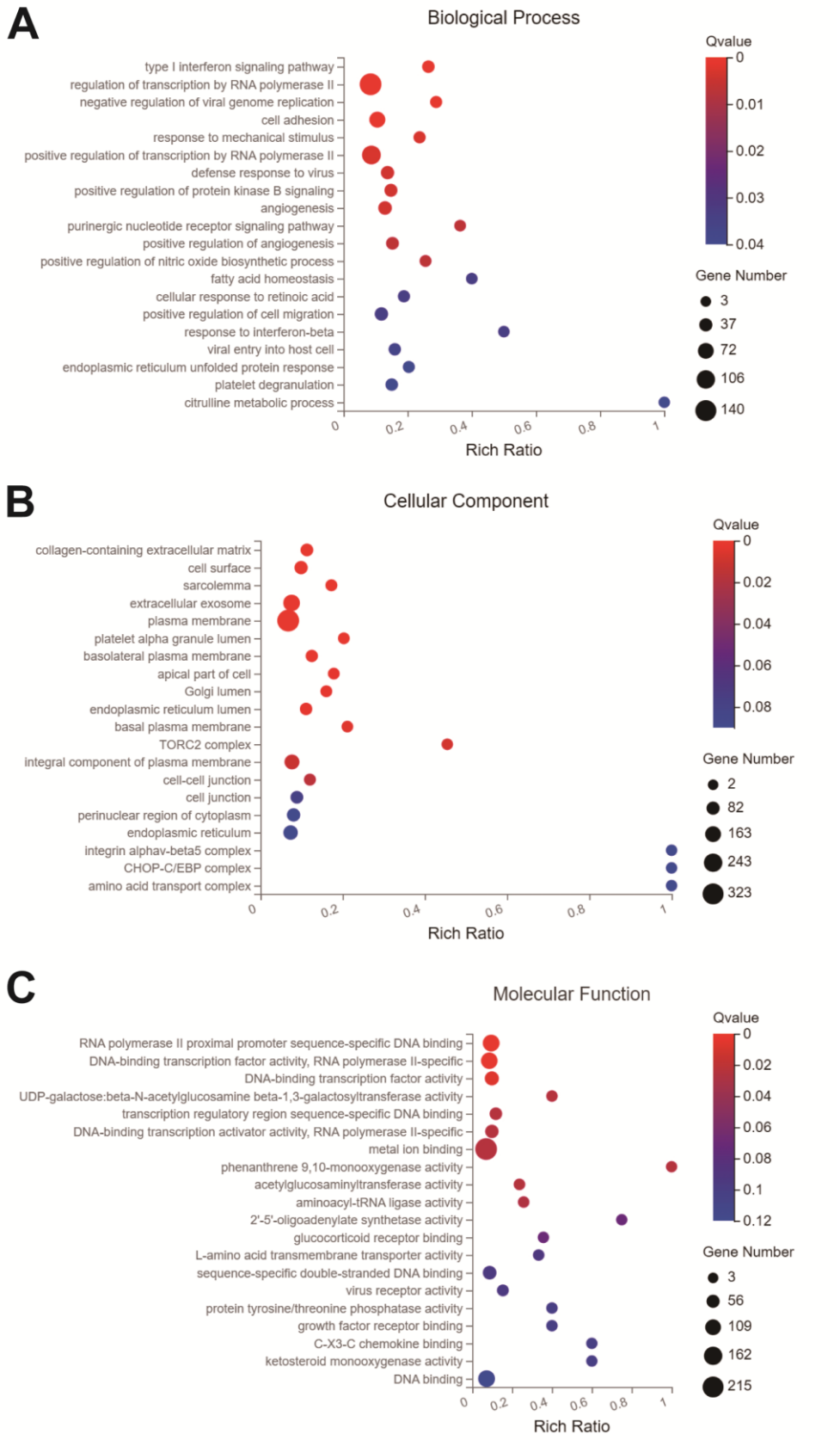

Undifferentiated cells

Upregulated DEGs

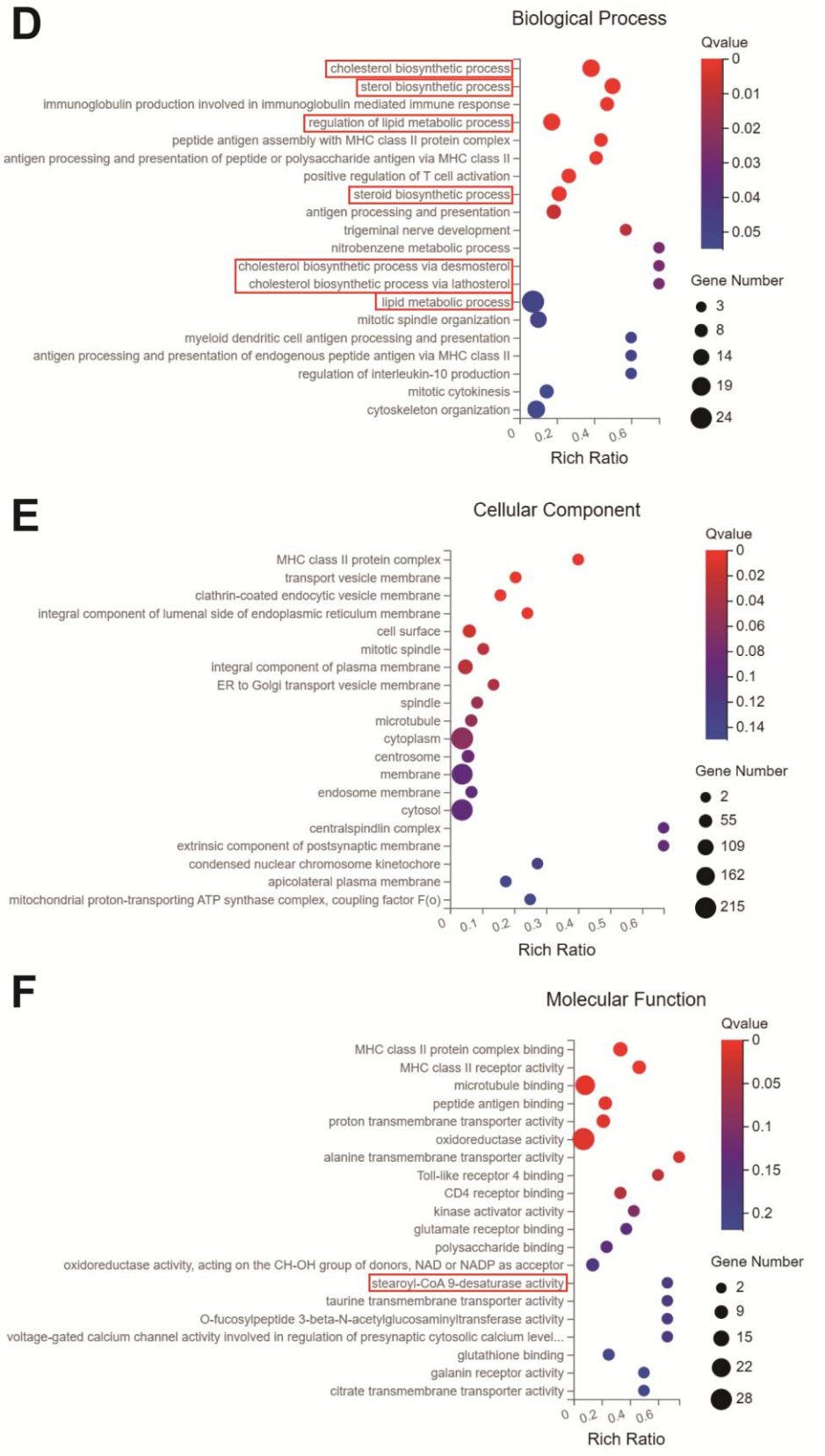

Fig. 3.29: Gene Ontology (GO) enrichment analysis of DEGs in RER1-deleted and wt undifferentiated THP-1 cells. GO enrichment analysis of genes related to biological process (A and D), cellular component (B and E) and molecular function (C and F) were performed in RER1 ko and wt THP-1 undifferentiated cells. Downregulated enrichment (A-C) and unregulated enrichment (D-F) are separately shown. Lipid metabolism related pathways in biological process and molecular function are shown in red rectangular box.

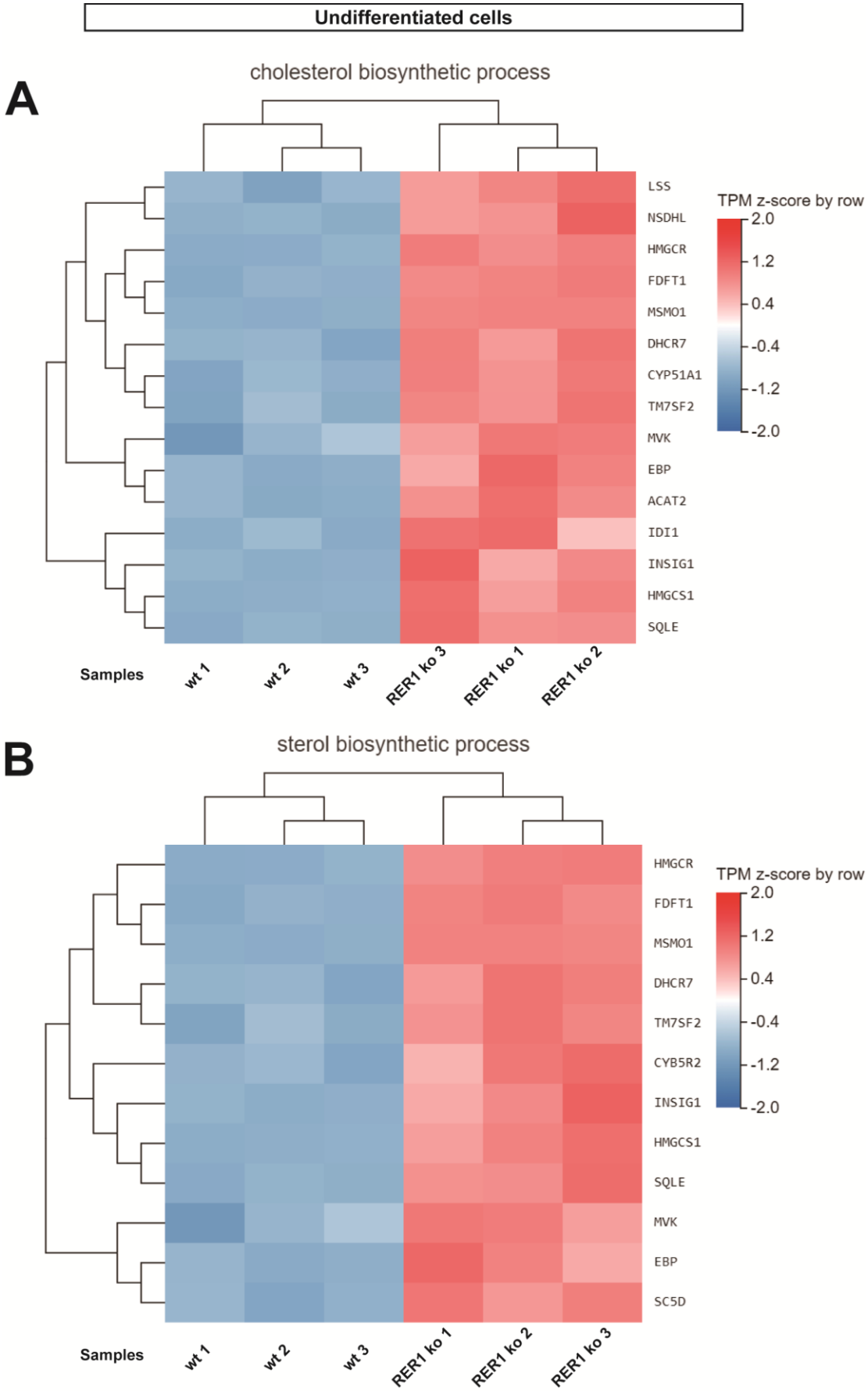
Undifferentiated cells
A
cholesterol biosynthetic process
LSS
NSDHL
HMGCR
FDFT1
MSMO1
DHCR7
CYP51A1
TM7SF2
MVK
EBP
ACAT2
IDI1
INSIG1
HMGCS1
SQLE
TPM z-score by row
2.0
1.2
0.4
-0.4
-1.2
-2.0
Samples
wt 1
wt 2
wt 3
RER1 ko 3
RER1 ko 1
RER1 ko 2
B
sterol biosynthetic process
HMGCR
FDFT1
MSMO1
DHCR7
TM7SF2
CYB5R2
INSIG1
HMGCS1
SQLE
MVK
EBP
SC5D
TPM z-score by row
2.0
1.2
0.4
-0.4
-1.2
-2.0
Samples
wt 1
wt 2
wt 3
RER1 ko 1
RER1 ko 2
RER1 ko 3

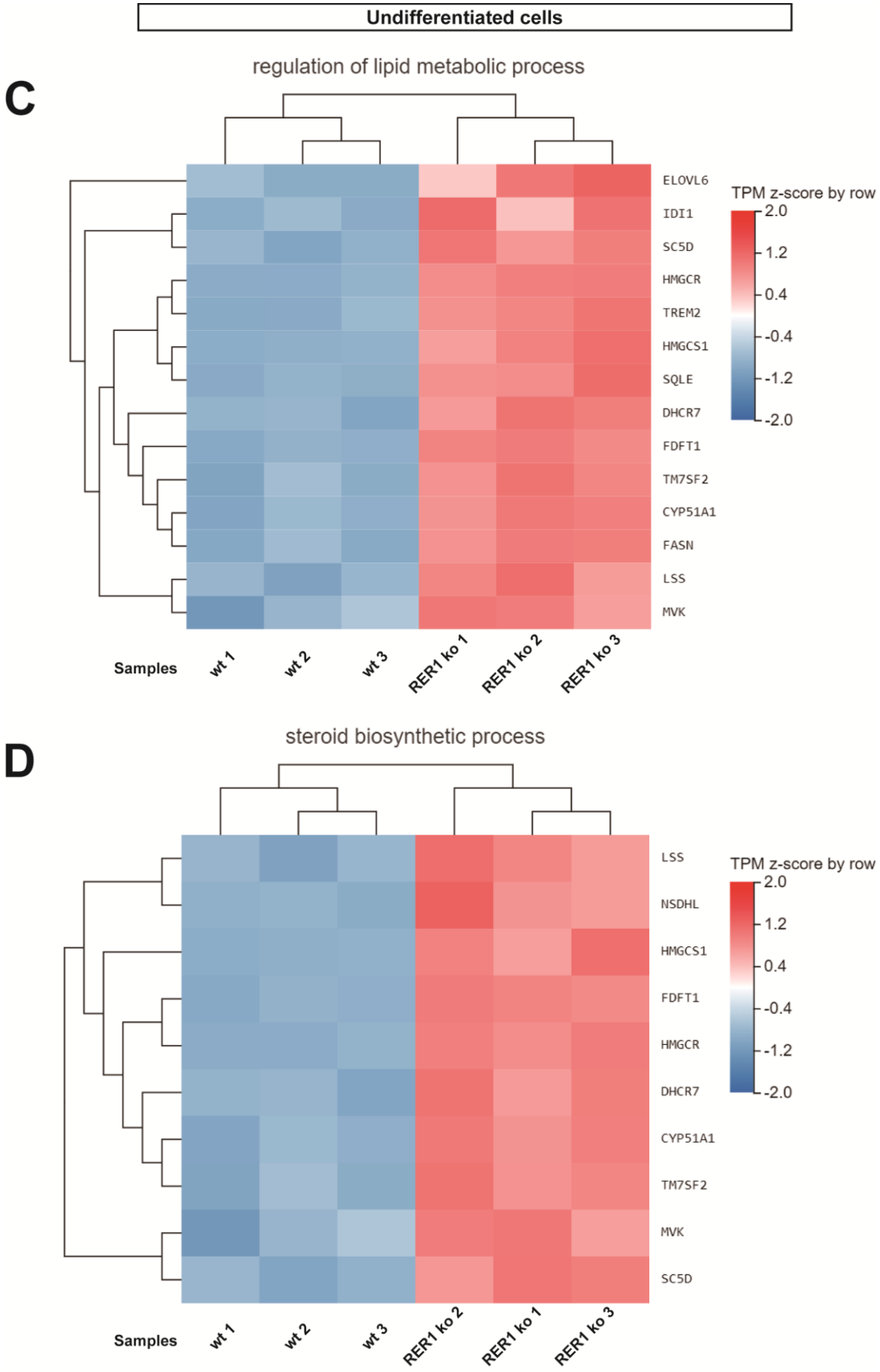
Undifferentiated cells
C
regulation of lipid metabolic process
ELOVL6
IDI1
SC5D
HMGCR
TREM2
HMGCS1
SQLE
DHCR7
FDFT1
TM7SF2
CYP51A1
FASN
LSS
MVK
TPM z-score by row
2.0
1.2
0.4
-0.4
-1.2
-2.0
Samples
wt 1
wt 2
wt 3
RER1 ko 1
RER1 ko 2
RER1 ko 3
D
steroid biosynthetic process
LSS
NSDHL
HMGCS1
FDFT1
HMGCR
DHCR7
CYP51A1
TM7SF2
MVK
SC5D
TPM z-score by row
2.0
1.2
0.4
-0.4
-1.2
-2.0
Samples
wt 1
wt 2
wt 3
RER1 ko 2
RER1 ko 1
RER1 ko 3

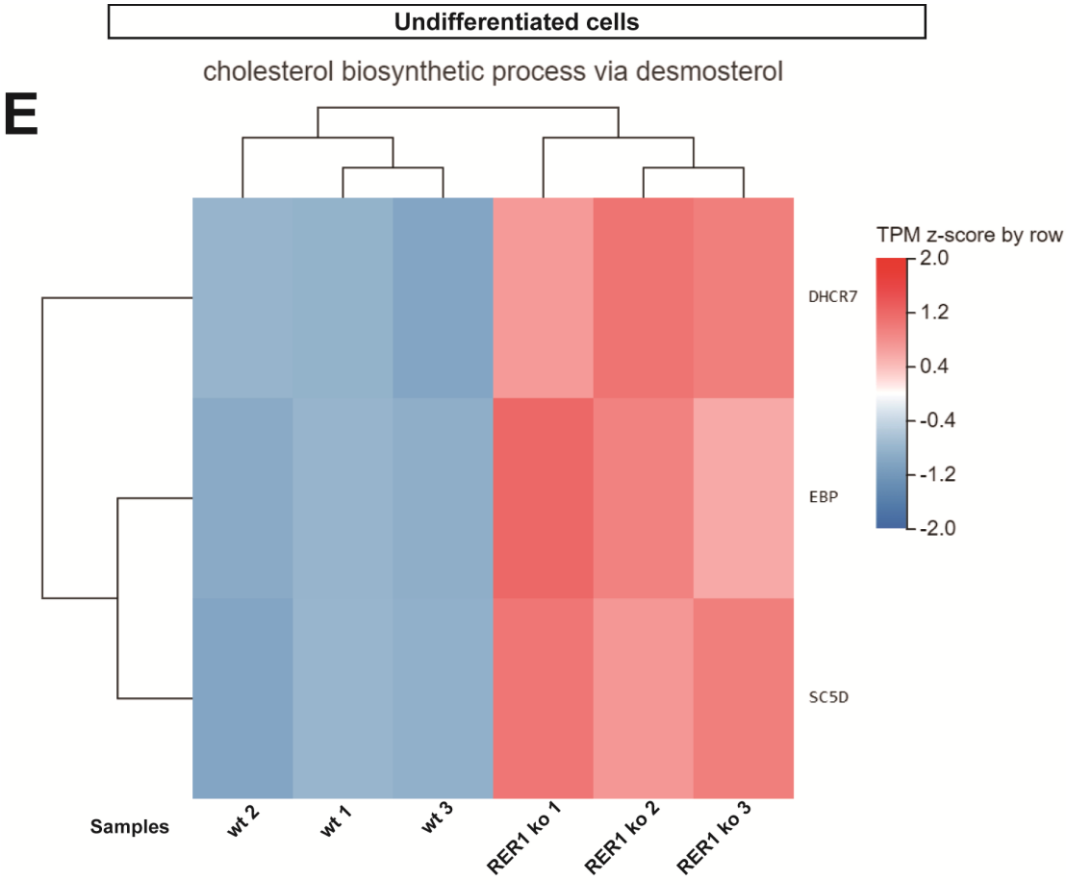
Undifferentiated cells
cholesterol biosynthetic process via desmosterol
E
TPM z-score by row
2.0
1.2
0.4
-0.4
-1.2
-2.0
DHCR7
EBP
SC5D
Samples
wt 2
wt 1
wt 3
RER1 ko 1
RER1 ko 2
RER1 ko 3

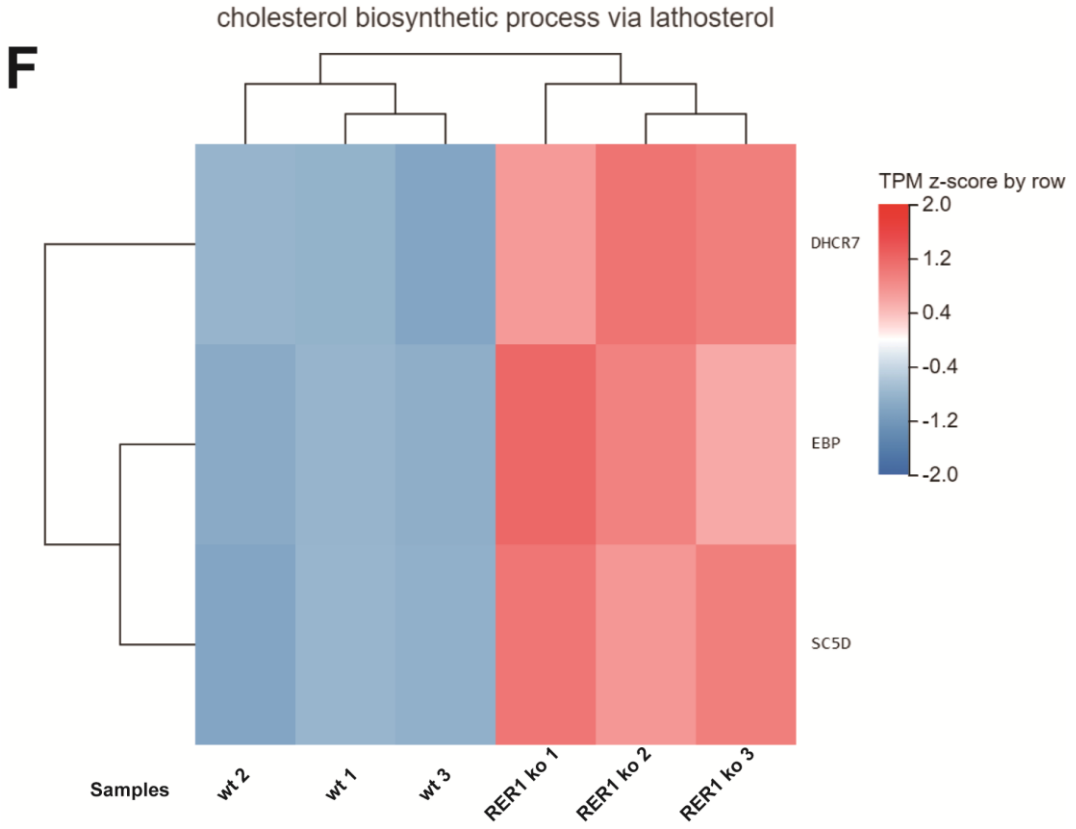
cholesterol biosynthetic process via lathosterol
F
TPM z-score by row
2.0
1.2
0.4
-0.4
-1.2
-2.0
DHCR7
EBP
SC5D
Samples
wt 2
wt 1
wt 3
RER1 ko 1
RER1 ko 2
RER1 ko 3

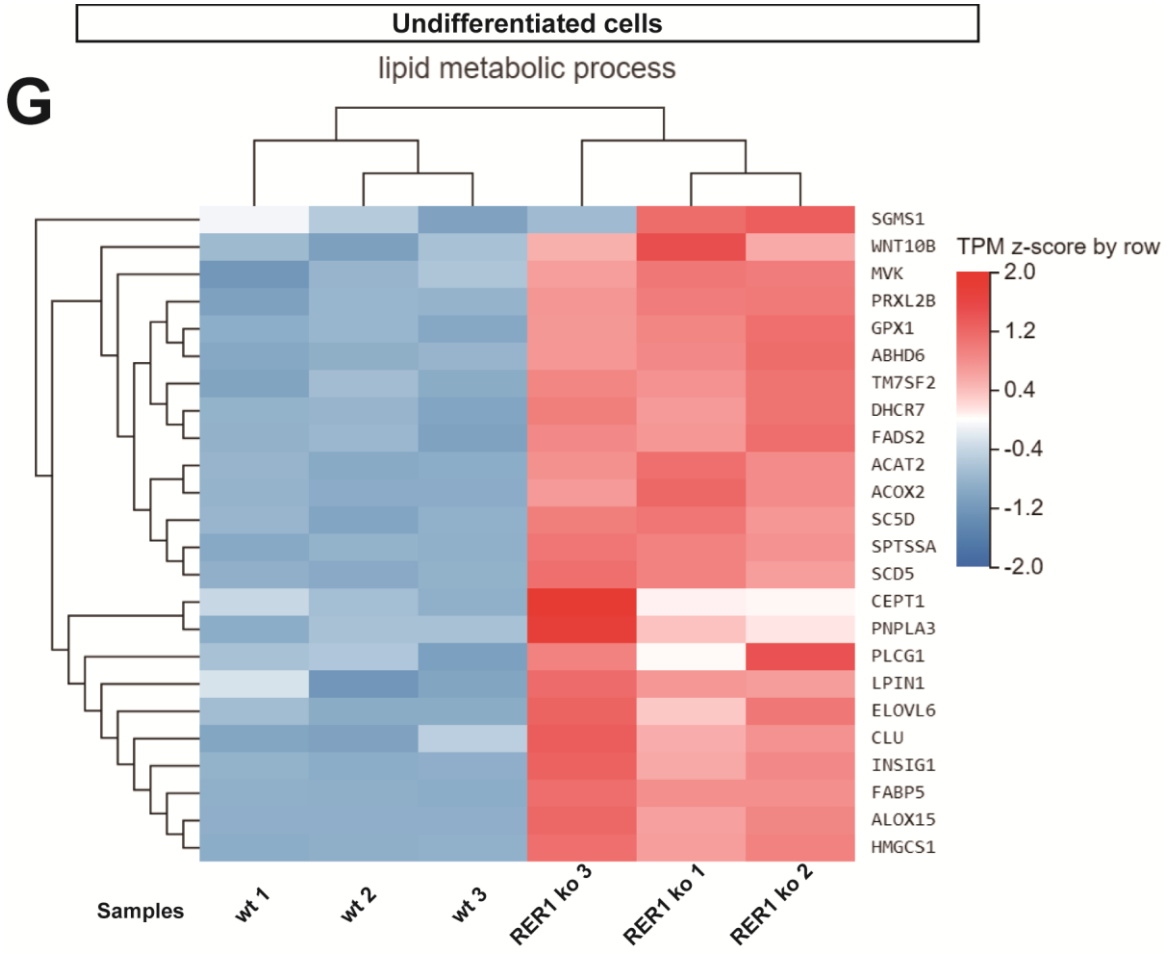

Fig. 3.30: Gene Ontology (GO) biological process enrichment analysis showed lipid metabolism related pathways are upregulated in RER1 ko undifferentiated THP-1 cells. Heatmap of lipid metabolism related pathways, including cholesterol biosynthetic process (A), sterol biosynthetic process (B), regulation of lipid metabolic process (C), steroid biosynthetic process (D), cholesterol biosynthetic process via desmosterol (E), cholesterol biosynthetic process via lathosterol (F) and lipid metabolic process (G). The genes involved in each pathway are shown in table 3.5-3.10.

Table 3.5: Upregulation of cholesterol biosynthetic process in RER1 ko undifferentiated THP-1 cells

Gene ID	Gene Symbol	Gene Name	Protein Name	Log2FoldChange (RER1KO_noPMA / WT_noPMA)	Qvalue (adjust p value) (RER1KO_noPMA / WT_noPMA)
6307	MSMO1	Methylsterol monooxygenase 1	Methylsterol monooxygenase 1	2.0842667	7.25E-50
39	ACAT2	Acetyl-CoA acetyltransferase 2	Acetyl-CoA acetyltransferase, cytosolic	2.007003217	3.79E-55
3156	HMGCR	3-hydroxy-3-methylglutaryl-CoA reductase	3-hydroxy-3-methylglutaryl-CoA reductase	1.931107601	9.83E-61
6713	SQLE	Squalene epoxidase	Squalene monooxygenase	1.882558907	4.64E-72
10682	EBP	EBP cholestenol delta-isomerase	3-beta-hydroxysteroid-Delta(8), Delta(7)-isomerase	1.731975796	3.91E-29
3638	INSIG1	insulin induced gene 1, CL6	Insulin-induced gene 1 protein	1.644743067	4.99E-57
1595	CYP51A1	Cytochrome P450 family 51 subfamily A member 1	Lanosterol 14-alpha demethylase	1.409495453	9.27E-39
50814	NSDHL	NAD(P) dependent steroid dehydrogenase-like	Sterol-4-alpha-carboxylate 3-dehydrogenase, decarboxylating	1.37597262	7.50E-13
1717	DHCR7	7-dehydrocholesterol reductase, SLOS	7-dehydrocholesterol reductase	1.323759153	2.29E-14
3157	HMGCS1	3-hydroxy-3-methylglutaryl-CoA synthase 1	Hydroxymethylglutaryl-CoA synthase, cytoplasmic	1.285537157	1.32E-42
4047	LSS	Lanosterol synthase	Lanosterol synthase	1.185656272	3.53E-07
2222	FDFT1	Farnesyl-diphosphate farnesyltransferase 1	Squalene synthase	1.167520997	1.06E-35
4598	MVK	Mevalonate kinase	Mevalonate kinase	1.146477972	1.34E-05
7108	TM7SF2	Transmembrane 7 superfamily member 2	Delta(14)-sterol reductase TM7SF2	1.07297873	5.41E-07
3422	IDI1	Isopentenyl-diphosphate delta isomerase 1	Isopentenyl-diphosphate Delta-isomerase 1	1.010133383	1.32E-10

Table 3.6: Upregulation of sterol biosynthetic process in RER1 ko undifferentiated cells

Gene ID	Gene Symbol	Gene Name	Protein Name	Log2FoldChange (RER1KO_noPMA / WT_noPMA)	Qvalue (adjust p value) (RER1KO_noPMA / WT_noPMA)
6307	MSMO1	Methylsterol monooxygenase 1	Methylsterol monooxygenase 1	2.0842667	7.25E-50
3156	HMGCR	3-hydroxy-3-methylglutaryl-CoA reductase	3-hydroxy-3-methylglutaryl-CoA reductase	1.931107601	9.83E-61
6713	SQLE	Squalene epoxidase	Squalene monooxygenase	1.882558907	4.64E-72
10682	EBP	EBP cholestenol delta-isomerase	3-beta-hydroxysteroid-Delta(8),Delta(7)-isomerase	1.731975796	3.91E-29
3638	INSIG1	Insulin induced gene 1	Insulin-induced gene 1 protein	1.644743067	4.99E-57
51700	CYB5R2	Cytochrome b5 reductase 2	NADH-cytochrome b5 reductase 2	1.362439787	3.00E-06
1717	DHCR7	7-dehydrocholesterol reductase	7-dehydrocholesterol reductase	1.323759153	2.29E-14
3157	HMGCS1	3-hydroxy-3-methylglutaryl-CoA synthase 1	Hydroxymethylglutaryl-CoA synthase, cytoplasmic	1.285537157	1.32E-42
6309	SC5D	Sterol-C5-desaturase, ERG3, S5DES	Lathosterol oxidase	1.246517242	8.83E-16
2222	FDFT1	Farnesyl-diphosphate farnesyltransferase 1	Squalene synthase	1.167520997	1.06E-35
4598	MVK	Mevalonate kinase	Mevalonate kinase	1.146477972	1.34E-05
7108	TM7SF2	Transmembrane 7 superfamily member 2	Delta(14)-sterol reductase TM7SF2	1.07297873	5.41E-07

Table 3.7: Regulation of lipid metabolic process is upregulated in RER1 ko undifferentiated cells

Gene ID	Gene Symbol	Gene Name	Protein Name	Log2FoldChange (RER1KO_noPMA / WT_noPMA)	Qvalue (adjust p value) (RER1KO_noPMA / WT_noPMA)
79071	ELOVL6	ELOVL fatty acid elongase 6	Very long chain fatty acid elongase 6	5.02457542	0.001995805
3156	HMGCR	3-hydroxy-3-methylglutaryl-CoA reductase	3-hydroxy-3-methylglutaryl-CoA reductase	1.931107601	9.83E-61
6713	SQLE	squalene epoxidase	Squalene monooxygenase	1.882558907	4.64E-72
1595	CYP51A1	cytochrome P450 family 51 subfamily A member 1	Lanosterol 14-alpha demethylase	1.409495453	9.27E-39
1717	DHCR7	7-dehydrocholesterol reductase	7-dehydrocholesterol reductase	1.323759153	2.29E-14
3157	HMGCS1	3-hydroxy-3-methylglutaryl-CoA synthase 1	Hydroxymethylglutaryl-CoA synthase, cytoplasmic	1.285537157	1.32E-42
2194	FASN	fatty acid synthase	Fatty acid synthase	1.251084436	4.21E-36
6309	SC5D	sterol-C5-desaturase	Lathosterol oxidase	1.246517242	8.83E-16
4047	LSS	lanosterol synthase	Lanosterol synthase	1.185656272	3.53E-07
2222	FDFT1	farnesyl-diphosphate farnesyltransferase 1	Squalene synthase	1.167520997	1.06E-35
4598	MVK	mevalonate kinase	Mevalonate kinase	1.146477972	1.34E-05
54209	TREM2	Triggering receptor expressed on myeloid cells 2		1.129664455	3.98E-11
7108	TM7SF2	transmembrane 7 superfamily member 2	Delta(14)-sterol reductase TM7SF2	1.07297873	5.41E-07
3422	IDI1	isopentenyl-diphosphate delta isomerase 1	Isopentenyl-diphosphate Delta-isomerase 1	1.010133383	1.32E-10

Table 3.8: The steroid biosynthetic process is upregulated in RER1 ko undifferentiated THP-1 cells

Gene ID	Gene Symbol	Gene Name	Protein Name	Log2FoldChange (RER1KO_noPMA / WT_noPMA)	Qvalue (adjust p value) (RER1KO_noPMA / WT_noPMA)
3156	HMGCR	3-hydroxy-3-methylglutaryl-CoA reductase	3-hydroxy-3-methylglutaryl-CoA reductase	1.931107601	9.83E-61
1595	CYP51A1	Cytochrome P450 family 51 subfamily A member 1	Lanosterol 14-alpha demethylase	1.409495453	9.27E-39
50814	NSDHL	NAD(P) dependent steroid dehydrogenase-like	Sterol-4-alpha-carboxylate 3-dehydrogenase, decarboxylating	1.37597262	7.50E-13
1717	DHCR7	7-dehydrocholesterol reductase	7-dehydrocholesterol reductase	1.323759153	2.29E-14
3157	HMGCS1	3-hydroxy-3-methylglutaryl-CoA synthase 1	Lanosterol 14-alpha demethylase	1.285537157	1.32E-42
6309	SC5D	Sterol-C5-desaturase	Lathosterol oxidase	1.246517242	8.83E-16
4047	LSS	Lanosterol synthase	Lanosterol synthase	1.185656272	3.53E-07
2222	FDFT1	Farnesyl-diphosphate farnesyltransferase 1	Squalene synthase	1.167520997	1.06E-35
4598	MVK	Mevalonate kinase	Mevalonate kinase	1.146477972	1.34E-05
7108	TM7SF2	Transmembrane 7 superfamily member 2	Delta(14)-sterol reductase TM7SF2	1.07297873	5.41E-07

Table 3.9: Cholesterol biosynthetic process via desmosterol and lathosterol is upregulated in RER1 ko undifferentiated cells

Gene ID	Gene Symbol	Gene Name	Protein Name	Log2FoldChange (RER1KO_noPMA / WT_noPMA)	Qvalue (adjust p value) (RER1KO_noPMA / WT_noPMA)
10682	EBP	EBP cholestenol delta-isomerase	3-beta-hydroxysteroid-Delta(8),Delta(7)-isomerase	1.731975796	3.91E-29
1717	DHCR7	7-dehydrocholesterol reductase	7-dehydrocholesterol reductase	1.323759153	2.29E-14
6309	SC5D	Sterol-C5-desaturase	Lathosterol oxidase	1.246517242	8.83E-16

Table 3.10: Lipid metabolic process is upregulated in RER1 ko undifferentiated THP-1 cells

Gene ID	Gene Symbol	Gene Name	Protein Name	Log2FoldChange (RER1KO_noPMA / WT_noPMA)	Qvalue (adjust p value) (RER1KO_noPMA / WT_noPMA)
8309	ACOX2	Acyl-CoA oxidase 2	Peroxisomal acyl-coenzyme A oxidase 2	5.40578578	4.58E-04
246	ALOX15	Arachidonate 15-lipoxygenase	Polyunsaturated fatty acid lipoxygenase ALOX15	5.134196348	0.005724019
79071	ELOVL6	ELOVL fatty acid elongase 6	Very long chain fatty acid elongase 6	5.02457542	0.001995805
79966	SCD5	Stearoyl-CoA desaturase 5	Stearoyl-CoA desaturase 5	2.780915058	9.74E-23
7480	WNT10B	Wnt family member 10B	Protein Wnt-10b	2.489258935	0.01048109
39	ACAT2	Acetyl-CoA acetyltransferase 2	acetyl-CoA acetyltransferase 2	2.007003217	3.79E-55
127281	PRXL2B	Peroxiredoxin like 2B	Prostamide/prostaglandin F synthase	1.941103681	1.13E-08
3638	INSIG1	Insulin induced gene 1	Insulin-induced gene 1 protein	1.644743067	4.99E-57
5335	PLCG1	Phospholipase C gamma 1	1-phosphatidylinositol 4,5-bisphosphate phosphodiesterase gamma-1	1.524097591	1.24E-04
2876	GPX1	Glutathione peroxidase 1	Glutathione peroxidase 1	1.413364161	6.91E-42
259230	SGMS1	Sphingomyelin synthase 1	Phosphatidylcholine:ceramide cholinephosphotransferase 1	1.389932176	0.033195848
57406	ABHD6	Abhydrolase domain containing 6, acylglycerol lipase	Monoacylglycerol lipase ABHD6	1.356112209	0.004410288
1717	DHCR7	7-dehydrocholesterol reductase	7-dehydrocholesterol reductase	1.323759153	2.29E-14
1191	CLU	Clusterin	Clusterin	1.300241265	0.017307615
3157	HMGCS1	3-hydroxy-3-methylglutaryl-CoA synthase 1	Lanosterol 14-alpha demethylase	1.285537157	1.32E-42
6309	SC5D	Sterol-C5-desaturase	Lathosterol oxidase	1.246517242	8.83E-16
9415	FADS2	Fatty acid desaturase 2	Acyl-CoA 6-desaturase	1.171429157	1.01E-15
2171	FABP5	Fatty acid binding protein 5	Fatty acid-binding protein 5	1.159770456	1.01E-33
80339	PNPLA3	Patatin like phospholipase domain containing 3	1-acylglycerol-3-phosphate O-acyltransferase PNPLA3	1.156253221	1.27E-07
4598	MVK	Mevalonate kinase	Mevalonate kinase	1.146477972	1.34E-05
7108	TM7SF2	Transmembrane 7 superfamily member 2	Delta(14)-sterol reductase TM7SF2	1.07297873	5.41E-07
171546	SPTSSA	Serine palmitoyltransferase small subunit A	Serine palmitoyltransferase small subunit A	1.033638595	1.22E-13
23175	LPIN1	Lipin 1	Phosphatidate phosphatase LPIN1	1.009996073	2.87E-05
10390	CEPT1	Choline/ethanolamine phosphotransferase 1	Choline/ethanolaminephosphotransferase 1	1.003102894	8.06E-07

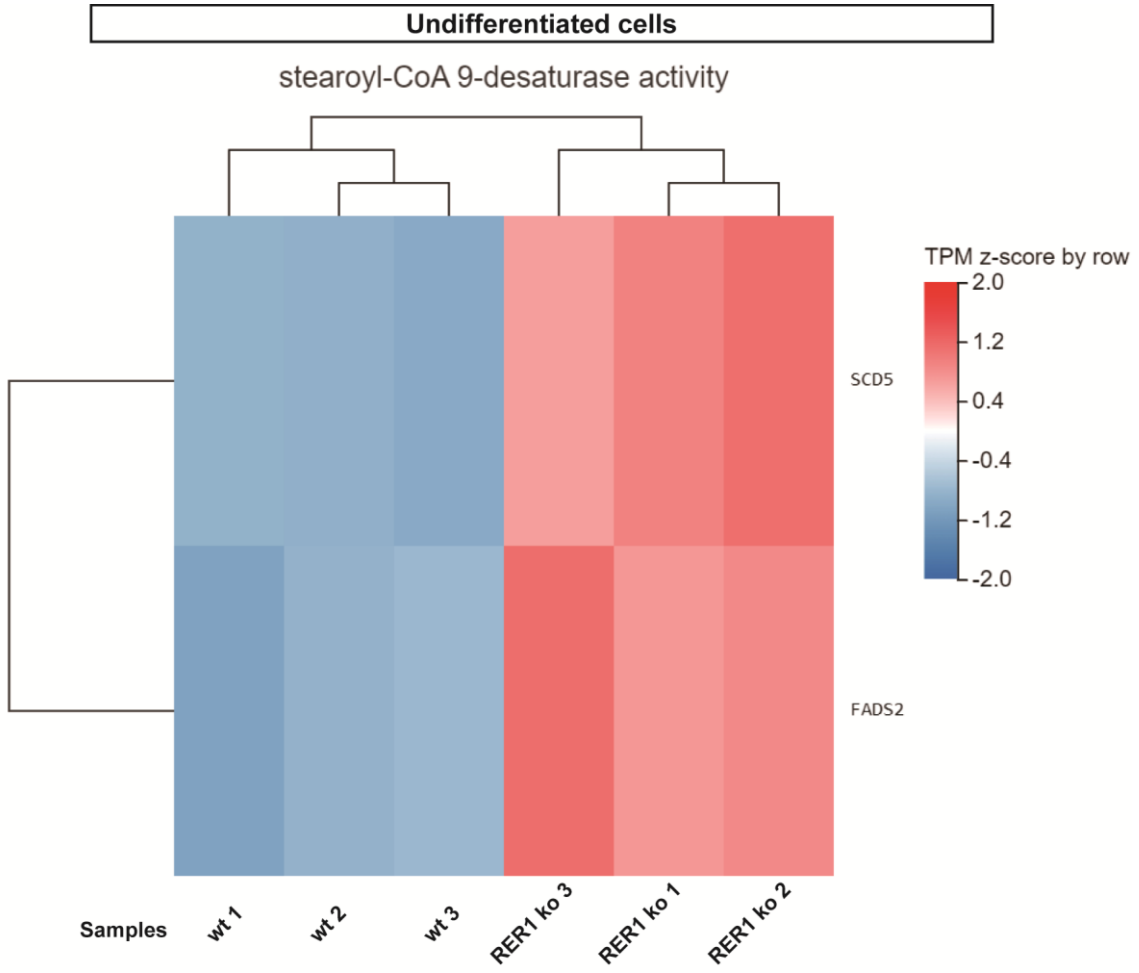

Fig. 3.31: Gene Ontology (GO) molecular function enrichment analysis stearoyl-CoA 9-desaturase activity is upregulated in RER1 ko undifferentiated THP-1 cells. Heatmap of two genes which are upregulated in stearoyl-CoA 9-desaturase activity. The genes involved in each pathway are shown in table 3.11.

Table 3.11: The stearoyl-coa 9-desaturase activity is upregulated in RER1 ko undifferentiated THP-1 cells

Gene ID	Gene Symbol	Gene Name	Protein Name	Log2FoldChange (RER1KO_noPMA / WT_noPMA)	Qvalue (adjust p value) (RER1KO_noPMA / WT_noPMA)
79966	SCD5	Stearoyl-CoA desaturase 5	Stearoyl-CoA desaturase 5	2.780915058	9.74E-23
9415	FADS2	Fatty acid desaturase 2	Acyl-CoA 6-desaturase	1.171429157	1.01E-15

Differentiated cells

Downregulated DEGs

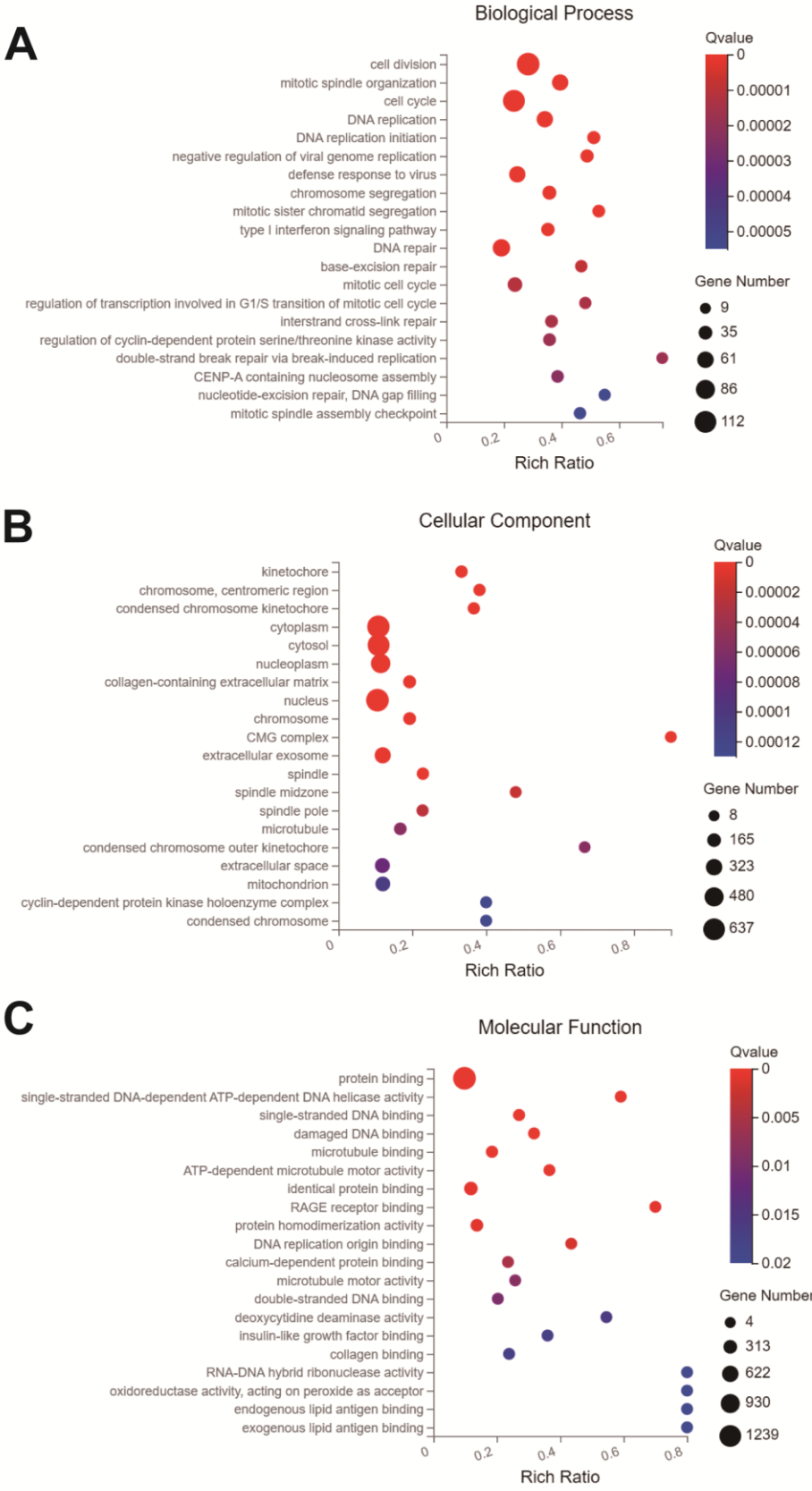

Differentiated cells

Upregulated DEGs

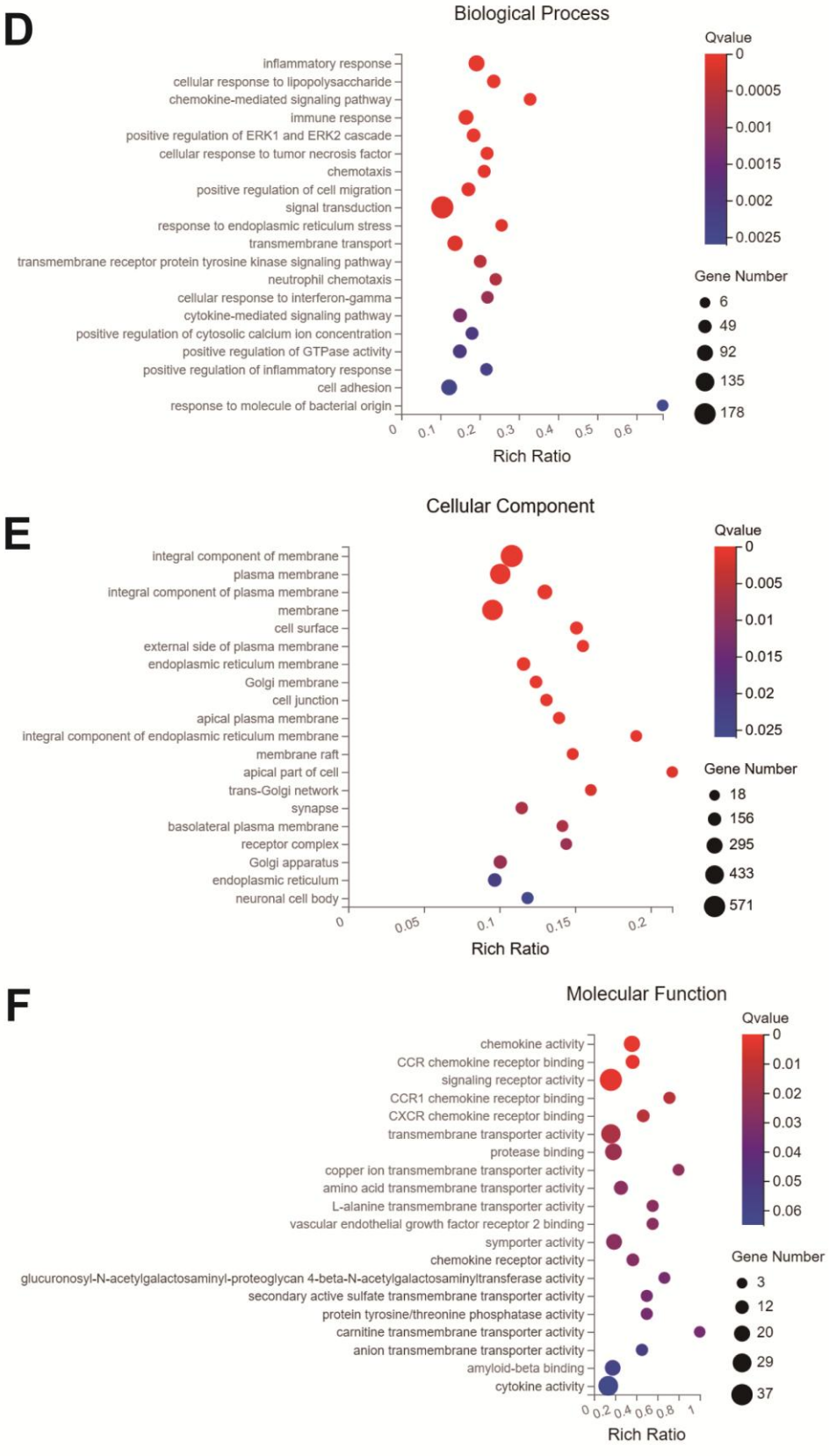

Fig. 3.32: Gene Ontology (GO) enrichment analysis of DEGs in RER1-deleted and wt differentiated THP-1 cells. GO enrichment analysis of genes related to biological process (A and D), cellular component (B and E) and molecular function (C and F) were performed in RER1 ko and wt THP-1 differentiated cells. Downregulated enrichment (A-C) and unregulated enrichment (D-F) are separately shown.

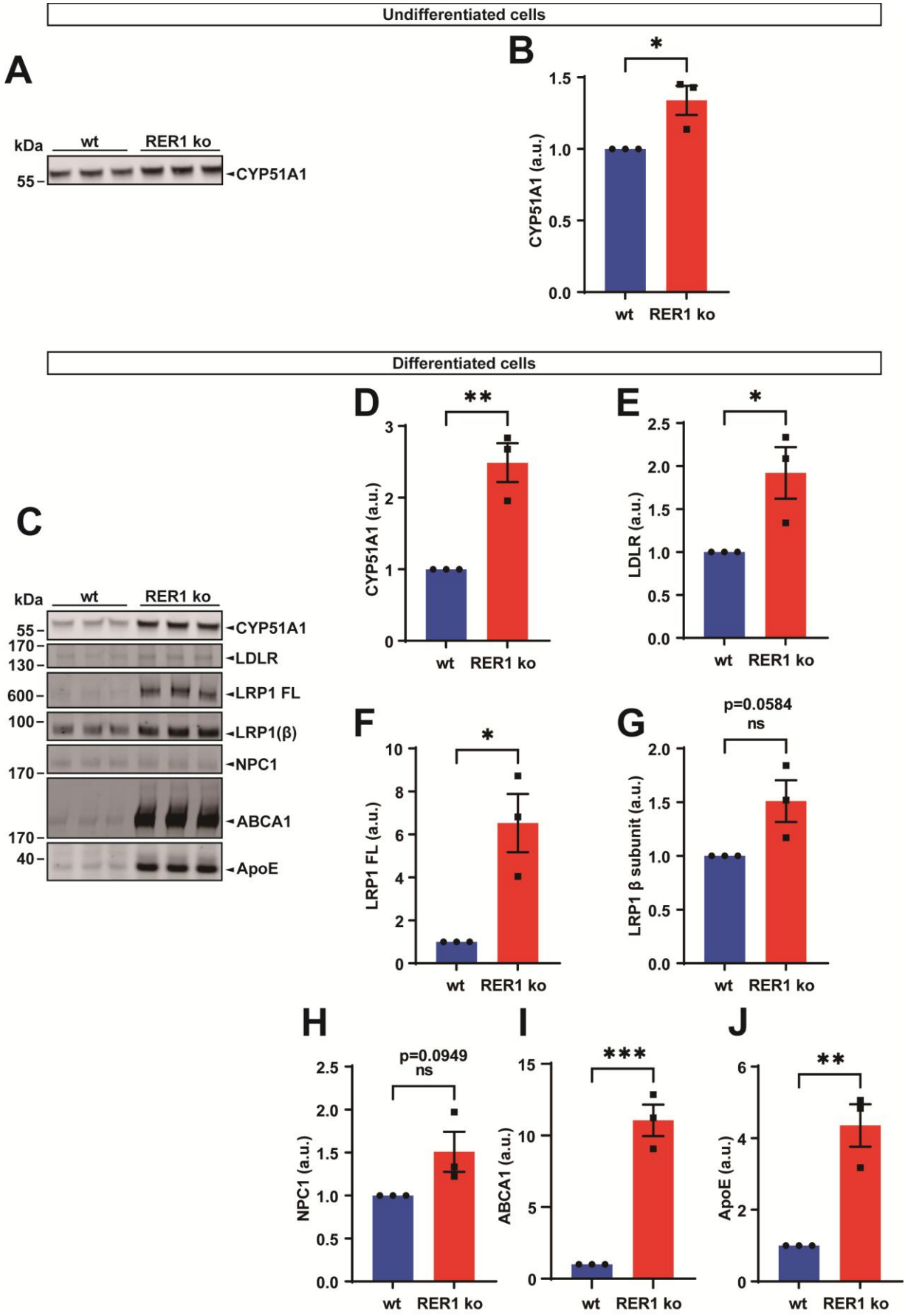
Undifferentiated cells
A
kDa
wt
RER1 ko
55
CYP51A1
B
*
CYP51A1 (a.u.)
1.5
1.0
0.5
0.0
wt
RER1 ko
Differentiated cells
C
kDa
wt
RER1 ko
55
CYP51A1
170
130
LDLR
600
LRP1 FL
100
LRP1(β)
170
NPC1
170
ABCA1
40
ApoE
D
**
CYP51A1 (a.u.)
3
2
1
0
wt
RER1 ko
E
*
LDLR (a.u.)
2.5
2.0
1.5
1.0
0.5
0.0
wt
RER1 ko
F
*
LRP1 FL (a.u.)
10
8
6
4
2
0
wt
RER1 ko
G
p=0.0584
ns
LRP1 β subunit (a.u.)
2.0
1.5
1.0
0.5
0.0
wt
RER1 ko
H
p=0.0949
ns
NPC1 (a.u.)
2.5
2.0
1.5
1.0
0.5
0.0
wt
RER1 ko
I
***
ABCA1 (a.u.)
15
10
5
0
wt
RER1 ko
J
**
ApoE (a.u.)
6
4
2
0
wt
RER1 ko

Fig. 3.33: Expressions of lipid metabolism related proteins in wt and RER1 ko THP-1 cells. (A) and (C) Detection of lipid metabolism related proteins in RER1 ko and wt THP-1 undifferentiated (A) and differentiated (C) cells. Cellular membranes were isolated and western immunoblotting was used for the detection of the indicated protein. Quantification of CYP51A1 (B and D), LDLR (E), LRP1 (F and G), NPC1 (H), ABCA1 (I) and ApoE (J) by western immunoblotting (as shown in A and C) Indicated proteins were normalized to the full protein stained by ponceau. Values represent Mean ± SEM of three independent experiments with one to three samples per experiment. Each data point represents the mean value of an individual experiment. Student's t-test (unpaired, two-tailed). *p <0.05, **p <0.01, ***p <0.001.

4 Discussion

DAP12, interacting with its co-receptors, including TREM2, plays important roles in the regulation of immune cell functions, including survival and proliferation, phagocytosis, chemotaxis, cytoskeletal remodeling and cytokine production (Koth et al., 2010, Otero et al., 2012, Takahashi et al., 2005, Wang et al., 2016). The physiological importance of DAP12 is demonstrated by loss of function mutations that cause NHD, a severe disorder characterized by bone abnormalities and progressive dementia (Paloneva et al., 2002). Notably, NHD can also be caused by mutations in TREM2, indicating that impaired TREM2-DAP12 signaling underlies the development of this disease (Liu et al., 2024, Sessa et al., 2004, Soragna et al., 2003).

In this study, we used THP-1 monocyte-derived macrophage-like cells as a model where the TREM2-DAP12 complex is endogenously expressed, and HEK293 cells as a model where the TREM2-DAP12 complex is overexpressed. The present data confirm that the interaction of DAP12 and TREM2 is mediated by the charged residues in the transmembrane domain of the two proteins. Trimeric and tetrameric assemblies of DAP12 are formed in transiently transfected HEK293 cells with DAP12 and TREM2 variants when DAP12 is not binding to TREM2. The absence of TREM2 or without the interaction with TREM2, DAP12 is instable and degraded efficiently by proteasome. Moreover, the assembly with TREM2 is necessary for the proper transport of DAP12 to the plasma membrane. The present work also indicates that the aspartic acid residue D50 in the transmembrane of DAP12 represents a retention signal, and that RER1 prevents cell surface transport of DAP12 by binding to this D50 residue when it is not assembled with one of its cognate immunoreceptors. The RXR motif in the cytoplasmic domain of DAP12 does not seem to play a role in the retention of unassembled DAP12. The deletion of RER1 also interferes with TREM2-DAP12 signaling and phagocytosis. In addition, RER1 alters lipid metabolism in both undifferentiated and differentiated THP-1 cells. Thus, RER1 is critically involved in the regulation of DAP12 mediated signaling and immune cell function.

4.1 Low concentration of PMA is sufficient to differentiate THP-1 cells into macrophage-like cells

THP-1 is a human acute monocytic leukemia cell line derived from the peripheral blood of a patient diagnosed with monocytic leukemia, which was established in 1980 (Tsuchiya et al., 1980). Macrophage-like cells differentiated from THP-1 cells have been widely used in inflammation related studies. A recent study compared the transcriptomes in undifferentiated and differentiated THP-1 cells by RNA sequencing and revealed that the differentiation of THP-1 cells to macrophage-like cells leads to the significant upregulation of more than 3000 genes, which are closely associated with the activation of immune cells, and to the downregulation of more than 2000 genes linking to cell cycle process and cell division (Liu et al., 2023), indicating that differentiated THP-1 cells acquire additional functions related to both innate and adaptive immunity while concurrently losing their ability to proliferate, as compared to undifferentiated THP-1 cells.

There are several inducers used for the differentiation of THP-1 cells into macrophage-like cells, including PMA, retinoic acid (RA), tumor necrosis factor-alpha (TNF-α) plus Interferon-gamma (IFN-γ), 1,25-Dihydroxyvitamin D3 (Vitamin D3) and colony-stimulating factors (CSF, e.g., M-CSF, GM-CSF), which act through different signaling pathways to drive THP-1 cell differentiation. During the differentiation, cells get adherent and undergo many morphological and physiological alterations, resulting in diverse phenotypes and functional characteristics of the differentiated macrophage-like cells (Chanput et al., 2014, Chen et al., 1996, Chen & Ross, 2004, Schwende et al., 1996, Tsuchiya et al., 1982). PMA is the most commonly used inducer for the differentiation of THP-1 monocytes into macrophage-like cells and it is an analog of diacyl glycerol which can activate PKC, in particular the classical and the novel PKC isoforms (Tsuchiya et al., 1982). However, there are many different protocols about the choice for the concentration of PMA, ranging from 5 ng/mL to 400 ng/mL, and treatment time, ranging from 24 h to 72 h (Park et al., 2007). Here, we also tried different conditions, including the different concentrations of PMA, ranging from 5 ng/mL to 50 ng/mL, and different treatment time for PMA, 48 h and 72 h, to differentiate THP-1 cells into macrophage-like cells. We observed the treatment of PMA 5 ng/mL for 48 h and recovery of cells in RPMI completed medium was sufficient to induce TREM2 and DAP12 expression in THP-1 differentiated macrophage-like cells (Fig. 3.1).

The expression of DAP12 and TREM2 at both mRNA and protein level were increased robustly in macrophage-like cells compared to undifferentiated THP-1 monocytes (Fig.3.1). Similar findings were obtained previously in a study for optimizing differentiation conditions of THP-1 cells (Park et al., 2007). They proposed that THP-1 cells are effectively differentiated with 5 ng/ml PMA, and subsequently, the differentiated macrophages exhibit a robust response to weak stimuli without excessive gene upregulation induced by PMA. The expression of TREM2 in monocytes is controversial (Bouchon et al., 2000). Here, we observed a low level of TREM2 expression at both protein and mRNA level in THP-1 monocytes cell line (Fig. 3.1).

Moreover, we conducted a comparison of DAP12 and TREM2 migration in SDS gels by western immunoblotting under non-reducing (sample buffer without DTT) and reducing (sample buffer with DTT) conditions. We found that addition of DTT to the loading buffer led to the complete reduction of DAP12 dimers into monomers. However, under the non-reducing condition, we observed well-defined DAP12 homodimers, which are crucial for interaction with co-receptors (Fig. 3.1). A previous study demonstrated that KIR2DS, a co-receptor of DAP12, interacts with DAP12 dimers, and DAP12 oligomers were only observable under non-reducing conditions (Knoblich et al., 2015). Consequently, we opted for the non-reducing condition throughout our study, as our focus is on understanding the mechanisms governing the assembly of the TREM2-DAP12 complex.

4.2 The interaction of DAP12 and TREM2 is mediated by the charged residues in the transmembrane domain of the proteins

Previous findings indicated the interaction of DAP12 and its co-receptors is mediated via charged amino acid residues in their TMDs, including the aspartic acid residue D50 in DAP12, and a lysine (K) or arginine (R) residue in the respective the co-receptors (Bouchon et al., 2001, Feng et al., 2006, Lanier et al., 1998a). The presence of a central transmembrane (TM) lysine is a critical characteristic of DAP12-associated receptors, and assembly and surface expression is not interfered even the lysine is placed in a TM sequence full of hydrophobic amino acids, such as valine or leucine residues (Feng et al., 2006, Feng et al., 2005). Here we generated the mutations of TREM2-DAP12 interaction sites, D50A and K186N, by site-directed mutagenesis and HEK293 cells were transiently

transfected with the cDNA constructs coding those two mutations as well as TRM2 wt+DAP12 wt. Further coimmunoprecipitation assays showed that the interaction of TREM2 and DAP12 didn't exist in those two mutations (Fig. 3.3). Similar results were obtained in a previous study showing that both TREM2 FL and CTF were not precipitated by anti-DAP12 antibody in TREM2 and DAP12 D50A co-transfected cells (Zhong et al., 2015). Interestingly, a K186N substitution is one of the TREM2 mutant causing NHD which was identified in Norwegian NHD family (Paloneva et al., 2002). The K186N mutation is predicted to result in defects in signal transduction due to the impairment of the interaction with DAP12 (Call et al., 2010). Here, our results confirmed the interaction of DAP12 and one of its co-receptors, TREM2, is mediated by DAP12 D50 and TREM2 K186. This similar assembly structure, one basic and two acid residues, exists in other different immunoreceptor-adapter interaction. Important examples include TCR that interacts with its adaptor CD3, which contains three signaling modules, CD3δε, CD3γε, and ζζ (Call et al., 2002), and NKG2D that assembles with DAP10 (Feng et al., 2006, Feng et al., 2005, Garrity et al., 2005). The threonine residue in DAP12 TMD (T54) is also involved for the interaction of DAP12 and its co-receptors, since these two T54 residues in the dimer of DAP12 contribute to the complex electrostatic network between DAP12 and its co-receptors, and T54 could stabilize the D50 side chain in a position that favors contact with the lysine amino group (Call et al., 2010). The presence of polar amino acids at specific positions in the TMD is sufficient for the interaction between adapter proteins and immune receptors (Feng et al., 2006). In our research, the complete loss of interaction resulting from mutations at interaction sites further confirms this. Furthermore, there are other factors affecting the binding specificity between immunoreceptors and their adaptors, including spatial hindrance of the immunoreceptor extracellular domains (Feng et al., 2006).

We also noted that compared with the HEK 293 cells overexpressed TREM2 wt-DAP12 wt, both DAP12 D50A and TREM2 K186N mutants, which showed no interaction between DAP12 and TREM2, formed increased levels of SDS resistant trimers and tetramers (Fig. 3.3). A previous study also showed that in addition to dimeric form, DAP12 formed into trimer and tetramer when it is not assembled with KIR2DS, one of its co-immunoreceptors. Those trimeric or tetrameric structures are competitive with receptor association in the ER (Knoblich et al., 2015). As shown by *in vitro* translation experiments with different amounts

of KIR2DS mRNA mixing with the same amounts of DAP12 wt and D50N mutation mRNA, the levels of trimer and tetramer decreased as the amount of KIR2DS mRNA increased in DAP12 wt while DAP12 D50N exhibited consistent levels of trimer and tetramer regardless of the increased amounts of KIR2DS mRNA.

For the co-immunoprecipitation experiments, we used transiently transfected HEK293 cells which have robust protein overexpression. However, studies have demonstrated that excessive protein overexpression may overwhelm retention and quality control mechanisms within the ER, consequently facilitating the export of misfolded or immature proteins (Barlowe & Helenius, 2016, Hammond et al., 1994, Spear & Ng, 2003). To avoid saturation of cellular degradation pathways or induction of cell stress responses, stable cell clones in HEK293 cells that overexpress the indicated TREM2 and DAP12 variants were generated for further experiments on the turnover and localization of these proteins in this study.

4.3 DAP12 protein expression level is decreased without assembly with TREM2

To investigate the characteristics of TREM2-DAP12 complex assembly, especially the effect of TREM2 on the metabolism of DAP12, TREM2 was deleted in THP-1 cells and direct comparison of DAP12 expression level in differentiated wt and TREM2 ko THP-1 cells showed a significant decrease of DAP12 dimer and monomer at protein level (Fig. 3.4), but not at mRNA level (Fig. 3.4), indicating that the deletion of TREM2 might impair the translational or post-translational process of DAP12 protein (Liu et al., 2024). A similar result was observed in a prior study showing that DAP12 was decreased in TREM2 ko THP-1 cells at protein level (Boudesco et al., 2022), while there was no comparison of mRNA expression level between wt and TREM2 ko THP-1 cells in this study. In another transmembrane protein complex, the absence of PS1 or PS1/PS2 leads to a significant reduction in PEN2 levels. Similarly, the downregulation of Nct by RNA interference results in reduced levels of PEN2. Conversely, the downregulation of PEN2 via RNA interference is also associated with decreased levels of PS, impaired Nct maturation, and the formation of a deficient γ-secretase complex, indicating that components of the multiprotein complex can influence the expression levels of each other (Steiner et al., 2002). Another sample is that TREM2 CTF was significantly increased in the presence of DAP12 (Zhong et al.,

2015). Those evidences might indicate that complex formation stabilizes the individual proteins. When any component is removed, it leads to a decrease in the overall abundance of the complex, consequently resulting in a loss of complex activity (Edbauer et al., 2002, Francis et al., 2002, Steiner et al., 2002, Zhong et al., 2015). To further find out the reason why DAP12 protein expression level was so strongly decreased in TREM2 ko cells, we explored the turnover of DAP12 by cycloheximide chase assay in the following experiments.

4.4 TREM2 stabilizes DAP12

Previous study showed that DAP12 could stabilize the TREM2 CTF, indicating the importance of DAP12 for its co-receptor metabolism (Zhong et al., 2015). However, there is no evidence about the effect of assembly with co-receptors on DAP12 metabolisms. Here, we found the expression of DAP12 at protein level in TREM2 ko was strongly decreased compared with wt cells (Fig. 3.4). Therefore, we wanted to explore the effects of TREM2 on the stability of DAP12 using a THP-1 differentiated macrophage-like cell model with endogenous expression of TREM2 and DAP12. Different approaches have been applied to measure the kinetics of protein turnover, including radionuclide-labeled amino acids based pulse-chase assay, pharmacological inhibitors of the synthesis, the degradation based chase assay or mass spectrometry technology based assay (Ross et al., 2021). Cycloheximide, a protein synthesis inhibitor, is commonly used to analyze protein turnover by measuring changes in protein levels over time to determine their half-life. By blocking new protein synthesis, cycloheximide allows existing proteins to degrade, and the rate of protein degradation can be quantified to determine protein turnover rates (Belle et al., 2006). Cycloheximide is a small molecule derived from *Streptomyces griseus* that is used as a fungicide. Cycloheximide works by inhibiting protein synthesis at the translation elongation stage. Specifically, it binds to the 60S ribosomal subunit of eukaryotic ribosomes and interferes with the translocation step of protein synthesis (Garreau de Loubresse et al., 2014, Schneider-Poetsch et al., 2010). This inhibition prevents the elongation of polypeptide chains, leading to the cessation of protein synthesis (Kao et al., 2015, Li et al., 2021, Miao et al., 2023). By inhibiting protein synthesis, cycloheximide is used to investigate the turnover rates of specific proteins and to study

the mechanisms underlying protein degradation pathways, such as the ubiquitin-proteasome pathway and autophagy.

In the present study, cycloheximide chase assay was used to assess the turnover of DAP12 in both differentiated THP-1 cell model and HEK293 cell model with overexpression of DAP12 and TREM2 variants. Interestingly, deletion of TREM2 strongly increased the degradation of DAP12 dimer in THP-1 differentiated cells. The half-life time of DAP12 dimer was shortened from around 6 h in wt cells to around 3 h in TREM2 ko cells, while the deletion of TREM2 had little effect on the turnover rate of DAP12 monomer (Fig. 3.4). These results indicated destabilization of DAP12 dimer when it is not assembled with an appropriate immune receptor. Similar results were also obtained in a non-immune related HEK293 Flp-In cell model with overexpressed DAP12 and/or TREM2. We observed that dimeric DAP12 was quickly degraded in cells expressing DAP12 alone or together with the TREM2 K186N variant, but not in cells expressing DAP12 together with TREM2 wt, indicating that the stabilization of DAP12 dimer by TREM2 does not require other factors selectively expressed in immune cells (Liu et al., 2024).

However, monomeric DAP12 in HEK293 cells co-expressing DAP12 wt and TREM2 wt was quite stable upon the treatment with cycloheximide (Fig. 3.5). In HEK293 cells with the co-overexpression of DAP12 and TREM2 wt, the generation of TREM2 and DAP12 proteins are comparable because of this bicistronic cDNA construct encoding TREM2 and DAP12 separated by a T2A linker sequence to ensure stoichiometric expression of both proteins. However, in THP-1 wt cells, the DAP12 protein might be present as a pool available for the binding to different co-receptors. We assume that the amount of endogenously expressed DAP12 is more than TREM2 in THP-1 cells. Therefore, the free DAP12 pool in THP-1 cells is higher than that in HEK293 cells with the overexpression of DAP12 and TREM2 and unstable without the binding to the co-receptors (Liu et al., 2024).

4.5 DAP12 is mainly degraded by the ubiquitin-proteasome pathway

Degradation pathways of DAP12 and TREM2 have not been widely explored. In cells, there are two main degradation pathways responsible for maintaining cellular homeostasis and disposing of unwanted or damaged components: the ubiquitin-proteasomal pathway

and the autophagy-lysosomal pathway (Ciechanover, 2005, Dikic, 2017). The ubiquitin-proteasomal pathway targets individual intracellular short-lived proteins (Majumder & Baumeister, 2019). This process involves the covalent attachment of a small protein known as ubiquitin to target proteins, thereby tagging them for degradation (Majumder & Baumeister, 2019). The proteasome recognizes the polyubiquitin chain attached to the target protein, unfolds it, and degrades it into short peptides (Inobe & Matouschek, 2014, Tanaka, 2009). The autophagy-lysosomal pathway is mainly responsible for the degradation and recycling of organelles, membrane proteins, and invading pathogens (Kraft & Martens, 2012, Yang & Klionsky, 2009).

Here, lacatacystin and MG132 were used as inhibitors for the proteasome. Lactacystin is a natural product and a potent and specific inhibitor of the proteasome. It was originally isolated from the bacterium *Streptomyces lactacystinaeus* (Ōmura & Crump, 2019). Lactacystin inhibits the proteasome by forming a covalent bond with the active site of the proteasome's beta subunits and irreversibly inhibits the chymotrypsin-like activity of the proteasome, which is responsible for the cleavage of peptide bonds after hydrophobic amino acids (Tomoda & Omura, 2000). Differently, MG132 binds reversibly to the active site of the proteasome, where it forms a covalent bond with the catalytic threonine residues located within the β subunits of the proteasome and further inhibits the activation of proteasome (Albornoz et al., 2019, Harer et al., 2012). However, the inhibitory effect of MG132 is not specific for the proteasome, since it can also inhibit other proteases including calpains and cathepsins (Tsubuki et al., 1996).

Chloroquine is known to inhibit lysosomal function. Chloroquine accumulates within lysosomes, where it raises the pH of the acidic lysosomal environment (Homewood et al., 1972, Pasquier, 2016, Slater, 1993). Lysosomes normally maintain an acidic pH (pH 4.6-5.0) to facilitate the activity of hydrolytic enzymes responsible for degrading macromolecules. By raising the lysosomal pH, chloroquine disrupts the optimal conditions required for lysosomal enzyme activity. As a result, the degradation of macromolecules within lysosomes is impaired, leading to the accumulation of undegraded materials and dysfunctional lysosomes. Chloroquine also inhibits autophagy by disrupting the fusion of autophagosomes with lysosomes, thereby preventing the degradation of autophagic cargo (Mauthe et al., 2018).

In the present study, we firstly treated the THP-1 wt and TREM2 ko cells with inhibitors for proteasome and lysosome for 4 h. Interestingly, a strong stabilization of the DAP12 dimer could be observed upon the inhibition of proteasome in TREM2 ko cells but not in wt cells, while the treatment of chloroquine had no effect on DAP12 dimer in both wt and TREM2 ko cells (Fig. 3.6), indicating that DAP12 dimer is mainly degraded by proteasome and the stability of DAP12 dimer is decreased without the assembly with TREM2. DAP12 monomer was slightly increased upon the inhibition of proteasome in both wt and TREM2 ko cells (Fig. 3.6), indicating that DAP12 monomer is also mainly degraded by proteasomal activity. Similar results were also observed in HEK293 cells with the stable transfection of DAP12 and TREM2 variants. Dimeric DAP12 was significantly increased in the cells overexpressing DAP12 wt alone with or without TREM2 K186N variants but not in the cells co-expressing TREM2 wt. Monomeric DAP12 was increased in all of three mutations upon the inhibition of proteasomal activity, but the difference between the lactacystin, MG132 treated and no-treated condition was only significant in DAP12 co-expressed with TREM2 K186N variant (Fig. 3.7). These results confirmed the observation obtained in THP-1 cells, that DAP12 not interacting with TREM2 is mainly degraded by proteasome. Moreover, the observation of trimeric DAP12 in TREM2 ko THP-1 differentiated macrophage-like cells and TREM2 K186N+DAP12 wt overexpressing HEK293 cells treated with proteasome inhibitors suggests that DAP12 can form trimer independently of co-receptor assembly (Fig. 3.7). However, the stability of DAP12 trimeric forms in TREM2 ko THP-1 differentiated macrophage-like cells and TREM2 K186N+DAP12 wt overexpressing HEK293 cells is transient, as they are only detected under proteasomal degradation inhibition (Liu et al., 2024). Similar findings were reported in a prior study, indicating that DAP12 homotrimers compete with DAP12-co-receptor heterotrimers during the assembly process (Knoblich et al., 2015).

The treatment of THP-1 wt cells with lactacystin and MG132 decreased levels TREM2 FL, but increased levels of TREM2 CTFs, albeit the effect of lactacystin on the level of TREM2 CTFs was not significant (Fig. 3.6). Similarly, the treatment of HEK293 cells with lactacystin and MG132 slightly decreased levels of full-length TREM2 in DAP12 co-expressing with TREM2 wt but no effect in DAP12 co-expressing with TREM2 K186N, while increased levels of the CTFs of TREM2 in both variants, but the effect of lactacystin was slight (Fig. 3.7). The inhibition of lysosomal activity by chloroquine had no significant

effect on TREM2 CTFs in both THP-1 cells and HEK293 cells with the overexpression of DAP12 and TREM2 variants, suggesting that the degradation of TREM2 CTFs rather involves proteasomal activity than lysosomal activity (Fig. 3.6 and Fig. 3.7). However, TREM2 CTFs are generated by ectodomain shedding, and can be processed further by γ-secretase (Glebov et al., 2016, Lichtenthaler et al., 2022, Oikawa & Walter, 2019, Wunderlich et al., 2013), and it remains to be tested whether these pathways are affected by proteasomal inhibition under our experimental conditions (Liu et al., 2024).

The strong accumulation of APP CTFs upon chloroquine treatment in both cells is in line with previous findings, and indicates efficient inhibition of lysosomal activity under these experimental conditions. However, both TREM2 CTFs and APP CTFs can undergo intramembrane proteolysis by γ-secretase that also could contribute to their degradation. Proteasome inhibition could lead to enhanced autophagic activity (Ge et al., 2009, Kyrychenko et al., 2014, Tang et al., 2014). Therefore, the decreased levels of TREM2 FL and APP FL with the treatment of proteasomal inhibitors could result from activation of another degradation pathway and/or increased shedding, which could also result in increased production of CTFs (Liu et al., 2024).

4.6 Unassembled DAP12 is retained in early secretory compartments

The ER-to-Golgi transport of newly synthesized proteins is highly selective. Generally, only properly folded and assembled soluble and membrane-associated secretory proteins undergo this journey. Those misfolded and unassembled proteins could be retained in or retrieved to ER compartment (Barlowe & Helenius, 2016). Previous flow cytometry studies with Ba/F3 cells indicated that overexpressed DAP12 is not efficiently transported to the cell surface without overexpression of CD94/NKG2C suggesting a retention mechanism for DAP12 when it is not properly complexed with an immunoreceptor (Lanier et al., 1998a). It was also suggested that DAP12 could facilitate surface transport of its co-immunoreceptor, including TREM2 and KIR2DS (Mulrooney et al., 2013, Zhong et al., 2015). However, overexpressed TREM2 is also transported to the cell surface and secreted in the absence of DAP12 (Kleinberger et al., 2014, Sirkis et al., 2017). It was indicated in previous studies that DAP12 might only be required for the surface transport of C-lectin co-receptors but not be generally necessary for the surface transport of

immunoglobulin co-receptors (Tomasello et al., 1998). For example, one of the C-lectin coreceptors of DAP12, CD94/NKG2C, could not be expressed on the cell surface when it was transfected alone or co-transfected with DAP12 D50A mutant in Ba/F3 cells (Lanier et al., 1998a).

Here, we noticed that DAP12 was not transported to the cell surface in the absence of TREM2 or when the interaction with TREM2 is prevented by mutating lysine residue K186 in the TMD of TREM2 that is critical for the interaction with DAP12 (Fig. 3.8). Immunocytochemistry also revealed DAP12 was mainly colocalized with calnexin and EGRIC53, which are expressed in the ER and ERGIC, respectively, indicating that unassembled DAP12 is mainly retained in compartments of the early secretory pathway, including the ER and ERGIC. However, in cells overexpressing TREM2 wt and DAP12 wt, assembled DAP12 with TREM2 was predominantly localized at the cell surface, with partial localization in the Golgi compartment. There, DAP12 colocalized with alpha 1 sodium potassium ATPase (α1 Na+/K+ ATPase), a plasma membrane protein, and partially with Giantin, a cis-Golgi marker (Fig. 3.9). These findings strongly indicate that the expression of co-receptors is required for the transport of DAP12. The localization of TREM2 on the cell surface in TREM2 K186N co-expressing with DAP12 and TREM2 wt co-expressing with DAP12 D50A could confirm that DAP12 might not be required for the cellular transportation of TREM2 (Fig. 3.8) (Liu et al., 2024). The retention of unassembled subunits of complex in the early secretory pathway could avoid proteins to be transported to further compartments before the complete assemble of the complex. Those retained proteins in the early secretory compartments would be further degraded for maintaining the cellular homeostasis (Cosson et al., 2013).

4.7 The aspartic acid residue in the transmembrane domain is critical for retention of unassembled DAP12 in early secretory compartments

The retrieval and retention signals, including the dilysine motifs (KKXX or KXKXX) recognized by the COPI coat and an arginine-based RXR motif, are found in the C-terminal of the proteins that cycle between the ER and the Golgi. Additionaly, the H/KDEL motifs binding to KDEL receptors are found in the C-terminal sequences of soluble ER-resident proteins (Michelsen et al., 2005, Munro & Pelham, 1987, Papanikou & Glick, 2014,

Semenza et al., 1990). Some transmembrane proteins do not have C-terminal retrieval motifs for COPI recognition. In this case, the RER1 protein, characterized as a multispanning transmembrane protein with a COPI binding signal, could bind to the proteins that have escaped into post-ER compartments through interactions involving its transmembrane domains (Boehm et al., 1997b, Füllekrug et al., 1997, Sato et al., 2003). The existence of charged residues or polar residues in the TMD of transmembrane proteins is required for the interaction with RER1 (Cosson et al., 2013).

DAP12 contains a negatively charged residue, asparitic acid residue, in the TMD and it is also responsible for the interaction with the co-immunoreceptors. Therefore, we explored if this charged residue in the TMD of DAP12 mediates the ER retention and/or retrieval of unassembled DAP12. In the present study, we firstly observed that DAP12 with the D50A mutations was transported to the cell surface expressed with or without TREM2 (Fig. 3.10), indicating that the mutation of D to A in DAP12 led to the escape of DAP12 from the ER to post ER compartments and the cell surface. This observation was further confirmed by the colocalization of DAP12 with Golgi maker giantin and plasma membrane maker alpha 1 sodium potassium ATPase in the cells overexpressing DAP12 D50A variants (Fig. 3.11). Similar observations were made previously using flow cytometry of Ba/F3 cells upon virally transduced DAP12 constructs (Lanier et al., 1998a). Indeed, charged or polar amino acid residues in TMDs could be important determinants in the ER retention of several membrane proteins, such as CD3, which is associated with TCR and mediates the signal transduction (Bonifacino et al., 1990, Bonifacino et al., 1991, Cosson et al., 1991).

RER1 is a sorting receptor for the retrieval of ER membrane proteins and selected unassembled subunits of larger protein complexes. It can retrieve clients from early Golgi compartments by recognizing charged or other polar amino acid residues within the respective transmembrane domains. Human client proteins of RER1 include unassembled PEN2, immature nicastrin, the α-units of skeletal muscle nicotinic acetylcholine receptor (nAChR), and peripheral myelin protein 22 (PMP22) (Hara et al., 2014, Kaether et al., 2007, Spasic et al., 2007, Valkova et al., 2011). Additional RER1 client proteins have been identified in yeast, including the ER resident membrane proteins Sec12p, Sec71p, Sec63p (Sato et al., 1995, Sato et al., 1997), and unassembled subunits of oligomeric membrane complexes like Fet3 (Sato et al., 2004). By co-

immunoprecipitation assays in HEK293 cells transiently transfected with DAP12 and TREM2 variants, we could demonstrate that RER1 interacts with DAP12, and that the charged D50 residue in the DAP12 TMD is critical for this interaction (Fig. 3.12). We also observed that DAP12 and RER1 interacted independently of the presence of TREM2 in THP-1 cells, whereas in HEK293 cells with the overexpression of DAP12 and TREM2 mutants, this interaction was observed only in the absence of TREM2. Thus, a pool of unassembled DAP12 might exist in THP-1 cells that is stabilized by the interaction with RER1 in early secretory compartments, and is available on demand for assembly with TREM2 or other immunoreceptors capable to interact with DAP12. In the HEK293 cell model, we used a bicistronic construct encoding TREM2 and DAP12 linked by a T2A sequence to assure stoichiometric expression of both proteins. Thus, in this model likely most of DAP12 (dimers) associate with TREM2 thereby precluding interaction with RER1. However, the relative contribution of RER1 to the retention/retrieval of unassembled DAP12 and the exact molecular mode of interaction of both proteins remains to be dissected in more detail. These combined results provide evidence for a molecular mechanism mediating the retention and regulated degradation of unassembled DAP12.

Another observation was that DAP12 wt formed increased levels of SDS resistant trimers and tetramers when expressed in the absence of TREM2 in the transiently transfected HEK293 cells (Fig. 3.12), similar to the two mutations of interaction sites for TREM2 and DAP12 (Fig. 3.3). A similar observation was made previously by Call et al. studying the assembly of DAP12 with the NK cell activating receptor KIR2DS2 by *in vitro* translation experiments, and it had been proposed that DAP12 interacting immunoreceptors compete with additional DAP12 molecules for binding to covalently linked DAP12 dimers during complex assembly (Knoblich et al., 2015). In addition, proteasomal inhibition also led to the detection of trimeric DAP12 in HEK293 cells stably overexpressing DAP12 with the TREM2 K186N mutant, further supporting the notion that TREM2 or other receptors compete with monomeric DAP12 for binding to covalently linked DAP12 dimers (Liu et al., 2024).

4.8 RGR motif is not important for the retention of unassembled DAP12 in early secretory compartments

Arginine (Arg)-based ER-localization signals (RXR) were firstly identified to be involved in the transport of major histocompatibility complex (MHC) class II (Bakke & Dobberstein, 1990, Lotteau et al., 1990). Afterwards, RXR motifs were identified in many transmembrane proteins, such as G-protein coupled receptor 1 for gamma-aminobutyric acid ($GABA_BR1$), the delta opioid receptor, the N-methyl-D-aspartate (NMDA) receptor, the ATP-sensitive potassium channel subunit (Kir6.1), longer transmembrane protein 63B (TMEM63B) isoform, and others, mediating the ER retention of those proteins (Aziz et al., 2014, Margeta-Mitrovic et al., 2000, Shiwarski et al., 2019, Wu et al., 2023). It was shown that RXR motif is binding to the COPI retrieval vesicles and mediates the retention of respective proteins, especially the subunits of the transmembrane protein complexes in the early secretory compartments (Michelsen et al., 2005). However, the RXR motifs are masked when subunits of the transmembrane protein complex are fully assembled with or interact with other proteins, leading to the further transport to cell surface. For example, NMDA receptor (NR) 1 has four splice variants, NR1-1, NR1-2, NR1-3 and NR1-4. NR1-1 and NR1-3 contain RRR motifs in the C-terminal domain while only NR1-1 retains intracellularly. NR1-3 contains a terminal four amino acid PDZ-interacting domain in its C-terminus, which could mask the RRR motif, resulting in the further transport of NR1-3 (Standley et al., 2000).

A RXR (70RGR72) motif is also present in the cytoplasmic domain of DAP12, which is very close to its transmembrane domain. Therefore, we explored whether this RXR motif plays a role in the retention of unassembled DAP12. By mutating the two arginine residues at position 70 and 72 to the alanine residues (A), we observed that mutated arginine residues didn’t lead to the forward transport of DAP12 (Fig. 3.13 and Fig. 3.14), indicating that the RGR motif of DAP12 had little effect on the retention of unassembled DAP12. Therefore, the aspartic acid residue (D50) in the TMD of DAP12 plays a leading role for the retention/retrieval of unassembled DAP12 and the interaction between D50 with the positively charged residues localized in the TMD of its co-receptor masks this retention/retrieval signal, leading to the exit of assembled DAP12-co-receptor complexes.

4.9 RER1 deletion decreases levels of TREM2-DAP12 complex and impairs the TREM2-DAP12 signaling and phagocytosis of macrophage-like cells differentiated from THP-1 monocytes

A functional relevance of RER1 in the expression and signaling TREM2-DAP12 complexes was demonstrated by the deletion of the RER1 gene in THP-1 cells. As compared to wt cells, RER1 ko cells showed strongly decreased levels of both TREM2 and DAP12 at protein level, while the deletion of RER1 didn't significantly affect the mRNA level of both TREM2 and DAP12 (Fig. 3.15). It has been reported previously that knockdown of RER1 results in decreased levels of the AchR α-subunit, which is also a client protein of RER1 (Valkova et al., 2011). These findings suggest that RER1 not only controls the retention or retrieval of unassembled components of certain membrane protein complexes, but also may stabilize these proteins until they properly assemble into functional complexes prior to transport to the cell surface to interact with specific ligands and trigger membrane proximal signaling (Liu et al., 2024).

We also observed that the turnover of DAP12 was not affected while the inhibition of proteasome by MG132 partially stabilized DAP12 dimer in RER1 ko cells (Fig. 3.16 and Fig. 3.17). These findings suggest that additional posttranscriptional and/or posttranslational mechanisms could contribute to the strong decrease of DAP12 and TREM2 proteins in RER1 ko cells (Liu et al., 2024).

Indeed, RER1 ko THP-1 cells showed strongly reduced phosphorylation of SYK upon stimulation of TREM2 with agonistic antibodies (Fig. 3.18). Furthermore, the deletion of the RER1 gene in THP-1 cells significantly decreased phagocytic activity (Fig. 3.19), thereby showing the importance of RER1 in the maintenance of immune cell function (Liu et al., 2024).

RER1 is almost ubiquitously expressed in different cell types (Uhlén et al., 2015). An important function of RER1 is the modulation of Notch signaling during mouse cerebral cortex development by maintaining sufficient cell surface expression and activity of the γ-secretase complex (Hara et al., 2018). RER1 has also been recognized as one of the most stably expressed genes throughout choroid plexus development and aging in mice, and considered as a housekeeping gene (Ho & Patrizi, 2021). Abundant expression of

RER1 mRNA and protein is also detected in microglia and other immune cells (Karlsson et al., 2021, Sjöstedt et al., 2020, Uhlen et al., 2019). γ-Secretase dependent Notch signaling also regulates lymphocyte development, differentiation and proliferation (Radtke et al., 2010), and the inflammatory response of myeloid cells to various stimuli (Grandbarbe et al., 2007, Keewan & Naser, 2020). A recent study also revealed that RER1 is important in maintenance of proteostasis in *Drosophila* (Paul et al., 2024). The present data show that RER1 plays additional roles in the regulation of immune cell function by controlling assembly and surface expression of functional TREM2-DAP12 complexes. Thus, it will be important to further dissect RER1 function in immune cells, and its role in the regulation of inflammatory processes (Liu et al., 2024).

4.10 RER1 deletion alters the lipid metabolisms of both undifferentiated and differentiated THP-1 cells

The presented data indicate the strong accumulation of lipid droplets mainly containing TAGs in RER1 ko monocytes and macrophage-like cells as compared to wt cells. Additionally, RER1 is implicated in the cellular cholesterol metabolism, indicated by the changes of mRNA and protein expression of factors involved in cholesterol biosynthesis, uptake, intracellular transport, and efflux. Thus, RER1 plays a crucial role in lipid metabolism in those immune cells.

Lipid droplets (LDs) are dynamic organelles found in most cells, serving as storage sites for neutral lipids, including triacylglycerols (TAGs) and cholesterol esters (CEs).The accumulation of LDs has been related to inflammation and immune cell function in several diseases, including obesity, diabetes, atherosclerosis, neurodegenerative disorders (Accad et al., 2000, Bozza & Viola, 2010, den Brok et al., 2018, Farmer et al., 2020, Koliwad et al., 2010, Nagle et al., 2009, Stephenson et al., 2024, van Dierendonck et al., 2022, Walther & Farese, 2012). Previous studies showed LDs accumulation in presenilin (PS) ko mouse embryonic fibroblast (Fabiano et al., 2024, Gutierrez et al., 2020), which might be due to the impairment of γ secretase function. Interestingly, RER1 deletion in the HAP1 cell line leads to the reduction of PEN2, Nicastrin and PS1, which decreased the

assembly of the γ-secretase complex (Hara et al., 2018). Whether RER1 deletion affects lipid metabolism is not known so far.

Here we also explored the role of RER1 on the regulation of lipid metabolism in monocytes and macrophage-like cells. The accumulation of lipid droplets in RER1 ko cells (Fig. 3.20 and Fig. 3.21), which mainly contain TAGs, demonstrated that the RER1 deficiency increased cellular TAGs storge in immune cells. The increased cholesterol precursors and genes involved in sterol synthesis pathways in RER1-deficient monocytes indicated that RER1 deletion upregulated cholesterol biosynthesis in those cells. Additionally, expression of genes related to cholesterol uptake, intracellular transport and efflux was upregulated at both, mRNA and protein levels in RER1 ko macrophage-like cells, indicating the critical involvement of RER1 in the regulation of cholesterol metabolism in those cells.

Cholesterol is synthesized from acetate via a complex process that involves more than 30 different steps, which can be divided into four major processes, including condensation of acetate to isoprene, polymerization of isoprene to squalene, cyclization of squalene to lanosterol, and finally the conversion of lanosterol to cholesterol (Mitsche et al., 2015). Two biochemical pathways, including Bloch pathway and Kandutsch-Russell pathway, have been found for the synthesis of cholesterol from lanosterol (Bloch, 1965, Kandutsch & Russell, 1960a, Kandutsch & Russell, 1960b). The precursors of cholesterol, including lanosterol and desmosterol, were significantly increased in RER1 deleted THP-1 monocytes as compared to wt monocytes, while lathosterol was strongly decreased by RER1 deletion, indicating the *de novo* synthesis of cholesterol in the Bloch pathway was upregulated and the Kandutsch-Russell pathway was downregulated (Fig. 3.22). A previous study revealed the Bloch pathway as a main pathway for the biosynthesis of cholesterol (Mitsche et al., 2015). Surprisingly, in macrophage-like cells, RER1 deficiency resulted in decreased lanosterol, desmosterol and lathosterol, indicating the reduction of cholesterol biosynthesis in RER1 deleted cells as compared to wt cells (Fig. 3.22). The difference of the effects of RER1 on cholesterol biosynthesis in monocytes and macrophage-like cells needs to be further explored. However, in both monocytes and macrophage-like cells, the total amount of cholesterol was comparable in RER1 ko and wt cells, while increased free cholesterol and decreased cholesterol esters were observed

in RER1 ko cells (Fig. 3.22). Upregulation of the Bloch pathway leads to the accumulation of desmosterol, which can activate liver X receptors (LXR) and further promote the export of cholesterol, and also inactivate sterol response element-binding protein 2 (SREBP2) to suppress the biosynthesis of cholesterol (Mitsche et al., 2015). Our data showed that the total amount of cholesterol was not significantly changed in RER1 deleted undifferentiated cells, which might be due to compensatory regulation of cholesterol levels in these cells. Further experiments need to investigate effects of RER1 on those regulatory mechanisms of cholesterol.

Although LDs were strongly accumulated in RER1 ko cells in both monocytes and macrophage-like cells, detailed analysis revealed rather decreased levels of CEs (Fig. 3.22). Therefore, we analyzed the different species of CEs by mass spectrometry to further investigate the possible content of increased LDs in RER1 ko cells. Similarly, the level of CEs in RER1 ko monocytes was not much changed but was significantly decreased in RER1 ko macrophage-like cells (Fig. 3.23 and Fig. 3.24). Oppositely, we observed significant increases in TAGs and DAGs in RER1-deficient macrophages as compared to wt cells (Fig. 3.23 and Fig. 3.24). TAGs are stored in LDs in most mammalian cells (Barbosa & Siniossoglou, 2017a, Henne et al., 2018, Walther & Farese, 2012, Wang et al., 2017). Beside TAGs, previous studies showed the direct metabolic precursor diacylglycerol, DAG, can also accumulate in LDs (Cantley et al., 2013, Kuerschner et al., 2008). Therefore, our results suggested the increased amounts of both TAGs and DAGs in accumulated LDs in RER1 ko cells.

Next, we investigated the effects of RER1 on the expression of RNAs and proteins associated with lipid metabolism. Our RNA sequencing data showed that RER1 deletion upregulated many genes involved in lipid metabolism. In THP-1 monocytes, KEGG enrichment analysis of differentially expressed genes (DEGs) showed that steroid biosynthesis pathway was significantly upregulated in RER1 ko cells (Fig. 3.26). In this pathway, *MSMO1*, *SQLE*, *EBP*, *CYP51A1*, *NSDHL*, *DHCR7*, *SC5D*, *LSS*, *FDFT1*, *TM7SF2* were all involved in cholesterol *de novo* biosynthesis, which further proved the elevated cholesterol precursors in RER1 ko monocytes (Ershov et al., 2021). However, some of those genes were also upregulated in RER1 ko macrophage-like cells as compared to wt cells, while cholesterol precursors were strongly decreased in RER1 ko

cells, which needs to be further investigated. Further western immunoblotting proved the increased expression of CYP51A1 at protein level (Fig. 3.33). Besides steroid biosynthesis, KEGG enrichment analysis of DEGs in macrophage-like cells also showed that ‘lipid and atherosclerosis’ and ‘cholesterol metabolism’ were upregulated in RER1 deficient cells (Fig. 3.26 and Fig. 3.28). Genes involved in those pathways include ABC transporters, such as *ABCA1*, *ABCG1* and *ABCG8* which mediate the export of cholesterol (Yu & Tang, 2022, Yvan-Charvet et al., 2010). The receptors mediating the import and intracellular transport of cholesterol, including low density lipoprotein receptor (LDLR), LDL receptor related protein 1 (LRP1), NPC intracellular cholesterol transporter 1 and 2 (NPC1 and 2) were also increased in RER1 ko macrophage-like cells (Goldstein & Brown, 2009, Pfeffer, 2019). In addition of increased mRNA levels of those genes, we also observed elevated protein levels of ABCA1, LDLR, LRP1 and NPC1 in RER1 ko macrophage-like cells as compared to wt cells (Fig. 3.33). These results indicate the upregulation of both import and export of cholesterol in RER1 ko macrophage-like cells as compared to wt cells. Other genes related to cholesterol metabolism, such as *APOE*, *LPL*, *APOC1*, *LIPG*, *MYLIP*, were upregulated in RER1 deleted macrophage-like cells. Apolipoprotein E (ApoE), encoded by *APOE*, is a lipid transport protein and binds to lipoproteins, such as very low density lipoprotein (VLDL) (Mahley, 1988, Mahley & Rall, 2000). ApoE also binds to high density lipoprotein (HDL) and mediates the cholesterol efflux from macrophage (Tudorache et al., 2017). Apolipoprotein C1, encoded by *APOC1*, can inhibit the binding of ApoE-mediated lipoprotein with the corresponding receptors and also regulate the activity of lipoprotein lipase (Fuior & Gafencu, 2019). Lipases upregulated by RER1 deletion in macrophage-like cells include lipoprotein lipase encoded by *LPL*, and endothelial lipase G encoded by *LIPG*. *MYLIP* encodes myosin regulatory light chain interacting protein, also known as inducible degrader of LDLR (IDOL), which is an E3 ubiquitin ligase to promote the ubiquitination of LDLR for further degradation (Yu et al., 2021).

Further GO enrichment analysis of DEGs in monocytes revealed the upregulation of ‘cholesterol biosynthetic process’, ‘sterol biosynthetic process’, ‘regulation of lipid metabolic process’, ‘steroid biosynthetic process’, ‘cholesterol biosynthetic process via desmosterol and lathosterol’, ‘lipid metabolic process’ and ‘stearoyl-CoA 9-desaturase’ in

RER1 deleted monocytes (Fig. 3.29 and Fig. 3.30). This analysis showed another two upregulated genes, including *HMGCS1* and *HMGCR,* which are involved in the *de novo* synthesis of cholesterol, further demonstrating the upregulation of cholesterol biosynthesis in RER1 deleted monocytes. *INSIG1*, encoding insulin-induced gene 1 protein, was also upregulated in RER1 deleted monocytes. INSIG1 was shown to combine with Sterol regulatory element-binding protein Cleavage-Activating Protein (SCAP) when sterols accumulate in ER and further inhibit the transport of Sterol regulatory element-binding protein (SREBP)-SCAP complex from ER to Golgi, therefore gives a negative feedback of cholesterol biosynthesis (Adams et al., 2003, McPherson & Gauthier, 2004, Sun et al., 2005). Additionally, the increased fatty acid metabolism related genes, including *ELOVL6*, *FASN*, *SCD5*, *FADS2* and *FABP5* were found in RER1 deleted monocytes. It was shown that the enzymes encoded by *ELOVL6*, *FASN*, *SCD5* and *FADS2* were involved in the *de novo* lipogenesis from acetyl CoA (Koundouros & Poulogiannis, 2020). FABP5 (fatty acid binding protein 5), which belongs to FAs-binding proteins in transmembrane plasma, plays a role in FAs uptake and further transports FAs to cell compartments (Hou et al., 2022). The upregulation of these genes by RER1 deletion indicated the role of RER1 in fatty acid metabolisms.

The combined data demonstrate an important role of RER1 in the complex regulation of lipid metabolism of immune related monocytic and macrophage-like cells. Thus, it will be important to further investigate the molecular mechanisms underlying these observations, and to further characterize the implications of RER1 in immune cell function.

4.11 Limitation of the study

While the study identifies the impact of RER1 ko on the TREM2-DAP12 immunoreceptor-adapter complex in differentiated THP-1 cells, the lack of rescue experiments diminishes the depth of understanding. Introducing RER1 overexpression into the RER1 ko THP-1 cell line could provide crucial insights on that. Such experiments could elucidate whether restoring RER1 levels rescues the observed phenotypic changes, thereby confirming the specific role of RER1 in modulating TREM2-DAP12 complex expression, signaling, and cellular functions.

The exact role of RER1 in the transportation of unassembled DAP12 is still unclear. In present study, the observation of reduced levels of both DAP12 and TREM2 in THP-1 differentiated macrophage-like cells upon RER1 deletion complicates the assessment of DAP12 transport. To address this, utilizing a different cellular model system, such as HEK293 cells, could provide valuable insights. By deleting RER1 and overexpressing wild-type DAP12 (DAP12 wt) alone or in combination with wild-type TREM2 (TREM2 wt) or a mutant form of TREM2 (TREM2 K186N), one can investigate the role of RER1 in DAP12 transport in HEK293 cells without the interruption of endogenous expression of DAP12 and its co-receptors.

Although the study highlights that the deletion of RER1 impairs the TREM2-DAP12 signaling and phagocytosis in differentiated THP-1 cells, the precise molecular mechanisms remain elusive. Further investigation about how RER1 affects the activation and regulation of the TREM2-DAP12 complex will be needed.

While cell line models used in the present study included HEK293 and THP-1 cells, they may not fully capture the complexities of *in vivo* systems. Incorporating primary cell models, such as primary microglia isolated from animal models or human induced pluripotent stem cell (iPSC)-derived microglia, could provide a more physiologically relevant context. Primary cells better represent the diversity and functionality of native cell populations, offering insights that may not be evident in immortalized cell lines. Moreover, while cell-based studies provide valuable insights, validating findings in living organisms is essential for translational relevance.

Animal models with RER1 deletion, such as conditional RER1 ko in microglia, monocytes, and macrophages could be generated to assess the impact of RER1 deficiency on the TREM2-DAP12 pathway *in vivo*. This approach allows for the evaluation of RER1's role within the complex interplay of cellular networks and physiological systems, providing a more holistic understanding of its functions.

The present study only focuses on the TREM2-DAP12 complex and whether RER1 also regulate the transport and function of other immunoreceptor-adapter complexes is unknown. Therefore, other receptor-adapter pairs, such as the TCR-CD3 complex or the NKG2D-DAP10 complex could give us more view on common or distinct assembly

mechanisms. Comparative analyses across multiple complexes would enhance our understanding of the broader regulatory networks governing immune cell signaling and function.

Addressing these limitations through additional experimental approaches and model systems would strengthen the study's conclusions and contribute to a more comprehensive understanding of RER1's role in immune cell biology and disease pathology.

5 Abstract

DNAX-activating protein of 12 kDa (DAP12) is a transmembrane adapter protein expressed on lymphoid and myeloid lineage cells, and interacts with several immune receptors to form functional complexes that trigger intracellular signaling pathways. One of the DAP12 associated receptors is the triggering receptor expressed on myeloid cells 2 (TREM2), and mutations in both, DAP12 and TREM2, have been linked to neurodegenerative disease. However, mechanisms involved in the assembly of TREM2-DAP12 complexes and the turnover of both proteins are not well understood.

Here, we demonstrate that DAP12 is efficiently targeted to proteasomal degradation in the absence of TREM2. Interestingly, unassembled DAP12 was retained in the early secretory compartments, including the endoplasmic reticulum (ER) and the ER-Golgi intermediate compartment (ERGIC) while the mutation of aspartic acid residue at position 50 (D50) to alanine (A) in the transmembrane of DAP12 leads to the escape of unassembled DAP12 to the post-translational compartments as well as cytoplasm. Interaction studies showed that unassembled DAP12 interacts with the Retention in ER Sorting Receptor 1 (RER1) by electrostatic interaction, indicating that RER1 might play a role in unassembled DAP12 retention and/or retrieval. However, the RXR motif localized in the C-terminal of DAP12 has no effect on DAP12 retention. Additionally, the deletion of endogenous RER1 decreased expression of functional TREM2-DAP12 complexes and membrane proximal signaling, and resulted in almost complete inhibition of phagocytic activity in THP-1 differentiated macrophage-like cells. Furthermore, RER1 deficiency resulted in the accumulation of cellular triacylglycerols (TAGs) in both undifferentiated and differentiated THP-1 cells. The increased cholesterol

precursors and the differentially expressed genes involved in sterol synthesis pathways in RER1-deficient monocytes indicated a critical involvement of RER1 in cholesterol biosynthesis of this cell type. Additionally, the altered expression of genes related to the uptake, intracellular transport and efflux of cholesterol at the mRNA and protein level as well as the altered TAGs composition in RER1 ko macrophage-like cells indicated the critical involvement of RER1 in the complex regulation of lipid metabolism also in this cell type. These results indicate that RER1 acts as an important regulator of DAP12 containing immune receptor complexes, immune cell function as well as lipid metabolism in immune cells.

6 List of figures

7 List of tables

Tables

8 References

Abe T, Ohno M, Sato T, Murakami M, Kajiki M, Kodaira R. "Differentiation Induction" culture of human leukemic myeloid cells stimulates high production of macrophage differentiation inducing factor. Cytotechnology 1991; 5: 75-93

Accad M, Smith SJ, Newland DL, Sanan DA, King LE, Jr., Linton MF, Fazio S, Farese RV, Jr. Massive xanthomatosis and altered composition of atherosclerotic lesions in hyperlipidemic mice lacking acyl CoA:cholesterol acyltransferase 1. J Clin Invest 2000; 105: 711-719

Adams CM, Goldstein JL, Brown MS. Cholesterol-induced conformational change in SCAP enhanced by Insig proteins and mimicked by cationic amphiphiles. Proceedings of the National Academy of Sciences 2003; 100: 10647-10652

Albornoz N, Bustamante H, Soza A, Burgos P. Cellular Responses to Proteasome Inhibition: Molecular Mechanisms and Beyond. Int J Mol Sci 2019; 20

Althafar ZM. Targeting Microglia in Alzheimer's Disease: From Molecular Mechanisms to Potential Therapeutic Targets for Small Molecules. Molecules 2022; 27

Angata T, Hayakawa T, Yamanaka M, Varki A, Nakamura M. Discovery of Siglec-14, a novel sialic acid receptor undergoing concerted evolution with Siglec-5 in primates. Faseb j 2006; 20: 1964-1973

Angata T, Kerr SC, Greaves DR, Varki NM, Crocker PR, Varki A. Cloning and characterization of human Siglec-11. A recently evolved signaling molecule that can interact with SHP-1 and SHP-2 and is expressed by tissue macrophages, including brain microglia. J Biol Chem 2002; 277: 24466-24474

Annaert W, Kaether C. Bring it back, bring it back, don't take it away from me - the sorting receptor RER1. J Cell Sci 2020; 133

Ansa-Addo EA, Lange S, Stratton D, Antwi-Baffour S, Cestari I, Ramirez MI, McCrossan MV, Inal JM. Human plasma membrane-derived vesicles halt proliferation and induce differentiation of THP-1 acute monocytic leukemia cells. J Immunol 2010; 185: 5236-5246

Atagi Y, Liu CC, Painter MM, Chen XF, Verbeeck C, Zheng H, Li X, Rademakers R, Kang SS, Xu H, Younkin S, Das P, Fryer JD, Bu G. Apolipoprotein E Is a Ligand for Triggering Receptor Expressed on Myeloid Cells 2 (TREM2). J Biol Chem 2015; 290: 26043-26050

Audrain M, Haure-Mirande JV, Mleczko J, Wang M, Griffin JK, St George-Hyslop PH, Fraser P, Zhang B, Gandy S, Ehrlich ME. Reactive or transgenic increase in microglial TYROBP reveals a TREM2-independent TYROBP-APOE link in wild-type and Alzheimer's-related mice. Alzheimers Dement 2021; 17: 149-163

Audrain M, Haure-Mirande JV, Wang M, Kim SH, Fanutza T, Chakrabarty P, Fraser P, St George-Hyslop PH, Golde TE, Blitzer RD, Schadt EE, Zhang B, Ehrlich ME, Gandy S.

Integrative approach to sporadic Alzheimer's disease: deficiency of TYROBP in a tauopathy mouse model reduces C1q and normalizes clinical phenotype while increasing spread and state of phosphorylation of tau. Mol Psychiatry 2019; 24: 1383-1397

Aziz Q, Thomas AM, Gomes J, Ang R, Sones WR, Li Y, Ng KE, Gee L, Tinker A. The ATP-sensitive potassium channel subunit, Kir6.1, in vascular smooth muscle plays a major role in blood pressure control. Hypertension 2014; 64: 523-529

Bailey CC, DeVaux LB, Farzan M. The Triggering Receptor Expressed on Myeloid Cells 2 Binds Apolipoprotein E. J Biol Chem 2015; 290: 26033-26042

Bakke O, Dobberstein B. MHC class II-associated invariant chain contains a sorting signal for endosomal compartments. Cell 1990; 63: 707-716

Bakker AB, Baker E, Sutherland GR, Phillips JH, Lanier LL. Myeloid DAP12-associating lectin (MDL)-1 is a cell surface receptor involved in the activation of myeloid cells. Proc Natl Acad Sci U S A 1999; 96: 9792-9796

Balch WE, Morimoto RI, Dillin A, Kelly JW. Adapting proteostasis for disease intervention. Science 2008; 319: 916-919

Barbosa AD, Siniossoglou S. Function of lipid droplet-organelle interactions in lipid homeostasis. Biochimica et Biophysica Acta (BBA) - Molecular Cell Research 2017a; 1864: 1459-1468

Barbosa AD, Siniossoglou S. Function of lipid droplet-organelle interactions in lipid homeostasis. Biochim Biophys Acta Mol Cell Res 2017b; 1864: 1459-1468

Bard F, Cannon C, Barbour R, Burke RL, Games D, Grajeda H, Guido T, Hu K, Huang J, Johnson-Wood K, Khan K, Kholodenko D, Lee M, Lieberburg I, Motter R, Nguyen M, Soriano F, Vasquez N, Weiss K, Welch B, Seubert P, Schenk D, Yednock T. Peripherally administered antibodies against amyloid beta-peptide enter the central nervous system and reduce pathology in a mouse model of Alzheimer disease. Nat Med 2000; 6: 916-919

Barlowe C, Helenius A. Cargo Capture and Bulk Flow in the Early Secretory Pathway. Annu Rev Cell Dev Biol 2016; 32: 197-222

Baumeister W, Walz J, Zühl F, Seemüller E. The proteasome: paradigm of a self-compartmentalizing protease. Cell 1998; 92: 367-380

Belle A, Tanay A, Bitincka L, Shamir R, O'Shea EK. Quantification of protein half-lives in the budding yeast proteome. Proc Natl Acad Sci U S A 2006; 103: 13004-13009

Biassoni R, Cantoni C, Falco M, Verdiani S, Bottino C, Vitale M, Conte R, Poggi A, Moretta A, Moretta L. The human leukocyte antigen (HLA)-C-specific "activatory" or "inhibitory" natural killer cell receptors display highly homologous extracellular domains but differ in their transmembrane and intracytoplasmic portions. J Exp Med 1996; 183: 645-650

Blasius A, Vermi W, Krug A, Facchetti F, Cella M, Colonna M. A cell-surface molecule selectively expressed on murine natural interferon-producing cells that blocks secretion of interferon-alpha. Blood 2004; 103: 4201-4206

Blasius AL, Cella M, Maldonado J, Takai T, Colonna M. Siglec-H is an IPC-specific receptor that modulates type I IFN secretion through DAP12. Blood 2006; 107: 2474-2476

Bloch K. The biological synthesis of cholesterol. Science 1965; 150: 19-28

Bochtler M, Ditzel L, Groll M, Hartmann C, Huber R. THE PROTEASOME. Annual Review of Biophysics 1999; 28: 295-317

Boehm J, Letourneur F, Ballensiefen W, Ossipov D, Démollière C, Schmitt HD. Sec12p requires Rer1p for sorting to coatomer (COPI)-coated vesicles and retrieval to the ER. J Cell Sci 1997a; 110 (Pt 8): 991-1003

Boehm U, Klamp T, Groot M, Howard JC. Cellular responses to interferon-gamma. Annu Rev Immunol 1997b; 15: 749-795

Bonifacino JS, Cosson P, Klausner RD. Colocalized transmembrane determinants for ER degradation and subunit assembly explain the intracellular fate of TCR chains. Cell 1990; 63: 503-513

Bonifacino JS, Cosson P, Shah N, Klausner RD. Role of potentially charged transmembrane residues in targeting proteins for retention and degradation within the endoplasmic reticulum. Embo j 1991; 10: 2783-2793

Bouchon A, Dietrich J, Colonna M. Cutting edge: inflammatory responses can be triggered by TREM-1, a novel receptor expressed on neutrophils and monocytes. J Immunol 2000; 164: 4991-4995

Bouchon A, Hernández-Munain C, Cella M, Colonna M. A DAP12-mediated pathway regulates expression of CC chemokine receptor 7 and maturation of human dendritic cells. J Exp Med 2001; 194: 1111-1122

Boudesco C, Nonneman A, Cinti A, Picardi P, Redaelli L, Swijsen S, Roewe J, Reinhardt P, Ibach M, Walter J, Pocock JM, Ren Y, Driguez PA, Dargazanli G, Eyquem S, Proto J, Flores-Morales A, Pradier L. Novel potent liposome agonists of triggering receptor expressed on myeloid cells 2 phenocopy antibody treatment in cells. Glia 2022; 70: 2290-2308

Bozza PT, Viola JPB. Lipid droplets in inflammation and cancer. Prostaglandins, Leukotrienes and Essential Fatty Acids (PLEFA) 2010; 82: 243-250

Brodsky JL, McCracken AA. ER protein quality control and proteasome-mediated protein degradation. Semin Cell Dev Biol 1999; 10: 507-513

Brooks AG, Posch PE, Scorzelli CJ, Borrego F, Coligan JE. NKG2A complexed with CD94 defines a novel inhibitory natural killer cell receptor. J Exp Med 1997; 185: 795-800

Buchanan BW, Lloyd ME, Engle SM, Rubenstein EM. Cycloheximide Chase Analysis of Protein Degradation in Saccharomyces cerevisiae. J Vis Exp 2016;

Call ME, Pyrdol J, Wiedmann M, Wucherpfennig KW. The organizing principle in the formation of the T cell receptor-CD3 complex. Cell 2002; 111: 967-979

Call ME, Wucherpfennig KW, Chou JJ. The structural basis for intramembrane assembly of an activating immunoreceptor complex. Nat Immunol 2010; 11: 1023-1029

Campbell KS, Cella M, Carretero M, López-Botet M, Colonna M. Signaling through human killer cell activating receptors triggers tyrosine phosphorylation of an associated protein complex. Eur J Immunol 1998; 28: 599-609

Campbell KS, Yusa S, Kikuchi-Maki A, Catina TL. NKp44 triggers NK cell activation through DAP12 association that is not influenced by a putative cytoplasmic inhibitory sequence. J Immunol 2004; 172: 899-906

Cannon JP, O'Driscoll M, Litman GW. Specific lipid recognition is a general feature of CD300 and TREM molecules. Immunogenetics 2012; 64: 39-47

Cantley JL, Yoshimura T, Camporez JPG, Zhang D, Jornayvaz FR, Kumashiro N, Guebre-Egziabher F, Jurczak MJ, Kahn M, Guigni BA, Serr J, Hankin J, Murphy RC, Cline GW, Bhanot S, Manchem VP, Brown JM, Samuel VT, Shulman GI. CGI-58 knockdown sequesters diacylglycerols in lipid droplets/ER-preventing diacylglycerol-mediated hepatic insulin resistance. Proceedings of the National Academy of Sciences 2013; 110: 1869-1874

Cantoni C, Biassoni R, Pende D, Sivori S, Accame L, Pareti L, Semenzato G, Moretta L, Moretta A, Bottino C. The activating form of CD94 receptor complex: CD94 covalently associates with the Kp39 protein that represents the product of the NKG2-C gene. Eur J Immunol 1998; 28: 327-338

Cao H, Crocker PR. Evolution of CD33-related siglecs: regulating host immune functions and escaping pathogen exploitation? Immunology 2011; 132: 18-26

Cao J, Zhong MB, Toro CA, Zhang L, Cai D. Endo-lysosomal pathway and ubiquitin-proteasome system dysfunction in Alzheimer's disease pathogenesis. Neurosci Lett 2019; 703: 68-78

Carretero M, Cantoni C, Bellón T, Bottino C, Biassoni R, Rodríguez A, Pérez-Villar JJ, Moretta L, Moretta A, López-Botet M. The CD94 and NKG2-A C-type lectins covalently assemble to form a natural killer cell inhibitory receptor for HLA class I molecules. Eur J Immunol 1997; 27: 563-567

Cella M, Buonsanti C, Strader C, Kondo T, Salmaggi A, Colonna M. Impaired differentiation of osteoclasts in TREM-2-deficient individuals. J Exp Med 2003; 198: 645-651

Chan G, White CC, Winn PA, Cimpean M, Replogle JM, Glick LR, Cuerdon NE, Ryan KJ, Johnson KA, Schneider JA, Bennett DA, Chibnik LB, Sperling RA, Bradshaw EM, De Jager PL. CD33 modulates TREM2: convergence of Alzheimer loci. Nat Neurosci 2015; 18: 1556-1558

Chanput W, Mes JJ, Wichers HJ. THP-1 cell line: an in vitro cell model for immune modulation approach. Int Immunopharmacol 2014; 23: 37-45

Chen H, Qi X, Faulkner RA, Schumacher MM, Donnelly LM, DeBose-Boyd RA, Li X. Regulated degradation of HMG CoA reductase requires conformational changes in sterol-sensing domain. Nature Communications 2022; 13: 4273

Chen Q, DeFrances MC, Zarnegar R. Induction of met proto-oncogene (hepatocyte growth factor receptor) expression during human monocyte-macrophage differentiation. Cell Growth Differ 1996; 7: 821-832

Chen Q, Ross AC. Retinoic acid regulates cell cycle progression and cell differentiation in human monocytic THP-1 cells. Exp Cell Res 2004; 297: 68-81

Chen S, Zhang J, Chen J, Wang Y, Zhou S, Huang L, Bai Y, Peng C, Shen B, Chen H, Tian Y. RER1 enhances carcinogenesis and stemness of pancreatic cancer under hypoxic environment. J Exp Clin Cancer Res 2019; 38: 15

Cheng-Hathaway PJ, Reed-Geaghan EG, Jay TR, Casali BT, Bemiller SM, Puntambekar SS, von Saucken VE, Williams RY, Karlo JC, Moutinho M, Xu G, Ransohoff RM, Lamb BT, Landreth GE. The Trem2 R47H variant confers loss-of-function-like phenotypes in Alzheimer's disease. Mol Neurodegener 2018; 13: 29

Chiesa S, Mingueneau M, Fuseri N, Malissen B, Raulet DH, Malissen M, Vivier E, Tomasello E. Multiplicity and plasticity of natural killer cell signaling pathways. Blood 2006; 107: 2364-2372

Chiu IM, Morimoto ET, Goodarzi H, Liao JT, O'Keeffe S, Phatnani HP, Muratet M, Carroll MC, Levy S, Tavazoie S, Myers RM, Maniatis T. A neurodegeneration-specific gene-expression signature of acutely isolated microglia from an amyotrophic lateral sclerosis mouse model. Cell Rep 2013; 4: 385-401

Cho SW, Kim S, Kim JM, Kim JS. Targeted genome engineering in human cells with the Cas9 RNA-guided endonuclease. Nat Biotechnol 2013; 31: 230-232

Choi GE, Park JY, Park MR, Yoon JH, Han HJ. Glucocorticoid enhances presenilin1-dependent Aβ production at ER's mitochondrial-associated membrane by downregulating Rer1 in neuronal cells. Redox Biol 2023; 65: 102821

Chung DH, Seaman WE, Daws MR. Characterization of TREM-3, an activating receptor on mouse macrophages: definition of a family of single Ig domain receptors on mouse chromosome 17. Eur J Immunol 2002; 32: 59-66

Ciechanover A. Proteolysis: from the lysosome to ubiquitin and the proteasome. Nat Rev Mol Cell Biol 2005; 6: 79-87

Claes C, Danhash EP, Hasselmann J, Chadarevian JP, Shabestari SK, England WE, Lim TE, Hidalgo JLS, Spitale RC, Davtyan H, Blurton-Jones M. Plaque-associated human microglia accumulate lipid droplets in a chimeric model of Alzheimer's disease. Molecular Neurodegeneration 2021; 16: 50

Cock PJ, Fields CJ, Goto N, Heuer ML, Rice PM. The Sanger FASTQ file format for sequences with quality scores, and the Solexa/Illumina FASTQ variants. Nucleic Acids Res 2010; 38: 1767-1771

Colonna M. TREMs in the immune system and beyond. Nat Rev Immunol 2003; 3: 445-453

Connerly PL, Esaki M, Montegna EA, Strongin DE, Levi S, Soderholm J, Glick BS. Sec16 is a determinant of transitional ER organization. Curr Biol 2005; 15: 1439-1447

Cosson P, Lankford SP, Bonifacino JS, Klausner RD. Membrane protein association by potential intramembrane charge pairs. Nature 1991; 351: 414-416

Cosson P, Perrin J, Bonifacino JS. Anchors aweigh: protein localization and transport mediated by transmembrane domains. Trends Cell Biol 2013; 23: 511-517

Crocker PR, Paulson JC, Varki A. Siglecs and their roles in the immune system. Nature Reviews Immunology 2007; 7: 255-266

Daigneault M, Preston JA, Marriott HM, Whyte MK, Dockrell DH. The identification of markers of macrophage differentiation in PMA-stimulated THP-1 cells and monocyte-derived macrophages. PLoS One 2010; 5: e8668

Dardiotis E, Siokas V, Pantazi E, Dardioti M, Rikos D, Xiromerisiou G, Markou A, Papadimitriou D, Speletas M, Hadjigeorgiou GM. A novel mutation in TREM2 gene causing Nasu-Hakola disease and review of the literature. Neurobiol Aging 2017; 53: 194.e113-194.e122

Daws MR, Sullam PM, Niemi EC, Chen TT, Tchao NK, Seaman WE. Pattern recognition by TREM-2: binding of anionic ligands. J Immunol 2003; 171: 594-599

Dejanovic B, Wu T, Tsai MC, Graykowski D, Gandham VD, Rose CM, Bakalarski CE, Ngu H, Wang Y, Pandey S, Rezzonico MG, Friedman BA, Edmonds R, De Mazière A, Rakosi-Schmidt R, Singh T, Klumperman J, Foreman O, Chang MC, Xie L, Sheng M, Hanson JE. Complement C1q-dependent excitatory and inhibitory synapse elimination by astrocytes and microglia in Alzheimer's disease mouse models. Nat Aging 2022; 2: 837-850

den Brok MH, Raaijmakers TK, Collado-Camps E, Adema GJ. Lipid Droplets as Immune Modulators in Myeloid Cells. Trends in Immunology 2018; 39: 380-392

Di Meco A, Curtis ME, Lauretti E, Praticò D. Autophagy Dysfunction in Alzheimer's Disease: Mechanistic Insights and New Therapeutic Opportunities. Biol Psychiatry 2020; 87: 797-807

Dick SA, Wong A, Hamidzada H, Nejat S, Nechanitzky R, Vohra S, Mueller B, Zaman R, Kantores C, Aronoff L, Momen A, Nechanitzky D, Li WY, Ramachandran P, Crome SQ, Becher B, Cybulsky MI, Billia F, Keshavjee S, Mital S, Robbins CS, Mak TW, Epelman S. Three tissue resident macrophage subsets coexist across organs with conserved origins and life cycles. Sci Immunol 2022; 7: eabf7777

Dietrich J, Cella M, Seiffert M, Bühring HJ, Colonna M. Cutting edge: signal-regulatory protein beta 1 is a DAP12-associated activating receptor expressed in myeloid cells. J Immunol 2000; 164: 9-12

Dikic I. Proteasomal and Autophagic Degradation Systems. Annu Rev Biochem 2017; 86: 193-224

Doherty GJ, McMahon HT. Mechanisms of endocytosis. Annu Rev Biochem 2009; 78: 857-902

Dries DR, Yu G. Assembly, maturation, and trafficking of the gamma-secretase complex in Alzheimer's disease. Curr Alzheimer Res 2008; 5: 132-146

Driscoll JJ, Dechowdhury R. Therapeutically targeting the SUMOylation, Ubiquitination and Proteasome pathways as a novel anticancer strategy. Target Oncol 2010; 5: 281-289

Edbauer D, Winkler E, Haass C, Steiner H. Presenilin and nicastrin regulate each other and determine amyloid beta-peptide production via complex formation. Proc Natl Acad Sci U S A 2002; 99: 8666-8671

El Khoury JB, Moore KJ, Means TK, Leung J, Terada K, Toft M, Freeman MW, Luster AD. CD36 mediates the innate host response to beta-amyloid. J Exp Med 2003; 197: 1657-1666

Ellgaard L, Molinari M, Helenius A. Setting the standards: quality control in the secretory pathway. Science 1999; 286: 1882-1888

Ershov P, Kaluzhskiy L, Mezentsev Y, Yablokov E, Gnedenko O, Ivanov A. Enzymes in the Cholesterol Synthesis Pathway: Interactomics in the Cancer Context. Biomedicines 2021; 9

Fabiano M, Oikawa N, Kerksiek A, Furukawa JI, Yagi H, Kato K, Schweizer U, Annaert W, Kang J, Shen J, Lütjohann D, Walter J. Presenilin Deficiency Results in Cellular Cholesterol Accumulation by Impairment of Protein Glycosylation and NPC1 Function. Int J Mol Sci 2024; 25

Farmer BC, Walsh AE, Kluemper JC, Johnson LA. Lipid Droplets in Neurodegenerative Disorders. Front Neurosci 2020; 14: 742

Feingold KR, Shigenaga JK, Kazemi MR, McDonald CM, Patzek SM, Cross AS, Moser A, Grunfeld C. Mechanisms of triglyceride accumulation in activated macrophages. J Leukoc Biol 2012; 92: 829-839

Feng J, Call ME, Wucherpfennig KW. The assembly of diverse immune receptors is focused on a polar membrane-embedded interaction site. PLoS Biol 2006; 4: e142

Feng J, Garrity D, Call ME, Moffett H, Wucherpfennig KW. Convergence on a distinctive assembly mechanism by unrelated families of activating immune receptors. Immunity 2005; 22: 427-438

Feng Y, He D, Yao Z, Klionsky DJ. The machinery of macroautophagy. Cell Res 2014; 24: 24-41

Fenoglio C, Galimberti D, Piccio L, Scalabrini D, Panina P, Buonsanti C, Venturelli E, Lovati C, Forloni G, Mariani C, Bresolin N, Scarpini E. Absence of TREM2 polymorphisms in patients with Alzheimer's disease and Frontotemporal Lobar Degeneration. Neurosci Lett 2007; 411: 133-137

Florance I, Ramasubbu S. Current Understanding on the Role of Lipids in Macrophages and Associated Diseases. Int J Mol Sci 2022; 24

Forabosco P, Ramasamy A, Trabzuni D, Walker R, Smith C, Bras J, Levine AP, Hardy J, Pocock JM, Guerreiro R, Weale ME, Ryten M. Insights into TREM2 biology by network analysis of human brain gene expression data. Neurobiol Aging 2013; 34: 2699-2714

Fowler SD, Mayer EP, Greenspan P. Foam cells and atherogenesis. Ann N Y Acad Sci 1985; 454: 79-90

Francis R, McGrath G, Zhang J, Ruddy DA, Sym M, Apfeld J, Nicoll M, Maxwell M, Hai B, Ellis MC, Parks AL, Xu W, Li J, Gurney M, Myers RL, Himes CS, Hiebsch R, Ruble C, Nye JS, Curtis D. aph-1 and pen-2 are required for Notch pathway signaling, gamma-secretase cleavage of betaAPP, and presenilin protein accumulation. Dev Cell 2002; 3: 85-97

Fuchs A, Cella M, Kondo T, Colonna M. Paradoxic inhibition of human natural interferon-producing cells by the activating receptor NKp44. Blood 2005; 106: 2076-2082

Fuior EV, Gafencu AV. Apolipoprotein C1: Its Pleiotropic Effects in Lipid Metabolism and Beyond. Int J Mol Sci 2019; 20

Füllekrug J, Boehm J, Röttger S, Nilsson T, Mieskes G, Schmitt HD. Human Rer1 is localized to the Golgi apparatus and complements the deletion of the homologous Rer1 protein of Saccharomyces cerevisiae. Eur J Cell Biol 1997; 74: 31-40

Garreau de Loubresse N, Prokhorova I, Holtkamp W, Rodnina MV, Yusupova G, Yusupov M. Structural basis for the inhibition of the eukaryotic ribosome. Nature 2014; 513: 517-522

Garrity D, Call ME, Feng J, Wucherpfennig KW. The activating NKG2D receptor assembles in the membrane with two signaling dimers into a hexameric structure. Proc Natl Acad Sci U S A 2005; 102: 7641-7646

Gawish R, Martins R, Böhm B, Wimberger T, Sharif O, Lakovits K, Schmidt M, Knapp S. Triggering receptor expressed on myeloid cells-2 fine-tunes inflammatory responses in murine Gram-negative sepsis. Faseb j 2015; 29: 1247-1257

Ge PF, Zhang JZ, Wang XF, Meng FK, Li WC, Luan YX, Ling F, Luo YN. Inhibition of autophagy induced by proteasome inhibition increases cell death in human SHG-44 glioma cells. Acta Pharmacol Sin 2009; 30: 1046-1052

Geissmann F, Jung S, Littman DR. Blood monocytes consist of two principal subsets with distinct migratory properties. Immunity 2003; 19: 71-82

Ghavidel A, Baxi K, Ignatchenko V, Prusinkiewicz M, Arnason TG, Kislinger T, Carvalho CE, Harkness TA. A Genome Scale Screen for Mutants with Delayed Exit from Mitosis: Ire1-Independent Induction of Autophagy Integrates ER Homeostasis into Mitotic Lifespan. PLoS Genet 2015; 11: e1005429

Gilroy DW, Lawrence T, Perretti M, Rossi AG. Inflammatory resolution: new opportunities for drug discovery. Nat Rev Drug Discov 2004; 3: 401-416

Gingras MC, Lapillonne H, Margolin JF. TREM-1, MDL-1, and DAP12 expression is associated with a mature stage of myeloid development. Mol Immunol 2002; 38: 817-824

Ginhoux F, Greter M, Leboeuf M, Nandi S, See P, Gokhan S, Mehler MF, Conway SJ, Ng LG, Stanley ER, Samokhvalov IM, Merad M. Fate mapping analysis reveals that adult microglia derive from primitive macrophages. Science 2010; 330: 841-845

Glebov K, Wunderlich P, Karaca I, Walter J. Functional involvement of γ-secretase in signaling of the triggering receptor expressed on myeloid cells-2 (TREM2). J Neuroinflammation 2016; 13: 17

Glickman MH, Ciechanover A. The ubiquitin-proteasome proteolytic pathway: destruction for the sake of construction. Physiol Rev 2002; 82: 373-428

Goldstein JL, Brown MS. The LDL Receptor. Arteriosclerosis, Thrombosis, and Vascular Biology 2009; 29: 431-438

Gomez Perdiguero E, Klapproth K, Schulz C, Busch K, Azzoni E, Crozet L, Garner H, Trouillet C, de Bruijn MF, Geissmann F, Rodewald HR. Tissue-resident macrophages originate from yolk-sac-derived erythro-myeloid progenitors. Nature 2015; 518: 547-551

Gordon S. The macrophage: past, present and future. Eur J Immunol 2007; 37 Suppl 1: S9-17

Gordon S, Plüddemann A. Tissue macrophages: heterogeneity and functions. BMC Biology 2017; 15: 53

Gordon S, Plüddemann A, Mukhopadhyay S. Plasma membrane receptors of tissue macrophages: functions and role in pathology. The Journal of Pathology 2020; 250: 656-666

Grandbarbe L, Michelucci A, Heurtaux T, Hemmer K, Morga E, Heuschling P. Notch signaling modulates the activation of microglial cells. Glia 2007; 55: 1519-1530

Greenberg AS, Egan JJ, Wek SA, Garty NB, Blanchette-Mackie EJ, Londos C. Perilipin, a major hormonally regulated adipocyte-specific phosphoprotein associated with the periphery of lipid storage droplets. J Biol Chem 1991; 266: 11341-11346

Griseti E, Bello AA, Bieth E, Sabbagh B, Iacovoni JS, Bigay J, Laurell H, Čopič A. Molecular mechanisms of perilipin protein function in lipid droplet metabolism. FEBS Lett 2024; 598: 1170-1198

Groll M, Bajorek M, Köhler A, Moroder L, Rubin DM, Huber R, Glickman MH, Finley D. A gated channel into the proteasome core particle. Nat Struct Biol 2000; 7: 1062-1067

Gross DA, Silver DL. Cytosolic lipid droplets: from mechanisms of fat storage to disease. Crit Rev Biochem Mol Biol 2014; 49: 304-326

Grubman A, Choo XY, Chew G, Ouyang JF, Sun G, Croft NP, Rossello FJ, Simmons R, Buckberry S, Landin DV, Pflueger J, Vandekolk TH, Abay Z, Zhou Y, Liu X, Chen J, Larcombe M, Haynes JM, McLean C, Williams S, Chai SY, Wilson T, Lister R, Pouton CW, Purcell AW, Rackham OJL, Petretto E, Polo JM. Transcriptional signature in microglia associated with Aβ plaque phagocytosis. Nat Commun 2021; 12: 3015

Guerreiro R, Wojtas A, Bras J, Carrasquillo M, Rogaeva E, Majounie E, Cruchaga C, Sassi C, Kauwe JS, Younkin S, Hazrati L, Collinge J, Pocock J, Lashley T, Williams J, Lambert JC, Amouyel P, Goate A, Rademakers R, Morgan K, Powell J, St George-Hyslop P, Singleton A, Hardy J. TREM2 variants in Alzheimer's disease. N Engl J Med 2013a; 368: 117-127

Guerreiro RJ, Lohmann E, Brás JM, Gibbs JR, Rohrer JD, Gurunlian N, Dursun B, Bilgic B, Hanagasi H, Gurvit H, Emre M, Singleton A, Hardy J. Using exome sequencing to reveal mutations in TREM2 presenting as a frontotemporal dementia-like syndrome without bone involvement. JAMA Neurol 2013b; 70: 78-84

Gutierrez E, Lütjohann D, Kerksiek A, Fabiano M, Oikawa N, Kuerschner L, Thiele C, Walter J. Importance of γ-secretase in the regulation of liver X receptor and cellular lipid metabolism. Life Sci Alliance 2020; 3

Haapasalo A, Kovacs DM. The many substrates of presenilin/γ-secretase. J Alzheimers Dis 2011; 25: 3-28

Haass C. Take five--BACE and the gamma-secretase quartet conduct Alzheimer's amyloid beta-peptide generation. Embo j 2004; 23: 483-488

Haass C, Koo EH, Mellon A, Hung AY, Selkoe DJ. Targeting of cell-surface beta-amyloid precursor protein to lysosomes: alternative processing into amyloid-bearing fragments. Nature 1992; 357: 500-503

Hamerman JA, Jarjoura JR, Humphrey MB, Nakamura MC, Seaman WE, Lanier LL. Cutting edge: inhibition of TLR and FcR responses in macrophages by triggering receptor expressed on myeloid cells (TREM)-2 and DAP12. J Immunol 2006; 177: 2051-2055

Hamerman JA, Tchao NK, Lowell CA, Lanier LL. Enhanced Toll-like receptor responses in the absence of signaling adaptor DAP12. Nat Immunol 2005; 6: 579-586

Hammond C, Braakman I, Helenius A. Role of N-linked oligosaccharide recognition, glucose trimming, and calnexin in glycoprotein folding and quality control. Proc Natl Acad Sci U S A 1994; 91: 913-917

Hammond TR, Dufort C, Dissing-Olesen L, Giera S, Young A, Wysoker A, Walker AJ, Gergits F, Segel M, Nemesh J, Marsh SE, Saunders A, Macosko E, Ginhoux F, Chen J, Franklin RJM, Piao X, McCarroll SA, Stevens B. Single-Cell RNA Sequencing of Microglia throughout the Mouse Lifespan and in the Injured Brain Reveals Complex Cell-State Changes. Immunity 2019; 50: 253-271.e256

Haney MS, Pálovics R, Munson CN, Long C, Johansson PK, Yip O, Dong W, Rawat E, West E, Schlachetzki JCM, Tsai A, Guldner IH, Lamichhane BS, Smith A, Schaum N, Calcuttawala K, Shin A, Wang Y-H, Wang C, Koutsodendris N, Serrano GE, Beach TG, Reiman EM, Glass CK, Abu-Remaileh M, Enejder A, Huang Y, Wyss-Coray T. APOE4/4 is linked to damaging lipid droplets in Alzheimer's disease microglia. Nature 2024; 628: 154-161

Hanley SE, Cooper KF. Sorting Nexins in Protein Homeostasis. Cells 2020; 10

Hara T, Hashimoto Y, Akuzawa T, Hirai R, Kobayashi H, Sato K. Rer1 and calnexin regulate endoplasmic reticulum retention of a peripheral myelin protein 22 mutant that causes type 1A Charcot-Marie-Tooth disease. Sci Rep 2014; 4: 6992

Hara T, Maejima I, Akuzawa T, Hirai R, Kobayashi H, Tsukamoto S, Tsunoda M, Ono A, Yamakoshi S, Oikawa S, Sato K. Rer1-mediated quality control system is required for neural stem cell maintenance during cerebral cortex development. PLoS Genet 2018; 14: e1007647

Harada Y, Ohkawa Y, Maeda K, Taniguchi N. Glycan quality control in and out of the endoplasmic reticulum of mammalian cells. Febs j 2022; 289: 7147-7162

Harer SL, Bhatia MS, Bhatia NM. Proteasome inhibitors mechanism; source for design of newer therapeutic agents. The Journal of Antibiotics 2012; 65: 279-288

Haure-Mirande JV, Audrain M, Fanutza T, Kim SH, Klein WL, Glabe C, Readhead B, Dudley JT, Blitzer RD, Wang M, Zhang B, Schadt EE, Gandy S, Ehrlich ME. Deficiency of TYROBP, an adapter protein for TREM2 and CR3 receptors, is neuroprotective in a mouse model of early Alzheimer's pathology. Acta Neuropathol 2017; 134: 769-788

Haure-Mirande JV, Wang M, Audrain M, Fanutza T, Kim SH, Heja S, Readhead B, Dudley JT, Blitzer RD, Schadt EE, Zhang B, Gandy S, Ehrlich ME. Integrative approach to sporadic Alzheimer's disease: deficiency of TYROBP in cerebral Aβ amyloidosis mouse normalizes clinical phenotype and complement subnetwork molecular pathology without reducing Aβ burden. Mol Psychiatry 2019; 24: 431-446

Heinemeyer W, Ramos PC, Dohmen RJ. Ubiquitin-proteasome system. Cellular and Molecular Life Sciences CMLS 2004; 61: 1562-1578

Hellwig S, Masuch A, Nestel S, Katzmarski N, Meyer-Luehmann M, Biber K. Forebrain microglia from wild-type but not adult 5xFAD mice prevent amyloid-β plaque formation in organotypic hippocampal slice cultures. Sci Rep 2015; 5: 14624

Heneka MT, van der Flier WM, Jessen F, Hoozemanns J, Thal DR, Boche D, Brosseron F, Teunissen C, Zetterberg H, Jacobs AH, Edison P, Ramirez A, Cruchaga C, Lambert JC, Laza AR, Sanchez-Mut JV, Fischer A, Castro-Gomez S, Stein TD, Kleineidam L, Wagner M, Neher JJ, Cunningham C, Singhrao SK, Prinz M, Glass CK, Schlachetzki JCM, Butovsky O, Kleemann K, De Jaeger PL, Scheiblich H, Brown GC, Landreth G, Moutinho M, Grutzendler J, Gomez-Nicola D, McManus RM, Andreasson K, Ising C, Karabag D, Baker DJ, Liddelow SA, Verkhratsky A, Tansey M, Monsonego A, Aigner L, Dorothée G, Nave KA, Simons M, Constantin G, Rosenzweig N, Pascual A, Petzold GC, Kipnis J, Venegas C, Colonna M, Walter J, Tenner AJ, O'Banion MK, Steinert JR, Feinstein DL, Sastre M, Bhaskar K, Hong S, Schafer DP, Golde T, Ransohoff RM, Morgan D, Breitner J, Mancuso R, Riechers SP. Neuroinflammation in Alzheimer disease. Nat Rev Immunol 2024;

Henne WM, Reese ML, Goodman JM. The assembly of lipid droplets and their roles in challenged cells. Embo j 2018; 37

Hershko A, Ciechanover A. The ubiquitin system for protein degradation. Annu Rev Biochem 1992; 61: 761-807

Hickman SE, El Khoury J. TREM2 and the neuroimmunology of Alzheimer's disease. Biochem Pharmacol 2014; 88: 495-498

Hickman SE, Kingery ND, Ohsumi TK, Borowsky ML, Wang LC, Means TK, El Khoury J. The microglial sensome revealed by direct RNA sequencing. Nat Neurosci 2013; 16: 1896-1905

Ho KH, Patrizi A. Assessment of common housekeeping genes as reference for gene expression studies using RT-qPCR in mouse choroid plexus. Sci Rep 2021; 11: 3278

Hoeffel G, Chen J, Lavin Y, Low D, Almeida FF, See P, Beaudin AE, Lum J, Low I, Forsberg EC, Poidinger M, Zolezzi F, Larbi A, Ng LG, Chan JK, Greter M, Becher B, Samokhvalov IM, Merad M, Ginhoux F. C-Myb(+) erythro-myeloid progenitor-derived fetal monocytes give rise to adult tissue-resident macrophages. Immunity 2015; 42: 665-678

Homewood CA, Warhurst DC, Peters W, Baggaley VC. Lysosomes, pH and the anti-malarial action of chloroquine. Nature 1972; 235: 50-52

Hooli BV, Parrado AR, Mullin K, Yip WK, Liu T, Roehr JT, Qiao D, Jessen F, Peters O, Becker T, Ramirez A, Lange C, Bertram L, Tanzi RE. The rare TREM2 R47H variant exerts only a modest effect on Alzheimer disease risk. Neurology 2014; 83: 1353-1358

Hou Y, Wei D, Zhang Z, Guo H, Li S, Zhang J, Zhang P, Zhang L, Zhao Y. FABP5 controls macrophage alternative activation and allergic asthma by selectively programming long-chain unsaturated fatty acid metabolism. Cell Reports 2022; 41: 111668

Houchins JP, Lanier LL, Niemi EC, Phillips JH, Ryan JC. Natural killer cell cytolytic activity is inhibited by NKG2-A and activated by NKG2-C. J Immunol 1997; 158: 3603-3609

Hsieh CL, Koike M, Spusta SC, Niemi EC, Yenari M, Nakamura MC, Seaman WE. A role for TREM2 ligands in the phagocytosis of apoptotic neuronal cells by microglia. J Neurochem 2009; 109: 1144-1156

Hu N, Tan MS, Yu JT, Sun L, Tan L, Wang YL, Jiang T, Tan L. Increased expression of TREM2 in peripheral blood of Alzheimer's disease patients. J Alzheimers Dis 2014; 38: 497-501

Huang Y, Lemke G. Early death in a mouse model of Alzheimer's disease exacerbated by microglial loss of TAM receptor signaling. Proc Natl Acad Sci U S A 2022; 119: e2204306119

Hume DA, Irvine KM, Pridans C. The Mononuclear Phagocyte System: The Relationship between Monocytes and Macrophages. Trends in Immunology 2019; 40: 98-112

Ibach M, Mathews M, Linnartz-Gerlach B, Theil S, Kumar S, Feederle R, Brüstle O, Neumann H, Walter J. A reporter cell system for the triggering receptor expressed on myeloid cells 2 reveals differential effects of disease-associated variants on receptor signaling and activation by antibodies against the stalk region. Glia 2021; 69: 1126-1139

Inobe T, Matouschek A. Paradigms of protein degradation by the proteasome. Curr Opin Struct Biol 2014; 24: 156-164

Jaeger PA, Pickford F, Sun CH, Lucin KM, Masliah E, Wyss-Coray T. Regulation of amyloid precursor protein processing by the Beclin 1 complex. PLoS One 2010; 5: e11102

Jarosch E, Geiss-Friedlander R, Meusser B, Walter J, Sommer T. Protein dislocation from the endoplasmic reticulum--pulling out the suspect. Traffic 2002; 3: 530-536

Jay TR, von Saucken VE, Landreth GE. TREM2 in Neurodegenerative Diseases. Mol Neurodegener 2017; 12: 56

Jenkins SJ, Allen JE. The expanding world of tissue-resident macrophages. Eur J Immunol 2021; 51: 1882-1896

Jiang K, Zhong B, Gilvary DL, Corliss BC, Vivier E, Hong-Geller E, Wei S, Djeu JY. Syk regulation of phosphoinositide 3-kinase-dependent NK cell function. J Immunol 2002; 168: 3155-3164

Jiang S, Li Y, Zhang X, Bu G, Xu H, Zhang YW. Trafficking regulation of proteins in Alzheimer's disease. Mol Neurodegener 2014; 9: 6

Jonsson T, Stefansson H, Steinberg S, Jonsdottir I, Jonsson PV, Snaedal J, Bjornsson S, Huttenlocher J, Levey AI, Lah JJ, Rujescu D, Hampel H, Giegling I, Andreassen OA, Engedal K, Ulstein I, Djurovic S, Ibrahim-Verbaas C, Hofman A, Ikram MA, van Duijn CM, Thorsteinsdottir U, Kong A, Stefansson K. Variant of TREM2 associated with the risk of Alzheimer's disease. N Engl J Med 2013; 368: 107-116

Jurisch-Yaksi N, Rose AJ, Lu H, Raemaekers T, Munck S, Baatsen P, Baert V, Vermeire W, Scales SJ, Verleyen D, Vandepoel R, Tylzanowski P, Yaksi E, de Ravel T, Yost HJ, Froyen G, Arrington CB, Annaert W. Rer1p maintains ciliary length and signaling by regulating γ-secretase activity and Foxj1a levels. J Cell Biol 2013a; 200: 709-720

Jurisch-Yaksi N, Sannerud R, Annaert W. A fast growing spectrum of biological functions of γ-secretase in development and disease. Biochim Biophys Acta 2013b; 1828: 2815-2827

Kaether C, Scheuermann J, Fassler M, Zilow S, Shirotani K, Valkova C, Novak B, Kacmar S, Steiner H, Haass C. Endoplasmic reticulum retention of the gamma-secretase complex component Pen2 by Rer1. EMBO Rep 2007; 8: 743-748

Kaifu T, Nakahara J, Inui M, Mishima K, Momiyama T, Kaji M, Sugahara A, Koito H, Ujike-Asai A, Nakamura A, Kanazawa K, Tan-Takeuchi K, Iwasaki K, Yokoyama WM, Kudo A, Fujiwara M, Asou H, Takai T. Osteopetrosis and thalamic hypomyelinosis with synaptic degeneration in DAP12-deficient mice. J Clin Invest 2003; 111: 323-332

Kandutsch AA, Russell AE. Preputial gland tumor sterols. 2. The identification of 4 alpha-methyl-Delta 8-cholesten-3 beta-ol. J Biol Chem 1960a; 235: 2253-2255

Kandutsch AA, Russell AE. Preputial gland tumor sterols. 3. A metabolic pathway from lanosterol to cholesterol. J Biol Chem 1960b; 235: 2256-2261

Kanekiyo T, Zhang J, Liu Q, Liu CC, Zhang L, Bu G. Heparan sulphate proteoglycan and the low-density lipoprotein receptor-related protein 1 constitute major pathways for neuronal amyloid-beta uptake. J Neurosci 2011; 31: 1644-1651

Kao SH, Wang WL, Chen CY, Chang YL, Wu YY, Wang YT, Wang SP, Nesvizhskii AI, Chen YJ, Hong TM, Yang PC. Analysis of Protein Stability by the Cycloheximide Chase Assay. Bio Protoc 2015; 5

Karaca I, Tamboli IY, Glebov K, Richter J, Fell LH, Grimm MO, Haupenthal VJ, Hartmann T, Gräler MH, van Echten-Deckert G, Walter J. Deficiency of sphingosine-1-phosphate lyase impairs lysosomal metabolism of the amyloid precursor protein. J Biol Chem 2014; 289: 16761-16772

Karlsson M, Zhang C, Méar L, Zhong W, Digre A, Katona B, Sjöstedt E, Butler L, Odeberg J, Dusart P, Edfors F, Oksvold P, von Feilitzen K, Zwahlen M, Arif M, Altay O, Li X, Ozcan

M, Mardinoglu A, Fagerberg L, Mulder J, Luo Y, Ponten F, Uhlén M, Lindskog C. A single-cell type transcriptomics map of human tissues. Sci Adv 2021; 7

Kaushik S, Cuervo AM. The coming of age of chaperone-mediated autophagy. Nat Rev Mol Cell Biol 2018; 19: 365-381

Kawabori M, Kacimi R, Kauppinen T, Calosing C, Kim JY, Hsieh CL, Nakamura MC, Yenari MA. Triggering receptor expressed on myeloid cells 2 (TREM2) deficiency attenuates phagocytic activities of microglia and exacerbates ischemic damage in experimental stroke. J Neurosci 2015; 35: 3384-3396

Keewan E, Naser SA. The Role of Notch Signaling in Macrophages during Inflammation and Infection: Implication in Rheumatoid Arthritis? Cells 2020; 9

Keren-Shaul H, Spinrad A, Weiner A, Matcovitch-Natan O, Dvir-Szternfeld R, Ulland TK, David E, Baruch K, Lara-Astaiso D, Toth B, Itzkovitz S, Colonna M, Schwartz M, Amit I. A Unique Microglia Type Associated with Restricting Development of Alzheimer's Disease. Cell 2017; 169: 1276-1290.e1217

Kettenmann H, Kirchhoff F, Verkhratsky A. Microglia: new roles for the synaptic stripper. Neuron 2013; 77: 10-18

Khaminets A, Behl C, Dikic I. Ubiquitin-Dependent And Independent Signals In Selective Autophagy. Trends Cell Biol 2016; 26: 6-16

Khatchadourian A, Bourque SD, Richard VR, Titorenko VI, Maysinger D. Dynamics and regulation of lipid droplet formation in lipopolysaccharide (LPS)-stimulated microglia. Biochim Biophys Acta 2012; 1821: 607-617

Kiialainen A, Veckman V, Saharinen J, Paloneva J, Gentile M, Hakola P, Hemelsoet D, Ridha B, Kopra O, Julkunen I, Peltonen L. Transcript profiles of dendritic cells of PLOSL patients link demyelinating CNS disorders with abnormalities in pathways of actin bundling and immune response. J Mol Med (Berl) 2007; 85: 971-983

Kiianitsa K, Lukes ME, Hayes BJ, Brutman J, Valdmanis PN, Bird TD, Raskind WH, Korvatska O. TREM2 variants that cause early dementia and increase Alzheimer's disease risk affect gene splicing. Brain 2024;

Kim D, Langmead B, Salzberg SL. HISAT: a fast spliced aligner with low memory requirements. Nat Methods 2015; 12: 357-360

Kim J, Han D, Byun SH, Kwon M, Cho JY, Pleasure SJ, Yoon K. Ttyh1 regulates embryonic neural stem cell properties by enhancing the Notch signaling pathway. EMBO Rep 2018; 19

Kim S, Kim D, Cho SW, Kim J, Kim JS. Highly efficient RNA-guided genome editing in human cells via delivery of purified Cas9 ribonucleoproteins. Genome Res 2014; 24: 1012-1019

Kisselev AF, Goldberg AL. Proteasome inhibitors: from research tools to drug candidates. Chem Biol 2001; 8: 739-758

Klausner RD, Sitia R. Protein degradation in the endoplasmic reticulum. Cell 1990; 62: 611-614

Kleinberger G, Yamanishi Y, Suárez-Calvet M, Czirr E, Lohmann E, Cuyvers E, Struyfs H, Pettkus N, Wenninger-Weinzierl A, Mazaheri F, Tahirovic S, Lleó A, Alcolea D, Fortea J, Willem M, Lammich S, Molinuevo JL, Sánchez-Valle R, Antonell A, Ramirez A, Heneka MT, Sleegers K, van der Zee J, Martin JJ, Engelborghs S, Demirtas-Tatlidede A, Zetterberg H, Van Broeckhoven C, Gurvit H, Wyss-Coray T, Hardy J, Colonna M, Haass C. TREM2 mutations implicated in neurodegeneration impair cell surface transport and phagocytosis. Sci Transl Med 2014; 6: 243ra286

Klünemann HH, Ridha BH, Magy L, Wherrett JR, Hemelsoet DM, Keen RW, De Bleecker JL, Rossor MN, Marienhagen J, Klein HE, Peltonen L, Paloneva J. The genetic causes of basal ganglia calcification, dementia, and bone cysts: DAP12 and TREM2. Neurology 2005; 64: 1502-1507

Knoblich K, Park S, Lutfi M, van 't Hag L, Conn CE, Seabrook SA, Newman J, Czabotar PE, Im W, Call ME, Call MJ. Transmembrane Complexes of DAP12 Crystallized in Lipid Membranes Provide Insights into Control of Oligomerization in Immunoreceptor Assembly. Cell Rep 2015; 11: 1184-1192

Kober DL, Alexander-Brett JM, Karch CM, Cruchaga C, Colonna M, Holtzman MJ, Brett TJ. Neurodegenerative disease mutations in TREM2 reveal a functional surface and distinct loss-of-function mechanisms. Elife 2016; 5

Kohro T, Tanaka T, Murakami T, Wada Y, Aburatani H, Hamakubo T, Kodama T. A comparison of differences in the gene expression profiles of phorbol 12-myristate 13-acetate differentiated THP-1 cells and human monocyte-derived macrophage. J Atheroscler Thromb 2004; 11: 88-97

Koliwad SK, Streeper RS, Monetti M, Cornelissen I, Chan L, Terayama K, Naylor S, Rao M, Hubbard B, Farese RV, Jr. DGAT1-dependent triacylglycerol storage by macrophages protects mice from diet-induced insulin resistance and inflammation. J Clin Invest 2010; 120: 756-767

Kory N, Farese RV, Jr., Walther TC. Targeting Fat: Mechanisms of Protein Localization to Lipid Droplets. Trends Cell Biol 2016; 26: 535-546

Koth LL, Cambier CJ, Ellwanger A, Solon M, Hou L, Lanier LL, Abram CL, Hamerman JA, Woodruff PG. DAP12 is required for macrophage recruitment to the lung in response to cigarette smoke and chemotaxis toward CCL2. J Immunol 2010; 184: 6522-6528

Koundouros N, Poulogiannis G. Reprogramming of fatty acid metabolism in cancer. British Journal of Cancer 2020; 122: 4-22

Kraft C, Martens S. Mechanisms and regulation of autophagosome formation. Curr Opin Cell Biol 2012; 24: 496-501

Krshnan L, van de Weijer ML, Carvalho P. Endoplasmic Reticulum-Associated Protein Degradation. Cold Spring Harb Perspect Biol 2022; 14

Kuerschner L, Moessinger C, Thiele C. Imaging of Lipid Biosynthesis: How a Neutral Lipid Enters Lipid Droplets. Traffic 2008; 9: 338-352

Kyrychenko VO, Nagibin VS, Tumanovska LV, Pashevin DO, Gurianova VL, Moibenko AA, Dosenko VE, Klionsky DJ. Knockdown of PSMB7 induces autophagy in cardiomyocyte cultures: possible role in endoplasmic reticulum stress. Pathobiology 2014; 81: 8-14

Lancaster CE, Ho CY, Hipolito VEB, Botelho RJ, Terebiznik MR. Phagocytosis: what's on the menu? (1). Biochem Cell Biol 2019; 97: 21-29

Lanier LL, Bakker AB. The ITAM-bearing transmembrane adaptor DAP12 in lymphoid and myeloid cell function. Immunol Today 2000; 21: 611-614

Lanier LL, Corliss B, Wu J, Phillips JH. Association of DAP12 with activating CD94/NKG2C NK cell receptors. Immunity 1998a; 8: 693-701

Lanier LL, Corliss BC, Wu J, Leong C, Phillips JH. Immunoreceptor DAP12 bearing a tyrosine-based activation motif is involved in activating NK cells. Nature 1998b; 391: 703-707

Lawrence T, Willoughby DA, Gilroy DW. Anti-inflammatory lipid mediators and insights into the resolution of inflammation. Nat Rev Immunol 2002; 2: 787-795

Lazetic S, Chang C, Houchins JP, Lanier LL, Phillips JH. Human natural killer cell receptors involved in MHC class I recognition are disulfide-linked heterodimers of CD94 and NKG2 subunits. J Immunol 1996; 157: 4741-4745

Le Dréan E, Vély F, Olcese L, Cambiaggi A, Guia S, Krystal G, Gervois N, Moretta A, Jotereau F, Vivier E. Inhibition of antigen-induced T cell response and antibody-induced NK cell cytotoxicity by NKG2A: association of NKG2A with SHP-1 and SHP-2 protein-tyrosine phosphatases. Eur J Immunol 1998; 28: 264-276

Lecker SH, Goldberg AL, Mitch WE. Protein degradation by the ubiquitin-proteasome pathway in normal and disease states. J Am Soc Nephrol 2006; 17: 1807-1819

Lee MJ, Lee JH, Rubinsztein DC. Tau degradation: the ubiquitin-proteasome system versus the autophagy-lysosome system. Prog Neurobiol 2013; 105: 49-59

Lepesheva GI, Waterman MR. Sterol 14alpha-demethylase cytochrome P450 (CYP51), a P450 in all biological kingdoms. Biochim Biophys Acta 2007; 1770: 467-477

Li J, Cai Z, Vaites LP, Shen N, Mitchell DC, Huttlin EL, Paulo JA, Harry BL, Gygi SP. Proteome-wide mapping of short-lived proteins in human cells. Mol Cell 2021; 81: 4722-4735.e4725

Li Q, Liu Y, Sun M. Autophagy and Alzheimer's Disease. Cellular and Molecular Neurobiology 2017; 37: 377-388

Libby P. Inflammation in atherosclerosis. Nature 2002; 420: 868-874

Lichtenthaler SF, Tschirner SK, Steiner H. Secretases in Alzheimer's disease: Novel insights into proteolysis of APP and TREM2. Curr Opin Neurobiol 2022; 72: 101-110

Liu CC, Liu CC, Kanekiyo T, Xu H, Bu G. Apolipoprotein E and Alzheimer disease: risk, mechanisms and therapy. Nat Rev Neurol 2013; 9: 106-118

Liu T, Huang T, Li J, Li A, Li C, Huang X, Li D, Wang S, Liang M. Optimization of differentiation and transcriptomic profile of THP-1 cells into macrophage by PMA. PLoS One 2023; 18: e0286056

Liu WS, Heckman CA. The sevenfold way of PKC regulation. Cell Signal 1998; 10: 529-542

Liu X, Zhang L, Zhang H, Liang X, Zhang B, Tu J, Zhao Y. Nedd4-2 Haploinsufficiency in Mice Impairs the Ubiquitination of Rer1 and Increases the Susceptibility to Endoplasmic Reticulum Stress and Seizures. Front Mol Neurosci 2022; 15: 919718

Liu Y, Theil S, Ibach M, Walter J. DAP12 interacts with RER1 and is retained in the secretory pathway before assembly with TREM2. Cell Mol Life Sci 2024; 81: 302

Lotteau V, Teyton L, Peleraux A, Nilsson T, Karlsson L, Schmid SL, Quaranta V, Peterson PA. Intracellular transport of class II MHC molecules directed by invariant chain. Nature 1990; 348: 600-605

Luzio JP, Pryor PR, Bright NA. Lysosomes: fusion and function. Nat Rev Mol Cell Biol 2007; 8: 622-632

Ma L, Allen M, Sakae N, Ertekin-Taner N, Graff-Radford NR, Dickson DW, Younkin SG, Sevlever D. Expression and processing analyses of wild type and p.R47H TREM2 variant in Alzheimer's disease brains. Mol Neurodegener 2016; 11: 72

Mahley RW. Apolipoprotein E: cholesterol transport protein with expanding role in cell biology. Science 1988; 240: 622-630

Mahley RW, Rall SC. Apolipoprotein E: Far More Than a Lipid Transport Protein. Annual Review of Genomics and Human Genetics 2000; 1: 507-537

Majumder P, Baumeister W. Proteasomes: unfoldase-assisted protein degradation machines. Biol Chem 2019; 401: 183-199

Makrigiannis AP, Gosselin P, Mason LH, Taylor LS, McVicar DW, Ortaldo JR, Anderson SK. Cloning and characterization of a novel activating Ly49 closely related to Ly49A. J Immunol 1999; 163: 4931-4938

Margeta-Mitrovic M, Jan YN, Jan LY. A Trafficking Checkpoint Controls GABAB Receptor Heterodimerization. Neuron 2000; 27: 97-106

Marinko JT, Wright MT, Schlebach JP, Clowes KR, Heintzman DR, Plate L, Sanders CR. Glycosylation limits forward trafficking of the tetraspan membrane protein PMP22. J Biol Chem 2021; 296: 100719

Marschallinger J, Iram T, Zardeneta M, Lee SE, Lehallier B, Haney MS, Pluvinage JV, Mathur V, Hahn O, Morgens DW, Kim J, Tevini J, Felder TK, Wolinski H, Bertozzi CR, Bassik MC, Aigner L, Wyss-Coray T. Lipid-droplet-accumulating microglia represent a dysfunctional and proinflammatory state in the aging brain. Nature Neuroscience 2020; 23: 194-208

Mason LH, Willette-Brown J, Anderson SK, Gosselin P, Shores EW, Love PE, Ortaldo JR, McVicar DW. Characterization of an associated 16-kDa tyrosine phosphoprotein required for Ly-49D signal transduction. J Immunol 1998; 160: 4148-4152

Mass E, Ballesteros I, Farlik M, Halbritter F, Günther P, Crozet L, Jacome-Galarza CE, Händler K, Klughammer J, Kobayashi Y, Gomez-Perdiguero E, Schultze JL, Beyer M, Bock C, Geissmann F. Specification of tissue-resident macrophages during organogenesis. Science 2016; 353

Mass E, Nimmerjahn F, Kierdorf K, Schlitzer A. Tissue-specific macrophages: how they develop and choreograph tissue biology. Nature Reviews Immunology 2023; 23: 563-579

Masuda T, Sankowski R, Staszewski O, Böttcher C, Amann L, Sagar, Scheiwe C, Nessler S, Kunz P, van Loo G, Coenen VA, Reinacher PC, Michel A, Sure U, Gold R, Grün D, Priller J, Stadelmann C, Prinz M. Spatial and temporal heterogeneity of mouse and human microglia at single-cell resolution. Nature 2019; 566: 388-392

Mauthe M, Orhon I, Rocchi C, Zhou X, Luhr M, Hijlkema KJ, Coppes RP, Engedal N, Mari M, Reggiori F. Chloroquine inhibits autophagic flux by decreasing autophagosome-lysosome fusion. Autophagy 2018; 14: 1435-1455

McPherson R, Gauthier A. Molecular regulation of SREBP function: the Insig-SCAP connection and isoform-specific modulation of lipid synthesis. Biochemistry and Cell Biology 2004; 82: 201-211

McVicar DW, Burshtyn DN. Intracellular signaling by the killer immunoglobulin-like receptors and Ly49. Sci STKE 2001; 2001: re1

McVicar DW, Taylor LS, Gosselin P, Willette-Brown J, Mikhael AI, Geahlen RL, Nakamura MC, Linnemeyer P, Seaman WE, Anderson SK, Ortaldo JR, Mason LH. DAP12-mediated signal transduction in natural killer cells. A dominant role for the Syk protein-tyrosine kinase. J Biol Chem 1998; 273: 32934-32942

Mellman I, Fuchs R, Helenius A. Acidification of the endocytic and exocytic pathways. Annu Rev Biochem 1986; 55: 663-700

Menzies FM, Moreau K, Rubinsztein DC. Protein misfolding disorders and macroautophagy. Curr Opin Cell Biol 2011; 23: 190-197

Miao Y, Du Q, Zhang HG, Yuan Y, Zuo Y, Zheng H. Cycloheximide (CHX) Chase Assay to Examine Protein Half-life. Bio Protoc 2023; 13: e4690

Michelsen K, Yuan H, Schwappach B. Hide and run. Arginine-based endoplasmic-reticulum-sorting motifs in the assembly of heteromultimeric membrane proteins. EMBO Rep 2005; 6: 717-722

Mitsche MA, McDonald JG, Hobbs HH, Cohen JC. Flux analysis of cholesterol biosynthesis in vivo reveals multiple tissue and cell-type specific pathways. Elife 2015; 4: e07999

Mizushima N, Komatsu M. Autophagy: renovation of cells and tissues. Cell 2011; 147: 728-741

Molineaux SM. Molecular Pathways: Targeting Proteasomal Protein Degradation in Cancer. Clinical Cancer Research 2012; 18: 15-20

Mori Y, Yoshino Y, Ochi S, Yamazaki K, Kawabe K, Abe M, Kitano T, Ozaki Y, Yoshida T, Numata S, Mori T, Iga J, Kuroda N, Ohmori T, Ueno S. TREM2 mRNA Expression in Leukocytes Is Increased in Alzheimer's Disease and Schizophrenia. PLoS One 2015; 10: e0136835

Mullard A. Inhibiting γ-secretase activity. Nature Reviews Molecular Cell Biology 2007; 8: 272-273

Mulrooney TJ, Posch PE, Hurley CK. DAP12 impacts trafficking and surface stability of killer immunoglobulin-like receptors on natural killer cells. J Leukoc Biol 2013; 94: 301-313

Munro S, Pelham HR. A C-terminal signal prevents secretion of luminal ER proteins. Cell 1987; 48: 899-907

Murata S, Yashiroda H, Tanaka K. Molecular mechanisms of proteasome assembly. Nat Rev Mol Cell Biol 2009; 10: 104-115

N'Diaye EN, Branda CS, Branda SS, Nevarez L, Colonna M, Lowell C, Hamerman JA, Seaman WE. TREM-2 (triggering receptor expressed on myeloid cells 2) is a phagocytic receptor for bacteria. J Cell Biol 2009; 184: 215-223

Nagle CA, Klett EL, Coleman RA. Hepatic triacylglycerol accumulation and insulin resistance. J Lipid Res 2009; 50 Suppl: S74-79

Nalepa G, Rolfe M, Harper JW. Drug discovery in the ubiquitin-proteasome system. Nat Rev Drug Discov 2006; 5: 596-613

Nishikawa S, Nakano A. Identification of a gene required for membrane protein retention in the early secretory pathway. Proc Natl Acad Sci U S A 1993; 90: 8179-8183

Nixon RA, Wegiel J, Kumar A, Yu WH, Peterhoff C, Cataldo A, Cuervo AM. Extensive involvement of autophagy in Alzheimer disease: an immuno-electron microscopy study. J Neuropathol Exp Neurol 2005; 64: 113-122

Numasawa Y, Yamaura C, Ishihara S, Shintani S, Yamazaki M, Tabunoki H, Satoh JI. Nasu-Hakola disease with a splicing mutation of TREM2 in a Japanese family. Eur J Neurol 2011; 18: 1179-1183

O'Gorman S, Fox DT, Wahl GM. Recombinase-mediated gene activation and site-specific integration in mammalian cells. Science 1991; 251: 1351-1355

Obrig TG, Culp WJ, McKeehan WL, Hardesty B. The mechanism by which cycloheximide and related glutarimide antibiotics inhibit peptide synthesis on reticulocyte ribosomes. J Biol Chem 1971; 246: 174-181

Oikawa N, Walter J. Presenilins and γ-Secretase in Membrane Proteostasis. Cells 2019; 8

Olah M, Menon V, Habib N, Taga MF, Ma Y, Yung CJ, Cimpean M, Khairallah A, Coronas-Samano G, Sankowski R, Grün D, Kroshilina AA, Dionne D, Sarkis RA, Cosgrove GR, Helgager J, Golden JA, Pennell PB, Prinz M, Vonsattel JPG, Teich AF, Schneider JA, Bennett DA, Regev A, Elyaman W, Bradshaw EM, De Jager PL. Single cell RNA sequencing of human microglia uncovers a subset associated with Alzheimer's disease. Nat Commun 2020; 11: 6129

Olcese L, Cambiaggi A, Semenzato G, Bottino C, Moretta A, Vivier E. Human killer cell activatory receptors for MHC class I molecules are included in a multimeric complex expressed by natural killer cells. J Immunol 1997; 158: 5083-5086

Ōmura S, Crump A. Lactacystin: first-in-class proteasome inhibitor still excelling and an exemplar for future antibiotic research. J Antibiot (Tokyo) 2019; 72: 189-201

Otero K, Shinohara M, Zhao H, Cella M, Gilfillan S, Colucci A, Faccio R, Ross FP, Teitelbaum SL, Takayanagi H, Colonna M. TREM2 and β-catenin regulate bone homeostasis by controlling the rate of osteoclastogenesis. J Immunol 2012; 188: 2612-2621

Ozaki Y, Yoshino Y, Yamazaki K, Sao T, Mori Y, Ochi S, Yoshida T, Mori T, Iga JI, Ueno SI. DNA methylation changes at TREM2 intron 1 and TREM2 mRNA expression in patients with Alzheimer's disease. J Psychiatr Res 2017; 92: 74-80

Paloneva J, Kestilä M, Wu J, Salminen A, Böhling T, Ruotsalainen V, Hakola P, Bakker AB, Phillips JH, Pekkarinen P, Lanier LL, Timonen T, Peltonen L. Loss-of-function mutations in TYROBP (DAP12) result in a presenile dementia with bone cysts. Nat Genet 2000; 25: 357-361

Paloneva J, Manninen T, Christman G, Hovanes K, Mandelin J, Adolfsson R, Bianchin M, Bird T, Miranda R, Salmaggi A, Tranebjaerg L, Konttinen Y, Peltonen L. Mutations in two genes encoding different subunits of a receptor signaling complex result in an identical disease phenotype. Am J Hum Genet 2002; 71: 656-662

Papanikou E, Glick BS. Golgi compartmentation and identity. Curr Opin Cell Biol 2014; 29: 74-81

Park EK, Jung HS, Yang HI, Yoo MC, Kim C, Kim KS. Optimized THP-1 differentiation is required for the detection of responses to weak stimuli. Inflamm Res 2007; 56: 45-50

Park HJ, Ryu D, Parmar M, Giasson BI, McFarland NR. The ER retention protein RER1 promotes alpha-synuclein degradation via the proteasome. PLoS One 2017; 12: e0184262

Park HJ, Shabashvili D, Nekorchuk MD, Shyqyriu E, Jung JI, Ladd TB, Moore BD, Felsenstein KM, Golde TE, Kim SH. Retention in endoplasmic reticulum 1 (RER1) modulates amyloid-β (Aβ) production by altering trafficking of γ-secretase and amyloid precursor protein (APP). J Biol Chem 2012; 287: 40629-40640

Park JS, Ji IJ, An HJ, Kang MJ, Kang SW, Kim DH, Yoon SY. Disease-Associated Mutations of TREM2 Alter the Processing of N-Linked Oligosaccharides in the Golgi Apparatus. Traffic 2015a; 16: 510-518

Park JS, Ji IJ, Kim DH, An HJ, Yoon SY. The Alzheimer's Disease-Associated R47H Variant of TREM2 Has an Altered Glycosylation Pattern and Protein Stability. Front Neurosci 2016; 10: 618

Park M, Yi JW, Kim EM, Yoon IJ, Lee EH, Lee HY, Ji KY, Lee KH, Jang JH, Oh SS, Yun CH, Kim SH, Lee KM, Song MG, Kim DH, Kang HS. Triggering receptor expressed on myeloid cells 2 (TREM2) promotes adipogenesis and diet-induced obesity. Diabetes 2015b; 64: 117-127

Park MD, Silvin A, Ginhoux F, Merad M. Macrophages in health and disease. Cell 2022; 185: 4259-4279

Parodi M, Favoreel H, Candiano G, Gaggero S, Sivori S, Mingari MC, Moretta L, Vitale M, Cantoni C. NKp44-NKp44 Ligand Interactions in the Regulation of Natural Killer Cells and Other Innate Lymphoid Cells in Humans. Front Immunol 2019; 10: 719

Pasquier B. Autophagy inhibitors. Cellular and Molecular Life Sciences 2016; 73: 985-1001

Paul PK, Umarvaish S, Bajaj S, S RF, Mohan H, Annaert W, Chaudhary V. Maintenance of proteostasis by Drosophila Rer1 is essential for competitive cell survival and Myc-driven overgrowth. PLoS Genet 2024; 20: e1011171

Pekkarinen P, Hovatta I, Hakola P, Järvi O, Kestilä M, Lenkkeri U, Adolfsson R, Holmgren G, Nylander PO, Tranebjaerg L, Terwilliger JD, Lönnqvist J, Peltonen L. Assignment of

the locus for PLO-SL, a frontal-lobe dementia with bone cysts, to 19q13. Am J Hum Genet 1998a; 62: 362-372

Pekkarinen P, Kestilä M, Paloneva J, Terwillign J, Varilo T, Järvi O, Hakola P, Peltonen L. Fine-scale mapping of a novel dementia gene, PLOSL, by linkage disequilibrium. Genomics 1998b; 54: 307-315

Pfeffer SR. NPC intracellular cholesterol transporter 1 (NPC1)-mediated cholesterol export from lysosomes. J Biol Chem 2019; 294: 1706-1709

Phongsisay V. Campylobacter jejuni targets immunoglobulin-like receptor LMIR5. Mol Immunol 2015; 63: 574-578

Phongsisay V, Iizasa E, Hara H, Yamasaki S. 3-O-sulfo-β-D-galactose moiety of endogenous sulfoglycolipids is a potential ligand for immunoglobulin-like receptor LMIR5. Mol Immunol 2015a; 63: 595-599

Phongsisay V, Iizasa E, Hara H, Yoshida H. Evidence for TLR4 and FcRγ-CARD9 activation by cholera toxin B subunit and its direct bindings to TREM2 and LMIR5 receptors. Mol Immunol 2015b; 66: 463-471

Phongsisay V, Iizasa E, Hara H, Yoshida H. Pertussis toxin targets the innate immunity through DAP12, FcRγ, and MyD88 adaptor proteins. Immunobiology 2017; 222: 664-671

Piccio L, Deming Y, Del-Águila JL, Ghezzi L, Holtzman DM, Fagan AM, Fenoglio C, Galimberti D, Borroni B, Cruchaga C. Cerebrospinal fluid soluble TREM2 is higher in Alzheimer disease and associated with mutation status. Acta Neuropathol 2016; 131: 925-933

Poliani PL, Wang Y, Fontana E, Robinette ML, Yamanishi Y, Gilfillan S, Colonna M. TREM2 sustains microglial expansion during aging and response to demyelination. J Clin Invest 2015; 125: 2161-2170

Pottier C, Ravenscroft TA, Brown PH, Finch NA, Baker M, Parsons M, Asmann YW, Ren Y, Christopher E, Levitch D, van Blitterswijk M, Cruchaga C, Campion D, Nicolas G, Richard AC, Guerreiro R, Bras JT, Zuchner S, Gonzalez MA, Bu G, Younkin S, Knopman DS, Josephs KA, Parisi JE, Petersen RC, Ertekin-Taner N, Graff-Radford NR, Boeve BF, Dickson DW, Rademakers R. TYROBP genetic variants in early-onset Alzheimer's disease. Neurobiol Aging 2016; 48: 222.e229-222.e215

Prieur X, Mok CY, Velagapudi VR, Núñez V, Fuentes L, Montaner D, Ishikawa K, Camacho A, Barbarroja N, O'Rahilly S, Sethi JK, Dopazo J, Orešič M, Ricote M, Vidal-Puig A. Differential lipid partitioning between adipocytes and tissue macrophages modulates macrophage lipotoxicity and M2/M1 polarization in obese mice. Diabetes 2011; 60: 797-809

Qin J, Ma Z, Chen X, Shu S. Microglia activation in central nervous system disorders: A review of recent mechanistic investigations and development efforts. Frontiers in Neurology 2023; 14

Quan DN, Cooper MD, Potter JL, Roberts MH, Cheng H, Jarvis GA. TREM-2 binds to lipooligosaccharides of Neisseria gonorrhoeae and is expressed on reproductive tract epithelial cells. Mucosal Immunol 2008; 1: 229-238

Radtke F, Fasnacht N, Macdonald HR. Notch signaling in the immune system. Immunity 2010; 32: 14-27

Rahim MM, Makrigiannis AP. Ly49 receptors: evolution, genetic diversity, and impact on immunity. Immunol Rev 2015; 267: 137-147

Randolph GJ, Beaulieu S, Lebecque S, Steinman RM, Muller WA. Differentiation of monocytes into dendritic cells in a model of transendothelial trafficking. Science 1998; 282: 480-483

Randolph GJ, Inaba K, Robbiani DF, Steinman RM, Muller WA. Differentiation of phagocytic monocytes into lymph node dendritic cells in vivo. Immunity 1999; 11: 753-761

Ross AB, Langer JD, Jovanovic M. Proteome Turnover in the Spotlight: Approaches, Applications, and Perspectives. Mol Cell Proteomics 2021; 20: 100016

Ross R. The pathogenesis of atherosclerosis: a perspective for the 1990s. Nature 1993; 362: 801-809

Saito K, Yamashiro K, Shimazu N, Tanabe T, Kontani K, Katada T. Concentration of Sec12 at ER exit sites via interaction with cTAGE5 is required for collagen export. J Cell Biol 2014; 206: 751-762

Salamanca L, Mechawar N, Murai KK, Balling R, Bouvier DS, Skupin A. MIC-MAC: An automated pipeline for high-throughput characterization and classification of three-dimensional microglia morphologies in mouse and human postmortem brain samples. Glia 2019; 67: 1496-1509

Sato K, Nishikawa S, Nakano A. Membrane protein retrieval from the Golgi apparatus to the endoplasmic reticulum (ER): characterization of the RER1 gene product as a component involved in ER localization of Sec12p. Mol Biol Cell 1995; 6: 1459-1477

Sato K, Sato M, Nakano A. Rer1p as common machinery for the endoplasmic reticulum localization of membrane proteins. Proc Natl Acad Sci U S A 1997; 94: 9693-9698

Sato K, Sato M, Nakano A. Rer1p, a retrieval receptor for endoplasmic reticulum membrane proteins, is dynamically localized to the Golgi apparatus by coatomer. J Cell Biol 2001; 152: 935-944

Sato K, Sato M, Nakano A. Rer1p, a retrieval receptor for ER membrane proteins, recognizes transmembrane domains in multiple modes. Mol Biol Cell 2003; 14: 3605-3616

Sato M, Sato K, Nakano A. Endoplasmic reticulum localization of Sec12p is achieved by two mechanisms: Rer1p-dependent retrieval that requires the transmembrane domain

and Rer1p-independent retention that involves the cytoplasmic domain. J Cell Biol 1996; 134: 279-293

Sato M, Sato K, Nakano A. Endoplasmic reticulum quality control of unassembled iron transporter depends on Rer1p-mediated retrieval from the golgi. Mol Biol Cell 2004; 15: 1417-1424

Satoh J, Shimamura Y, Tabunoki H. Gene expression profile of THP-1 monocytes following knockdown of DAP12, a causative gene for Nasu-Hakola disease. Cell Mol Neurobiol 2012; 32: 337-343

Satoh JI, Yanaizu M, Tosaki Y, Sakai K, Kino Y. Targeted sequencing approach to identify genetic mutations in Nasu-Hakola disease. Intractable Rare Dis Res 2016; 5: 269-274

Schafer DP, Stevens B. Microglia Function in Central Nervous System Development and Plasticity. Cold Spring Harb Perspect Biol 2015; 7: a020545

Schlepckow K, Kleinberger G, Fukumori A, Feederle R, Lichtenthaler SF, Steiner H, Haass C. An Alzheimer-associated TREM2 variant occurs at the ADAM cleavage site and affects shedding and phagocytic function. EMBO Mol Med 2017; 9: 1356-1365

Schlepckow K, Monroe KM, Kleinberger G, Cantuti-Castelvetri L, Parhizkar S, Xia D, Willem M, Werner G, Pettkus N, Brunner B, Sülzen A, Nuscher B, Hampel H, Xiang X, Feederle R, Tahirovic S, Park JI, Prorok R, Mahon C, Liang CC, Shi J, Kim DJ, Sabelström H, Huang F, Di Paolo G, Simons M, Lewcock JW, Haass C. Enhancing protective microglial activities with a dual function TREM2 antibody to the stalk region. EMBO Mol Med 2020; 12: e11227

Schneider-Poetsch T, Ju J, Eyler DE, Dang Y, Bhat S, Merrick WC, Green R, Shen B, Liu JO. Inhibition of eukaryotic translation elongation by cycloheximide and lactimidomycin. Nat Chem Biol 2010; 6: 209-217

Schuck S. Microautophagy - distinct molecular mechanisms handle cargoes of many sizes. J Cell Sci 2020; 133

Schwarz DS, Blower MD. The endoplasmic reticulum: structure, function and response to cellular signaling. Cell Mol Life Sci 2016; 73: 79-94

Schwende H, Fitzke E, Ambs P, Dieter P. Differences in the state of differentiation of THP-1 cells induced by phorbol ester and 1,25-dihydroxyvitamin D3. J Leukoc Biol 1996; 59: 555-561

Semenza JC, Hardwick KG, Dean N, Pelham HR. ERD2, a yeast gene required for the receptor-mediated retrieval of luminal ER proteins from the secretory pathway. Cell 1990; 61: 1349-1357

Serbina NV, Pamer EG. Monocyte emigration from bone marrow during bacterial infection requires signals mediated by chemokine receptor CCR2. Nat Immunol 2006; 7: 311-317

Sessa G, Podini P, Mariani M, Meroni A, Spreafico R, Sinigaglia F, Colonna M, Panina P, Meldolesi J. Distribution and signaling of TREM2/DAP12, the receptor system mutated in human polycystic lipomembraneous osteodysplasia with sclerosing leukoencephalopathy dementia. Eur J Neurosci 2004; 20: 2617-2628

Shaywitz DA, Espenshade PJ, Gimeno RE, Kaiser CA. COPII subunit interactions in the assembly of the vesicle coat. J Biol Chem 1997; 272: 25413-25416

Shiwarski DJ, Crilly SE, Dates A, Puthenveedu MA. Dual RXR motifs regulate nerve growth factor-mediated intracellular retention of the delta opioid receptor. Mol Biol Cell 2019; 30: 680-690

Sirkis DW, Aparicio RE, Schekman R. Neurodegeneration-associated mutant TREM2 proteins abortively cycle between the ER and ER-Golgi intermediate compartment. Mol Biol Cell 2017; 28: 2723-2733

Sjöstedt E, Zhong W, Fagerberg L, Karlsson M, Mitsios N, Adori C, Oksvold P, Edfors F, Limiszewska A, Hikmet F, Huang J, Du Y, Lin L, Dong Z, Yang L, Liu X, Jiang H, Xu X, Wang J, Yang H, Bolund L, Mardinoglu A, Zhang C, von Feilitzen K, Lindskog C, Pontén F, Luo Y, Hökfelt T, Uhlén M, Mulder J. An atlas of the protein-coding genes in the human, pig, and mouse brain. Science 2020; 367

Slater AF. Chloroquine: mechanism of drug action and resistance in Plasmodium falciparum. Pharmacol Ther 1993; 57: 203-235

Song W, Hooli B, Mullin K, Jin SC, Cella M, Ulland TK, Wang Y, Tanzi RE, Colonna M. Alzheimer's disease-associated TREM2 variants exhibit either decreased or increased ligand-dependent activation. Alzheimers Dement 2017; 13: 381-387

Soragna D, Papi L, Ratti MT, Sestini R, Tupler R, Montalbetti L. An Italian family affected by Nasu-Hakola disease with a novel genetic mutation in the TREM2 gene. J Neurol Neurosurg Psychiatry 2003; 74: 825-826

Šošić-Jurjević B, Lütjohann D, Renko K, Filipović B, Radulović N, Ajdžanović V, Trifunović S, Nestorović N, Živanović J, Manojlović Stojanoski M, Köhrle J, Milošević V. The isoflavones genistein and daidzein increase hepatic concentration of thyroid hormones and affect cholesterol metabolism in middle-aged male rats. The Journal of Steroid Biochemistry and Molecular Biology 2019; 190: 1-10

Spasic D, Raemaekers T, Dillen K, Declerck I, Baert V, Serneels L, Füllekrug J, Annaert W. Rer1p competes with APH-1 for binding to nicastrin and regulates gamma-secretase complex assembly in the early secretory pathway. J Cell Biol 2007; 176: 629-640

Spear ED, Ng DT. Stress tolerance of misfolded carboxypeptidase Y requires maintenance of protein trafficking and degradative pathways. Mol Biol Cell 2003; 14: 2756-2767

Standley S, Roche KW, McCallum J, Sans N, Wenthold RJ. PDZ domain suppression of an ER retention signal in NMDA receptor NR1 splice variants. Neuron 2000; 28: 887-898

Stefano L, Racchetti G, Bianco F, Passini N, Gupta RS, Panina Bordignon P, Meldolesi J. The surface-exposed chaperone, Hsp60, is an agonist of the microglial TREM2 receptor. J Neurochem 2009; 110: 284-294

Steiner H, Winkler E, Edbauer D, Prokop S, Basset G, Yamasaki A, Kostka M, Haass C. PEN-2 is an integral component of the gamma-secretase complex required for coordinated expression of presenilin and nicastrin. J Biol Chem 2002; 277: 39062-39065

Stephenson RA, Johnson KR, Cheng L, Yang LG, Root JT, Gopalakrishnan J, Shih H-Y, Narayan PS. Triglyceride metabolism controls inflammation and APOE4-associated disease states in microglia. bioRxiv 2024: 2024.2004.2011.589145

Sterz J, von Metzler I, Hahne JC, Lamottke B, Rademacher J, Heider U, Terpos E, Sezer O. The potential of proteasome inhibitors in cancer therapy. Expert Opin Investig Drugs 2008; 17: 879-895

Stewart CR, Stuart LM, Wilkinson K, van Gils JM, Deng J, Halle A, Rayner KJ, Boyer L, Zhong R, Frazier WA, Lacy-Hulbert A, El Khoury J, Golenbock DT, Moore KJ. CD36 ligands promote sterile inflammation through assembly of a Toll-like receptor 4 and 6 heterodimer. Nat Immunol 2010; 11: 155-161

Strittmatter WJ, Saunders AM, Schmechel D, Pericak-Vance M, Enghild J, Salvesen GS, Roses AD. Apolipoprotein E: high-avidity binding to beta-amyloid and increased frequency of type 4 allele in late-onset familial Alzheimer disease. Proc Natl Acad Sci U S A 1993; 90: 1977-1981

Sullivan LC, Clements CS, Beddoe T, Johnson D, Hoare HL, Lin J, Huyton T, Hopkins EJ, Reid HH, Wilce MCJ, Kabat J, Borrego F, Coligan JE, Rossjohn J, Brooks AG. The Heterodimeric Assembly of the CD94-NKG2 Receptor Family and Implications for Human Leukocyte Antigen-E Recognition. Immunity 2007; 27: 900-911

Sun L-P, Li L, Goldstein JL, Brown MS. Insig Required for Sterol-mediated Inhibition of Scap/SREBP Binding to COPII Proteins in Vitro*, ♦. Journal of Biological Chemistry 2005; 280: 26483-26490

Sun Z, Brodsky JL. Protein quality control in the secretory pathway. Journal of Cell Biology 2019; 218: 3171-3187

Suzuki K, Kirisako T, Kamada Y, Mizushima N, Noda T, Ohsumi Y. The pre-autophagosomal structure organized by concerted functions of APG genes is essential for autophagosome formation. Embo j 2001; 20: 5971-5981

Tai LM, Mehra S, Shete V, Estus S, Rebeck GW, Bu G, LaDu MJ. Soluble apoE/Aβ complex: mechanism and therapeutic target for APOE4-induced AD risk. Mol Neurodegener 2014; 9: 2

Takahashi K, Rochford CD, Neumann H. Clearance of apoptotic neurons without inflammation by microglial triggering receptor expressed on myeloid cells-2. J Exp Med 2005; 201: 647-657

Tamboli IY, Hampel H, Tien NT, Tolksdorf K, Breiden B, Mathews PM, Saftig P, Sandhoff K, Walter J. Sphingolipid storage affects autophagic metabolism of the amyloid precursor protein and promotes Abeta generation. J Neurosci 2011; 31: 1837-1849

Tan YJ, Ng ASL, Vipin A, Lim JKW, Chander RJ, Ji F, Qiu Y, Ting SKS, Hameed S, Lee TS, Zeng L, Kandiah N, Zhou J. Higher Peripheral TREM2 mRNA Levels Relate to Cognitive Deficits and Hippocampal Atrophy in Alzheimer's Disease and Amnestic Mild Cognitive Impairment. J Alzheimers Dis 2017; 58: 413-423

Tanabe C, Maeda T, Zou K, Liu J, Liu S, Nakajima T, Komano H. The ubiquitin ligase synoviolin up-regulates amyloid β production by targeting a negative regulator of γ-secretase, Rer1, for degradation. J Biol Chem 2012; 287: 44203-44211

Tanaka K. The proteasome: overview of structure and functions. Proc Jpn Acad Ser B Phys Biol Sci 2009; 85: 12-36

Tang B, Cai J, Sun L, Li Y, Qu J, Snider BJ, Wu S. Proteasome inhibitors activate autophagy involving inhibition of PI3K-Akt-mTOR pathway as an anti-oxidation defense in human RPE cells. PLoS One 2014; 9: e103364

Teasdale RD, Jackson MR. Signal-mediated sorting of membrane proteins between the endoplasmic reticulum and the golgi apparatus. Annu Rev Cell Dev Biol 1996; 12: 27-54

Tien NT, Karaca I, Tamboli IY, Walter J. Trehalose Alters Subcellular Trafficking and the Metabolism of the Alzheimer-associated Amyloid Precursor Protein. J Biol Chem 2016; 291: 10528-10540

Tomasello E, Cant C, Bühring HJ, Vély F, André P, Seiffert M, Ullrich A, Vivier E. Association of signal-regulatory proteins beta with KARAP/DAP-12. Eur J Immunol 2000; 30: 2147-2156

Tomasello E, Olcese L, Vély F, Geourgeon C, Bléry M, Moqrich A, Gautheret D, Djabali M, Mattei MG, Vivier E. Gene structure, expression pattern, and biological activity of mouse killer cell activating receptor-associated protein (KARAP)/DAP-12. J Biol Chem 1998; 273: 34115-34119

Tomoda H, Omura S. Lactacystin, a proteasome inhibitor: discovery and its application in cell biology. Yakugaku Zasshi 2000; 120: 935-949

Tremblay M. The role of microglia at synapses in the healthy CNS: novel insights from recent imaging studies. Neuron Glia Biol 2011; 7: 67-76

Tremblay M, Stevens B, Sierra A, Wake H, Bessis A, Nimmerjahn A. The role of microglia in the healthy brain. J Neurosci 2011; 31: 16064-16069

Tsai B, Ye Y, Rapoport TA. Retro-translocation of proteins from the endoplasmic reticulum into the cytosol. Nat Rev Mol Cell Biol 2002; 3: 246-255

Tserel L, Kolde R, Rebane A, Kisand K, Org T, Peterson H, Vilo J, Peterson P. Genome-wide promoter analysis of histone modifications in human monocyte-derived antigen presenting cells. BMC Genomics 2010; 11: 642

Tsubuki S, Saito Y, Tomioka M, Ito H, Kawashima S. Differential inhibition of calpain and proteasome activities by peptidyl aldehydes of di-leucine and tri-leucine. J Biochem 1996; 119: 572-576

Tsuchiya S, Kobayashi Y, Goto Y, Okumura H, Nakae S, Konno T, Tada K. Induction of maturation in cultured human monocytic leukemia cells by a phorbol diester. Cancer Res 1982; 42: 1530-1536

Tsuchiya S, Yamabe M, Yamaguchi Y, Kobayashi Y, Konno T, Tada K. Establishment and characterization of a human acute monocytic leukemia cell line (THP-1). Int J Cancer 1980; 26: 171-176

Tudorache IF, Trusca VG, Gafencu AV. Apolipoprotein E - A Multifunctional Protein with Implications in Various Pathologies as a Result of Its Structural Features. Comput Struct Biotechnol J 2017; 15: 359-365

Turnbull IR, Colonna M. Activating and inhibitory functions of DAP12. Nat Rev Immunol 2007; 7: 155-161

Turnbull IR, Gilfillan S, Cella M, Aoshi T, Miller M, Piccio L, Hernandez M, Colonna M. Cutting edge: TREM-2 attenuates macrophage activation. J Immunol 2006; 177: 3520-3524

Uhlén M, Fagerberg L, Hallström BM, Lindskog C, Oksvold P, Mardinoglu A, Sivertsson Å, Kampf C, Sjöstedt E, Asplund A, Olsson I, Edlund K, Lundberg E, Navani S, Szigyarto CA, Odeberg J, Djureinovic D, Takanen JO, Hober S, Alm T, Edqvist PH, Berling H, Tegel H, Mulder J, Rockberg J, Nilsson P, Schwenk JM, Hamsten M, von Feilitzen K, Forsberg M, Persson L, Johansson F, Zwahlen M, von Heijne G, Nielsen J, Pontén F. Proteomics. Tissue-based map of the human proteome. Science 2015; 347: 1260419

Uhlen M, Karlsson MJ, Zhong W, Tebani A, Pou C, Mikes J, Lakshmikanth T, Forsström B, Edfors F, Odeberg J, Mardinoglu A, Zhang C, von Feilitzen K, Mulder J, Sjöstedt E, Hober A, Oksvold P, Zwahlen M, Ponten F, Lindskog C, Sivertsson Å, Fagerberg L, Brodin P. A genome-wide transcriptomic analysis of protein-coding genes in human blood cells. Science 2019; 366

Valkova C, Albrizio M, Röder IV, Schwake M, Betto R, Rudolf R, Kaether C. Sorting receptor Rer1 controls surface expression of muscle acetylcholine receptors by ER retention of unassembled alpha-subunits. Proc Natl Acad Sci U S A 2011; 108: 621-625

Valkova C, Liebmann L, Krämer A, Hübner CA, Kaether C. The sorting receptor Rer1 controls Purkinje cell function via voltage gated sodium channels. Sci Rep 2017; 7: 41248

van Dierendonck X, Vrieling F, Smeehuijzen L, Deng L, Boogaard JP, Croes CA, Temmerman L, Wetzels S, Biessen E, Kersten S, Stienstra R. Triglyceride breakdown

from lipid droplets regulates the inflammatory response in macrophages. Proc Natl Acad Sci U S A 2022; 119: e2114739119

van Furth R, Cohn ZA. The origin and kinetics of mononuclear phagocytes. J Exp Med 1968; 128: 415-435

van Furth R, Raeburn JA, van Zwet TL. Characteristics of human mononuclear phagocytes. Blood 1979; 54: 485-500

Vargas JNS, Hamasaki M, Kawabata T, Youle RJ, Yoshimori T. The mechanisms and roles of selective autophagy in mammals. Nature Reviews Molecular Cell Biology 2023; 24: 167-185

Varnum MM, Clayton KA, Yoshii-Kitahara A, Yonemoto G, Koro L, Ikezu S, Ikezu T. A split-luciferase complementation, real-time reporting assay enables monitoring of the disease-associated transmembrane protein TREM2 in live cells. J Biol Chem 2017; 292: 10651-10663

Verghese PB, Castellano JM, Garai K, Wang Y, Jiang H, Shah A, Bu G, Frieden C, Holtzman DM. ApoE influences amyloid-β (Aβ) clearance despite minimal apoE/Aβ association in physiological conditions. Proc Natl Acad Sci U S A 2013; 110: E1807-1816

Verloes A, Maquet P, Sadzot B, Vivario M, Thiry A, Franck G. Nasu-Hakola syndrome: polycystic lipomembranous osteodysplasia with sclerosing leucoencephalopathy and presenile dementia. J Med Genet 1997; 34: 753-757

Vitale M, Bottino C, Sivori S, Sanseverino L, Castriconi R, Marcenaro E, Augugliaro R, Moretta L, Moretta A. NKp44, a novel triggering surface molecule specifically expressed by activated natural killer cells, is involved in non-major histocompatibility complex-restricted tumor cell lysis. J Exp Med 1998; 187: 2065-2072

Vivier E, Nunès JA, Vély F. Natural killer cell signaling pathways. Science 2004; 306: 1517-1519

Voges D, Zwickl P, Baumeister W. The 26S proteasome: a molecular machine designed for controlled proteolysis. Annu Rev Biochem 1999; 68: 1015-1068

Walter J. The Triggering Receptor Expressed on Myeloid Cells 2: A Molecular Link of Neuroinflammation and Neurodegenerative Diseases. J Biol Chem 2016; 291: 4334-4341

Walther TC, Farese RV, Jr. Lipid droplets and cellular lipid metabolism. Annu Rev Biochem 2012; 81: 687-714

Wang DW, Peng ZJ, Ren GF, Wang GX. The different roles of selective autophagic protein degradation in mammalian cells. Oncotarget 2015a; 6: 37098-37116

Wang H, Airola MV, Reue K. How lipid droplets “TAG” along: Glycerolipid synthetic enzymes and lipid storage. Biochimica et Biophysica Acta (BBA) - Molecular and Cell Biology of Lipids 2017; 1862: 1131-1145

Wang J-M, Zhang L, Yao Y, Viroonchatapan N, Rothe E, Wang Z-Z. A transmembrane motif governs the surface trafficking of nicotinic acetylcholine receptors. Nature Neuroscience 2002; 5: 963-970

Wang S, Mustafa M, Yuede CM, Salazar SV, Kong P, Long H, Ward M, Siddiqui O, Paul R, Gilfillan S, Ibrahim A, Rhinn H, Tassi I, Rosenthal A, Schwabe T, Colonna M. Anti-human TREM2 induces microglia proliferation and reduces pathology in an Alzheimer's disease model. J Exp Med 2020; 217

Wang Y, Cella M, Mallinson K, Ulrich JD, Young KL, Robinette ML, Gilfillan S, Krishnan GM, Sudhakar S, Zinselmeyer BH, Holtzman DM, Cirrito JR, Colonna M. TREM2 lipid sensing sustains the microglial response in an Alzheimer's disease model. Cell 2015b; 160: 1061-1071

Wang Y, Ulland TK, Ulrich JD, Song W, Tzaferis JA, Hole JT, Yuan P, Mahan TE, Shi Y, Gilfillan S, Cella M, Grutzendler J, DeMattos RB, Cirrito JR, Holtzman DM, Colonna M. TREM2-mediated early microglial response limits diffusion and toxicity of amyloid plaques. J Exp Med 2016; 213: 667-675

Wei P, Zheng BK, Guo PR, Kawakami T, Luo SZ. The association of polar residues in the DAP12 homodimer: TOXCAT and molecular dynamics simulation studies. Biophys J 2013; 104: 1435-1444

Welte MA, Gould AP. Lipid droplet functions beyond energy storage. Biochim Biophys Acta Mol Cell Biol Lipids 2017; 1862: 1260-1272

Wilson MJ, Lindquist JA, Trowsdale J. DAP12 and KAP10 (DAP10)-novel transmembrane adapter proteins of the CD3zeta family. Immunol Res 2000; 22: 21-42

Wójcik C, DeMartino GN. Intracellular localization of proteasomes. Int J Biochem Cell Biol 2003; 35: 579-589

Wu D, Xu L, Cai WM, Zhan SY, Wan G, Xu Y, Shi YS. A splicing-dependent ER retention signal regulates surface expression of the mechanosensitive TMEM63B cation channel. J Biol Chem 2023; 299: 102781

Wu K, Byers DE, Jin X, Agapov E, Alexander-Brett J, Patel AC, Cella M, Gilfilan S, Colonna M, Kober DL, Brett TJ, Holtzman MJ. TREM-2 promotes macrophage survival and lung disease after respiratory viral infection. J Exp Med 2015; 212: 681-697

Wu X, Rapoport TA. Mechanistic insights into ER-associated protein degradation. Curr Opin Cell Biol 2018; 53: 22-28

Wunderlich P, Glebov K, Kemmerling N, Tien NT, Neumann H, Walter J. Sequential proteolytic processing of the triggering receptor expressed on myeloid cells-2 (TREM2) protein by ectodomain shedding and γ-secretase-dependent intramembranous cleavage. J Biol Chem 2013; 288: 33027-33036

Xue J, Schmidt SV, Sander J, Draffehn A, Krebs W, Quester I, De Nardo D, Gohel TD, Emde M, Schmidleithner L, Ganesan H, Nino-Castro A, Mallmann MR, Labzin L, Theis H, Kraut M, Beyer M, Latz E, Freeman TC, Ulas T, Schultze JL. Transcriptome-based network analysis reveals a spectrum model of human macrophage activation. Immunity 2014; 40: 274-288

Yaghmour MH, Thiele C, Kuerschner L. An advanced method for propargylcholine phospholipid detection by direct-infusion MS. J Lipid Res 2021; 62: 100022

Yamasaki A, Hara T, Maejima I, Sato M, Sato K, Sato K. Rer1p regulates the ER retention of immature rhodopsin and modulates its intracellular trafficking. Sci Rep 2014; 4: 5973

Yang Z, Klionsky DJ. An overview of the molecular mechanism of autophagy. Curr Top Microbiol Immunol 2009; 335: 1-32

Yona S, Jung S. Monocytes: subsets, origins, fates and functions. Current Opinion in Hematology 2010; 17: 53-59

Yu Q, Zheng H, Zhang Y. Inducible degrader of LDLR: A potential novel therapeutic target and emerging treatment for hyperlipidemia. Vascular Pharmacology 2021; 140: 106878

Yu X-H, Tang C-K (2022) ABCA1, ABCG1, and Cholesterol Homeostasis. In *HDL Metabolism and Diseases*, Zheng L (ed) pp 95-107. Singapore: Springer Nature Singapore

Yvan-Charvet L, Wang N, Tall AR. Role of HDL, ABCA1, and ABCG1 transporters in cholesterol efflux and immune responses. Arterioscler Thromb Vasc Biol 2010; 30: 139-143

Zaffagnini G, Martens S. Mechanisms of Selective Autophagy. J Mol Biol 2016; 428: 1714-1724

Zanetti G, Pahuja KB, Studer S, Shim S, Schekman R. COPII and the regulation of protein sorting in mammals. Nat Cell Biol 2011; 14: 20-28

Zhang B, Gaiteri C, Bodea LG, Wang Z, McElwee J, Podtelezhnikov AA, Zhang C, Xie T, Tran L, Dobrin R, Fluder E, Clurman B, Melquist S, Narayanan M, Suver C, Shah H, Mahajan M, Gillis T, Mysore J, MacDonald ME, Lamb JR, Bennett DA, Molony C, Stone DJ, Gudnason V, Myers AJ, Schadt EE, Neumann H, Zhu J, Emilsson V. Integrated systems approach identifies genetic nodes and networks in late-onset Alzheimer's disease. Cell 2013; 153: 707-720

Zhang J, Raper A, Sugita N, Hingorani R, Salio M, Palmowski MJ, Cerundolo V, Crocker PR. Characterization of Siglec-H as a novel endocytic receptor expressed on murine plasmacytoid dendritic cell precursors. Blood 2006; 107: 3600-3608

Zhao J, Goldberg AL. Coordinate regulation of autophagy and the ubiquitin proteasome system by MTOR. Autophagy 2016; 12: 1967-1970

Zhao J, Zhai B, Gygi SP, Goldberg AL. mTOR inhibition activates overall protein degradation by the ubiquitin proteasome system as well as by autophagy. Proc Natl Acad Sci U S A 2015; 112: 15790-15797

Zhao L, Zhao J, Zhong K, Tong A, Jia D. Targeted protein degradation: mechanisms, strategies and application. Signal Transduct Target Ther 2022; 7: 113

Zhong L, Chen XF, Wang T, Wang Z, Liao C, Wang Z, Huang R, Wang D, Li X, Wu L, Jia L, Zheng H, Painter M, Atagi Y, Liu CC, Zhang YW, Fryer JD, Xu H, Bu G. Soluble TREM2 induces inflammatory responses and enhances microglial survival. J Exp Med 2017; 214: 597-607

Zhong L, Chen XF, Zhang ZL, Wang Z, Shi XZ, Xu K, Zhang YW, Xu H, Bu G. DAP12 Stabilizes the C-terminal Fragment of the Triggering Receptor Expressed on Myeloid Cells-2 (TREM2) and Protects against LPS-induced Pro-inflammatory Response. J Biol Chem 2015; 290: 15866-15877

Zuris JA, Thompson DB, Shu Y, Guilinger JP, Bessen JL, Hu JH, Maeder ML, Joung JK, Chen ZY, Liu DR. Cationic lipid-mediated delivery of proteins enables efficient protein-based genome editing in vitro and in vivo. Nat Biotechnol 2015; 33: 73-80

9 Acknowledgements

This thesis represents the culmination of years of dedication, collaboration, and support from many wonderful individuals. It is with profound gratitude that I take this opportunity to thank everyone who has contributed to my academic and personal journey. First and foremost, I would like to express my deepest gratitude to my supervisor, Prof. Dr. Jochen Walter, for his unwavering guidance, patience, and encouragement throughout this journey. His expertise and mentorship have been invaluable in shaping my research and personal growth. I would also like to extend my heartfelt thanks to my committee members, Prof. Dr. Thorsten Lang, Prof. Dr. Ina Maja Vorberg, and Prof. Dr. Michael Heneka, for their insightful feedback, support, and guidance throughout my work.

Special thanks go to Sandra Theil, not only for her technical expertise and assistance with the projects and experiments but also for being a true friend throughout this process. My sincere gratitude also extends to all the colleagues and members of Prof. Walter's lab and Prof. Wüllner's lab, who generously shared their knowledge, helped me refine my experimental skills, and created an inspiring and collaborative environment. I am immensely thankful to Thomas Bajaj and Dr. Fabian Stahl for their invaluable assistance with CRISPR/Cas9 technology and their constructive discussions, which were pivotal for advancing my projects. I would like to express my gratitude to Dr. Regina Feederle, Dr. Kai Schlepckow, and Dr. Christian Haass for providing the anti-TREM2 antibody (9D11), as well as to Dr. Sathish Kumar for the characterization of anti-DAP12 antibodies (DAP12.1 and DAP12.2). Thank you to Prof. Dr. Christoph Kaether, Prof, Dr. Guy Brown, and Prof. Dr. Harald Neumann for critically offering helpful discussions.

I also deeply appreciate the contributions of Anja Kerksiek and Prof. Dr. Dieter Lütjohann in assisting with the detection of cholesterol and its precursors, as well as Mohamed H. Yaghmour and Prof. Dr. Christoph Thiele for their support with lipidomic analysis. Many thanks to Peng Chen and Prof. Dr. Ingo Schmidt-Wolf for their guidance and expertise with flow cytometry.

On a personal note, I want to thank my boyfriend, Jianxun Li, who has stood by my side throughout the highs and lows of this Ph.D. journey. His unwavering support, love, and encouragement have meant everything to me. To my parents, brother, and sister-in-law, your constant love, sacrifices, and belief in me have been the cornerstone of my strength. Words cannot express how much your presence has meant to me. I am also profoundly grateful to my friends who have made this journey less daunting and more joyful. To my dear friends in Germany—Xinyu Han, Mengjun Xie, and Ruizhi Bao and friends in China— Yujiao Zhang, Qingping Xu and Jie Li, thank you for your companionship and for being my pillars of support during my Ph.D. years.

Finally, to all my friends, colleagues, and mentors who have touched my life in one way or another, thank you for your kindness, encouragement, and belief in me. This thesis is as much a reflection of your contributions as it is of my own effort.

Publications:

1. **Liu Y**, Theil S, Ibach M, Walter J, DAP12 interacts with RER1 and is retained in the secretory pathway before assembly with TREM2. Cell Mol Life Sci, 2024. 81(1): p. 302. https://doi.org/10.1007/s00018-024-05298-w.

2. Cui D[#], **Liu Y[#]**, Jin L, Hu L, Cao L, A novel compound heterozygous mutation in the arginase-1 gene identified in a Chinese patient with argininemia: A case report. Medicine (Baltimore), 2020. 99(32): p. e21634. https://doi.org/10.1097/MD.0000000000021634.

3. Liu T, Pu J, Theil S, **Liu Y,** Jiang L, Liu H, Maciaczyk J, Schmidt-Wolf IGH, Walter J, Sharma A. Potential role of TNFRSF12A in linking glioblastoma and alzheimer's disease via shared tumour suppressor pathways. Sci Rep. 2025 Jul 1;15(1):21535. https://doi.org/10.1038/s41598-025-08000-7.

4. Ying, C., Ying, L., **Yanxia, L.,** Le, W., Lili, C., High mobility group box 1 antibody represses autophagy and alleviates hippocampus damage in pilocarpine-induced mouse epilepsy model. Acta Histochem, 2020. 122(2): p. 151485. https://doi.org/10.1016/j.acthis.2019.151485.